

# Physics of coral reef systems in a shallow tidal embayment

Fysica van koraalrif systemen in een ondiepe baai  
onder invloed van getijwerking

(met een samenvatting in het Nederlands)

Proefschrift

ter verkrijging van de graad van doctor aan de  
Universiteit Utrecht op gezag van de Rector Magnificus,  
Prof. Dr. W.H. Gispen, ingevolge het besluit van het  
College voor Promoties in het openbaar te verdedigen  
op vrijdag 2 mei 2003 des namiddags te 2.30 uur

door

Antonius Johannes Fransiscus Hoitink

geboren op 20 december 1973 te Hoogkarspel

Promotores

Prof. Dr. P. Hoekstra

Prof. Dr. J.H.J. Terwindt

Dit proefschrift werd financieel mogelijk gemaakt door de Stichting voor Wetenschappelijk Onderzoek van de Tropen en Ontwikkelingslanden (WOTRO).

# Physics of coral reef systems in a shallow tidal embayment



Netherlands Geographical Studies 313

# Physics of coral reef systems in a shallow tidal embayment

A.J.F. Hoitink

Utrecht 2003

Royal Dutch Geographical Society /  
Faculty of Geographical Sciences, Utrecht University

This publication is identical to a thesis submitted in partial fulfilment of the requirements for the degree of Doctor (Ph.D.) at Utrecht University, The Netherlands, 2 May 2003.

Promotores

Prof. Dr. P. Hoekstra, Faculty of Geographical Sciences, Utrecht University  
Prof. Dr. J.H.J. Terwindt, Faculty of Geographical Sciences, Utrecht University

Examination committee

Prof. Dr. H.J. de Vriend, Delft University of Technology  
Prof. Dr. W.P.M. de Ruijter, Utrecht University  
Prof. Dr. R.P.M. Bak, University of Amsterdam  
Prof. Dr. S.J.H.M. Hulscher, University of Twente  
Prof. Dr. S.R. Massel, Institute of Oceanology (Sopot, Poland)

ISBN 90-6809-351-7

Copyright ©A.J.F. Hoitink p/a Faculty of Geographical Sciences, Utrecht University, 2003.

Cover photographs provided by Gerard Nieuwland, Royal Netherlands Institute for Sea Research, lay-out by Kartlab, Utrecht University

Niets uit deze uitgave mag worden vermenigvuldigd en/of openbaar gemaakt door middel van druk, fotokopie of op welke andere wijze dan ook zonder voorafgaande schriftelijke toestemming van de uitgevers.

All rights reserved. No part of this publication may be reproduced in any form, by print or photo print, microfilm or any other means, without written permission by the publishers.

Printed in the Netherlands by Labor Grafimedia b.v. - Utrecht.

# Contents

<b>1</b>	<b>General introduction</b>	<b>14</b>
1.1	Problem definition . . . . .	14
1.2	Physical oceanography of coral reef systems . . . . .	16
1.2.1	Introduction . . . . .	16
1.2.2	Eddy formation . . . . .	16
1.2.3	Mixing and stratification effects . . . . .	18
1.2.4	Drift currents . . . . .	19
1.2.5	Waves . . . . .	19
1.3	Objectives and thesis outline . . . . .	21
<b>2</b>	<b>Field site</b>	<b>23</b>
2.1	Introduction . . . . .	23
2.2	Marine geology of the Bay of Banten . . . . .	25
2.3	Tidal dynamics of the Java Sea . . . . .	27
2.4	Monsoonal climate . . . . .	32
2.5	Sea surface topography and throughflow . . . . .	35
2.6	Concluding remarks . . . . .	38
<b>3</b>	<b>Topographic influence on mixing and stratification in a tropical tidal embayment</b>	<b>39</b>
3.1	Abstract . . . . .	39
3.2	Introduction . . . . .	39
3.3	Observational program . . . . .	41
3.4	The tidal boundary layer . . . . .	42
3.5	Gravitational circulation and Ekman forcing . . . . .	45
3.6	Water column stability . . . . .	48
3.7	Discussion and conclusion . . . . .	50
<b>4</b>	<b>Flow asymmetry associated with astronomical tides: implications for the residual transport of sediment</b>	<b>52</b>
4.1	Abstract . . . . .	52
4.2	Introduction . . . . .	52
4.3	Asymmetry associated with the $K_1$ , $O_1$ and $M_2$ tides . . . . .	53
4.4	Generalization to other tidal constituents . . . . .	57
4.5	Implications for residual bedload transport . . . . .	58
4.6	Implications for residual suspended load transport . . . . .	60
4.7	Conclusions and relevance . . . . .	64

<b>5</b>	<b>Hydrodynamic control on the supply of reworked terrigenous sediment to coral reefs</b>	<b>66</b>
5.1	Abstract . . . . .	66
5.2	Introduction . . . . .	66
5.3	Field site . . . . .	68
5.4	Data acquisition and processing . . . . .	70
5.5	Transport of terrigenous sediment by monsoon-driven flow . . . . .	70
5.5.1	Monsoonal wind and wave climate . . . . .	71
5.5.2	Resuspension by waves . . . . .	72
5.5.3	Seasonal coupling between wave attack, wind-driven throughflow and river discharge . . . . .	74
5.6	Tidally-driven residual transport . . . . .	76
5.6.1	Flow-induced resuspension . . . . .	76
5.6.2	Residual transport associated with tidal asymmetry . . . . .	77
5.6.3	Residual effect of spatial current variation . . . . .	79
5.7	Summary and discussion . . . . .	80
<b>6</b>	<b>Observation of fine-grained suspended sediment from ADCP and OBS measurements</b>	<b>83</b>
6.1	Abstract . . . . .	83
6.2	Introduction . . . . .	83
6.3	Acoustic formulation . . . . .	85
6.3.1	Application of the sonar equation . . . . .	85
6.3.2	Volume backscattering strength related to SSC . . . . .	85
6.3.3	Sound absorption . . . . .	86
6.4	Site and instrumentation . . . . .	88
6.5	Calibrations . . . . .	91
6.5.1	OBS calibration using water samples . . . . .	91
6.5.2	ADCP backscatter conversion to SSC . . . . .	91
6.6	Comparison of ADCP and OBS estimates of mass concentration . . . . .	93
6.6.1	20-day moorings . . . . .	93
6.6.2	25-hour anchor stations . . . . .	98
6.7	Spatial turbidity patterns . . . . .	99
6.8	Discussion . . . . .	99
6.9	Conclusion . . . . .	102
<b>7</b>	<b>Tidally-induced clouds of suspended sediment connected to shallow-water coral reefs</b>	<b>104</b>
7.1	Abstract . . . . .	104
7.2	Introduction . . . . .	104
7.3	Field site . . . . .	105
7.4	Observational program and methods . . . . .	107
7.4.1	Field surveys . . . . .	107
7.4.2	Directional wave spectra . . . . .	108
7.4.3	OBS calibration . . . . .	108
7.4.4	SSC spectra . . . . .	109
7.4.5	Calibration of ADCP backscatter intensity . . . . .	109
7.5	Turbidity variation . . . . .	110
7.6	Flow structure and coastal morphology . . . . .	115



7.7	Implications for reef development . . . . .	117
7.8	Discussion . . . . .	118
7.9	Conclusions . . . . .	120
<b>8</b>	<b>Synthesis</b>	<b>122</b>
8.1	Introduction . . . . .	122
8.2	Physical processes in the Bay of Banten . . . . .	122
8.2.1	Direct river impacts . . . . .	122
8.2.2	Regional sediment supply . . . . .	123
8.2.3	Local sedimentary processes at coral reefs . . . . .	124
8.3	General implications and recommendations . . . . .	124
8.3.1	Coral reefs in marginal regimes . . . . .	124
8.3.2	Physical oceanography of continental shelves . . . . .	125

# List of Tables

1.1	First-order determinants of global reef distribution . . . . .	15
2.1	Tidal amplitude and Greenwich phase lag for selected tidal constituents in the Bay of Banten . . . . .	31
4.1	Doodson numbers and relative amplitude in the Equilibrium Tide of the main diurnal and semidiurnal tidal constituents . . . . .	54
7.1	Mean and maximum of hourly averaged SSC at Kubur and Pamujan Besar .	114
7.2	Coherence between SSC and $u^2$ oscillation . . . . .	115

# List of Figures

1.1	Island wake circulation . . . . .	17
1.2	Internal circulation by boundary mixing in a stratified flow along a reef slope . . . . .	18
1.3	Wave transformation at coral reefs associated to coral cay formation . . . . .	20
2.1	Global patterns of diversity in reef-building scleractinian corals . . . . .	24
2.2	Coastline changes in the Bay of Banten over the past century . . . . .	25
2.3	Bathymetry of the Bay of Banten . . . . .	26
2.4	Recent accumulation rates in Teluk Banten . . . . .	27
2.5	Co-tidal charts of the semidiurnal tides in the Java Sea . . . . .	28
2.6	Co-tidal charts of the diurnal tides in the Java Sea . . . . .	29
2.7	Tidal amplitude change in the Strait Sunda . . . . .	30
2.8	Precipitation and temperature in the region of the Bay of Banten . . . . .	32
2.9	Wind climate in the western part of the Java Sea . . . . .	33
2.10	Seasonality of significant wave heights in the western part of the Java Sea and North of Teluk Banten . . . . .	34
2.11	Low-passed wind speed from a meteorological station at Bojonegara . . . . .	35
2.12	Throughflow in the Strait Sunda . . . . .	36
2.13	Annual variation of the sealevel topography in the Java Sea . . . . .	37
3.1	Location map showing sampling stations in the Bay of Banten . . . . .	41
3.2	Surface current tidal ellipses of $K_1$ and $M_2$ . . . . .	43
3.3	Amplitude and phase of the diurnal currents during spring tide and neap tide conditions . . . . .	44
3.4	Variation of stratification and depth-mean flow at Besar . . . . .	45
3.5	Depth-mean values of $\sigma_t$ from quasi-synoptic CTD data . . . . .	46
3.6	Time-averaged vertical velocity profiles of cross-isobath and along-isobath current components at Besar . . . . .	47
3.7	Time-series based on moored data from Besar . . . . .	48
3.8	Time-series based on moored data from Kubur . . . . .	49
3.9	Time-series of the tidal elevation ( $\eta_{\text{harm}}$ ) in the Bay of Banten . . . . .	51
4.1	Variation of $U$ for $A_{K_1} = A_{M_2} = 1$ , $A_{O_1} = 1/2$ and $\phi_{K_1} = \phi_{O_1} = \phi_{M_2} = 0$ , which yields an asymmetrical periodic pattern . . . . .	55
4.2	Variation of $U$ , $a_1/a_2$ and $2\varphi_1 - \varphi_2$ over two spring-neap cycles . . . . .	56
4.3	Variation of $F_d$ as a function of $\Theta_d$ and $T_a$ . . . . .	61
4.4	Variation of $F_d$ as a function of $T_a$ . . . . .	62
4.5	Variation of $F_s$ as a function of $\Theta_s$ and $T_a$ . . . . .	63
4.6	Variation of $F_s$ as a function of $T_a$ . . . . .	63

4.7	Tidal regimes of the world, classified according to the tidal form factor $F = (A_{K_1} + A_{O_1})/(A_{M_2} + A_{S_2})$ . . . . .	65
5.1	Index map showing shoreline changes associated to the diversion of the Ciu-jung in the 1920's . . . . .	68
5.2	Surface current ellipses of the major diurnal and semidiurnal tidal constituents	69
5.3	Wind vectors and wave climatology for the western part of the Java Sea . . .	71
5.4	Wind frequency distribution and a time-averaged directional wave spectrum representing the wet season of 1998/1999 . . . . .	72
5.5	Turbidity variation at the abandoned delta front compared to hydrodynamic conditions at Utara . . . . .	73
5.6	Vector plot of surface current velocity at Utara, wind velocity at Bojonegara and the angular difference between current and wind vectors . . . . .	74
5.7	Coherence of the low-frequency flow in the Bay of Banten . . . . .	75
5.8	Interpretation of the depth-mean SSC variation in the former delta region at 8 m water depth . . . . .	77
5.9	Variation of depth-mean SSC and along-isobath flow at Kubur . . . . .	78
5.10	Asymmetrical tidal cycles induced by $K_1$ , $O_1$ and $M_2$ oscillation at Kubur and Besar . . . . .	79
6.1	Isolines of sound absorption in water . . . . .	87
6.2	Isolines of sound absorption due to sediment . . . . .	88
6.3	Location of the five experimental sites . . . . .	89
6.4	OBS calibration using <i>in situ</i> mass in water samples . . . . .	91
6.5	Calibration of the ADCP signal volume strength for the 20-day moorings at Besar and Kubur . . . . .	93
6.6	Time-series of ADCP and OBS estimates of suspended mass concentration and environmental variables at Besar . . . . .	94
6.7	Time-series of ADCP and OBS estimates of suspended mass concentration and environmental variables at Kubur . . . . .	95
6.8	Calibration of the ADCP signal volume strength for shipboard 25-hour measurements . . . . .	100
6.9	Quasi-synoptic spatial turbidity patterns at the reef slope of Kubur . . . . .	101
7.1	Bathymetry and tidal flow properties of the Bay of Banten . . . . .	106
7.2	OBS-derived SSC time series corrupted by algae growth . . . . .	107
7.3	Calibration of the ADCP backscatter intensity . . . . .	108
7.4	SSC variation at the reef slope of Besar, wave height and wave energy directional distribution at Utara and along-isobath flow velocity at the far-field station near Besar . . . . .	111
7.5	Quasi-synoptic spatial turbidity patterns at the reef slope of Pamujan Besar .	112
7.6	SSC spectra from OBS measurements at the reef slopes of Kubur and Pamujan Besar . . . . .	113
7.7	Horizontal flow affected by flow curvature and the high hydraulic roughness of the island fringe . . . . .	116
7.8	Depth-mean flow structure around Kubur . . . . .	117
7.9	Sedimentation in tube traps deployed at Kubur and Pamujan Besar, as a function of depth . . . . .	118

# Voorwoord / Foreword

## *In het Nederlands*

Het uitvoeren van een promotieonderzoek dat handelt over een tropisch gebied ergens aan de andere kant van de wereld heeft een fix aantal voordelen. Het grootste pluspunt is dat je veel op reis bent en inderdaad, ik heb daar erg veel plezier in gehad. Indonesië is zoals in de folders een exotisch paradijs en ik beschouw het als een voorrecht dat ik er een pioniersstudie heb mogen verrichten. Daarnaast ben ik ervan overtuigd dat het doen van onderzoek ver over de grens zeer bevorderlijk is voor de wetenschappelijke creativiteit. Ik hoop dat ik met dit proefschrift mensen ervan overtuig dat tropenstudies zoals die van mij niet slechts bijdragen aan de kennis van de regio waar het onderzoek heeft plaats gevonden. Onderzoek gefinancierd door de Stichting ter Bevordering van Onderzoek in de Tropen (WOTRO) kan daadwerkelijk een weerslag hebben op onderzoek dat zich richt op, laten we zeggen, een nogal fris gebied als de Noordzee. Ik bedank WOTRO en de Koninklijke Nederlandse Akademie van Wetenschappen (KNAW) voor de financiële ondersteuning.

In het veld heb ik veel hulp gehad van de andere onderzoekers binnen het Teluk Banten Onderzoeksprogramma, waarvoor ik hen bedank. Met name wil ik noemen Wawan Kiswara, Tiwi Dwi Abad, Siti Nuraini, Yus Rusila Noor, Budianto Ontowirjo, Nyoman Sukmantalya, Erik Meesters, Gert van den Bergh en Wim Douven. Erik heeft me veel bijgebracht over koraalriffen, en heeft mijn onderzoek sterk beïnvloed vanaf het prille begin. Ik heb met erg veel plezier met hem gewerkt. Het was ook plezierig werken met Gert van den Bergh, als partner tijdens vele scheepsmetingen. Gerts rijkelijke kennis van het Indonesisch heeft vele deuren voor me geopend. Wim bewonder ik zeer om het geduld waarmee hij de resultaten van ons onderzoek onder de mensen brengt bij lokale overheden.

Evenals deze collega-onderzoekers bedank ik de andere mensen waarmee ik in het veld heb samengewerkt, waaronder kapitein Dulah van het onderzoeksschip H3 en zijn bemanning, Dhr. Muhajir, Dhr. Pram, Fausi de bootsman, Firman en Tono. Met hen heb ik een meer dan plezierige tijd gehad. Marcel van Maarseveen en zijn collega's van het Fysisch Geografisch Laboratorium hebben een vitale rol gespeeld op technisch gebied. Vijf studenten hebben mij geholpen tijdens veldwerk: Bas van Maren, Daan Rijks, Mieke Steenbruggen, Andrew West en Mark Reinders. Later werd Bas mijn kamergenoot, hetgeen ik heb ervaren, en nog altijd ervaar, als een perfecte match. De voorzet die hij gaf voor het getij-asymmetrie verhaal zal ik niet vergeten.

Veel dank gericht aan mijn eerste promotor: Piet Hoekstra. Hij was een ideale begeleider aangezien hij me nooit een kant op duwde die ik zelf niet op wilde gaan. Alle middelen die ik me kon wensen stonden tot mijn beschikking en Piets commentaar

was altijd to-the-point, bondig en constructief. Zijn commentaar werd aangevuld door de meer poëtische opmerkingen van mijn tweede promotor, Joost Terwindt. Met zijn pensioen, samen met dat van Pieter Augustinus, komt er een einde aan een tijdperk van verhalen vertellende fysisch geografen. Het overige deel van de kustengroep wordt gevormd door Aart Kroon, Bart Grasmeijer, Irene van Enckevoort, Susanne Quartel, Pim van Santen, Nicolas Grunnet, Sandra Vermeer, Leo van Rijn, Gerben Ruessink en Maarten Kleinhans. Ik bedank hen voor de stimulerende werksfeer. Ik bedank ook een aantal oud-collega's, waaronder Hennie Schans, Klaas Houwman, Brigit Janssen-Stelder, Arjan de Boer en Willem van der Lee. Veel van de figuren in dit proefschrift zijn vervaardigd door het Kartlab. Met name Ton Markus heeft fantastisch werk geleverd in dit opzicht.

Graag zou ik mijn collega's van de vakgroep Fysische Oceanografie binnen het IMAU willen bedanken. Gesprekken met Huib de Swart en Johan van der Molen waren erg vruchtbaar. Ik bedank WL|Delft Hydraulics voor de toestemming om gebruik te maken van het Getijsys pakket en voor het aanleveren van altimeter data van getij-amplitudes. Ik betreur het feit dat uiteindelijk onvoldoende basis informatie aanwezig was om een hydrodynamisch model op te zetten met Delft3D. Ik ben David Johnson van de Universiteit van West Australië erkentelijk voor het mogen gebruiken van zijn software pakket waarmee richtingspectra van golven zijn te berekenen uit veldgegevens. Ik bedank Jan-Willem Mol en zijn collega's van Aquavision BV voor het commentaar dat zij hebben geleverd op het hoofdstuk over ADCP echo-intensiteit.

Als allerbelangrijkste bedank ik mijn vrienden, schoonfamilie en familie. Ik ben zeer dankbaar voor de ruggesteun van mijn ouders. De hoeveelheid energie die zij op hun leeftijd nog hebben geeft mij vertrouwen in mijn eigen capaciteiten. Mijn oudere zussen Petra en Conny hebben beiden in Wageningen gestudeerd, waar iedere student een wereldreiziger is. Hun reizen hebben mij zeer geïnspireerd. Ik heb veel te danken aan Irene; zij zorgde letterlijk voor een gespreid bed toen ik aankwam in Utrecht. En dan, eindelijk, bedank ik Linda, de ware liefde van mijn leven. Wat kan er ook gebeuren met een vrouw zoals jij aan mijn zij?

### *In English*

Doing a PhD study about some tropical place on the other side of the globe has a number of advantages. The foremost plus point is that you get to travel a lot and indeed, I really enjoyed the journeys. Indonesia truly is an exotic paradise and I see it as a privilege to do a pioneering study there. Moreover, I am convinced that doing research abroad promotes scientific creativity. With this thesis I hope I can convince people that the results of studies like mine are not merely to the benefit of the region where measurements were taken. Research funded by the Foundation for the Advancement of Tropical Research (WOTRO) can have a spin-off on other research that focusses on, let's say, the chilly North Sea. I thank WOTRO and the Royal Dutch Academy of Sciences (KNAW) for the financial support.

Out in the field I have received a lot of help of the other researchers in the Teluk Banten Research Programme. I would like to mention Wawan Kiswara, Tiwi Dwi Abad, Siti Nuraini, Yus Rusila Noor, Budianto Ontowirjo, Nyoman Sukmantalya, Erik Meesters, Gert van den Bergh and Wim Douven. Erik taught me all about coral

reefs, and he has had a strong influence on my work from the beginning. I really had a great time working with him. It was also pleasant to work with Gert, who was a partner on various ship cruises. Gert's skills concerning the Indonesian language have opened many doors. Wim I admire for his patience to retail the results of our research to local governments.

Besides these fellow-researchers, I thank captain Dulah from the RV H3 and his crew, Mr. Muhajir, Mr. Pram, Fausi the boatman, Firman and Tono. I have had a more than pleasant time with these people. Marcel van Maarseveen and his colleagues of the Physical Geographical Laboratory were vital for all their technical support. Five students assisted me with the daily things to do during fieldwork: Bas van Maren, Daan Rijks, Mieke Steenbruggen, Adrew West en Mark Reinders. Later on Bas became my roommate, which I have experienced, and still experience, as a perfect match. The assist he gave for the tidal asymmetry story I will not forget.

Many thanks to my first promotor, Piet Hoeksta. He was an ideal supervisor since I was never pushed into a direction I didn't want to go to. I was given all the opportunities a PhD student could wish and Piet's comments were always to-the-point, concise and constructive. These comments were supplemented with the more poetic remarks made by my second promotor, Joost Terwindt. His retirement, together with that of Pieter Augustinus, heralds the end of an era of story-telling physical geographers in Utrecht. The remainder of the coastal group includes Aart Kroon, Bart Grasmeyer, Irene van Enckevoort, Susanne Quartel, Pim van Santen, Nicolas Grunnet, Sandra Vermeer, Leo van Rijn, Gerben Ruessink en Maarten Kleinhans. I thank them for the pleasant atmosphere at work. I also thank ex-colleagues amongst whom are Hennie Schans, Klaas Houwman, Brigit Janssen-Stelder, Arjan de Boer and Willem van der Lee. Many of the graphics in this thesis have been prepared by Kartlab. In particular, Ton Markus has done a excellent job.

I would like to thank my colleagues of the Physical Oceanography Department within the IMAU. Meetings with Huib de Swart and Johan van der Molen have been very fruitful. Thanks to WL|Delft Hydraulics for permitting the use of Getijsys, and for providing me with the altimeter data on tidal elevations. I regret the fact that insufficient basic data was available to set up a hydrodynamic model using Delft3D. David Johnson of the University of Western Australia I acknowledge for giving me his toolbox to calculate directional wave spectra from field data. I thank Jan-Willem Mol and his colleagues from Aquavision BV for commenting on the chapter on ADCP echo-intensity.

Most importantly, I thank my friends, in-laws and family. I am very grateful for the support of my parents. The amount of energy they still have in their mid sixties gives me faith in my own capacities. Petra and Conny have studied in Wageningen, where every student is a world traveller. Their journeys have inspired me a lot. I owe a lot to Irene, who took good take of me when I arrived here in Utrecht. Then, finally, I thank Linda, the true love of my life. Nothing can happen with a woman like her on my side.

# 1

## General introduction

### 1.1 Problem definition

Coral reefs constitute a vital resource for tropical marine life. About half the world's coastline is situated in the tropics and about one third of the tropical coastlines are made of coral reef. The first order determinants of reef distribution at a global scale include temperature, salinity, light, nutrient concentration, and the saturation degree of aragonite, which is a carbonate mineral (Table. 1.1, adopted from Kleypas (1999)). Provided that those variables are favorable and hard substrate is present for settlement of larvae, coral reefs can be found in all shallow regions of tropical coastal waters, continental shelves and oceans. Tropical areas where reefs are virtually absent are West Africa, probably due to low temperatures during the Pleistocene and upwelling of cold deep water, the Gulfs of Bengal and Arabia, which may be associated to sediment influx from rivers, and the continental coast of South America, as a result of low temperatures caused by upwelling and of high runoff.

In spite of their ability to create the most massive structures in the world made by living creatures, coral reefs are particularly vulnerable to natural disturbances and the effects of human activities. Over the past century, tropical coastal areas have been subjected to increasing river discharges carrying freshwater and terrestrial sediment, which is associated with land degradation due to deforesting and channelling of river branches. Both increase and redistribution of river discharges may change the zoning of coastal areas where coral growth is potentially feasible, through modification of seawater salinity, siltation and water clarity. Moreover, altered buoyancy inputs disrupt the existing competition between mixing and stratification, which determines vertical nutrient exchange. Levels of turbidity and sedimentation in coral reef waters are in this respect amongst the most determinative factors (Hayward, 1982; Rogers, 1990; Hopley, 1994). In particular, fringing reefs and patch reefs near the coast are often affected by runoff of terrestrial sediment from catchments.

The biological consequences of increased water turbidity and sedimentation are numerous. Because the depth distribution of corals is largely limited by the ambient light regime, coral growth becomes restricted to shallow areas when clarity decreases (Hallock & Schlager, 1986). Physiologically, reduced solar irradiance affects the energy balance of the coral-symbiont association (Meesters et al., in prep). It should be mentioned that to some degree corals may adapt to lower irradiance by applying



**Table 1.1.** First-order determinants of global reef distribution, adopted from Kleypas (1999)

Variable	Reef limits	Temporal scale	Notes
Min. temperature [ $^{\circ}\text{C}$ ]	18	'annual minima'	see Coles & Fadlallah (1991) for a review
	18	'prolonged'	
	16	'short-term'	
	15	'few days exposure'	
	15-16	'long-term limit'	
	18	1-2 wk. cont. exposure	
Salinity [PSU]	11.5-14.0	2-30 days	Arabian Gulf
	25-42	continuous	see Coles & Jokiel (1992) for a review
	20	<1 day exposure	
Light [ $\mu\text{E m}^{-2} \text{ s}^{-1}$ ]	50-450		range of $I_k$ for individual corals; $I_k$ is a measure of coral adaptation to light (Chalker, 1981)
	30-40% of surface value	limits reefs	see Achituv & Dubinsky (1990)
	10% of surface value	limits corals	
Aragonite saturation $\Omega$ -arag	not established		function of $[\text{Ca}^{2+}]$ , $[\text{Ca}^{2-}]$ , temperature, salinity
Max. nutrients [ $\mu\text{mol liter}^{-1}$ ]	0.5-3.0 $\text{NO}_3?$		No limits established for $\text{NO}_3$ or $\text{PO}_4$ ; see Szmant (1997)
	0.1-1.2 $\text{PO}_4?$		

strategies collectively named photoadaptation, which encompass morphological, biochemical and physiological adaptations, and behavioral responses (Brown, 1997). The stresses that suspended sediments provoke are not all related to a decrease of light levels. Direct impacts regard the damage of the soft tissues of corals through abrasion by sediment particles and reduction of coral performance through excessive use of energy in activating sediment rejection mechanisms (Woolfe & Larcombe, 1999). Turbidity and increased sedimentation are also known to affect coral recruitment by decreasing the amount of substratum that is available for settlement of larvae (Babcock & Davies, 1991).

Despite decades of research on these issues, the effective resilience of coral reefs with regard to increased turbidity and sedimentation remains largely unknown. This is primarily due to the limited variety in environmental conditions that reef scientists have considered, as most reef studies have been carried out in relatively clear and undisturbed waters. Only recently, the focus of reef research has shifted towards reef behavior under turbid, or marginal conditions. Since reef development is to a large extent determined by 'hydromechanic' factors, progress in the biology of marginal reefs is largely dependent on knowledge of the physical oceanography in these regimes (Wolanski & Sarsenski, 1997). Tropical marine processes concerning freshwater effects, tidal motion and suspended sediment dynamics are in turn still poorly understood when compared to marine processes in temperate regions. Few studies have analyzed the mechanisms determining oceanographic variables of the relatively dynamic coral reef environments near the coast. To understand the impact of altered coastal characteristics on coral reef dynamics, increased knowledge is needed of the physical processes that govern the hydrodynamic and sedimentary regimes on and around coral reefs.

The present thesis aims to improve the understanding of (1) the physical mechanisms that govern the regional variability of vertical mixing, salinity, turbidity, and the supply of terrestrial sediment in marginal reef environments and (2) local sedimentary processes at reef slopes, determining turbidity levels and sedimentation.

## 1.2 Physical oceanography of coral reef systems

### 1.2.1 Introduction

Over the past century, the center of gravity of physical research of coral reefs has been located in the Great Barrier Reef, Australia. These studies have been well documented, and reviewed by Wiens (1962), Pickard et al. (1977) and Andrews & Pickard (1990). More recently, Massel (1999) has described physical marine processes from the perspective of marine ecologists and Wolanski (2001) focussed on the physics-biology links in the Great Barrier Reef. In the remainder of this section a brief overview is presented on a selection of physical processes that characterize coral reef environments.

### 1.2.2 Eddy formation

Reef islands in shallow coastal waters interact with the prevailing flows, which results in complex downstream currents. Wolanski et al. (1984a) proposed a model of the flow in the wake of coral reef islands, which captures the essential elements of the three-dimensional wake behavior in a substantial number of islands (cf. Pattiaratchi et al., 1986). The basic assumption in the model is the symmetric situation of two counter rotating eddies driven by the ambient currents (Fig. 1.1). At the base of the wake recirculation regions an Ekman benthic boundary layer exists, established by rotation in the wake and thus not by the earth's rotation. Focussing on a single eddy, vorticity is supposed to be introduced at the tip of the island, at the point of separation, which is to be cancelled by that generated at the bottom and so to disappear from the water column. A vorticity balance can be formulated as follows. The time scale  $T$  for the spin-down within the boundary layer due to Ekman pumping, is known from Ekman theory (Greenspan, 1968):

$$T = \frac{H}{\omega^{1/2} K_z^{1/2}} \quad (1.1)$$

where  $H$  denotes depth,  $\omega$  is the angular velocity within the eddy and  $K_z$  is the vertical eddy diffusivity. Since the vorticity contained in a cylinder of radius  $R$  is  $O(\omega R^2 H)$ , the flux of vorticity  $F$  from the core region is given by:

$$F = \frac{\omega R^2 H}{T} = \omega^{3/2} K_z^{1/2} R^2 \quad (1.2)$$

Assuming a linear velocity profile, the vorticity flux entering the region at the point of separation through the thin vertical turbulent boundary layer is  $O(HV^2)$ , where  $V$  is the azimuthal horizontal velocity. A vorticity balance then yields an expression for the length scale of the eddy:

$$R = \frac{H^{1/2} V}{\omega^{3/4} K_z^{1/4}} \quad (1.3)$$

Conservation of mass requires  $V \simeq U \simeq \omega R$  (Greenspan, 1968), where  $U$  is the free stream velocity, and thus Eq. 1.3 reduces to:

$$R = \frac{H^2 U}{K_z} \quad (1.4)$$

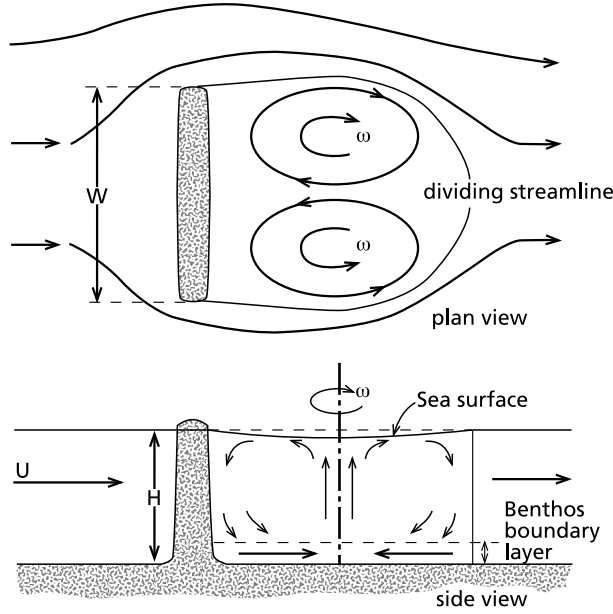


**Figure 1.1.** Sketch of the internal circulation in an island wake in shallow coastal waters. The vertical scale is exaggerated, as typically depths are less than 40 m, whereas horizontal scales are of the order of 1 km. The governing parameters determining the characteristics of an island wake are the free stream velocity ( $U$ ), the water depth ( $H$ ), and the island width  $W$ . After Wolanski & Hamner (1988)

The ratio of  $R$  and the island width  $W$  is known as the 'island wake parameter'  $P$ , which reads:

$$P = \frac{H^2 U}{W K_z} \quad (1.5)$$

For  $P \ll 1$ , friction dominates and quasi-potential flow is expected; a stable wake is characterized by  $P \simeq 1$  and when  $P \gg 1$  the wake becomes unsteady, shedding vortices as in a Karman vortex street (e.g. Ingram & Chu, 1987).

A force balance associated to Wolanski's model yields details of the secondary flow within the eddy (Fig. 1.1). The slope of the surface of the eddy, which is upward from the eddy center, generates a pressure gradient that is in equilibrium with the centrifugal acceleration. This balance cannot hold near the bottom because friction decreases the azimuthal velocity, whereas the radial pressure gradient is maintained everywhere throughout the eddy, including the bottom. As a result, water that is near the bottom flows radially toward the eddy center, which induces upwelling near the eddy center and downwelling near the outer edges. This secondary circulation affects sediment transport and distribution. Fine, clay-sized sediment is carried to the surface near the eddy center. From there, the sediment-enriched water spirals out from the eddy center because the waters have a radial velocity. High turbidity of surface waters in island wakes has been illustrated by many authors, using remote sensing images (Pattiaratchi et al., 1986; Ingram & Chu, 1987; Tomczak, 1988; Tseng, 2002).

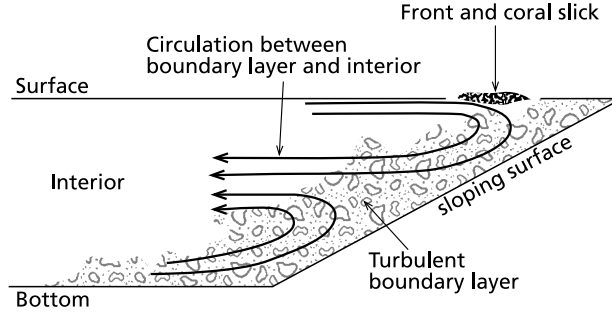


**Figure 1.2.** Sketch of an internal circulation that is generated by boundary mixing in a stratified flow along a reef slope. After Wolanski & Hamner (1988)

### 1.2.3 Mixing and stratification effects

Barrier reefs on the outer edge of continental shelves are known to be affected by stratification of the ocean they face. Thompson & Golding (1981) and later Thompson & Wolanski (1984) introduced a mechanism referred to as tidal suction (or Bernoulli suction), which results in upwelling of nutrients from below the thermocline. During rising tide, flood currents accelerate through narrow reef passages at the outer edge of the barrier reef, pulling relatively cold, saline, negatively buoyant water across the reef slopes upwards. During the ebb, the outflow is relatively warm and of low salinity, and concentrates near the surface due to its buoyancy. Hence, over the time span of a tidal cycle residual upwelling occurs. This mechanism may be relevant to the sedimentary regime of nearshore reefs, where stratification prevails. However, the strength of vertical currents along the slopes of shallow-water reef passages is generally weak compared to these at the shelf break.

Another residual effect of density stratification occurs in case of a stratified flow along a rugged reef slope, which generates a secondary current (Fig. 1.2). The secondary circulation results from boundary mixing, which produces a net downward buoyancy flux implying an upward salt flux in case of salinity stratification. The residual effect is a flow towards the solid boundary both near the surface and near the bottom and with a flow away from the boundary in between. The latter intermediate flow, which intrudes from the boundary layer into the ambient fluid, is largest at the depth of the maximum vertical density gradient (Fig. 1.2). Within the boundary layer, the flow converges somewhere at mid-depth. Phillips et al. (1986) developed a theory which yields an expression for the associated buoyancy flux  $F_B$ , which reads:

$$F_B = 0.60 \left( \frac{\nu_e N}{\sin \theta} \right)^{\frac{3}{2}} \cos^2 \theta \quad (1.6)$$

and for the 'intrusion' velocity  $v_I$ , corresponding to the current that recedes from the reef, which was found to be:

$$v_I = 0.42 \frac{\nu_e^{\frac{3}{2}} \cos^2 \theta}{N^{\frac{1}{2}} h^2 (\sin \theta)^{\frac{3}{2}}} \quad (1.7)$$

where  $N$  is the ambient stability frequency, reflecting the degree of stratification,  $\nu_e$  is the eddy viscosity,  $\theta$  is the angle of the sloping bed and  $h$  is the half-thickness of

the pycnocline. Herein,  $h$  is defined as:

$$h^{-1} = 2 \left( \frac{\partial \rho}{\partial z} \right)_{max} / \Delta \rho \quad (1.8)$$

where  $\rho$  denotes density and  $N$  is defined as:

$$N = \sqrt{\frac{g}{\rho} \frac{d\rho}{dz}} \quad (1.9)$$

Equation 1.7 was derived in a tank with a stratification level of  $N=3.5 \text{ s}^{-1}$ . Wolanski & Hamner (1988) hypothesize that the theory by Phillips et al. (1986) explains why floating coral eggs accumulate in a lagoon on a line parallel to the trend of the coral reef when wind is light or calm. The coral slick would be situated at the front that divides the boundary layer and the transverse surface current.

#### 1.2.4 Drift currents

Although interaction with tidal currents may complicate spatial and temporal patterns of drift currents, wind-driven flow in the tropics is often very regular due to clear cycles of monsoons and trade winds. In general, the coastal currents dominated by friction follow the seasonal wind direction closely (Andrews & Pickard, 1990), albeit with a time lag. The persisting wind stresses may be capable of generating quasi-steady flows with velocities as large as 30 cm/s (Wolanski & Pickard, 1985). Due to bathymetric influences, the flow response to a certain wind stress may vary with the wind direction. This applies especially near the coast, where the wind-driven currents are forced to run largely alongshore. Despite the low-latitude, the earth's rotation produces Ekman circulation in the tropics as in temperate regions. Merely within the narrow range between 2° Southern Latitude to 2° Northern Latitude, Coriolis effects are expected to be absent (W.P.M. de Ruijter, pers. comm.).

The turbulence generated by the interaction of coastal flows with irregular coral formations may affect large-scale circulations on the continental shelf. Wolanski & Spagnol (2000) introduced the term 'sticky waters' to address the stagnation of drift currents in a juxtaposition of coral reefs. The stagnation resulted from high levels of turbulence induced by tidal flow through an alignment of reef islands, which steers the prevailing low-frequency flow away from the reefs. Consequently, local residence times may be much larger than what may be expected from large-scale circulation rates. Tidally-averaged levels of turbulence depend on variation in the tidal current amplitude, and therefore often exhibit a pronounced spring-neap cycle. During neap tide, the low-frequency flow may be admitted to the reef passages, whereas the high levels of turbulence during spring tide block the low-frequency flow.

#### 1.2.5 Waves

A comprehensive description of wave behavior at coral reefs has been presented by Massel (1996). Obviously, the irregular, semi-vegetated beds, the complex topographies and the steep slopes of the reefs provide a challenge for wave modelers. The one-

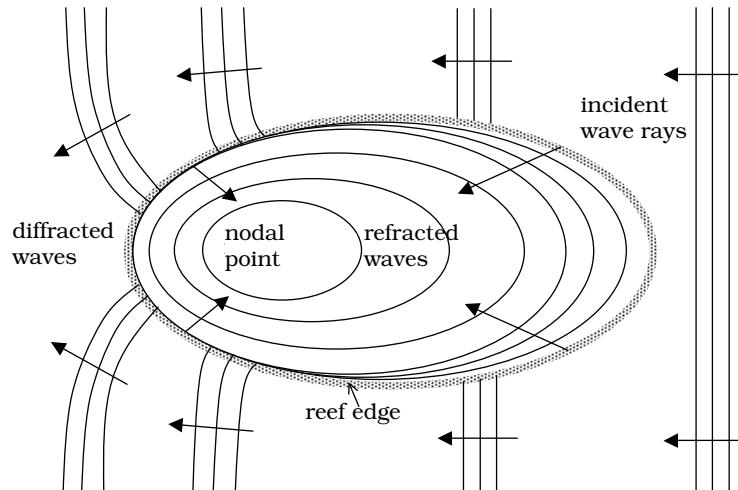


**Figure 1.3.** Wave transformation at coral reef slopes associated to coral cay formation; incident waves refract at the steep reef slopes and diffract at the lee of the island

dimensional wave propagation model by Massel (1993) assists the analysis of refraction, diffraction, reflection and dissipation at the reefs, using an extended mild-slope equation. The model requires calibration of a friction factor, a breaking coefficient and a coefficient of breaking waves recovery. Some general aspects of wave transformation at reef slopes have been shown to agree with observations, documented by Gourlay (1994). Steeper waves start to break early, at distance from the shallow reef edge, and their breaking intensity is higher than that of smaller waves. Waves of low steepness lose their stability closer to the reef edge and dissipate energy mostly on the reef platform, where water depth is in the order of 2 m. Since the tide modulates the water depth at the reef platform, it has a significant control on wave properties at the reef platform.

On top of the reef platform, wave-induced transport of coarse sediments at coral reefs, such as coral rubble, is evident from the Holocene sedimentary land forms known as coral cays (Gourlay, 1988). Coral rubble becomes easily transported by waves due to the relatively low density ( $\pm 2500 \text{ kg/m}^3$ ), high porosity (often in the order of 0.5-0.65) and large size. Located at the lee side of the reef platform, with respect to the predominant wind direction, at the nodal point where waves are focussed by refraction and diffraction an accretionary area of coral remnants may develop (Fig. 1.3, after Massel, 1999). Incident waves are refracted at the steep reef edges and diffracted at the lee side of the island. Broken waves partially continue to propagate over the reef slope. In many instances, coral cays become forested or vegetated by mangroves. The implications of wave transformation and breaking at the steep reef slopes on the resuspension of fine sediments are largely unexplored. Clearly, wave action is largest at the surface, which may be associated with a large capacity to mobilize sediments. But then again, at the reef crest coral cover is high which enhances bottom stresses and retains sediments. The intensity of coral growth gradually decreases towards the reef toe, where the bottom consists of a mixture of shoreface sediments and coral remnants, which tend to roll down slope.

## 1.3 Objectives and thesis outline

The present thesis aims to increase the understanding of regional and local physical mechanisms controlling the physical characteristics determinative to coral development near the coast. Field data were gathered within the framework of the Teluk Banten Research Programme, which is a Indonesian-Dutch research programme focussing on the social-economy, biology, geology and physical oceanography of to the Bay of Banten, Indonesia. The Teluk Banten Research Program is part of the Global Change Program of the Royal Netherlands Academy of Sciences (KNAW), and coordinated by the Foundation for the Advancement of Tropical Research (WOTRO).

The Bay of Banten provides an example of a shallow-water tidal embayment, harboring over ten coral reef islands, which is outlined in Chapter 2. The objectives and research questions of the five subsequent chapters are successively presented below.

### **Chapter 3: Identify the mechanisms controlling mixing and stratification as a product of buoyancy input, tidal forcing and wind-driven circulation.**

- Which are the main buoyancy sources to the region?
- How may the bottom boundary layer be characterized?
- Which are the mechanisms determining water column stability?
- Are there topographic controls on mixing and stratification?

### **Chapter 4: Characterize the asymmetry of tidal currents in diurnal regimes and quantify the associated residual transport of sediment.**

- Which are the causes of tidal velocity asymmetry in diurnal systems?
- Do tidal currents in these regimes feature persistent asymmetric patterns?
- Which are the implications for bedload and suspended load transport?
- How does tidal asymmetry in diurnal regimes compare to semidiurnal regimes?

### **Chapter 5: Identify the hydrodynamic controls on the supply of terrigenous sediment to coral reefs near the coast**

- Are near-coastal coral reefs directly exposed to inundation by river plumes?
- Which are the main hydrodynamic mechanisms causing the distribution of river discharges?
- May reworked deltaic sediments be transported towards coral reef localities?
- Can a zoning be distinguished regarding the areas where coral growth is potentially feasible?

### **Chapter 6: Reveal spatial patterns of turbidity in ambient reef waters using acoustic backscatter**

- How can acoustic backscatter be used as a measure of suspended sediment concentration?
- Which are the limiting factors when using this measure to render turbidity patterns in ambient reef waters?

**Chapter 7: Determine the hydrodynamic mechanisms controlling turbidity variation in ambient reef waters and establish the implications for reef development**

- What is the relative importance of local resuspension, when compared to regional advection?
- Do either waves or currents dominate local resuspension at reef fringes?
- Does the formation and evanescence of eddies play an eminent role in turbidity variation in ambient reef waters?
- Are ambient reef waters subject to upwelling or downwelling and if so, which are the driving mechanisms?
- Which are the sedimentary processes most determinative for reef development?

Each of the chapters 3 through 7 may be read independent of the remainder of the thesis, and has the format of a scientific paper. Especially chapters 4 and 6 serve a wider goal than the objectives formulated above. Chapter 4 addresses the asymmetry associated with astronomical tidal constituents in general, and analyzes the implications for residual sediment transport. The theory developed in Chapter 4 is applied in Chapter 5, which discusses the tidal asymmetry in the Bay of Banten. Chapter 6 presents a general analysis on the observation of fine-grained suspended sediment by combining the capabilities of an acoustic and a optical device, using the Bay of Banten merely as an example. By adopting the methodology expounded in Chapter 6, Chapter 7 analyzes turbidity patterns in ambient reef water. Chapter 8 concludes this thesis by synthesizing the main results.



# 2

## Field site

### 2.1 Introduction

The Indonesian Seas are biologically amongst the most productive and diverse reservoirs in the world (Fig. 2.1). Throughout the archipelago, 80 genera of corals can be found, covering a total area of approximately 87,700 km<sup>2</sup> (Tomascik et al., 1997). An important part of these reefs is scattered throughout the shallow and turbid continental seas of the Indonesian Archipelago, such as the Java Sea, the Natuna Sea and the Arafura Sea. Water clarity in these seas is low when compared to the oceanic waters of the Banda and the Flores Seas. Particularly in the coastal areas of Java, intensive surface runoff and changing land use in the coastal zone involve relative high levels of turbidity.

Teluk Banten (teluk means bay) consists of a semi-circular body of water where a number of small-scale rivers and canals from shrimp ponds debouch (Fig. 2.2). More than ten islands can be found in the bay, some of which are submerged, accommodating coral and coral reefs. The eastern flank of the bay is enclosed by the abandoned delta of the Ciujung (ci means river). In the beginning of the 1920's, the Ciujung river flow was diverted by a short-cut canal with a northeastern orientation towards the Java Sea. From that time, the abandoned delta has been subject to reworking while a new delta of elongate type was formed. This is illustrated in Fig. 2.2, where the coastlines of 1885, 1970 and 1995 are depicted, based on an old topographic map and aerial photographs. Two of the former distributaries of the Ciujung are still active, although they are disconnected from the present-day Ciujung river flow. The joint discharge of the Ciujung and Cidurian generally ranges between 20 and 220 m<sup>3</sup>/s, depending on the season. The rivers Banten, Anyer, Poncang (Fig. 2.2) currently have small discharges that we estimate between 1 and 10 m<sup>3</sup>/s each.

A low-lying coastal mud plain forms the southern boundary of the bay. The abundant sediment supply caused by retrogression of the old delta has led to accretion at the neighboring shorelines south of the former delta, which resulted in the formation of two tombolas that connect the two Pulau Dua islands to the coast. The last of the Pulau Dua islands has coalesced to the shore around 1980, to the detriment of coral reefs and their associated biota. Sedimentation of coarse coralline sand and gravel occurs at the exposed parts of the Pulau Dua tombolas and fine non-coralline sediments were deposited at shorelines relatively close to the tombolas.

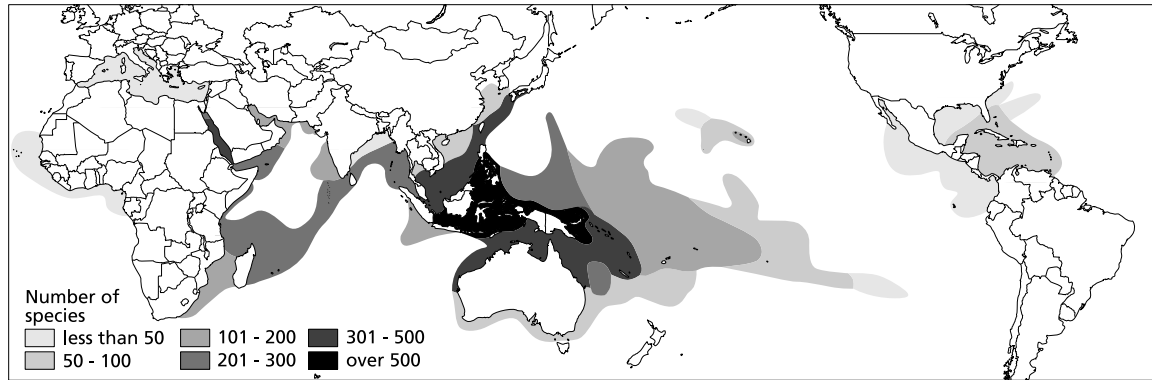


**Figure 2.1.** Patterns of diversity in reef-building scleractinian corals. The Indonesian Seas are the most diverse coral reef reservoirs in the world. Numbers in the legend indicate the number of coral species. After Spalding et al. (2001).

A circa 600 m high inactive volcano separates the western coast of the bay from the Strait Sunda. Industrial developments greatly impact the coast in this area, which is obvious from the presence of two expanding harbors, viz. Tanjung Awuran and Tanjung Kopo (Fig. 2.2). At the mid-western flank of Teluk Banten, a relatively large area of sea grass fields is located. Further southward, shorelines are characterized by an array of cross-shore bamboo structures to provoke land reclamation.

The present bathymetry of the bay is shown in Fig. 2.3. Depths gradually increase towards the northern margin, where the former late Pleistocene-Holocene coastline can be distinguished in between the 12 and 20 m isobaths. A north-west directed gully north of Panjang Island can be interpreted as a former river valley. The trenches at the south-western and south-eastern flanks of the bay are due to scour and reach a maximum depth of 20 m and 12 m, respectively. Scour trenches are also located north, and south east of Pamujan Besar Islands, revealing the principal direction of tidal currents.

All the islands in the bay, including the Pulau Dua tombolas, are low lying and are formed and classified as patch reefs. On most of the islands, cays of coral rubble have developed, hemmed by spits and cusped land forms. Patch reefs are generally found in the lagoons of barrier reef systems, but in the Indonesian Archipelago exceptions are numerous. In these instances, they develop on shallow shelves at varying distances from the shore where bathymetric highs are present. A well-studied patch reef complex is Kepulauan Seribu (Thousand Islands) (Tomascik et al., 1997), located northwest of Jakarta on top of the Seribu High, which is geologically considered to be a broad, shallow-water back-arc basin (Jordan et al., 1993). Patch reefs in Teluk Banten are similarly founded upon topographic paleo-highs of the Sunda Shelf.

In the following section, the marine geology of the Bay of Banten is further described. Subsequently, the boundary conditions of the embayment are presented, addressing the tidal behavior of the Java Sea (Section 2.3), the wind and wave climate of the Southwestern Java Sea (Section 2.4) and seasonal patterns of sea surface topography in the Java Sea and the Strait Sunda (Section 2.5). In the final section, some concluding remarks are made (Section 2.6).

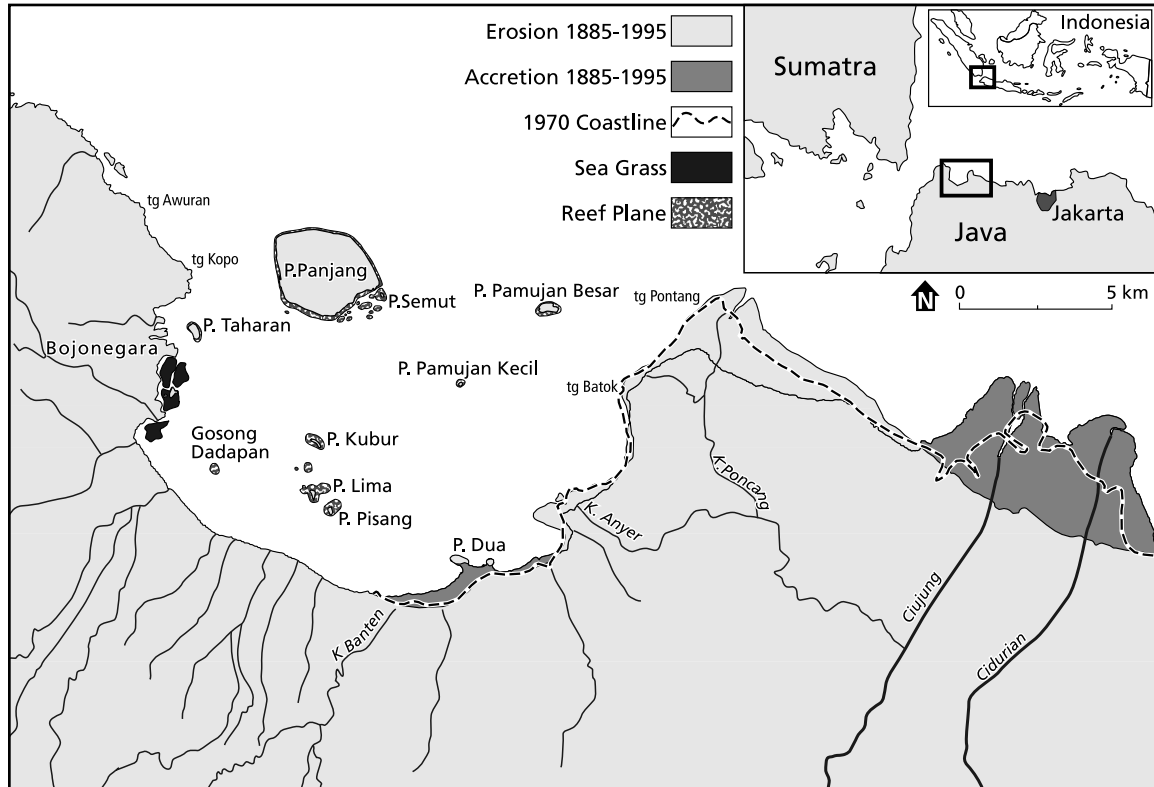


**Figure 2.2.** Coastline changes in the Bay of Banten over the past century, showing accretion and retrogression of the coastline, coalescence of the Pulau Islands with the present-day location of seagrass fields and coral reefs.

## 2.2 Marine geology of the Bay of Banten

An elaborate description of the Holocene depositional history of the Bay of Banten is given by Van den Bergh et al. (in prep a, b). They used seismic, sedimentological and geochronological methods to infer the origin and composition of marine sediments, and to determine sedimentation rates and historical sealevel changes. The present section briefly summarizes these results, successively focussing on the geological setting of the coral reefs in the bay, recent sedimentation rates and sediment composition.

The transgression of the bay's coastlines culminated during the Mid-Holocene, to a level that reached at least 2 m above present-day sealevel. The elevated sealevel lasted from about 6.5 ky until 5.0 ky BP, after which a shallowing of the area took place. During the period of high sealevel, deposition of fine-grained sediments appeared to have been mainly located in the southern bay area. The onset of coral reef formation started at about the same time on upwards protruding Pleistocene basement areas and on coarse substrates available in the transgressive fills of Pleistocene river valleys. The incipient reefs located on these valley fills were subsequently overrun by northwards prograding muddy sediments. During the following regressive phase, the remaining coral reefs became emerged to form the present-day islands in the bay.

The shallowing of the area at the stage of sealevel decline caused submarine erosion in the southern bay area, leading to the formation of sandy lag deposits and a shift of deposition in an offshore direction. In more recent times, mud accumulation has

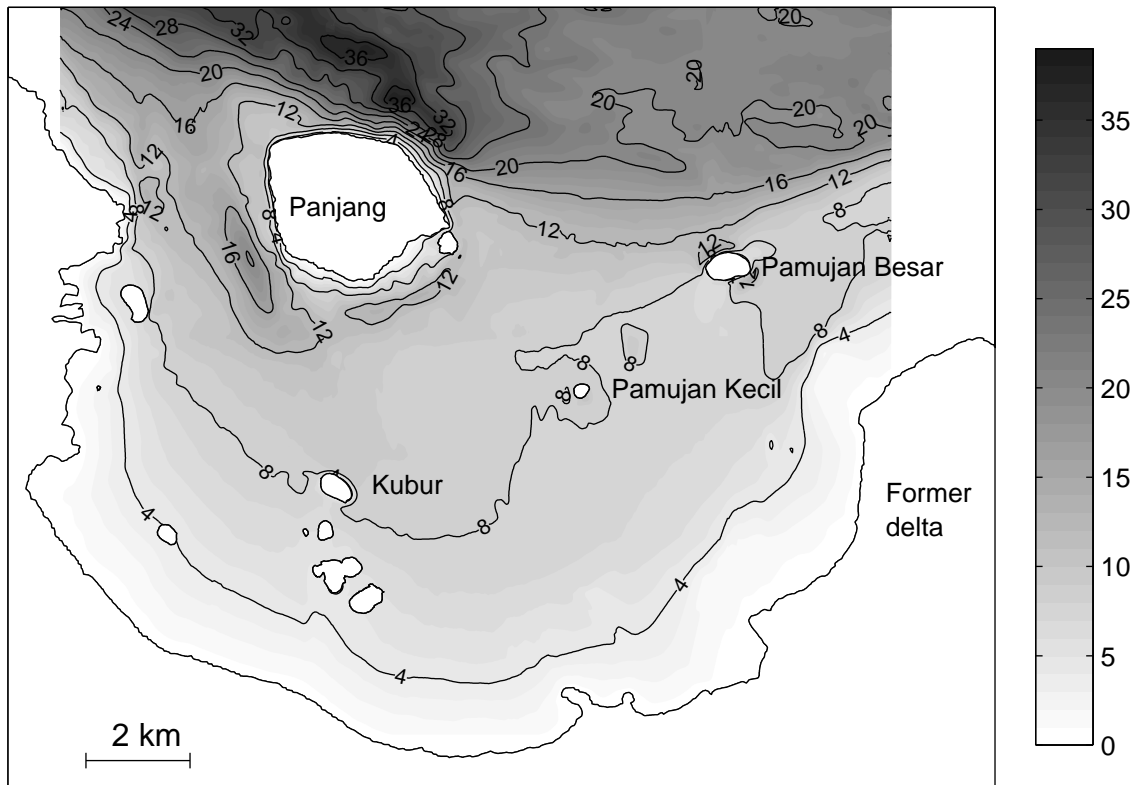


**Figure 2.3.** Bathymetry of the Bay of Banten. See Fig. 2.2 for location.

restarted even in the coastal regions, albeit at a slow rate, which continued until the redirection and canalization of the Ciujung River in the 1920's. The latter stage was shortly interrupted by the eruption of the Krakatau in 1883, which has led to the formation of a coarse-grained tsunami deposit. Fig. 2.4 demonstrates the current situation, based on a combination of results of a  $^{210}\text{Pb}$  analysis and assessment of the depth of the Krakatau layer. The shallow eastern part of the bay is subject to erosion, whereas deposition occurs in the remainder of the bay. Most of the muddy sediment accumulates on the sloping sea bottom facing the Java Sea, which marks the northwards prograding nature of the coastal system.

The bottom sediments in the bay are a mixture of fine-grained clays and clayey silts, containing variable amounts of shell material. Along the steeply sloping northern margin, muddy sediments extend to a depth of around 20 m, where the floreslope of the Holocene sediment wedge merges with the Java Sea bottom. Analysis of sediment samples taken at 2.5 cm below the bed surface throughout the bay yielded an average median grain size of  $15\ \mu\text{m}$ . Larger median grain sizes around  $23\ \mu\text{m}$  were encountered in the eastern area of the embayment, whereas sediments near the southern shoreline were found to be slightly finer than the average. In the western part of the bay, the bottom samples contained substantial amounts of faecal pellets, causing a peak in the particle size distribution at approximately  $100\ \mu\text{m}$ . These large amounts of faecal pellets are an indicator of fish abundance. In the vicinity of the coral islands the superficial mud contains a relatively high amount of carbonate sand, which is derived

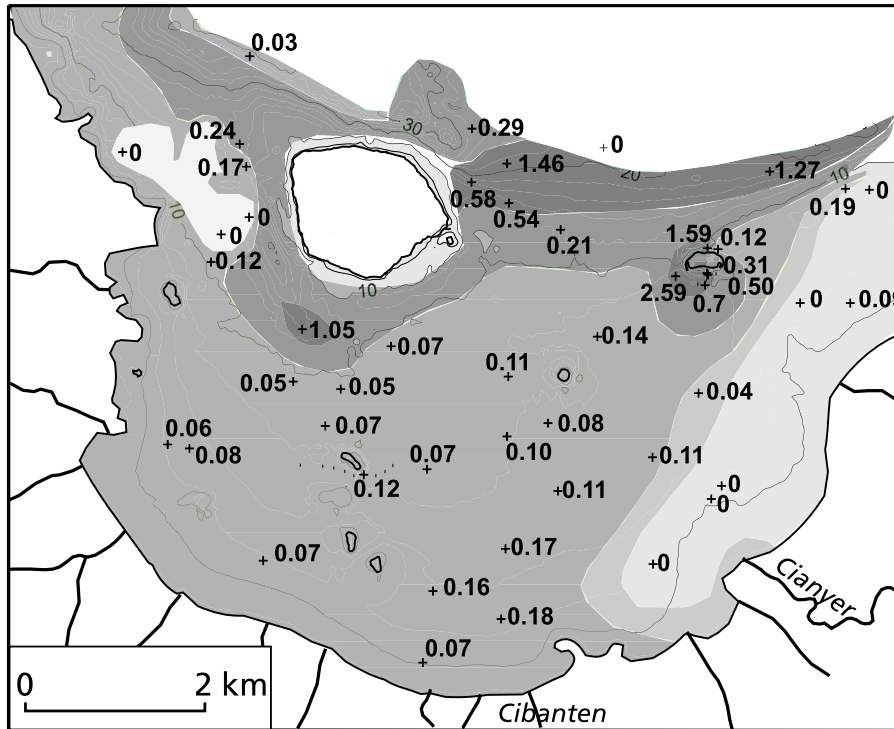


**Figure 2.4.** Recent accumulation rates in Teluk Banten in  $\text{g cm}^{-2} \text{ yr}^{-1}$ , based on  $^{210}\text{Pb}$  analysis and assessment of the depth of the 1883 Krakatau layer. Adapted from Van den Bergh et al. (2001)

from coral debris. Disregarding faecal pellets and coral remnants, bottom sediment in the bay can be regarded relatively homogenous.

## 2.3 Tidal dynamics of the Java Sea

Tides in the Bay of Banten are driven by the tidal motion in the southwesterly Java Sea. A comprehensive analysis of the tidal dynamics of the Java Sea is provided by Ali (1992). He used over thirty long-term tidal observational stations to construct co-phase and co-amplitude charts of the four principal tidal constituents, viz.  $M_2$ ,  $S_2$ ,  $K_1$  and  $O_1$ . In addition, a hydrodynamical numerical model was applied to reveal more kinematic information than possible on the basis of coastal observations only. In particular, the locations of amphidromic systems were determined. The model consists of an implementation of the depth-integrated equations of continuity and motion on a rectangular, spherical grid, containing advective, frictional, Coriolis and horizontal transport terms. A finite difference technique was adopted to solve these equations, using a procedure paralleling that of Mitchell et al. (1984). The following numerical properties and physical assumptions were applied.

- The grid resolution amounts to one sixth degree in both the latitudinal and the longitudinal direction.
- A Boussinesq approximation is applied, which assumes well-mixed conditions and a uniform density of sea water.

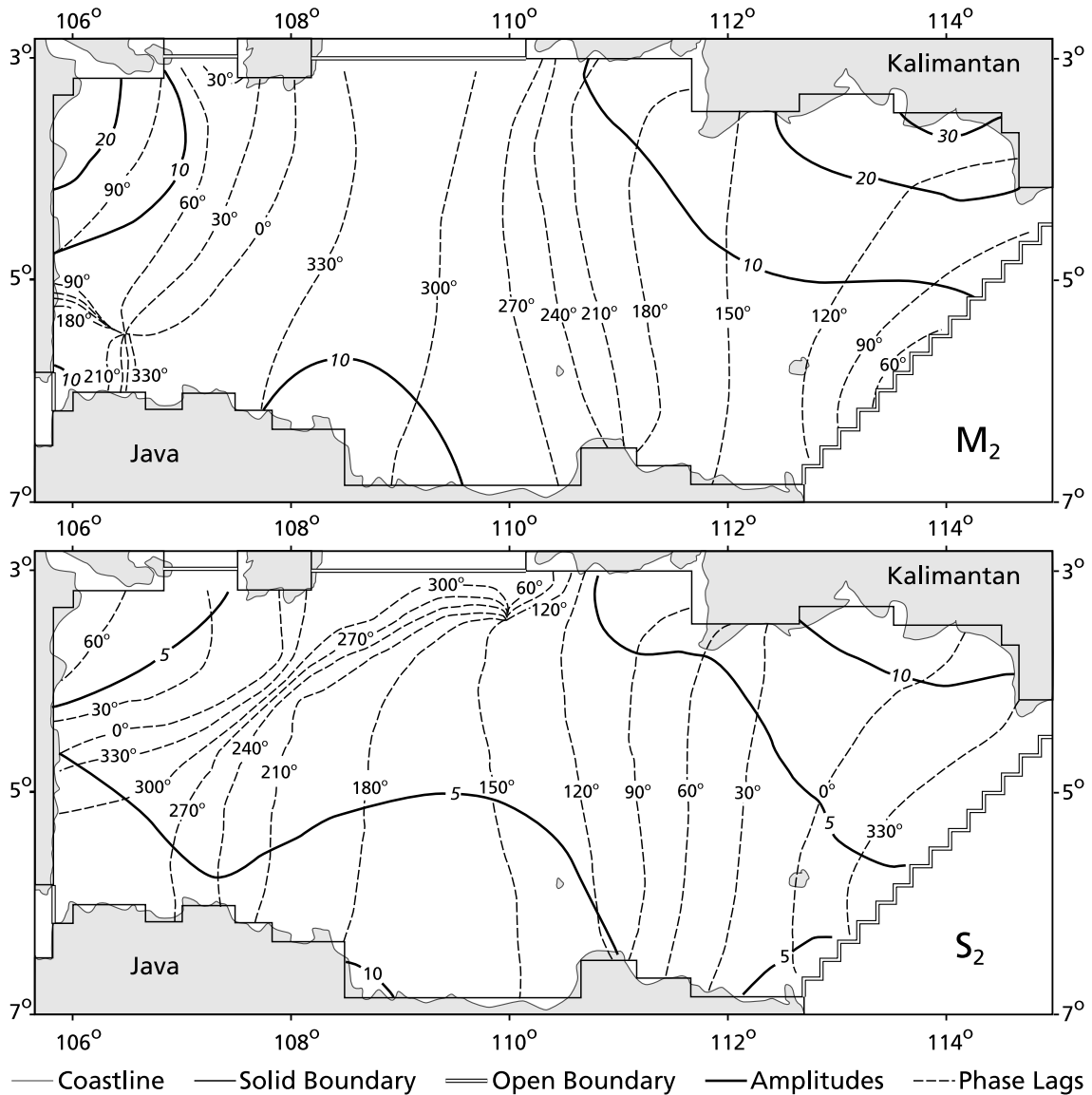
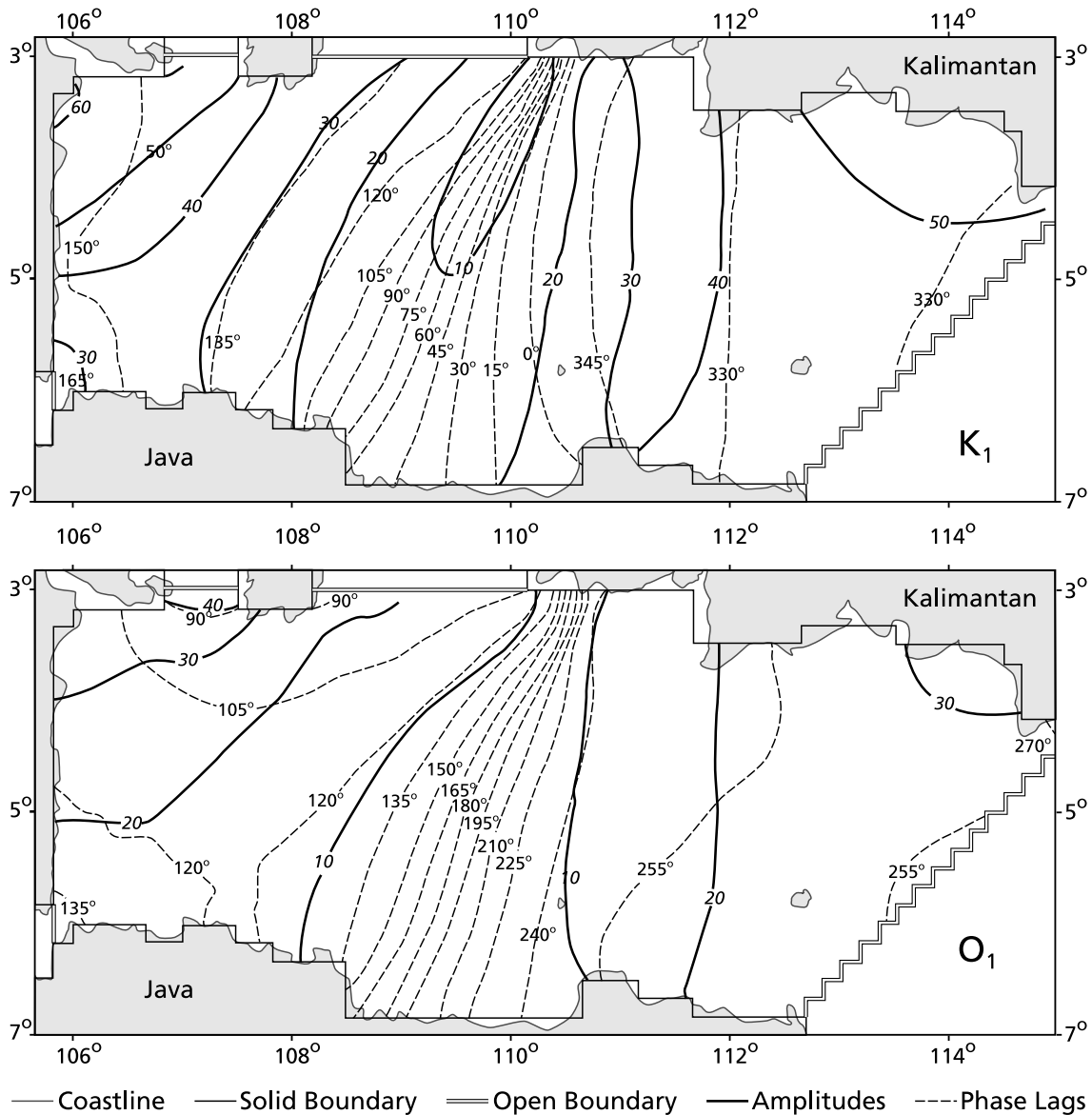


Figure 2.5. Co-tidal charts of the semidiurnal tides  $M_2$  and  $S_2$  in the Java Sea, after Ali (1992).

- The pressure term is assumed to be hydrostatic and air pressure is taken to be uniform for the entire modelled region.
- Horizontal stress gradients are neglected, and bottom frictional terms are given by a quadratic law with constant drag coefficients.
- A no-slip condition is applied at the sea bed and at the sides of the model.
- The calibration parameters, viz. the kinematic eddy viscosity  $A$  and the non-dimensional bottom drag coefficient  $C_d$ , were finally set to  $55 \text{ m}^2/\text{s}$  and  $0.003$ , respectively.
- The tide generating potential terms for the equilibrium tide were not incorporated in the equations of motion.



**Figure 2.6.** Co-tidal charts of the diurnal tides  $K_1$  and  $O_1$  in the Java Sea, after Ali (1992).

The co-tidal charts, derived from the modelling results by Ali (1992), are depicted in Figs. 2.6 and 2.5. The average discrepancies between the modelled and observed phase lags and amplitudes were  $8.87^\circ$  and  $2.73$  cm for the semi-diurnal tides and  $6.37^\circ$  in phase lag and  $3.68$  cm in amplitude for the diurnal tides. Hence, the modelling results showed a good agreement with the observations.

The dominant characteristic of the semidiurnal tides is a complex mix of progressive and co-oscillating wave components (Fig. 2.5). Near the western, northern and southern boundaries, representing the East Coast of Sumatra, the South Coast of Kalimantan and the North Coast of Java, respectively, reflection is apparent from the increase of amplitudes and the standing character of the  $M_2$  and  $S_2$  tidal waves. Further away from the reflective coasts, the semidiurnal tidal waves become more progressive in a west to northwesterly direction, towards the South China Sea. The

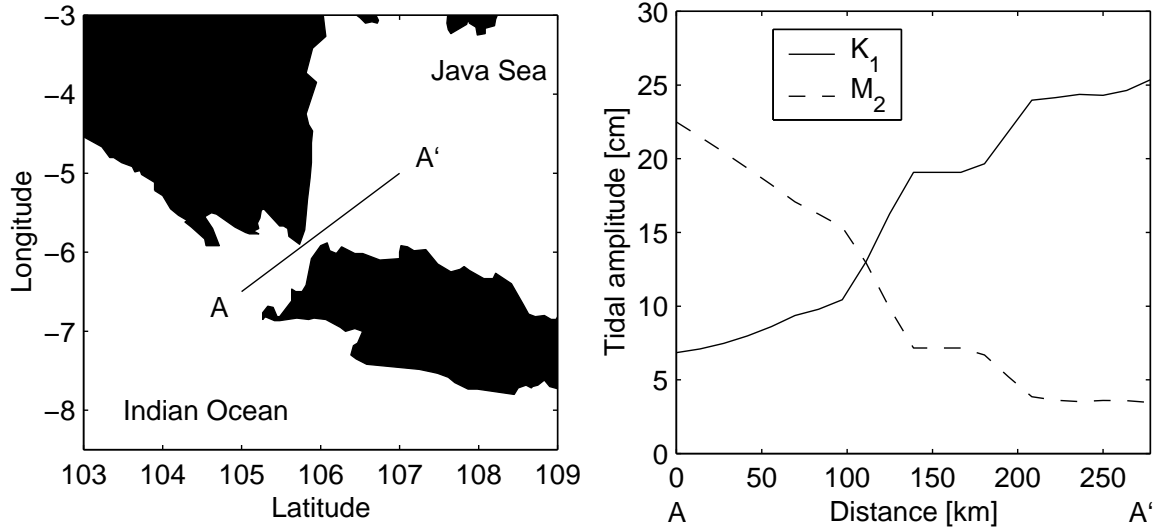


**Figure 2.7.** Tidal amplitude change in the Strait Sunda, where diurnal tides amplify and semi-diurnal tides attenuate towards the Java Sea. Based on altimeter data described by Schrama & Ray (1994)

amphidromic system of  $M_2$  in the western part of the Java Sea has an unusual progression, which does not conform to the Kelvin wave concept. Alternatively, it is associated to the superposition of the incoming wave from the Flores Sea, which is reflected at the western boundary, and the incoming wave from the Indian Ocean, travelling through the Strait Sunda. As a result, the  $M_2$  co-tidal lines are crowded near Teluk Banten. Theoretically, co-tidal charts for constituents with approximately the same angular frequency are supposed to be similar (Howarth & Pugh, 1983). Nevertheless, a slight inconsistency can be observed between the  $M_2$  and  $S_2$  co-tidal charts, which is attributed to the presence of radiational inputs in the observed  $S_2$  tide and a difference in response of the  $M_2$  and  $S_2$  tides to frictional dissipative effects. Consequently, the  $S_2$  tide has an amphidromic system near the southwesterly coast of Kalimantan and in the Strait Sunda, the  $S_2$  tide propagates towards the Indian Ocean.

The co-tidal charts of the diurnal tides clearly show that the conditions necessary for resonance are to an appreciable degree fulfilled (Fig. 2.6). The crowding of the lines of equal phase lag and the decrease of amplitude in the central part of the Java Sea suggest the presence of a node. A standing wave with a node in the central part and antinodes at the ends of the basin has a wave period that satisfies Merian's equation (Defant, 1961), which reads:

$$T = \frac{2L}{\sqrt{gH}} \quad (2.1)$$

- T = wave period (s)
- L = length of the basin (m)
- g = gravity acceleration ( $\text{m/s}^2$ )
- H = depth of the basin (m)



**Table 2.1.** Tidal amplitude (H) and Greenwich phase lag relative to UTC (g) for selected tidal constituents with amplitudes exceeding 1 cm; for shallow water tides equivalent angular speeds have been indicated. The tidal gauge was located at the reef slope of Pamujan Besar (Fig. 2.2).

Constituent	$\sigma$ ( $^{\circ}/hour$ )	Equivalent angular speed	$H$ (cm)	$g$ ( $^{\circ}$ )
$Q_1$	13.398661		3.0	133.0
$O_1$	13.943036		9.9	149.2
$M_1$	14.496694		1.5	151.0
$\chi_1$	14.569548		1.0	139.2
$P_1$	14.958931		5.6	161.9
$K_1$	15.041069		20.7	162.1
$KP_1$ *	15.123206	$2K_1 - P_1$	1.2	171.4
$J_1$	15.585443		1.7	217.8
$OO_1$	16.139102		1.9	223.2
$2MS_2$ *	27.968208	$2M_2 - S_2$	1.3	193.6
$M_2$	28.984104		5.5	220.8
$S_2$	30.000000		9.1	305.1
$K_2$	30.082137		3.3	296.0

\* also contain a significant gravitational component ( $KP_1 \equiv \phi_1$ ;  $2MS_2 \equiv \mu_2$ )

Assuming an estimated depth and length of the Java Sea of 50 m and 900 km, respectively, the period of free oscillation of the standing wave would amount to 23 hours, which indeed is close to the period of the forced oscillation of the diurnal tide. As a result, diurnal tides evidently dominate the Java Sea, even though the adjacent oceans, i.e. the Pacific and Indian Oceans, are basically semidiurnal in character. Obviously, reflection is more apparent in the vicinity of a closed boundary than near an open boundary (Fig. 2.6). As a consequence, in the eastern part of the Java Sea the diurnal tides have a predominantly progressive character, whereas at the western part the character of the standing wave is more pronounced. As in the case of the  $M_2$  and  $S_2$  tides, the co-tidal charts of  $K_1$  and  $O_1$  exhibit small dissimilarities. In the larger part of the modelling domain, the phase lags of the  $K_1$  and  $O_1$  increase in opposite directions. In the southwesterly part of the Java Sea, however, the phase lags of both constituents increase towards the Strait Sunda.

In addition to the construction of the co-tidal charts, Ali (1992) calculated tidal energy budgets of the Java Sea. The total energy flux of the principal tidal constituents into the Java Sea originates for approximately 63.5% from the Flores Sea and the Makassar Strait, for about 36.1% from the South China Sea and the remainder, roughly 0.4% from the Indian Ocean, through the Strait Sunda. The main source of tidal energy for the Java Sea is supplied by the  $K_1$  tide (about 75 % of the total energy flux). However, focussing at the Strait Sunda, the tidal energy fluxes of  $S_2$ ,  $K_1$  and  $O_1$  are comparatively small and directed towards Indian Ocean, whereas the  $M_2$  tidal wave energy transfer exceeds the total energy flux of the other three tidal constituents and is oppositely directed, towards the Java Sea (Fig. 2.7).

Teluk Banten is thus geographically located in a region where the dominant tidal characteristics turn from diurnal to semidiurnal over a very short distance. Table 2.1 gives a list of the main tidal amplitudes and Greenwich phase lags for surface tides in the bay, based on a harmonic analysis of seven months of surface elevation data. The

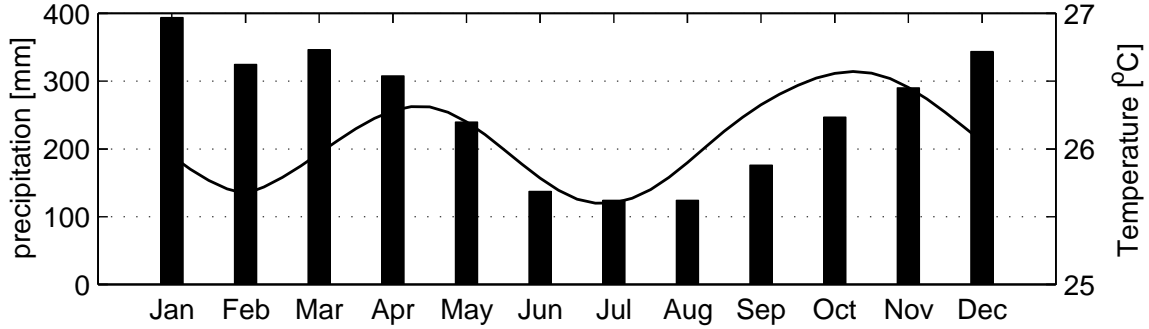


**Figure 2.8.** Average monthly precipitation (bars) and temperature (solid line) in the region of the Bay of Banten. Data source: University of East Anglia (grid size 0.5 x 0.5 degree; 1961-1990 Monthly Climatology)

tidal gauge was located at the reef slope of Pamujan Besar (Fig. 2.2). The amplitudes of the shallow water constituents are generally small. The largest third- and fourth-diurnal constituents are  $SO_3$  and  $M_4$ , respectively, which amplitudes amount to 0.6 and 0.9 cm. Hence, the role of compound and overtides in the dynamics of surface tides in the bay is only marginal.

## 2.4 Monsoonal climate

The Indonesian seas experience a typical monsoonal climate, determined by two opposing monsoons converging along the Inter-Tropical Convergence Zone (ITCZ). The ITCZ migrates north and south along with the position of the Sun, relative to the earth, heralding the change of monsoon characteristics (Tomascik et al., 1997). The location of the continental landmasses of Asia and Australia explain the southeast and northwest orientation of the monsoons. The Northwest Monsoon runs from December through February, whereas the Southeast Monsoon occurs from May until October. In both of these periods, winds are predominantly gentle and steady. During the transitional periods winds are light and more variable as a result of local land/sea breezes, which are then comparatively important. On an interannual timescale, El Nino - Southern Oscillation events sporadically disrupt the general weather pattern.

The seasonal variation of precipitation and temperature in the region of the Bay of Banten are a clear product of the monsoonal climate (Fig. 2.8). Monthly mean precipitation ranges between 100 mm during the dry season in July and 400 mm during the wet season in February. Monthly mean temperatures vary little and culminate during the monsoonal transition periods (Fig. 2.8). The temperature and precipitation are derived from a 1961-1990 monthly climatology data base from the University of East Anglia.

To gain an accurate estimate of the general wind and wave climate in the western part of the Java Sea, the CLAMS system from ARGOS Inc (Emmeloord, The Netherlands) was consulted. The CLAMS system computes climate parameters from satellite observations acquired over the past 15 years. Wind speed and directionality statistics are derived from the ERS-1/2 scatterometer data. The remotely sensed wind speeds have a standard deviation of 1.2 m/s from the wind speed measured by

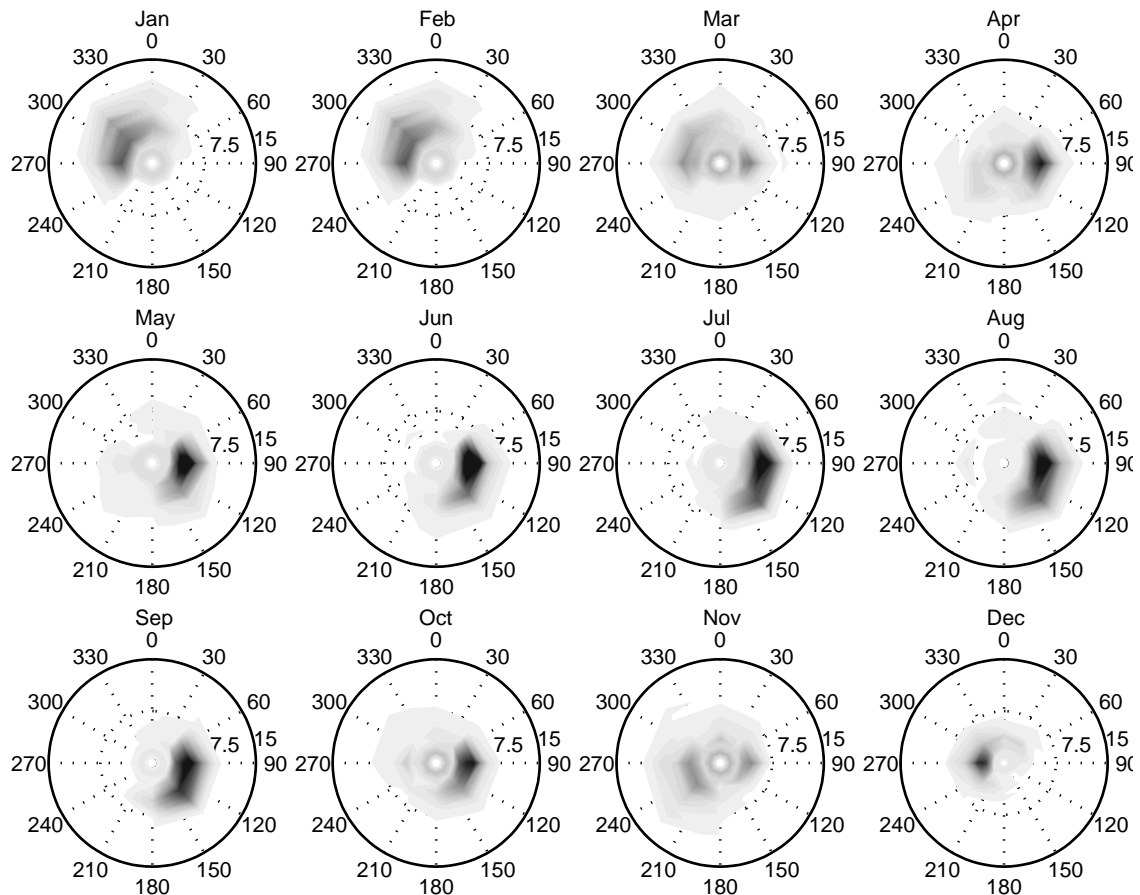


**Figure 2.9.** Wind climate in the western part of the Java Sea; annotation of circles indicate wind velocity in m/s; the gray shading scales the percentage of occurrence. Data source: ARGOS, Emmeloord.

an anemometer collocated at 5 m above sealevel, but converted to a reference height of 10 m. Spectral wave observations are acquired with the ERS-1/2 Synthetic Aperture Radar (SAR). The SAR observations complement the significant wave height measurements from the radar altimeters of the Geosat, ERS-1/2 and Topex/Poseidon missions. The standard deviation of the altimeter derived significant wave heights from the significant wave heights calculated from collocated wave buoys amounts to 0.45 m.

Fig. 2.9 displays the wind climate of the western part of the Java Sea, averaged over a 400 by 400 km square grid with its center located at 4° 45' South and 107° 45' East. In January and February northwestern winds prevail and wind speeds range between 0 to 9 m/s for 94% of the time, occasionally exceeding 10 m/s. In March the occurrence of easterly winds increases and the wind distribution becomes bidirectional. From April through October winds blow monotonously from the East and to a lesser degree from the Southeast. Wind speeds in this period are within the interval 0 to 9 m/s for 98% of the time. In November, southwesterly winds predominate, whereas the easterly winds have not yet entirely faded out. The southwesterly winds intensify in December and rotate clockwise towards the North West. Peak values of the time

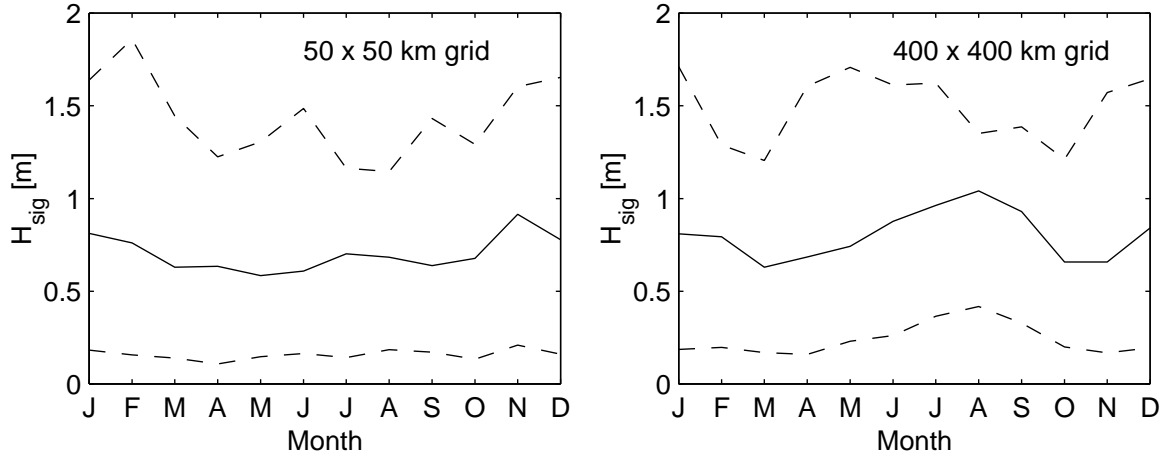


**Figure 2.10.** Seasonality of significant wave heights in the western part of the Java Sea (right) and North of Teluk Banten (left); solid line indicates the mean significant wave height; 5% of the occurring significant wave heights surpass the upper bound of the area in between the dashed lines and 5% remain below the lower bound.

averaged wind speeds are then as large as in January and February, exceeding 10 m/s for 6 percent of the time.

The seasonality of significant wave heights in the western part of the Java Sea are displayed in the left-hand panel of Fig. 2.10. A Weibull distribution was fitted to the population of  $H_{sig}$  estimates per month. The upper and lower bound of the areas in between the dashed lines in Fig. 2.10 correspond to the evaluation of the Weibull cumulative distribution function at 0.05 and 0.95. Hence, 5% of the occurring significant wave heights surpass the upper dashed line and 5% remain below the lower dashed line. The significant wave heights are generally small, within the range of 0.2 to 1.7 m. Monthly averages peak in August at 1.04 m, whereas in March and October to November, they drop to 0.63 and 0.66 m, respectively. The largest waves in the Java Sea are seemingly generated by the Southeast Monsoon, which has its peak mean wind velocity in August. The two periods of little wave action agree well with the transitional periods from one monsoonal regime to another.

In addition, a smaller (50 by 50 km) area north of Teluk Banten was selected in the CLAMS system with its center at  $5^{\circ} 46'$  South and  $106^{\circ} 10'$  East. The number of available satellite passes over this region appeared too limited to compute the seasonality of wind speed and direction. The variation of the significant wave height over the year could be estimated though, as depicted in the left-hand panel of Fig. 2.10. The yearly mean significant wave height amounts to 0.70 m, which is 10 cm less than the corresponding average for the westerly Java Sea. This may be associated to the location of Teluk Banten in the outer southwestern part of the Java Sea. Merely waves from the northeasterly quadrant may have developed over a considerable distance, others are highly fetch limited. The largest waves north of the Bay of Banten occur in November, when southwesterly winds prevail. Possibly, waves from the Strait Sunda penetrate the Java Sea in that month, reaching the Bay of Banten by means of diffraction.

To contrast the regional wind climate with the local conditions, a mobile anemome-

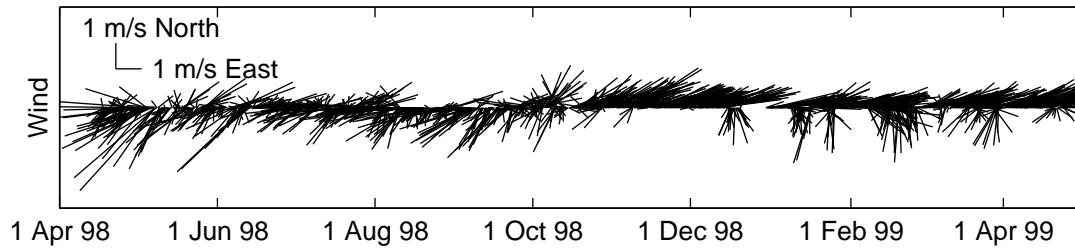


**Figure 2.11.** Low-passed wind speed from a meteorological station at Bojonegara (Fig. 2.2). Sticks indicate where the wind is blowing to. During the Northwest Monsoon local winds are from the west to southwest and during the Southwest Monsoon local winds blow from the east to northeast.

ter was deployed at the coast in Bojonegara (Fig. 2.2), recording wind speeds and directions at 8 m above ground, sampling every 10 minutes from March 1998 through April 1999. The wind speed time-series were low-pass filtered to exclude oscillations with frequencies higher than 0.8 cpd. The local winds have a counterclockwise deviation from the regional monsoonal cycle: during the Northwest Monsoon winds are from the west to southwest and during the Southeast Monsoon winds blow from the east to northeast (Fig. 2.11). Presumably, the discrepancy between the local and regional winds can be attributed to land/sea breezes.

## 2.5 Sea surface topography and throughflow

The prevailing trade winds over the tropical oceans cause an increase of sealevel on the western sides of the oceans and a lowering on its eastern sides (Wyrтки, 1987). Consequently, a significant pressure gradient exists between the western Pacific and the eastern Indian Ocean, driving a flow through the Indonesian Archipelago connecting the two Oceans. Wyrтки (1961) and coworkers conducted an extensive research on the dynamics of the sealevel topography in the Southeast Asian Waters, using surface current velocity measurements, a network of sealevel gauges and a simple force balance that relates wind stress, surface slope and mass transport. The difference between zero levels of a number of pairs of surface level gauges were estimated by comparison of local sealevel differences with shipborn observations of current velocity, someplace between the two stations. As a result of the semiannual change of monsoons, subtidal currents were mostly bidirectional. Assuming the absolute sealevel difference between two stations to equal zero when intermediate currents were reversing, the relative differences in level between stations were in general readily obtained.

In some cases, the subtidal currents were unidirectional throughout the year, which complicated acquiring the local zero level. In the Strait Sunda, outflow towards the Indian Ocean occurred during all measurements, which hampered the calculation of zero levels of the stations at the South Coast of Java. In Fig. 2.12 the seasonal variation of current velocity in the Strait Sunda is compared with surface level fluctuations in the harbor of Jakarta (Tanjung Priok, Northwest Java) and Pelabuhan Ratu (Southwest Java). The current velocity in the Strait Sunda and the sealevel difference

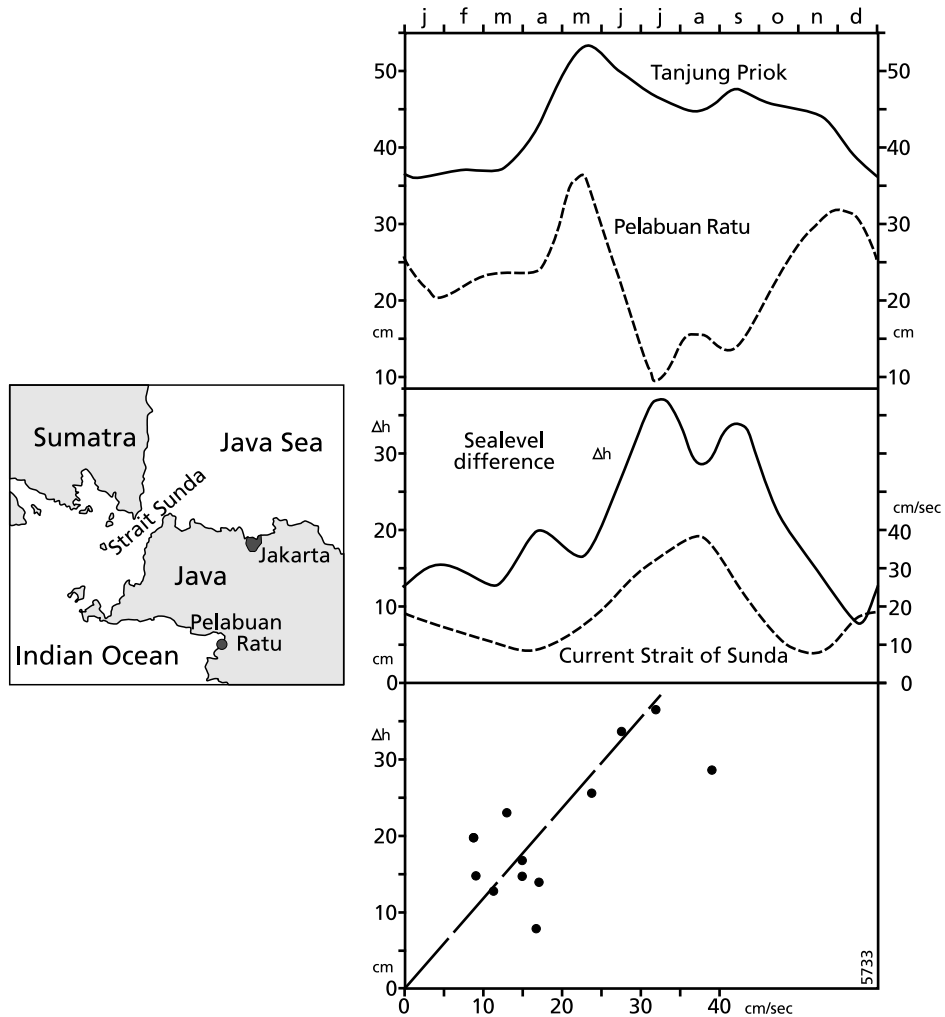


**Figure 2.12.** Top-right panel: subtidal sealevel variation at Tanjung Priok (TP) and at Pelabuan Ratu (PR). Mid-right panel: subtidal sealevel difference between TP and PR and currents in the Strait Sunda. Bottom-right panel: correlation between subtidal sealevel difference and current velocity. After Wyrtki (1961).

between the two stations are obviously linked. The linear relation indicated in the lower panel of Fig. 2.12 remains rather speculative, as both stations are situated approximately 120 km east of the strait.

The bimonthly charts of sea surface topography are presented in Fig. 2.13, in cm relative to 800 decibars air pressure. The average sealevel in the Java Sea remains consequently above the sealevel South of the Strait Sunda. The sealevel dynamics of the Java Sea show a seasonality with the largest sea surface slopes during the monsoonal periods, up to 4 cm per 100 km. During the Northwest Monsoon, the sealevel paradoxically increases towards the North, whereas during the Southeast Monsoon the surface gradient is positive towards the southwest. The transitional periods are characterized by a small surface gradient, which is positive towards the Northeast in April and towards the West in October.

The persisting outflow in the Strait Sunda towards the Indian Ocean suggests a westward residual current in the Teluk Banten area all through the year, which peaks

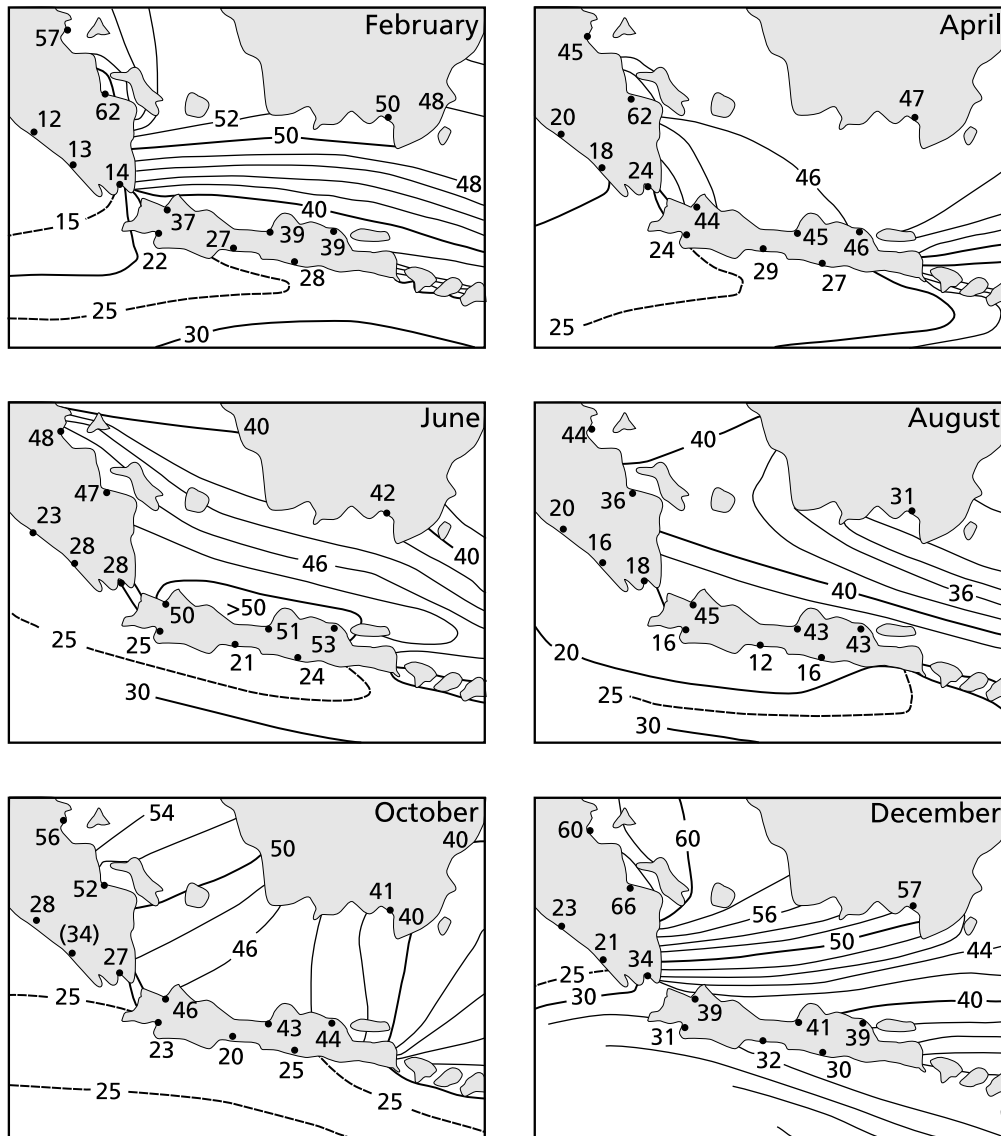


**Figure 2.13.** Annual variation of the sealevel topography in the Java Sea, in cm relative to 800 millibar air pressure (after Wyrтки (1961))

in August. However, surface current data collected within the period of October 1998 through March 1999 in the bay revealed that during the wet season, drift currents do reverse. A current meter was deployed at 1 m below local datum, attached to a wooden fishing platform in between Pamujan Besar and Panjang (Fig. 2.2), at 11 m depth. The average residual velocity amounted to 4.3 cm/s East and 0.9 cm/s North. Combining the results of Wyrтки (1961) with the recent wet season measurements, it seems very plausible that the bay is subject to an eastward throughflow during the wet season, and experiences a westward throughflow only during the dry season.

## 2.6 Concluding remarks

The Bay of Banten is hence subject to a typical monsoonal climate, resulting in clear seasonal cycles of wind and precipitation. Despite the regular atmospheric forcing, flow patterns in the bay are expected to be complex in space and time, due to the irregular topography and mixed diurnal-semidiurnal tidal motion. Both tidal and subtidal currents are influenced by the exchange of seawater and tidal energy between the Java Sea and the Indian Ocean, which are interconnected by the Strait Sunda. Wave energy in the bay is limited by low wind speeds and by the confined window of swell wave incidence. Wind waves do cause erosion of the eastern boundary of the bay though, which provides an important sediment source. Small amounts of terrestrial sediment are also delivered by the creeks that debouch into the embayment, especially by those along the eastern coastline. The seafloor sediments are relatively homogeneous and are composed of a mixture of silt and clay. In a coastal section along the eastern coastlines, erosion occurs and sediments are comparatively coarse. In the remainder of the bay accumulation takes place, and especially in the southern bay area sediments are relatively fine. Due to depositional processes, coral reefs in the bay are regionally being overrun by muddy sediment. However, the scour trenches suggest that the reefs may be able to create a local morphodynamic regime, where deposition rates differ from the regional trends.



# 3

## Topographic influence on mixing and stratification in a tropical tidal embayment

*With Piet Hoekstra and Bas van Maren, to be submitted to Journal of Marine Systems*

### 3.1 Abstract

The Bay of Banten provides an example of a semicircular shallow tidal embayment in a tropical ROFI (Region Of Freshwater Influence), subject to a mixed, mainly diurnal tidal regime and a monsoon-driven residual circulation. A partially inactivated delta shapes the east coast of the bay and constitutes the main freshwater source during the wet season. Based on bulk estimates of the Richardson number, the intratidal variation in stratification appeared to be primarily controlled by shear instability. The role of differential advection of salinity was inferred from the coherence between low-frequency variation of stratification and the subtidal flow. Most active mixing occurs when both the tidal and subtidal currents in the bay are directed towards the sources of buoyancy along the eastern coastline. The propensity for mixing is largest at the subaqueous plain in front of the former delta, where flow contracts around the protruding delta, which hydrodynamically acts as a headland. The cross-shore vertical circulation in the bay is composed of a baroclinic and an Ekman component. During the wet season, the secondary flow driven by the eastward monsoon-induced flow along the bay's isobaths reinforces the estuarine circulation, promoting offshore advection of freshwater buoyancy.

### 3.2 Introduction

Understanding the development and breakdown of stratification is a key objective of coastal oceanography. The level of stratification controls the intensity of vertical mixing and hence the vertical exchange of water-borne particles of various kinds. Studies addressing the processes of (de-) stratification have been strongly concentrated in midlatitude Regions Of Freshwater Influence, abbreviated ROFIs (e.g. Sharples &

Simpson, 1995; De Ruijter et al., 1997; Marmorino et al., 2000; Sanders & Garvine, 2001). In these regimes, buoyant spreading and its stratifying influence is largely constrained by the Earth's rotation, deflecting density currents to be trapped to the coastline (Woods & Beardsley, 1988; Munchow & Garvine, 1993). Apart from the effect of rotation, wind forcing often plays a central role in the topographic spreading of river effluents in midlatitude ROFIs, both locally by enhancing mixing with in the underlying saline waters, as well as regionally by generating longshore coastal flows and associated Ekman circulations (Fong et al., 1997; Sanders & Garvine, 2001).

Few studies have focussed on ROFIs at tropical low-latitudes, where rotation effects are less influential (Simpson, 1997) and where the monsoonal climate generally imposes a strong seasonal modulation of freshwater input and wind-driven circulation. Since tropical coastal environments are host to major fisheries and coral reefs, knowledge about flow mechanisms that control the vertical exchange in these waters provides an important basis for ecological studies (cf. Wolanski, 2001). Rivers in the tropics differ from these at low-latitudes because their freshwater and sediment discharges are generally an order of magnitude larger (Milliman & Meade, 1983). Consequently, they create protruding delta systems that interfere with the prevailing longshore flows (e.g. Allen et al., 1979; Hoekstra et al., 1989). The present study site, Bay of Banten, Indonesia, is located at 6° southern latitude and borders the partially inactivated Ciujung delta on its eastern flank (Fig. 3.1). The Bay of Banten is about 10 by 15 km wide, has a mean depth in the order of 8 m and merges with the Java Sea at the slope-break along its northern margin, where depths increase to 25 m. The Ciujung (ci means river in Indonesian language) was diverted to the east in the 1920's, reducing the total river discharge in the bay to an estimated range between 2 and 30 m<sup>3</sup>/s. Although similar shallow bays are often presumed *a priori* to be well-mixed, water masses in the Bay of Banten can be considerably stratified.

Apart from its low-latitude, the Bay of Banten differs from many well-studied embayments in that tides are mixed, mainly diurnal. The spring-neap cycle has a period of 13.4 days and results from the difference in angular speed of the main diurnal tidal constituents, viz.  $K_1$  and  $O_1$ . The semidiurnal  $M_2$  tide is dominant during neap tide, when  $K_1$  and  $O_1$  are in counter phase. Despite the small tidal range, which exceeds 85 cm only occasionally, tidal flow velocities attain peaks up to 0.65 m/s. The flow pathways largely parallel the coastline and are thus strongly curved. The alternate monsoonal winds drive a variable low-frequency flow in the order of 0.1 m/s, which is part of the large-scale circulation in the western Java Sea. During conditions of westward residual flow, the bay may be affected by buoyancy of the Ciujung and Cidurian (Fig. 3.1), which have a joint discharge ranging in between 20 and 220 m<sup>3</sup>/s. Local winds are merely of low intensity, exceeding 4 m/s only occasionally, and provide too little energy for generating a significant wind-mixed layer.

The present analysis aims to identify the mechanisms that control mixing and stratification in the Bay of Banten, with emphasis on the topographic influence on these mechanisms. This chapter is structured as follows. Section 2 describes the field measurement program. Section 3 presents observations of the tidal boundary layer structure, which provides a signature of the degree of mixing. In Section 4, mechanisms responsible for cross-shore water circulation are analyzed, as these are

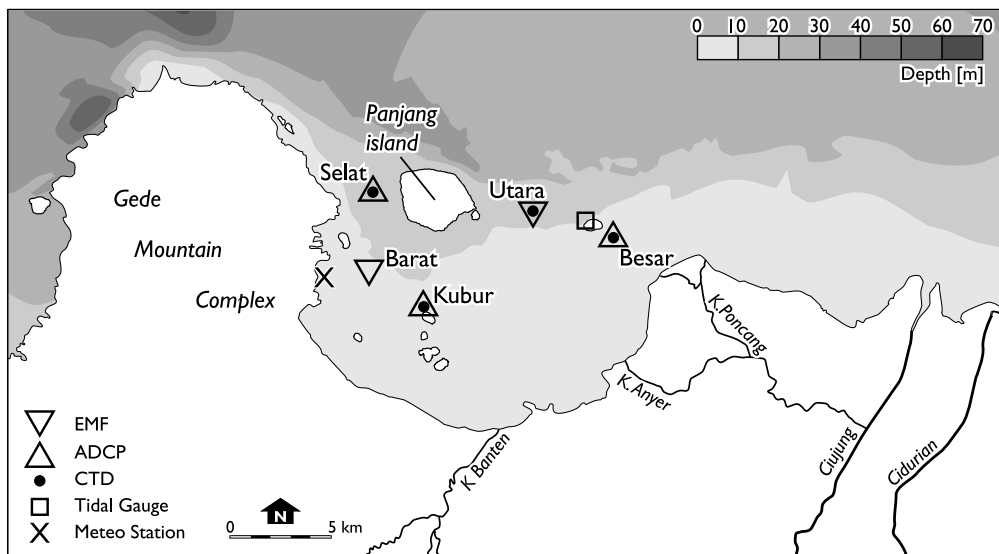
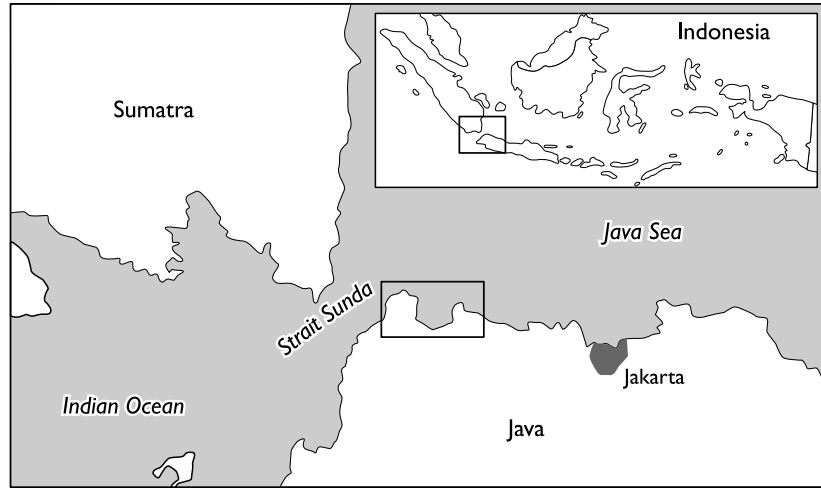


**Figure 3.1.** Location map showing sampling stations in the Bay of Banten. The larger portion of the Cuijung discharge enters the Java Sea by means of the shortcut canal east of the bay.

essential to the spreading of river effluents. Section 5 then describes the intra-tidal and subtidal variation in water column stability, which is followed by a discussion and conclusions.

### 3.3 Observational program

The major focus of the observations presented in this study was a period from September 1998 through April 1999, covering the wet season. An *Electro-Magnetic Flow* meter (EMF) was deployed 1 m below mean sealevel for three months at a northerly location in the bay, denoted Utara, and for a fortnight at a westerly location, denoted Barat (Fig. 3.1). At both locations, the EMF was moored on a wooden fishing platform. Additional velocity observations were made using a broad-banded 1.2 MHz

Acoustic Doppler Current Profiler (ADCP), with a vertical resolution of 0.25 m. At Besar and Kubur (Fig. 3.1) the ADCP was moored on a fishing platform for a fortnight and at Selat, shipboard ADCP measurements were taken during two 25-hour anchor stations. A mobile meteorological station recorded wind speeds and directions during the entire observational period. The anchor stations and moorings revealed the structure of the tidal boundary layer in the bay and the response of the subtidal water motion during wet season to the Northwest Monsoon and buoyancy issued by the small rivers in the bay.

A tidal analysis was performed to address the complex tidal behavior in the bay. Therefore, velocity vectors were transformed to result in components corresponding to the semi-major axis ( $u$ ) and semi-minor axis ( $v$ ) of the tidal flow. A tidal gauge yielded data on surface elevation ( $\zeta$ ), over the time-span of a year. Time-series of  $\zeta$ ,  $u$  and  $v$  were harmonically analyzed after applying a Godin filter (Godin, 1972). The  $u$ - and  $v$ -current records at Barat however were detrended by subtracting the best fit linear line instead of filtering the data, because the time-series would have become undesirably short. The tidal constituents to be included in the harmonic analysis of currents were selected based on the results of the analysis of the vertical tide. Constituents with a difference in frequency that was too small for proper resolution of both constituents were resolved in a coupled sense (WL|Delft Hydraulics, 1997).

Stratification of water masses in the bay was investigated by CTD (*Conductivity Temperature Depth*) sampling, synchronous with the ADCP observations. At Utara and Selat, CTD casts were taken hourly using a winch on a research vessel, during two 25-hour anchor stations at each location. At Besar and Kubur similar CTD casts were taken manually from the fishing platforms, once per hour during daytime. These obtained vertical profiles of salinity and temperature covered the entire water column except for the bottom 50 cm. From the salinity and temperature measurements water density was calculated, which is denoted in  $\sigma_t$  units throughout the text and relates to water density ( $\rho_w$ ) as in:

$$\sigma_t = \rho_w - 1000 \quad (3.1)$$

The 9-hour data gaps coinciding with nighttime inhibited a spectral analysis of the moored CTD data. Sufficient information was acquired though to establish the intratidal and subtidal variation of stratification. To gain insight into the spatial variability of the salinity distribution, additional CTD surveys were performed along three north to south transects, during two quasi-synoptic CTD cruises of the bay in September 1998 and February 1999.

### 3.4 The tidal boundary layer

Tides in the Bay of Banten are under the influence of the tidal motion in the Strait Sunda, where semidiurnal tidal energy penetrates the Java Sea from the Indian Ocean. The tidal regime in the Java Sea, in turn, is predominantly diurnal due to the resonant response of this basin to diurnal forcing. As observed at Utara, the tidal currents account for 64% of the current variance. The diurnal and semidiurnal current amplitudes are largest at Besar (Fig. 3.2), which represents the subaqueous plain in front of the delta that shapes the east coast. The old delta hydrodynamically acts as

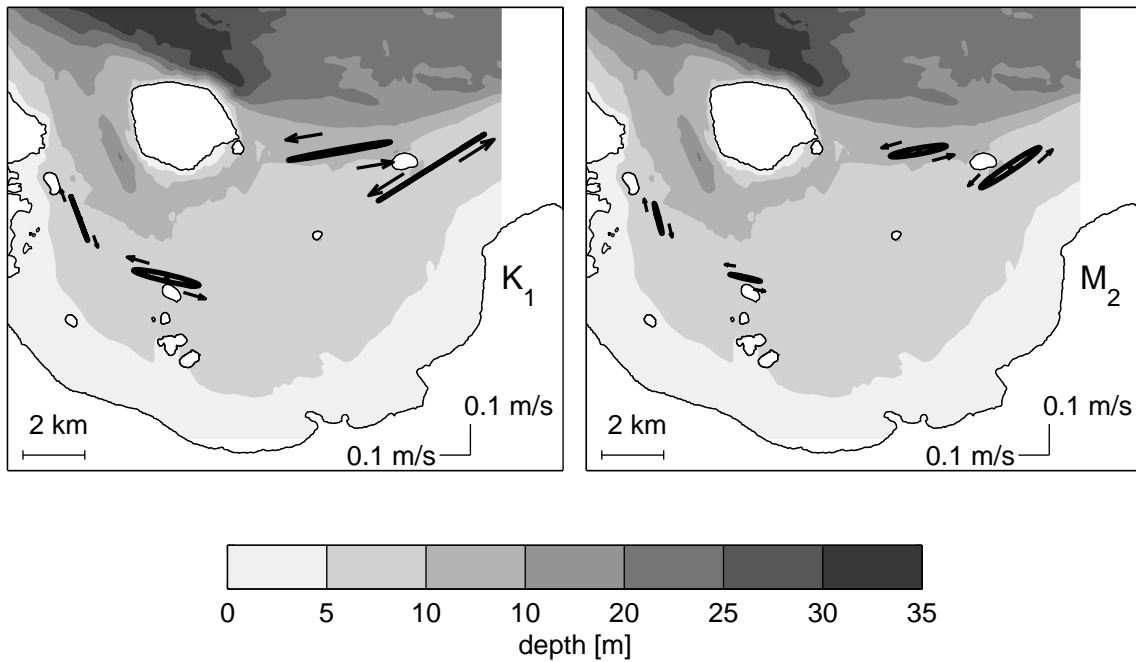


**Figure 3.2.** Surface current tidal ellipses of  $K_1$  and  $M_2$ , where arrows indicate the direction of rotation. Shading represents depth in meters.

a headland, where flow pathways contract. The surface tidal ellipses appear almost degenerate, with the semi-major axes running largely parallel to the bay's isobaths (Fig. 3.2). The baroclinic forcing on the boundary layer is thus insufficient to measurably modify the tidal ellipses (cf. Visser et al., 1994), not even at Besar which is approximately at right angles to the main buoyancy source.

The tidal boundary layer in the embayment generally occupies the entire water column (Fig. 3.3). At the subaqueous plain in front of the former delta, velocity profiles are logarithmic up to the surface indicating fully turbulent flow conditions, even at neap tide. Outside this region, a logarithmic layer is confined to the bottom few meters, and the largest portion of the water column is occupied by the outer layer, which is subject to influences of the earth's rotation and density gradients (cf. Soulsby, 1983). The stability of the outer layer allows for a general time-lag between surface and near-bottom current variation, in particular during neap tide. This is consistent with the theory of Bowden (1983) that regards the frictional effects on tidal waves. Friction transforms a progressive Kelvin wave, characterized by in-phase oscillation of elevation and the current, into a damped Kelvin wave, for which elevation lags on current variation. Due to the decrease of frictional stresses with increasing distance from the bottom, the tidal wave can concurrently be progressive at the surface and resemble a damped Kelvin wave near the bed, explaining the observed time-lag.

The limited vertical extent of the logarithmic layer in the larger part of the embayment is associated to a vertically continuous density stratification. Only at the subaqueous plain in front of the old delta, sufficient mixing energy is available to

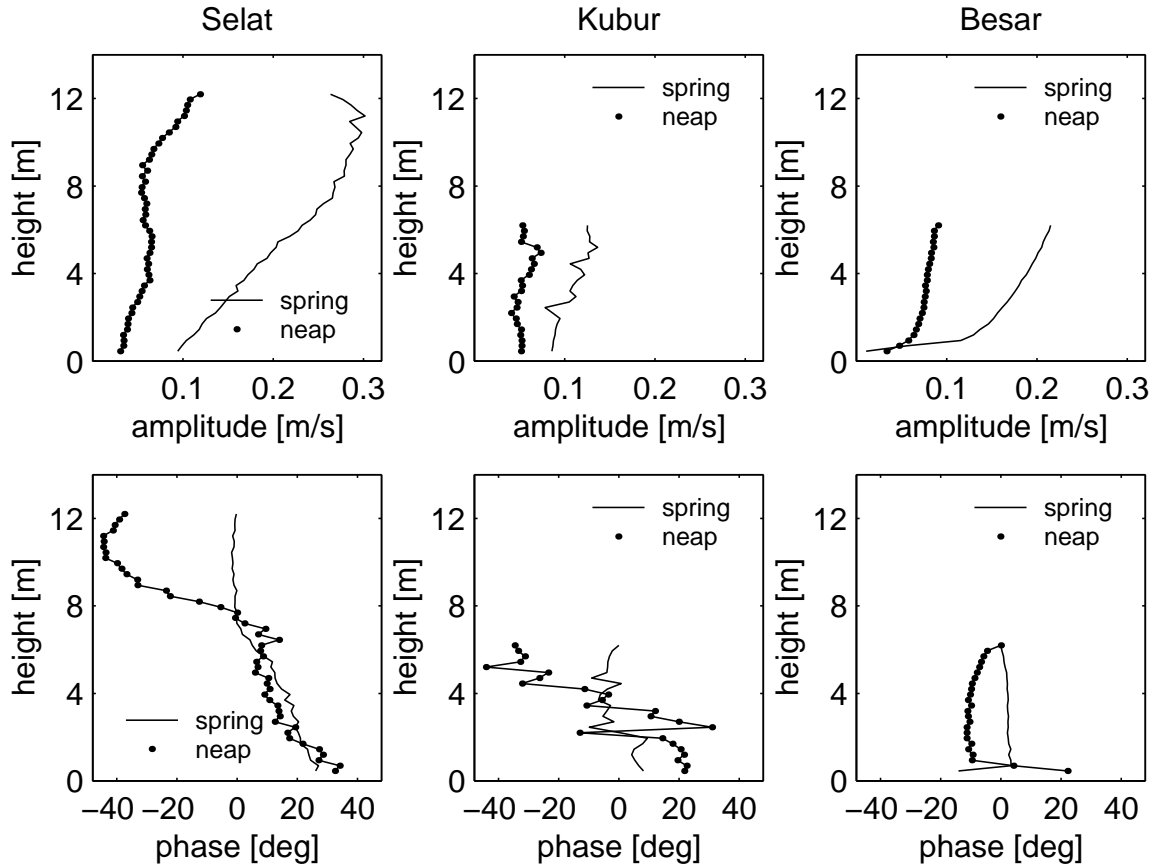


**Figure 3.3.** Amplitude and phase of the diurnal currents during spring tide and neap tide conditions, based on least squares harmonic analysis. Near the former delta (right panels) the logarithmic layer extends over the entire water depth, indicating strong mixing. In the remainder of the bay (left and mid panels), the outer layer occupies the largest portion of the water column.

produce an upward shifting halocline during conditions of increasing current velocity, and a vanishing downward moving halocline during deceleration of the flow (Fig. 3.4). In the absence of significant water temperature variation, baroclinic influences on the tidal boundary layer are due to salinity gradients. During the wet season, which coincides with the northwest monsoon, the small rivers constitute the main freshwater input to the bay. The northwest monsoon drives an eastward residual circulation that conveys saline waters from the Java Sea. This along-isobath residual flow intermittently persisted during the mooring at Utara and averaged 8 cm/s. In the dry season, river discharges are smaller, yet the corresponding southeast monsoon may drive a westward residual flow, carrying buoyancy from the Ciujung and Cidurian (Figs. 3.1 and 3.5). Stratifying forces in the Bay of Banten are thus present all through the year.

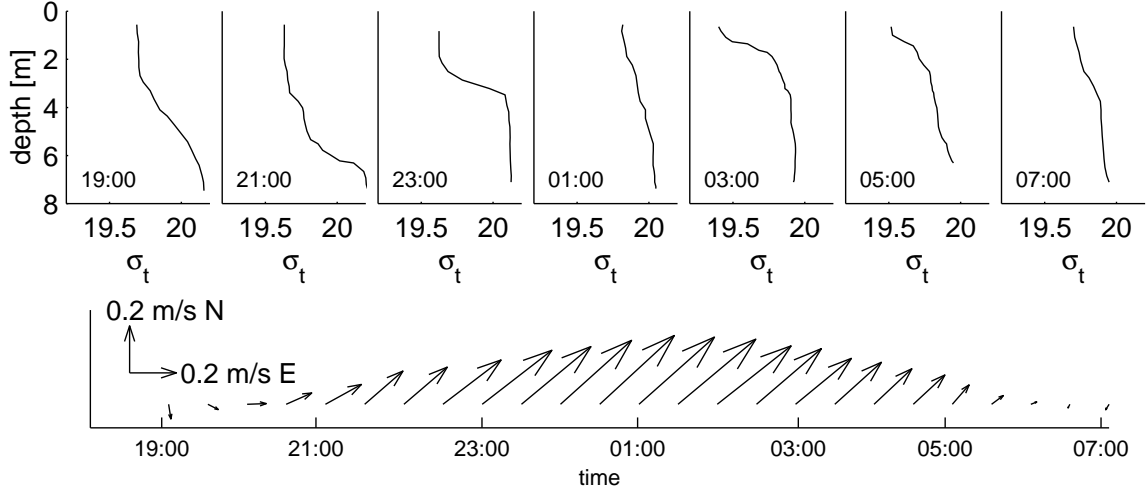


**Figure 3.4.** Variation of stratification (top panel) and depth-mean flow (bottom panel) at Besar. At the time of minimum and maximum current velocities the water column is continuously stratified. During conditions of increasing current velocity, a halocline is generated near the bottom and shifts upward. During decreasing flow, a halocline appears at the surface, but vanishes rapidly.

### 3.5 Gravitational circulation and Ekman forcing

Cross-shore vertical water circulations are essential to the seaward transport of buoyancy and have a direct stratifying influence (e.g Munchow & Garvine, 1993). During the mooring at Besar, a weak, though persistent vertical circulation was manifest, featuring a seaward moving layer over a land-ward directed return current (Fig. 3.6). To determine the hydrodynamic mechanisms responsible for this circulation, a scaling analysis of the cross-isobath momentum balance is here presented, using the moored data and the hydrographic measurements made during the wet season.

Assuming a horizontally uniform flow, the steady-state linear momentum equation for cross-isobath flow reads (Bowden, 1983):

$$fv + \frac{gz}{\rho} \frac{\partial \rho}{\partial x} = g \frac{\partial \zeta}{\partial x} - N_z \frac{\partial^2 u}{\partial z^2} \quad (3.2)$$

where  $u$  and  $v$  denote current components in the cross-isobath ( $x$ ) and along-isobath ( $y$ ) direction, respectively,  $f$  is the Coriolis parameter,  $\zeta$  denotes surface elevation,  $\rho$  is density and  $z$  is depth. The aim is to find the depth-mean values of the terms in Eq. 3.2. Differentiating (3.2) to  $z$  yields:

$$f \frac{\partial v}{\partial z} + \frac{g}{\rho} \frac{\partial \rho}{\partial x} = -N_z \frac{\partial^3 u}{\partial z^3} \quad (3.3)$$

Based on the wet season density structure displayed in Fig. 3.5 the depth-mean cross-isobath density gradient is estimated, which results in  $\partial \bar{\rho} / \partial x = 6 \cdot 10^{-5} \text{ kg/m}^4$ , where the overbar denotes depth-averaging. Using the vertical profiles of  $u$  and  $v$  in Fig. 3.6, the time-averaged eddy viscosity can be solved from Eq. 3.3, which gives  $N_z = 1.2$

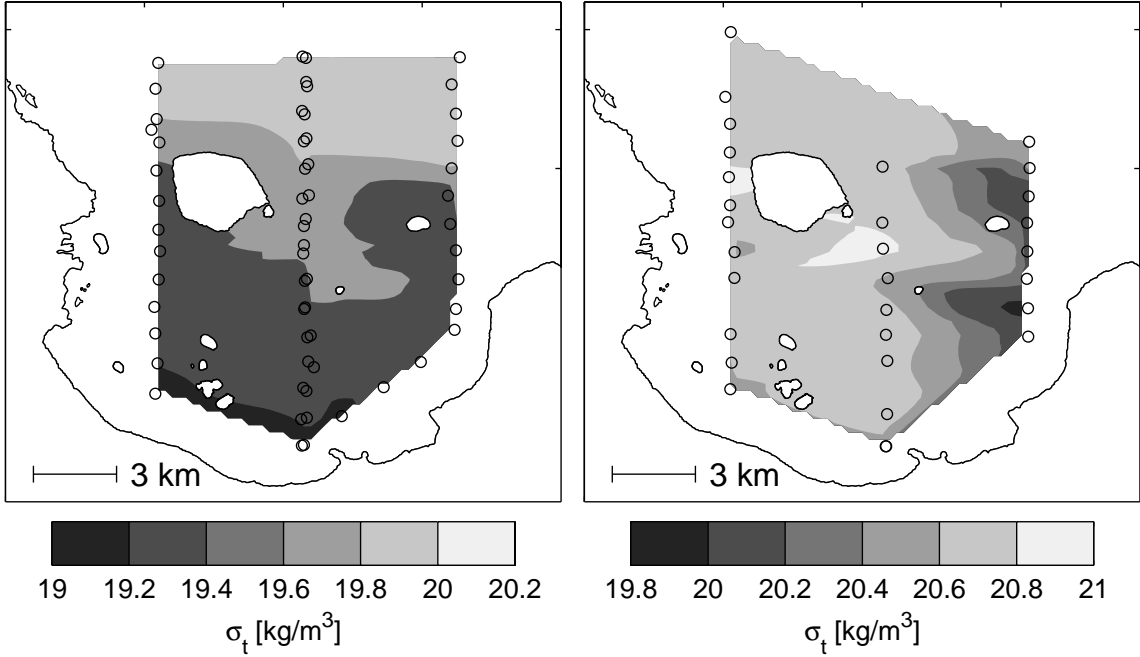


**Figure 3.5.** Depth-mean values of  $\sigma_t$  from quasi-synoptic CTD data collected on 17 and 18 September 1998 (left-hand panel, representing the dry season) and 14 February 1999 (right-hand panel, representing the wet season). During the dry season, westward circulation is expected, inducing an Ekman forcing that traps freshwater buoyancy derived from the Ciujung and Cidurian to the coast (see also Fig. 3.1). During the wet season, small rivers along the eastern coastline constitute the main sources of freshwater.

$\times 10^{-3} \text{ m}^2/\text{s}$ . This value can be verified using Bowden's formula for  $N_{z0}$  (Bowden, 1953):

$$N_{z0} \simeq 0.002|u_m|h, \quad (3.4)$$

which can be corrected for turbulence reduction due to stratification, using the functional relation formulated by Munk & Anderson (1948):

$$\frac{N_z}{N_{z0}} = \frac{1}{(1 + 10Ri_B)^{0.5}} \quad (3.5)$$

Herein,  $N_{z0}$  is the vertical eddy viscosity for well-mixed conditions,  $|u_m|$  denotes the depth-mean current magnitude and  $h$  is depth. The bulk Richardson number  $Ri_B$  is defined as (Lewis, 1997):

$$Ri_B = \frac{gh\Delta\rho}{\rho_m U^2} \quad (3.6)$$

where  $\Delta\rho$  is the density difference between surface and bottom and  $\rho_m$  is the depth-mean density. The mean value of  $N_z/N_{z0}$  equaled 0.65. This approach leads to  $N_z=1.5 \times 10^{-3} \text{ m}^2/\text{s}$ , which is in reasonable agreement with what was found by solving Eq. 3.3. Assuming  $N_z=1.2 \times 10^{-3} \text{ m}^2/\text{s}$ ,  $\partial\zeta/\partial x$  is subsequently obtained from (3.2) and amounts to  $2.1 \times 10^{-7}$ , representing a small cross-isobath setup towards the eastern



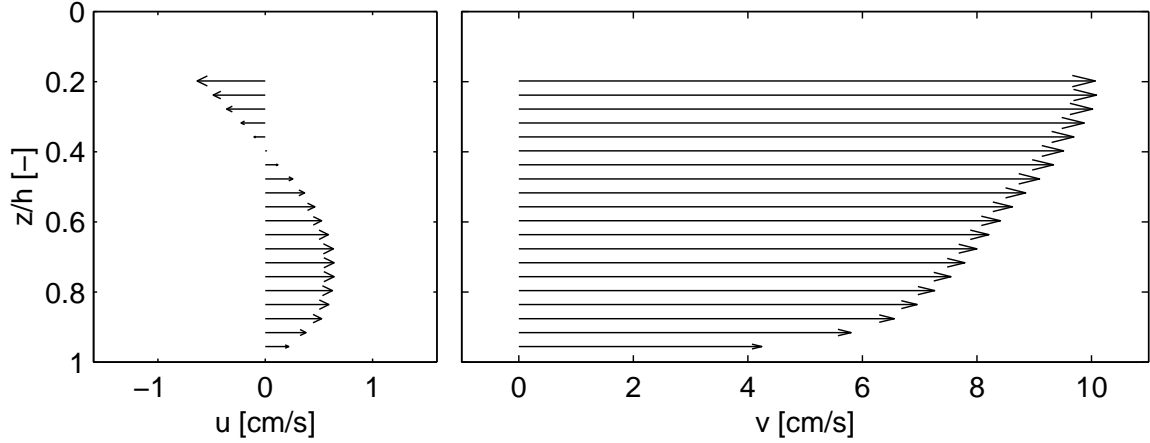


**Figure 3.6.** Time-averaged vertical velocity profiles of cross-isobath ( $u$ ) and along-isobath ( $v$ ) current components at Besar, where  $z/h$  denotes relative depth. Positive and negative values of  $u$  coincide with onshore and offshore flow, respectively. Positive and negative values of  $v$  represent flow towards E-NE and W-SW, respectively.

shoreline. Finally, the depth-mean values of the terms in the subtidal momentum balance are calculated and amount to  $1.3 \times 10^{-6} \text{ m s}^{-2}$  (Coriolis term),  $2.3 \times 10^{-6} \text{ m s}^{-2}$  (density gradient term),  $2.0 \times 10^{-6} \text{ m s}^{-2}$  (surface slope term) and  $1.6 \times 10^{-6} \text{ m s}^{-2}$  (friction term). Hence, the baroclinic momentum has the same sign and order of magnitude as the momentum induced by Coriolis forcing, and the two terms were counterbalanced by a surface slope and friction. This leads to the conclusion that the observed cross-shore circulation in Fig. 3.6 is driven both by gravitation and coastal Ekman forcing. The monsoon-induced current towards the east thus drives a secondary flow that reinforces the cross-isobath gravitational circulation, promoting seaward advection of buoyancy.

Although no long-term flow measurements were taken during the dry season, the Southeast Monsoon is expected to drive a westward residual current, with an associated reversed Ekman forcing. Consequently, freshwater buoyancy from the Ciujung, conveyed to the Bay of Banten along with a westward residual current, may be confined to the coast as the Ekman forcing then opposes the gravitational circulation. The quasi-synoptic spatial distributions of the depth-mean density, based on CTD surveys during the dry and wet season, indirectly support this hypothesis (Fig. 3.5). The longshore orientation of the isohalines during the dry season may indicate trapping of freshwater buoyancy to the coast. In addition, the relatively low mean density in the bay observed during the dry season can be explained by a westward longshore current carrying freshwater buoyancy from the Ciujung and Cidurian, which is absent during the wet season.

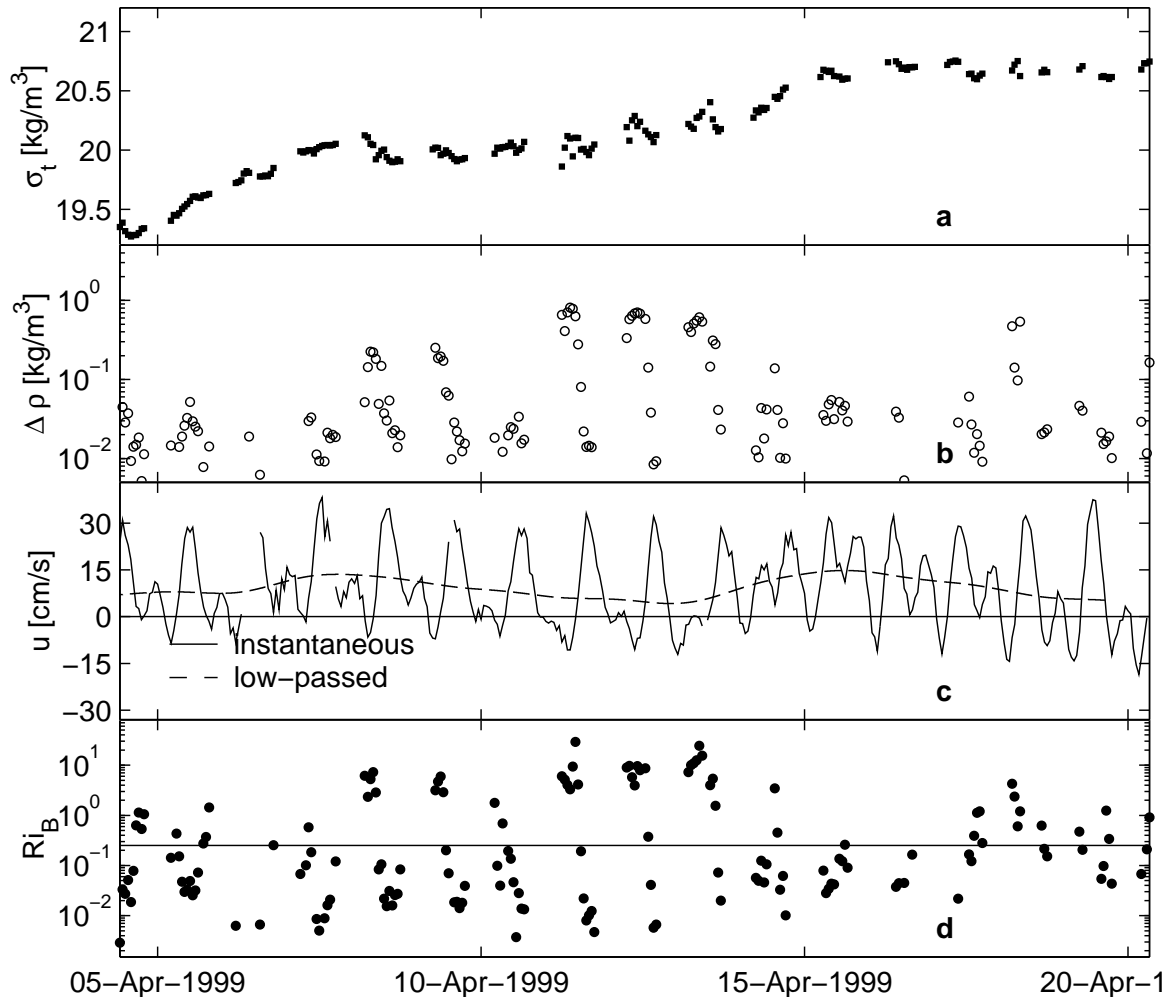


**Figure 3.7.** Time-series based on moored data from Besar. From top to bottom: depth-mean  $\sigma_t$  (a), density difference between the surface and the bottom (b), depth-mean values of the instantaneous and low-passed along-isobath current, defined positive for eastward flow (c), and bulk Richardson number (d). Note the logarithmic scaling for  $\Delta\rho$  and  $Ri_B$ . The solid line in the bottom panel indicates  $Ri_B=0.25$ .

### 3.6 Water column stability

An overall characterization of the stability of a stratified flow can be provided by a bulk Richardson number  $Ri_B$  (Eq. 3.6). When  $Ri_B < 0.25$ , mixing will generally occur, whereas for  $Ri_B > 0.25$  a stable water column is expected (Thorpe, 1971). For  $Ri_B > 0.25$  mixing is not unfeasible, owing to vertical variations in the velocity shear. However, based on field data documented by Geyer & Smith (1987) and Trowbridge & Kineke (1994), Geyer (1995) argues that  $Ri_B$  provides a reasonable estimate of the stability as  $Ri_B$  approaches its critical value, since shear and stratification tend toward linear profiles as mixing increases.

The Richardson number variation at the Besar mooring exhibits the predominant low stability of the water column (Fig. 3.7). The gradual increase of the mean density during the mooring confirms that the eastward residual circulation conveys comparatively high density water. A stable water column occurred only if the tidal current

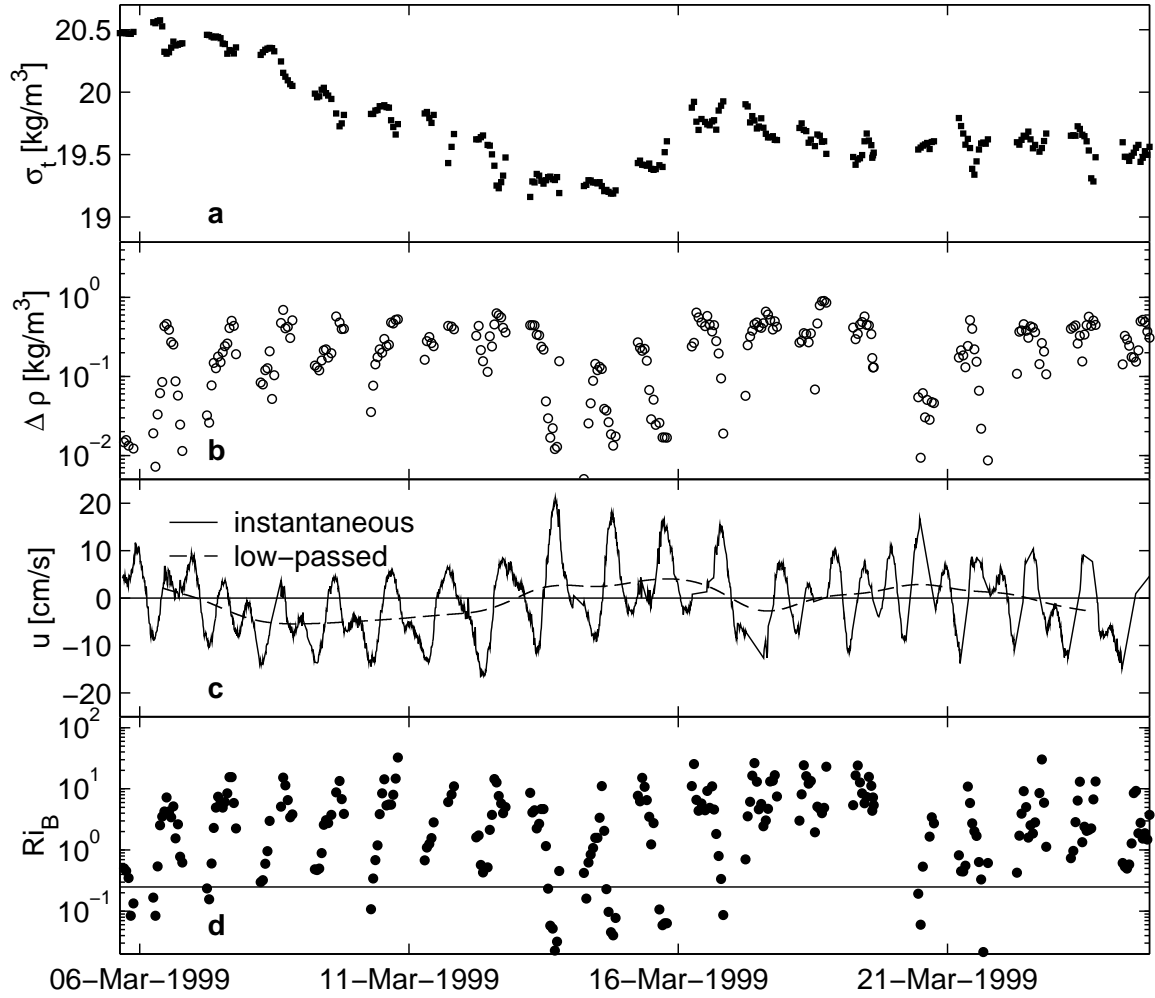


**Figure 3.8.** Time-series based on moored data from Kubur. From top to bottom: depth-mean  $\sigma_t$  (a), density difference between the surface and the bottom (b), depth-mean values of the instantaneous and low-passed along-isobath current, defined positive for eastward flow (c), and bulk Richardson number (d). Note the logarithmic scaling for  $\Delta\rho$  and  $Ri_B$ . The solid line in the bottom panel indicates  $Ri_B=0.25$ .

opposed the low-frequency flow, reducing current velocity and associated velocity shears to a minimum. The strong turbulence observed in the boundary layer suggests shear instability to be a likely mechanism for the diurnal breakdown of stratification in the area of the subaqueous delta front.

The role of differential advection of salinity (De Ruijter, 1983; Van Aken, 1986) appeared from the mooring in the central area of the bay, where the low-frequency flow reversed several times. In the presence of a horizontal density gradient, vertical velocity shear affects the degree of stratification, depending on the orientation of the shear relative to the density gradient. In the central area of the Bay of Banten, the horizontal density gradient is largely East to West and therefore aligned with the predominant pathways of the tidal and subtidal flow (Fig. 3.5). Comparison of the low-frequency variation of the Richardson number and the subtidal flow (Fig. 3.8) reveals that an eastward circulation tends to cancel the vertical salinity gradients, di-

minishing the degree of stratification, whereas a westward circulation has the opposite effect, straining the water column. In fact, the orientation of the low-frequency flow in the bay exerts a decisive influence on the stability of the water column, determining whether or not the mixing threshold is attained during maximum tidal current velocities.

In many estuaries, the tidal shear alternately destroys and induces stratification over a tidal cycle as a result of differential advection of salinity, which is often termed tidal straining (Simpson et al., 1990; Nepf & Geyer, 1996). The moored data from Kubur showed that increase of tidal current velocity and hence the shear produces a decline of stratification, irrespective of the direction of the tidal current (Fig. 3.8). Therefore, shear instability provides a more plausible candidate for controlling the intratidal variation of stratification, even in the central area of the bay where currents are relatively weak. The strength of tidal shear co-varies with tidal motion, which is typically diurnal during spring tide and semidiurnal during neap tide (Fig. 3.9). Due to the large number of tidal constituents that contribute to the mixed, mainly diurnal tidal motion, considerable differences are to be expected between successive spring-neap cycles.

### 3.7 Discussion and conclusion

The limited influx of buoyant waters into the Bay of Banten during the wet season affects the haline stratification dynamics in the embayment profoundly. Two dynamically different regimes were found, viz. the source region in the east part of the bay, where the tidal and subtidal flow is strongest and active mixing predominates, and the remainder of the bay, characterized by less vigorous currents and weak stratification. Tidal mixing in the source region was reflected in the nearly logarithmic tidal flow profiles and the degeneracy of the tidal ellipses at Besar, despite the orientation of the major axis of the tidal flow, largely aligned with the isohalines. The time-lag between surface and near-bottom currents in the remainder of the bay indicated an increase of friction towards the bottom. The reversals of the monsoon-driven subtidal flow at the Kubur mooring provided the opportunity to distinguish between the influences of differential advection of salinity and shear instability, which were shown to govern the intratidal, and subtidal variation of the water-column stability, respectively.

In addition to the effects of differential advection and shear-induced mixing, Nepf & Geyer (1996) discuss the role of vertical stretching in the process of (de-) stratification, which results from a vertical current component, for instance induced by a topographic irregularity. Vertical current components result in the advection of positive or negative buoyancy. The curved topography of the Bay of Banten suggests the presence of a secondary flow, with associated vertical current components. In particular, the flow around the protruding delta may generate upwelling at the subaqueous delta front, analogous to the spiral flow in the inner bend of a river (De Vriend, 1981). Kalkwijk & Booij (1986) theoretically found that stratified conditions may enhance secondary flow, which was confirmed from observations by Geyer (1993), who addressed the case of a headland. Therefore, it seems reasonable to presume that vertical stretching due to an upward salt flux resulting from a secondary flow reduces

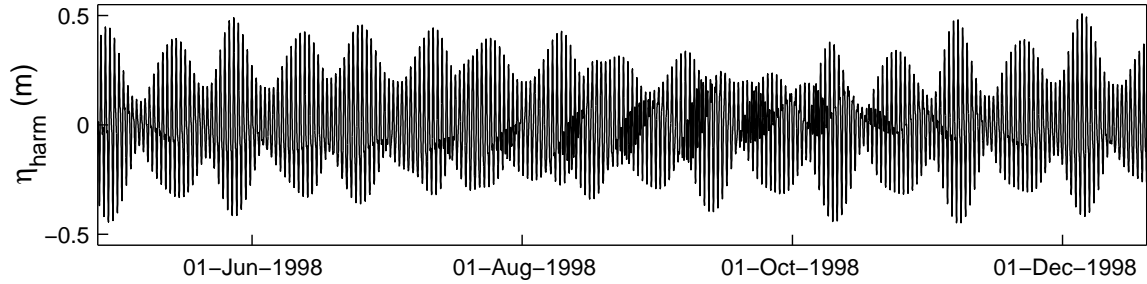


**Figure 3.9.** Time-series of the tidal elevation ( $\eta_{\text{harm}}$ ) in the Bay of Banten. The mixed, mainly diurnal tide exhibits significant differences between successive spring-neap cycles.

the stability of the water mass in front of the delta.

The spring-neap variation of the tidal currents and stratification is not as clear-cut as in prototype  $M_2$  dominated ROFIs (Simpson, 1997), which is due to the inherent complexity of the mixed, mainly diurnal tidal regime (Fig. 3.9). Consequently, the effect of tidal mixing cannot be inferred from a single spring-neap cycle, which does seem feasible in semidiurnal regimes such as the Amazon frontal zone (Geyer & Kineke, 1995; Geyer, 1995) and in the Liverpool Bay ROFI (Sharples, 1992). Whereas these regimes may be subject to  $N_2$  modulation of the spring-neap cycle (Sharples & Simpson, 1995), preventing strict fortnightly periodicity, differences between successive spring-neap cycles in mixed tidal regimes are more pronounced, due to the large number of tidal constituents involved. Using an analytical model, Nunes Vaz & Lennon (1991) showed that the low-frequency variation of turbulence is particularly important to stratification, which emphasizes the importance of these differences.

The spring-neap cycles in diurnal and semidiurnal tidal regimes have periods of 13.66 and 14.77 days, respectively (Godin, 1972). In mixed tidal regimes, these cycles interfere, and theoretically exhibit a virtually semiannual periodicity ( $13.66/(14.77 - 13.66) = 12.3$  cycles times 13.66 = 168 days). Examination of the entire scope of tidally-induced oscillations of stratification in a mixed tidal regime thus requires a data record covering half a year. The necessity of long-term observations is also marked by the unsteadiness of the monsoon-driven currents (Fig. 3.8). Based on measurements taken in the Great Barrier Reef, Wolanski & Spagnol (2000) showed that low-frequency currents with a non-tidal origin may be affected by the spring-neap undulations of turbulence. The low-frequency flow is steered away from regions of strong turbulence during spring tide, but not during neap tide. The coral reef islets in the Bay of Banten may constitute an important cause of energy dissipation and associated high levels of turbulence. Further research is needed to establish the relevance of interaction between spring-neap tidal cycles and low-frequency flow.

# 4

## Flow asymmetry associated with astronomical tides: implications for the residual transport of sediment

*With Piet Hoekstra and Bas van Maren, conditionally accepted by Journal of Geophysical Research*

### 4.1 Abstract

Tidal current asymmetry is usually associated to nonlinear tidal interactions in shallow water, generating compound tides and overtides. The present chapter demonstrates that tidal asymmetry is not only caused by nonlinear tidal interaction, but is also generated by astronomical tides in absence of shallow-water effects. In particular, the  $K_1$ ,  $O_1$  and  $M_2$  constituents give an asymmetrical periodic flow pattern, with the largest peak velocities persistently in the same direction. A theoretical explanation for this phenomenon is presented, and an inventory is made of other, subordinate constituents that may contribute to repetitive asymmetric flow patterns. Tidal current asymmetry may induce residual transport of sediment. Analytical expressions are derived which quantify the residual transport of sediment due to the  $K_1$ ,  $O_1$  and  $M_2$  tides, as a function of the phases and amplitudes of these constituents, and the time lag between variation in suspended sediment transport and flow velocity. The residual transport induced by the  $K_1$ ,  $O_1$  and  $M_2$  tides is compared to the residual transport due to the asymmetry associated with the  $M_2$  and  $M_4$  tides. The former mechanism is particularly relevant in diurnal, or mixed, mainly diurnal tidal regimes, where the  $K_1$  and  $O_1$  tides are dominant.

### 4.2 Introduction

Tidal current asymmetry may be defined as the periodic difference between the peak velocities and time span of ebb and flood currents. The importance of tidal asymmetries in the transport and accumulation of sediments in tidal systems is well established, which appears from studies of tidal rivers and estuaries (Dronkers, 1986;

Friedrichs, 1988; Van de Kreeke & Robaczewska, 1993; Van de Kreeke, 1997), tidal inlets (Aubrey & Friedrichs, 1988; Boon, 1988; Wang et al., 1995), tidal basins (Postma, 1961; Ridderinkhof, 1988a,b) and studies focussing on the offshore (Pingree & Maddock, 1978; Pingree & Griffiths, 1979; Van der Molen, 2000). The occurrence of tidal current asymmetry is generally associated with the nonlinear interaction of the barotropic  $M_2$  tide either with itself or with other, subordinate, principal tides such as  $S_2$ ,  $K_1$  and  $O_1$  (Aubrey & Speer, 1985; Aubrey & Friedrichs, 1988; Parker, 1991). In this chapter it is demonstrated that the systematic asymmetry of a tidal curve may also be caused by the astronomical tidal constituents, in absence of nonlinear tidal interaction, and that this general feature may be particularly relevant to the residual sediment transport in diurnal tidal regimes.

The role of astronomical tides in tidal flow asymmetry has been recently addressed by Ranasinghe & Pattiaratchi (2000). They found that in narrow inlets, located in diurnal regimes where nonlinear effects are insignificant, tidal velocity asymmetry is a direct consequence of the oceanic tidal forcing. In their paper, the conclusion is drawn that simple phase angle relationships to predict flood/ebb dominance cannot be derived for diurnal tidal systems, unlike in semidiurnal systems, where overtides and compound tides are the dominant cause of tidal asymmetry. However, the systematic asymmetry in a tidal signal is not restricted to tidal constituents whose periods can be expressed in terms of sums or differences of one or more principle tidal constituents, as in the cases of overtides and compound tides. The present chapter introduces a novel kind of tidal current asymmetry, caused by interaction of  $K_1$ ,  $O_1$  and  $M_2$ , which have angular frequencies composed of sums and differences of two basic astronomical frequencies. As a result of this interaction, a simple phase angle relationship to predict flood/ebb dominance does exist, which is presented here.

This chapter is structured as follows. Section 4.3 reveals that a tidal signal composed of  $K_1$ ,  $O_1$  and  $M_2$  oscillation may exhibit an asymmetrical periodic pattern, with the largest velocities during consecutive spring-neap cycles persistently in the same direction, despite the fact that the duration of the spring-neap cycle induced by the  $K_1$  and  $O_1$  tides does not coincide with a multiple of  $K_1$ ,  $O_1$  or  $M_2$  periods. It describes how this type of tidal asymmetry depends on an angular frequency relation between the three tidal constituents involved. Section 4.4 explores other constituents that contribute to the multi-constituent flow asymmetry. Sections 4.5 and 4.6 then discuss the implications for bedload and suspended-load transport of sediment, respectively, and Section 4.7 concludes this chapter by summarizing the main findings.

### 4.3 Asymmetry associated with the $K_1$ , $O_1$ and $M_2$ tides

The astronomical motions of the moon-earth-sun system that drive tides on earth involve six basic frequencies (Pugh, 1987). The angular frequency of each astronomical tidal constituent can be expressed in terms of sums and differences of these six basic

**Table 4.1.** Doodson numbers and relative amplitude in the Equilibrium Tide of the main diurnal and semidiurnal tidal constituents (see Eq. 4.1). Modified after Pugh (1987).

	$i_a$	$i_b$	$i_c$	$i_d$	$i_e$	$i_f$	H ( $M_2 = 1$ )
$2Q_1$	1	-3	0	2	0	0	0.011
$\sigma$	1	-3	2	0	0	0	0.013
$Q_1$	1	-2	0	1	0	0	0.079
$\rho$	1	-2	2	1	0	0	0.015
$O_1$	1	-1	0	0	0	0	0.415
$M_1$ {	1	0	0	-1	0	0	0.012
	1	0	0	0	0	0	0.007
	1	0	0	-1	0	0	0.033
$\Psi_1$	1	0	2	-1	0	0	0.006
$\pi_1$	1	1	-3	0	0	1	0.011
$P_1$	1	1	-2	0	0	0	0.193
$S_1$	1	1	-1	0	0	0	-
$K_1$ {	1	1	0	0	0	0	0.399
	1	1	0	0	0	0	0.185
$\chi$	1	1	1	0	0	-1	0.005
$\varphi$	1	1	2	0	0	0	0.008
$\theta$	1	2	-2	1	0	0	0.006
$J_1$	1	2	0	-1	0	0	0.033
$OO_1$	1	3	0	0	0	0	0.018
$2N_2$	2	-2	0	2	0	0	0.025
$\mu_2$	2	-2	2	0	0	0	0.031
$N_2$	2	-1	0	1	0	0	0.192
$\nu_2$	2	-1	2	-1	0	0	0.036
$M_2$	2	0	0	0	0	0	1.000
$\lambda_2$	2	1	-2	2	0	0	0.007
$L_2$ {	2	1	0	-1	0	0	0.028
	2	1	0	1	0	0	0.007
$T_2$	2	2	-3	0	0	1	0.027
$S_2$	2	2	-2	0	0	0	0.465
$R_2$	2	2	-1	0	0	-1	0.004
$K_2$ {	2	2	0	0	0	0	0.087
	2	2	0	0	0	0	0.040

frequencies  $\omega_1 - \omega_6$  (Doodson, 1921; Pugh, 1987):

$$\omega = i_a\omega_1 + i_b\omega_2 + i_c\omega_3 + i_d\omega_4 + i_e\omega_5 + i_f\omega_6 \quad (4.1)$$

where  $\omega_N$  denotes the angular frequency of constituent N, with unit rad/s, and the coefficients  $i_a$  to  $i_f$  are small integers known as Doodson numbers. A set of constituents with a common  $i_a$  is called a species (Doodson, 1921; Godin, 1972). Table 4.1 displays the Doodson numbers for the major astronomical tidal constituents and their amplitudes in the Equilibrium Tide, relative to  $M_2$ . The angular frequencies of the two largest diurnal species, viz.  $K_1$  and  $O_1$ , as well as the largest semidiurnal species, viz.  $M_2$ , are composed of merely two basic angular frequencies. A flow component,  $U$ , composed of these three constituents can be expressed as:

$$\begin{aligned} U = & A_{K_1} \cos((\omega_1 + \omega_2)t - \phi_{K_1}) \\ & + A_{O_1} \cos((\omega_1 - \omega_2)t - \phi_{O_1}) \\ & + A_{M_2} \cos(2\omega_1 t - \phi_{M_2}) \end{aligned} \quad (4.2)$$



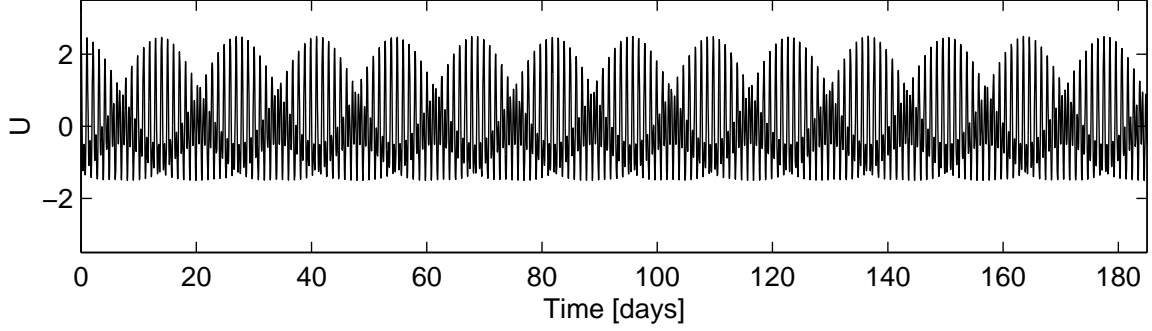


**Figure 4.1.** Variation of  $U$  for  $A_{K_1} = A_{M_2} = 1$ ,  $A_{O_1} = 1/2$  and  $\phi_{K_1} = \phi_{O_1} = \phi_{M_2} = 0$  (Eq. 4.2), which yields an asymmetrical periodic pattern. Peak velocities are largest for positive values of  $U$  during spring tide and for negative values of  $U$  during neap tide.

where  $A_N$  and  $\phi_N$  denote the amplitude and phase of constituent  $N$ , respectively. The duration of the spring-neap cycle, denoted  $T$ , coincides with the synodic period of  $K_1$  and  $O_1$ , which amounts to  $2\pi/\{(\omega_1 + \omega_2) - (\omega_1 - \omega_2)\} = \pi/\omega_2$ , or 13.66 days. Fig. 4.1 demonstrates that for  $A_{K_1} = A_{M_2} = 1$ ,  $A_{O_1} = 1/2$  and  $\phi_{K_1} = \phi_{O_1} = \phi_{M_2} = 0$ , consecutive spring-neap cycles of  $U$  over half a year show a systematic asymmetry, despite the fact that  $U(t) \neq U(t + T)$ .

To investigate the extent to which the observed asymmetry is restricted to the chosen phases and time span, a combined diurnal tide is defined as the summation of the complex representations of the  $K_1$  and  $O_1$  tides:

$$\begin{aligned} a_1(t)e^{i\varphi_1(t)} &= A_{K_1}e^{i((\omega_1+\omega_2)t-\phi_{K_1})} \\ &\quad + A_{O_1}e^{i((\omega_1-\omega_2)t-\phi_{O_1})} \end{aligned} \quad (4.3)$$

where  $a_1(t)$  and  $\varphi_1(t)$  are the time-varying amplitude and phase of the combined diurnal tide, respectively, and  $i$  is the imaginary unit. The analytical relationships that give the structures of the time-varying amplitude  $a_1$  and phase  $\varphi_1$  read

$$a_1 = \{A_{K_1}^2 + A_{O_1}^2 + 2A_{K_1}A_{O_1}\cos(2\omega_2t + \phi_{O_1} - \phi_{K_1})\}^{1/2} \quad (4.4)$$

$$\varphi_1 = \omega_1t - \lambda \quad (4.5)$$

where

$$\lambda = \arctan \frac{A_{K_1} \sin(\phi_{K_1} - \omega_2t) + A_{O_1} \sin(\phi_{O_1} + \omega_2t)}{A_{K_1} \cos(\phi_{K_1} - \omega_2t) + A_{O_1} \cos(\phi_{O_1} + \omega_2t)} \quad (4.6)$$

Similarly,  $a_2(t)$  and  $\varphi_2(t)$  are defined as:

$$a_2(t)e^{i\varphi_2(t)} = A_{M_2}e^{i(2\omega_1t-\phi_{M_2})} \quad (4.7)$$

This type of representation has been derived from Wang et al. (1999), who addressed a similar subject by analyzing amplitude ratios and phase differences between combined semidiurnal and quarter diurnal tides. Accordingly, an equivalent expression for (4.2) reads

$$\begin{aligned} U &= \text{Re} [a_1(t)e^{i\varphi_1(t)} + a_2(t)e^{i\varphi_2(t)}] \\ &= a_1 \cos(\omega_1t - \lambda) + a_2 \cos(2\omega_1t - \phi_{M_2}) \end{aligned} \quad (4.8)$$

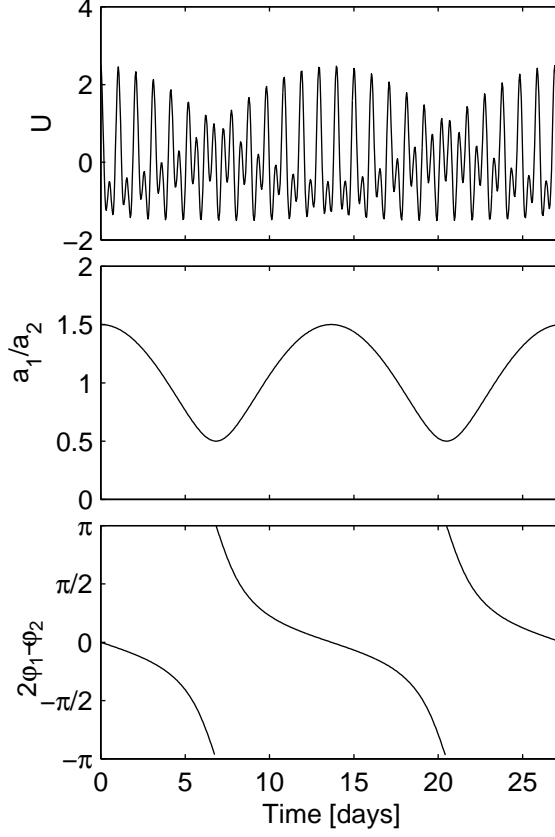


**Figure 4.2.** Variation of  $U$  (top panel),  $a_1/a_2$  (middle panel) and  $2\varphi_1 - \varphi_2$  (bottom panel) over two spring-neap cycles

where  $Re$  defines an operator to obtain the complex real part. Using the fact that  $\lambda$  is approximately constant over the time-span of a lunar day, the prerequisites for symmetry of  $U$  can be derived by defining a symmetry axis at the time of slack water for the diurnal tide:

$$\hat{t} = t - \frac{\lambda}{\omega_1} - \frac{\pi}{2\omega_1} \quad (4.9)$$

A symmetric velocity profile requires that

$$U(\hat{t}) + U(-\hat{t}) = 0 \quad (4.10)$$

This condition is satisfied provided that  $2\lambda - \phi_{M_2} = \pm\pi/2$ , which is equivalent to  $2\varphi_1 - \varphi_2 = \pm\pi/2$ , or trivially, if either  $a_1$  or  $a_2$  equals zero. This may be verified by substituting  $2\varphi_1 = \pm\pi/2 + \varphi_2$  into (4.8). Using Euler's formula, (4.8) then reduces to:

$$U = (a_1 \cos \frac{\pi}{4} + a_2) \cos \varphi_2 \pm a_1 \sin \frac{\pi}{4} \sin \varphi_2 \quad (4.11)$$

which denotes a symmetric signal when  $a_1$  is considered constant. For non-zero values of  $a_1$  and  $a_2$ , and values of  $2\varphi_1 - \varphi_2$  within the domain  $(-\pi/2, \pi/2)$ , the tide is asymmetric and the largest velocity peaks occur for positive values of  $U$ . Moreover,

for nonzero values of  $a_1$  and  $a_2$  and values of  $2\varphi_1 - \varphi_2$  within the domain  $[-\pi, -\pi/2) \cup (\pi/2, \pi]$ , the tide is asymmetric with the largest velocity peaks towards negative values of  $U$ . The asymmetry becomes more pronounced for values of the amplitude ratio  $a_1/a_2$  closer to one.

Fig. 4.2 illustrates the variation of  $a_1/a_2$  and  $2\varphi_1 - \varphi_2$  over two successive spring-neap cycles of  $U$ , for the same tidal parameters as in Fig. 4.1. The repetitive pattern of the amplitude ratio as well as phase difference parameter suggests that the variation of the degree and orientation of the occurring tidal asymmetry is identical for consecutive spring-neap cycles of period  $T$ . Using (4.3) and (4.7), it can be shown after elaboration that indeed  $a_1(t+T)/a_2(t+T) = a_1(t)/a_2(t)$ , and that  $2\varphi_1(t+T) - \varphi_2(t+T) = 2\varphi_1(t) - \varphi_2(t)$ :

$$\frac{a_1(t+T)}{a_2(t+T)} e^{i(2\varphi_1(t+T) - \varphi_2(t+T))} = \frac{a_1(t)}{a_2(t)} e^{i(2\varphi_1(t) - \varphi_2(t))} \quad (4.12)$$

This analysis demonstrates that the variation of the degree and orientation of the tidal asymmetry over a spring-neap cycle of  $U$  is identical to the variation of the tidal asymmetry in the spring-neap cycles that succeed, irrespective of the amplitudes  $A_{K_1}$ ,  $A_{O_1}$  and  $A_{M_2}$  and phases  $\phi_{K_1}$ ,  $\phi_{O_1}$  and  $\phi_{M_2}$ .

## 4.4 Generalization to other tidal constituents

A number of diurnal and semidiurnal tidal constituents other than  $K_1$ ,  $O_1$  and  $M_2$  have angular frequencies exclusively composed of the basic astronomic frequencies either both  $\omega_1$  and  $\omega_2$ , or one of these two basic frequencies. These include the astronomical tidal constituents  $OO_1$ ,  $K_2$ , the exact subharmonic  $M_1(\omega_1)$  (Table 4.1) and five nameless constituents with angular frequencies  $\omega_1 + 2\omega_2$ ,  $2\omega_1 - \omega_2$ ,  $2\omega_1 + \omega_2$ ,  $2\omega_1 + 3\omega_2$ ,  $2\omega_1 + 4\omega_2$ , as well as the diurnal and semidiurnal compound tides associated to the total of the aforementioned astronomical tides. The nameless tidal constituents and compound tides are not included in Table 4.1 for reasons of concision; a comprehensive list of constituents derived from Doodson's development of the tidal potential is provided by Doodson (1921) and Godin (1972). To analyze the asymmetry associated with diurnal and semidiurnal tidal constituents with frequencies composed of  $\omega_1$  and  $\omega_2$  only, the combined diurnal and semidiurnal tides in (4.3) and (4.7) may be generalized to:

$$a_1(t) e^{i\varphi_1(t)} = \sum_d A_d e^{i((\omega_1 + N_d \omega_2)t - \phi_d)} \quad (4.13)$$

and

$$a_2(t) e^{i\varphi_2(t)} = \sum_s A_s e^{i((2\omega_1 + N_s \omega_2)t - \phi_s)} \quad (4.14)$$

where  $A_d$ ,  $N_d$  and  $\phi_d$  are respectively the amplitude, Doodson number  $i_b$  and phase of diurnal tidal constituent  $d$  and  $A_s$ ,  $N_s$  and  $\phi_s$  are respectively the amplitude, Doodson number  $i_b$  and phase of semidiurnal tidal constituent  $s$ . For this generalized formulation the validity of (4.12) may be investigated by substituting (4.13) and (4.14)

in the term left from the equality sign in (4.12):

$$\frac{a_1(t+T)}{a_2(t+T)} e^{i(2\varphi_1(t+T)-\varphi_2(t+T))} = \frac{\sum_d A_d e^{i2\pi N_d} e^{i2((\omega_1+N_d\omega_2)t-\phi_d)}}{\sum_s A_s e^{i\pi N_s} e^{i((2\omega_1+N_s\omega_2)t-\phi_s)}} \quad (4.15)$$

Provided that  $N_s$  is even for each semidiurnal constituent, (4.15) reduces to (4.12). Similarly, it can be shown that if  $N_s$  is uneven for one of the semidiurnal constituents, the amplitude ratio  $a_1(t)/a_2(t)$  and phase difference  $2\varphi_1(t) - \varphi_2(t)$  are cyclic with period  $2T$ . Hence, the tidal current asymmetry associated to a subset of constituents within the diurnal and semidiurnal species satisfying  $i_c = i_d = i_e = i_f = 0$ , and for which values of  $N_s$  are even, may be analyzed from the variation of  $a_2(t)/a_1(t)$  and  $2\varphi_1(t) - \varphi_2(t)$  over a single spring-neap cycle with period  $\pi/\omega_2$ . If the former condition is met, but one or more values of  $N_s$  are uneven, the variation of  $a_2(t)/a_1(t)$  and  $2\varphi_1(t) - \varphi_2(t)$  features a cyclic pattern with a period of two spring-neap cycles.

Tidal constituents that satisfy  $i_c = i_d = i_e = i_f = 0$  are not restricted to the diurnal and semidiurnal species and these may also influence the degree and orientation of the tidal asymmetry. Within the long-period species ( $i_a = 0$ ), the angular frequency of lunar semi-monthly  $M_f$  tide coincides with  $2\omega_2$  and there is a nameless constituent with angular frequency  $3\omega_2$  (Doodson, 1921; Godin, 1972). Within the terdiurnal species ( $i_a = 3$ ),  $M_3$  has an angular frequency that corresponds to  $3\omega_1$  and a nameless constituent has angular frequency  $3\omega_1 + 2\omega_2$ . Furthermore, compound and overtides in the terdiurnal, quarterdiurnal, fifth-diurnal, etc., species, generated by astronomical tides satisfying  $i_c = i_d = i_e = i_f = 0$ , have angular frequencies that may also be written as sums and differences of the basic frequencies  $\omega_1$  and  $\omega_2$ . Each of these tidal constituents may systematically modify the asymmetry of a tidal curve for consecutive periods of one or two spring-neap cycles, yet many of them may be insignificant.

## 4.5 Implications for residual bedload transport

Marine sediments can move as either bedload or suspended load (see e.g. Dyer (1986)). In absence of waves, bedload transport,  $S_{bed}$ , can be assumed proportional to  $(|u| - u_{cr})^b$ , where  $|u|$  denotes the absolute flow velocity,  $u_{cr}$  is a critical value of the current velocity that accounts for the threshold of sediment motion and  $b$  is a constant power in between 2 and 7. The values of  $b$  and  $u_{cr}$  primarily depend on the prevailing sediment characteristics and bedforms. Provided that the threshold velocity for sediment motion is negligible and  $b = 3$ , the rate of the residual bedload transport due to the tidal motion is proportional to the  $\langle u^3 \rangle$ . Under these assumptions, the degree and orientation of a residual bedload transport due to a flow component  $U$ , defined as in Eq. 4.2, depends on the time-average of  $U^3$ . The average of  $U^3$  over a spring-neap cycle can be calculated from:

$$\langle U^3 \rangle_{s-n} = \frac{1}{T} \int_{t-T/2}^{t+T/2} U(t')^3 dt' \quad (4.16)$$

where  $\langle \cdot \rangle_{s-n}$  denotes the time-average over a spring-neap cycle. After elaboration, (4.16) yields a lengthy expression (not shown) that is time dependent due to the fact

that  $U(t) \neq U(t+T)$ . When integrating over an infinite number of spring-neap cycles, however, the time dependence vanishes and a more instructive expression is obtained:

$$\begin{aligned} \langle U^3 \rangle_\infty &= \lim_{\tau \rightarrow \infty} \frac{1}{\tau} \int_0^\tau U(t')^3 dt' \\ &= \frac{3}{2} A_{K_1} A_{O_1} A_{M_2} \cos(\phi_{K_1} + \phi_{O_1} - \phi_{M_2}) \end{aligned} \quad (4.17)$$

where  $\langle \cdot \rangle_\infty$  denotes the time-average over an infinitely long time interval. The presence of a threshold velocity has no severe implications, i.e. the orientation of a residual bedload transport is independent of the threshold of sediment motion. During the stages of the tide when the current velocity is below the threshold, the contribution to the residual bedload transport equals zero. For a flood-dominant system, the duration of zero-bedload conditions during flood is often shorter than that during the ebb, and vice versa for an ebb-dominant system. Consequently, the threshold velocity may even enhance the asymmetry of tidally driven bedload transport.

As indicated in the foregoing, the third power ( $b = 3$ ) in (4.17) may be lower or higher. The value of  $b$  only affects dependence of the bedload transport on the amplitudes, which is illustrated by the solution for  $\langle U^5 \rangle_\infty$ :

$$\begin{aligned} \langle U^5 \rangle_\infty &= \lim_{\tau \rightarrow \infty} \frac{1}{\tau} \int_0^\tau U(t')^5 dt' \\ &= \frac{15}{4} A_{K_1} A_{O_1} A_{M_2} (A_{K_1}^2 + A_{O_1}^2 + A_{M_2}^2) \cos(\phi_{K_1} + \phi_{O_1} - \phi_{M_2}) \end{aligned} \quad (4.18)$$

Inequality between flood and ebb velocity maxima may be termed maximum flow asymmetry (Nichols & Boon, 1994). Eqs. 4.17 and 4.18 indicate that the amplitudes of each of the three tidal constituents play an equal role in the degree in which maximum flow asymmetry induces residual transport of bedload material. The direction of the residual bedload transport is determined by the phase difference  $\phi_{K_1} + \phi_{O_1} - \phi_{M_2}$ .

The  $M_4$  tide is generally the most energetic amongst the occurring compound tides and overtides. The bedload transport mechanism due to the interaction between  $K_1$ ,  $O_1$ , and  $M_2$  can be compared to bedload transport due to  $M_2$  interaction with  $M_4$  by analyzing a flow component,  $V$ , composed of  $K_1$ ,  $O_1$ ,  $M_2$  and  $M_4$  oscillation. These four constituents generally capture a large portion of the cyclic asymmetry in a tidal signal in shallow waters, and are consequently likely to determine the magnitude and direction of bedload transport. A definition of  $V$  reads:

$$\begin{aligned} V &= A_{K_1} \cos((\omega_1 + \omega_2)t - \phi_{K_1}) \\ &\quad + A_{O_1} \cos((\omega_1 - \omega_2)t - \phi_{O_1}) \\ &\quad + A_{M_2} \cos(2\omega_1 t - \phi_{M_2}) \\ &\quad + A_{M_4} \cos(4\omega_1 t - \phi_{M_4}) \end{aligned} \quad (4.19)$$

where  $A_{M_4}$  and  $\phi_{M_4}$  are the phase and amplitude of the  $M_4$  tide and the other parameters are defined as in (4.2). Assuming  $b = 3$  and  $u_{cr} = 0$ , the residual bedload

transport associated to  $V$  is proportional to:

$$\begin{aligned} \langle V^3 \rangle_\infty &= \lim_{\tau \rightarrow \infty} \frac{1}{\tau} \int_0^\tau V(t')^3 dt' \\ &= \frac{3}{2} A_{K_1} A_{O_1} A_{M_2} \cos(\phi_{K_1} + \phi_{O_1} - \phi_{M_2}) \\ &\quad + \frac{3}{4} A_{M_2}^2 A_{M_4} \cos(2\phi_{M_2} - \phi_{M_4}) \end{aligned} \quad (4.20)$$

The first term in this solution coincides with the result in (4.17), expressing the contribution of the  $K_1$ ,  $O_1$  and  $M_2$  interaction. The second term expresses the contribution of  $M_2$  interacting with  $M_4$ , and was previously derived by Van de Kreeke & Robaczewska (1993). Eq. 4.20 shows that with no foreknowledge of the tidal phases, the relative importance of both contributions depends on the ratio  $\frac{3}{2} A_{K_1} A_{O_1} A_{M_2}$  to  $(\frac{3}{4} A_{M_2}^2 A_{M_4})$ . The residual bedload transport associated with the diurnal astronomical tides is then expectedly dominant if:

$$2A_{K_1} A_{O_1} > A_{M_2} A_{M_4} \quad (4.21)$$

Remarkably, none of the terms in (4.20) contains contributions of both the diurnal tides and  $M_4$ . This suggests there is no residual bedload transport due to interaction between  $K_1$ ,  $O_1$  and  $M_4$ . However, assuming  $b = 5$  the long-term average of  $V^b$  reads:

$$\begin{aligned} \langle V^5 \rangle_\infty &= \lim_{\tau \rightarrow \infty} \frac{1}{\tau} \int_0^\tau V(t')^5 dt' \\ &= \Lambda_1 \cos(\phi_{K_1} + \phi_{O_1} - \phi_{M_2}) \\ &\quad + \Lambda_2 \cos(2\phi_{M_2} - \phi_{M_4}) \\ &\quad + \Lambda_3 \cos(2\phi_{K_1} + 2\phi_{O_1} - \phi_{M_4}) \end{aligned} \quad (4.22)$$

where

$$\Lambda_1 = \frac{15}{4} (A_{K_1}^2 + A_{O_1}^2 + A_{M_2}^2 + 2A_{M_4}^2) A_{K_1} A_{O_1} A_{M_2} \quad (4.23)$$

$$\Lambda_2 = \frac{15}{4} (A_{K_1}^2 + A_{O_1}^2 + \frac{1}{3} A_{M_2}^2 + \frac{1}{2} A_{M_4}^2) A_{M_2}^2 A_{M_4} \quad (4.24)$$

$$\Lambda_3 = \frac{15}{8} A_{K_1}^2 A_{O_1}^2 A_{M_4} \quad (4.25)$$

Eqs. 4.22 to 4.25 demonstrate that for  $b = 5$  the bedload transport associated with interaction between the astronomical diurnal tidal constituents and  $M_2$  cannot be separated from the contribution of the interaction between  $M_2$  and the shallow-water  $M_4$  tide. Whether or not residual bedload transport due to interaction between  $K_1$ ,  $O_1$  and  $M_4$  occurs thus depends on the power  $b$ .

## 4.6 Implications for residual suspended load transport

Suspended load transport responds to changes in flow velocity with a time lag. For increasing flow rates, sediment is being entrained near the bed and moves vertically

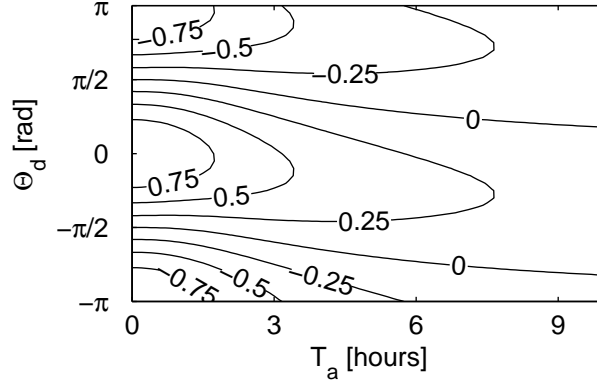


**Figure 4.3.** Variation of  $F_d$  as a function of  $\Theta_d$  and  $T_a$ . Isolines are drawn between -1 and 1 with intervals of 0.25

upward until a steady state is reached. This occurs when the upward forcing of sediment particles due to turbulence is balanced by downward forcing from gravity. In a decelerating flow, partial settling of sediments takes place until a new equilibrium transport rate is reached. A characteristic time scale for the adaptation of suspended load transport to flow velocity is  $d/w_s$ , where  $w_s$  is the particle settling velocity and  $d$  denotes water depth. The time lag between flow velocity variation and the associated response of the suspended sediment concentration is therefore particularly relevant for finer particles, with smaller settling velocities.

For fine sediments, suspended load transport rates thus depend on the history of the flow velocity. Consequently, tide-induced residual transports are not merely due to maximum flow asymmetry, but depend also on asymmetries in flow acceleration. This mechanism can be mathematically modelled starting from the relaxation process that describes the adaptation of the instantaneous depth-mean sediment concentration,  $c$ , to an equilibrium concentration  $c_e$ , which depends on the instantaneous flow velocity,  $u$  (Groen, 1967):

$$\frac{\partial c}{\partial t} = \frac{c_e - c}{T_a} \quad (4.26)$$

where  $T_a$  is the adaptation time. The general solution to (4.26) reads:

$$c = e^{-\frac{t}{T_a}} \left\{ c_0 + \int_0^t \frac{c_e}{T_a} e^{\frac{t'}{T_a}} dt' \right\} \quad (4.27)$$

in which  $c_0$  is an initial value of  $c$ . Adopting the theory of Bagnold (1966),  $c_e$  can be equated with  $ku^2$ , where  $k$  is a constant of proportionality. The suspended load transport rate,  $S_{sus}$ , can be approximated by  $S_{sus} = cu$  by ignoring depth variation of  $c$  and  $u$ . These assumptions allow for an analytical analysis of the residual transport induced by the tidal asymmetry associated to the  $K_1$ ,  $O_1$ ,  $M_2$  and  $M_4$  tides. Defining  $V$  as in (4.19), the residual transport of suspended-load material subject to these tidal

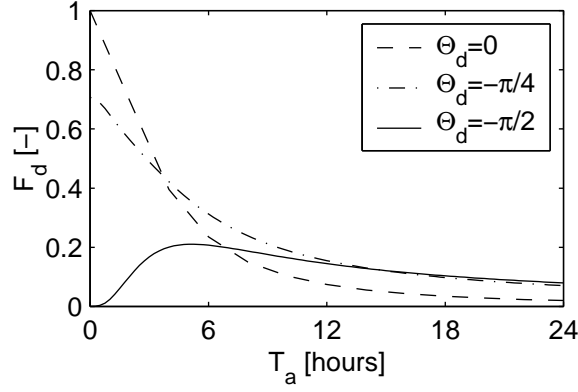


**Figure 4.4.** Variation of  $F_d$  as a function of  $T_a$  exemplified for  $\Theta_d = 0$ ,  $\Theta_d = -\pi/4$  and  $\Theta_d = -\pi/2$ .

constituents is described by:

$$\begin{aligned}
\langle S_{sus} \rangle_{\infty} &= \langle cV \rangle_{\infty} \\
&= \lim_{\tau \rightarrow \infty} \frac{1}{\tau} \\
&\quad \int_0^{\tau} V e^{-\frac{t}{T_a}} \left\{ c_0 + \int_0^t \frac{kV^2}{T_a} e^{-\frac{t'}{T_a}} dt' \right\} dt \\
&= \frac{3}{2} k A_{K_1} A_{O_1} A_{M_2} F_d + \\
&\quad \frac{3}{4} k A_{M_2}^2 A_{M_4} F_s
\end{aligned} \tag{4.28}$$

where

$$\begin{aligned}
F_d &= \frac{\cos \Theta_d + 2T_a \omega_1 \sin \Theta_d}{3 + 12T_a^2 \omega_1^2} \\
&\quad + \frac{\cos \Theta_d - T_a(\omega_1 + \omega_2) \sin \Theta_d}{3 + 3T_a^2(\omega_1^2 + 2\omega_1\omega_2 + \omega_2^2)} \\
&\quad + \frac{\cos \Theta_d - T_a(\omega_1 - \omega_2) \sin \Theta_d}{3 + 3T_a^2(\omega_1^2 - 2\omega_1\omega_2 + \omega_2^2)}
\end{aligned} \tag{4.29}$$

$$\Theta_d = \phi_{K_1} + \phi_{O_1} - \phi_{M_2} \tag{4.30}$$

$$\begin{aligned}
F_s &= \frac{\cos \Theta_s + 4T_a \omega_1 \sin \Theta_s}{3 + 48\omega_1^2 T_a^2} \\
&\quad + \frac{2 \cos \Theta_s - 4T_a \omega_1 \sin \Theta_s}{3 + 12\omega_1^2 T_a^2}
\end{aligned} \tag{4.31}$$

$$\Theta_s = 2\phi_{M_2} - \phi_{M_4} \tag{4.32}$$

Herein,  $F_d$  and  $F_s$  are attenuation factors within the range between -1 and 1, which depend on the phase differences  $\Theta_d$  and  $\Theta_s$ , respectively, and  $T_a$ . The component of the suspended load residual flux that relates to the  $K_1$  and  $O_1$  tides is independent of the  $M_4$  phase and amplitude, and vice versa, the residual flux component influenced by the  $M_4$  tide is independent of the phases and amplitudes of the  $K_1$  and  $O_1$  constituents. For  $T_a = 0$ ,  $\langle S_{sus} \rangle_{\infty} = k \langle V^3 \rangle_{\infty}$ , which coincides with  $c(t) = c_e(t)$ .



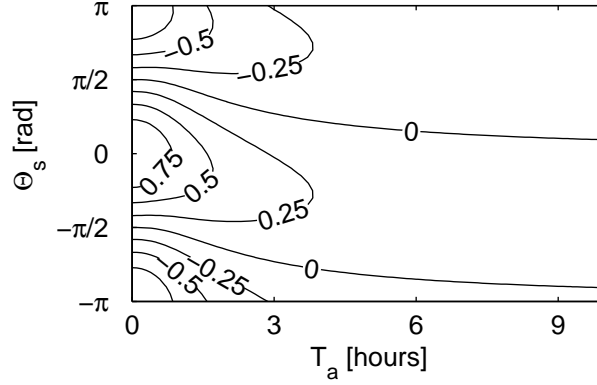


**Figure 4.5.** Variation of  $F_s$  as a function of  $\Theta_s$  and  $T_a$ . Isolines are drawn between -1 and 1 with intervals of 0.25

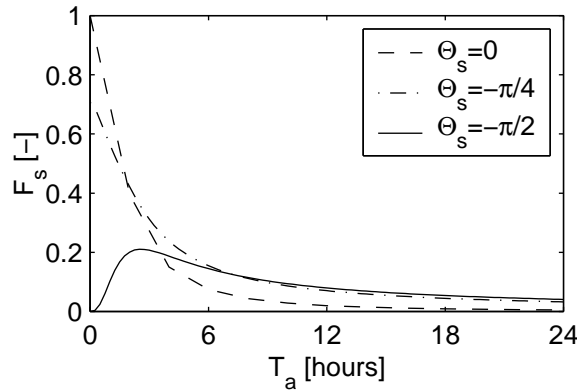


**Figure 4.6.** Variation of  $F_s$  as a function of  $T_a$  exemplified for  $\Theta_s = 0$ ,  $\Theta_s = -\pi/4$  and  $\Theta_s = -\pi/2$ .

The dependence of  $F_d$  on  $\Theta_d$  and  $T_a$  is illustrated in Figs. 4.3 and 4.4. For increasing  $T_a$ , the absolute value of  $F_d$ ,  $|F_d|$ , either decreases monotonously to zero or endures an initial increase followed by a monotonous decrease to zero. The dependence of  $F_s$  on  $\Theta_s$  and  $T_a$  qualitatively displays the same pattern (Figs. 4.5 and 4.6). It can be shown that  $F_s(T_a = x, \Theta_s = y) \simeq F_d(T_a = 2x, \Theta_d = y)$  for any  $(x, y)$ , by substituting  $\omega_2 = 0$  in (4.29), which is in a first order approximation allowable since  $\omega_1 \gg \omega_2$ . Consequently, the time lag mechanism generally has a stronger influence on the residual sediment flux associated to the  $M_2/M_4$ -induced flow asymmetry than on the residual flux due to the interaction of the  $K_1$ ,  $O_1$  and  $M_2$  tides.

Figs. 4.4 and 4.6 indicate that suspended sediment transport may occur in absence of maximum flow asymmetry, viz. when  $\Theta_d = \Theta_s = -\pi/2$ , which was already established by Groen (1967). Under these conditions, peak values of  $F_d$  and  $F_s$  both amount to 0.21, whereas values of  $F_d$  and  $F_s$  both culminate with 1 for  $\Theta_d = \Theta_s = 0$ , and zero time lag. These two extremes lead to the conclusion that maximum flow asymmetries are capable of generating a residual transport of suspended load material that is approximately five times larger than that caused by the lag effect in symmetrical flow.

## 4.7 Conclusions and relevance

The angular frequencies of astronomical and shallow-water tidal constituents can be expressed in terms of sums and differences of six basic astronomical frequencies, viz.  $\omega_1, \omega_2, \dots, \omega_6$  (Doodson, 1921). A subset of these constituents can be expressed in terms of sums and differences of  $\omega_1$  and  $\omega_2$  only, including the two major diurnal constituents, viz.  $K_1$  and  $O_1$ , and the major semidiurnal constituent,  $M_2$ . A tidal curve exclusively composed of these three principal constituents is subject to a spring-neap cycle with period  $\pi/\omega_2$ , or 13.66 days. The asymmetry of such a tidal curve is identical for consecutive spring-neap cycles, and therefore cyclic, despite the fact that the period of the spring-neap cycle is not an exact multiple of  $K_1, O_1$  or  $M_2$  periods. In particular, the maximum flow velocities for consecutive spring-neap cycles persistently have the same sign, which implies flood or ebb dominance, depending on the sign. Other tidal constituents which may enhance or counteract flood or ebb dominance include  $M_f, M_1, OO_1, K_2, M_3$ , a set of seven nameless constituents, and the shallow-water tides generated by the aforementioned astronomical tidal constituents. These constituents, however, are generally subordinate.

The rate of bedload transport bears a nonlinear relation with flow velocity. Therefore, flow asymmetry may govern the degree and direction of residual bedload transport. The asymmetry inherent to a flow component  $V$ , including contributions of the  $K_1, O_1, M_2$  and  $M_4$  tides, causes a residual bedload transport that was qualitatively analyzed by deriving theoretical expressions for the long-term averages of  $V^3$  and  $V^5$ . For the case of the long-term average of  $V^3$ , the contribution of the diurnal tides interacting with  $M_2$  is separable from the contribution due to the  $M_2$ - $M_4$  interaction. This is contrary to the case of  $V^5$ , for which interaction between  $K_1, O_1$  and  $M_4$  does contribute to the residual bedload transport.

The rate of suspended load transport responds to variation in flow velocity with a time lag that is larger for finer sediments. The suspended load transport rate is therefore not only influenced by the degree and orientation of the maximum flow asymmetry, but depends also on asymmetry in flow acceleration, in particular for fine sediments. These lag effects have been analyzed using a relaxation model that describes the response of the suspended load transport rate to a tidal current with contributions of the  $K_1, O_1, M_2$  and  $M_4$  tides. Asymmetries in flow maxima were found capable of generating a residual transport of suspended load material that is approximately five times larger than that caused by the lag effect in a symmetrical flow.

Tidally-induced residual transport of sediment is hence not restricted to shallow water, where nonlinear tidal interactions occur, but may be relevant to coastal dynamics in any marine environment subject to both diurnal and semidiurnal tidal motion. In regions where diurnal tides predominate, complete absence of semidiurnal tidal motion is exceptional, whereas in semidiurnal regimes, diurnal tides are often insignificant. The cyclic asymmetry association to the  $K_1, O_1$  and  $M_2$  tides is therefore particularly relevant to diurnal regimes. In Fig. 4.7 the worlds oceans and seas are classified according to the prevailing tidal regime, based on 12 months of altimeter

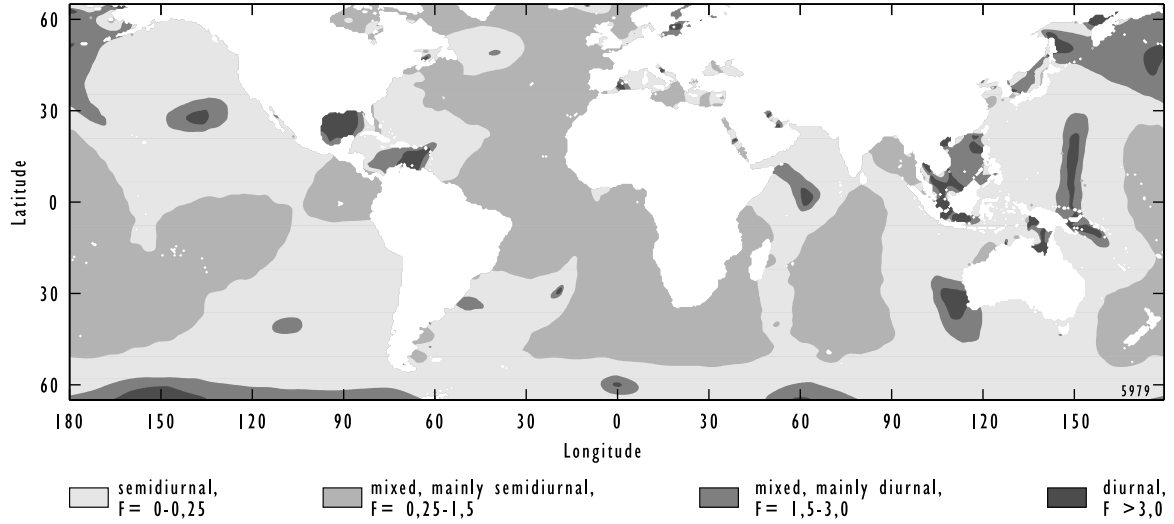


**Figure 4.7.** Tidal regimes of the world, classified according to the tidal form factor  $F = (A_{K_1} + A_{O_1}) / (A_{M_2} + A_{S_2})$ . The tidal amplitudes are derived from Schrama & Ray (1994).

data (cf. Schrama & Ray (1994)). The form factor  $F$  is defined as

$$F = \frac{A_{K_1} + A_{O_1}}{A_{M_2} + A_{S_2}} \quad (4.33)$$

where  $A_{S_2}$  is the amplitude of the  $S_2$  tide (Pugh, 1987). The areas subject to a diurnal regime cover large portions of the Southeast Asian waters, the Gulf of Mexico and the Caribbean Sea.

# 5

## Hydrodynamic control on the supply of reworked terrigenous sediment to coral reefs

*With Piet Hoekstra, conditionally accepted by Estuarine, Coastal and Shelf Sciences*

### 5.1 Abstract

The Bay of Banten (West Java, Indonesia) provides an extreme example of a shallow-water reef environment adjacent to an eroding delta system, where corals survive in turbid conditions. The present study addresses the hydrodynamic controls over residual fluxes of terrigenous sediment in the bay. Observations of wind, waves, currents and suspended sediment concentrations were made in 1998 and 1999. These revealed contrasting dynamic turbidity conditions influenced by tides, monsoon-driven flows and locally generated waves. The most sediment-rich suspensions originate from the shallow coastal margin of the inactive delta, where waves resuspend sediment and small creeks debouch. The coupling between monsoonal wind, throughflow in the bay and wave height entails that when wave-induced resuspension seasonally culminates, which occurs during the Northwest Monsoon, an eastward throughflow prevents the nearshore reefs in the bay from direct exposure to turbid water masses generated in the eroding delta. In offshore coastal waters, tidal asymmetry and spatial variation of current amplitudes cause residual sediment transport, largely depending on the availability of erodible sediment. Due to the relatively weak tidal and subtidal currents in the center of the bay where a patch reef complex is present, this region constitutes a sediment convergence zone.

### 5.2 Introduction

Over the past decades, it has been demonstrated that increased levels of turbidity and siltation in the coastal zone are a potential cause of coral reef degradation (Hubbard, 1986; Rogers, 1990; Babcock & Davies, 1991; Meesters et al., 1998; James et al., 2002). Whereas coral reefs are generally associated with pristine blue water

marine environments, many modern coral reefs experience prolonged inundation by suspensions of sediment with a terrigenous origin (Larcombe et al., 1995; Miller & Cruise, 1995; Fabricius & Wolanski, 2000). Local hydrodynamic mechanisms that may influence the sedimentary regime of coral reef environments have received ample attention in studies on eddy formation in the wake of reef islets (Wolanski et al., 1984a; Pattiaratchi et al., 1986; Deleersnijder et al., 1992), upwelling at reef slopes (Thompson & Golding, 1981; Thompson & Wolanski, 1984) and inter-reef dispersal of particles (Black, 1993; Wolanski & Sarsenski, 1997). Although the regional sedimentary regimes of nearshore reefs have been the focus of a number of geological studies (Roberts et al., 1992; Woolfe & Larcombe, 1999; Larcombe et al., 2001), the oceanographic sediment transport mechanisms in shallow-water reef environments are largely unexplored. Since these mechanisms determine the regional dispersion of terrigenous sediment, and the availability of terrigenous sediment in coastal waters surrounding the nearshore reefs, they need to be addressed.

The main forcing functions responsible for coastal flows dispersing coastal and riverine sediment include the astronomical tide, meteorological forcing and input of buoyancy. Gravitational circulation driven by the input of buoyancy constitutes the most apparent flow process, transporting sediment-laden river plumes in seaward direction. The degree in which a buoyant plume remains intact depends on turbulent mixing (e.g. Wolanski et al., 1984b; Geyer, 1995), exchanging salt and particles with the underlying saline waters, and on differential advection by coastal currents, which results in stretching of the plume and the formation of low-salinity patches (Wolanski et al., 1999). Our study site, the Bay of Banten, West Java, Indonesia (Fig. 5.1), presents a delta adjacent to a coral reef embayment, where the direct riverine impacts on coral reefs are subordinate due to reduced river discharges, vigorous mixing in the source region (Chapter 3) and rapid settling of riverine sediment. However, the former deltaic deposits are subject to reworking by waves in the shallow nearshore region (<3 m) and by currents in the deeper parts of the embayment. This chapter demonstrates that the regional dispersion of reworked sediment is controlled by the seasonal coupling between wave height, monsoon-driven flow and freshwater discharge, and by the asymmetry and spatial variation of the tidal currents.

The Bay of Banten provides an extreme example of a turbid shallow-water environment where coral reefs flourish or persist (Tomascik et al., 1997). The objective of the present study is to establish the hydrodynamic mechanisms controlling the supply of reworked terrigenous sediment to nearshore coral reefs, by focussing on the Bay of Banten. These mechanisms may not influence the levels of turbidity and siltation around coral reefs in a direct manner, but at least determine the amount of terrestrial sediment that is available for local resuspension by currents and waves at the reef slopes. This study is structured as follows. In Section 5.3 the field location is introduced, followed by a description of the data acquisition and processing in Section 5.4. Section 5.5 discusses the transport of sediment released from the delta as a result of wave erosion, associated to the monsoon-driven throughflow in the bay. Subsequently, the residual transport due to tidal asymmetry and spatial variation of tidal currents are addressed in Section 5.6. Section 5.7 concludes this chapter with a summary of the main results and a discussion.

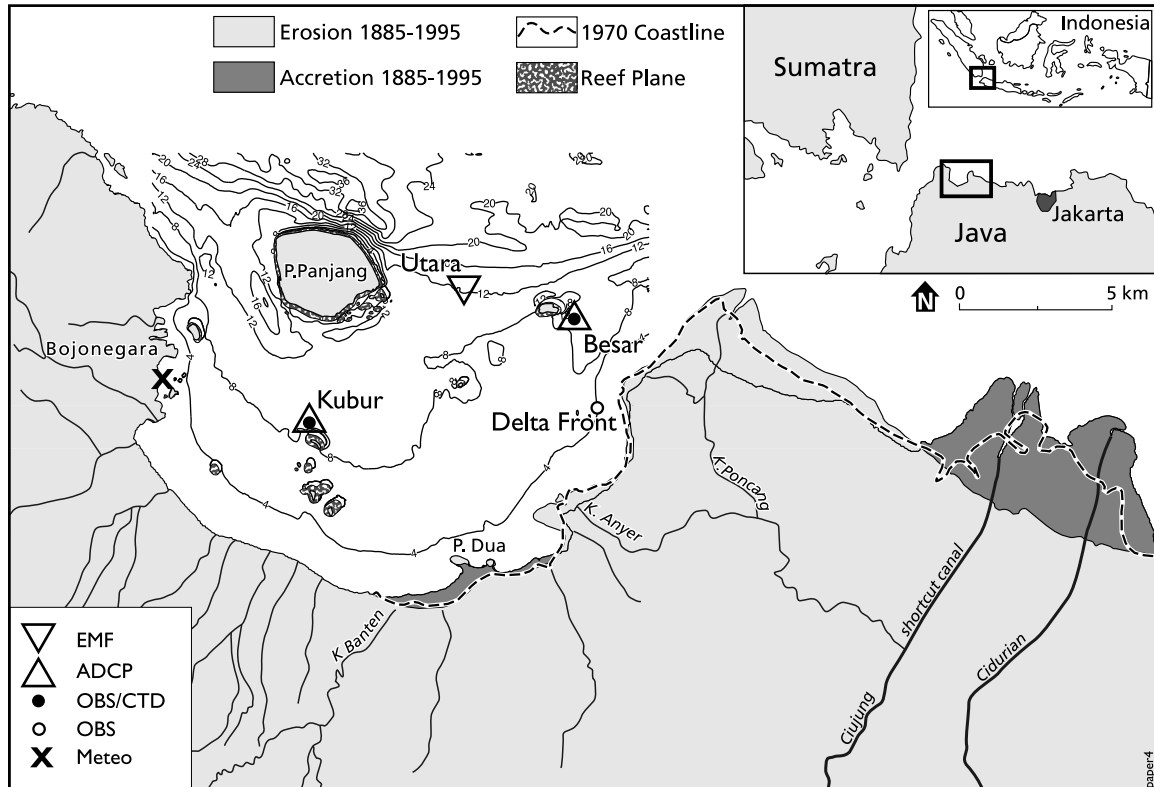


**Figure 5.1.** Index map showing shoreline changes associated to the diversion of the Ciujung in the 1920's, the reef flat areas in Teluk Banten and the location of the five experimental sites including the meteorological station

### 5.3 Field site

Teluk Banten (teluk means bay) is a shallow bowl-shaped embayment located along the northwestern coast of Java, which has experienced severe land degradation over the past century. The bay represents a circa 10 by 15 km wide Holocene sediment wedge containing predominantly silty clays, which are largely derived from the adjacent Ciujung (ci means river). The main distributary of the Ciujung was diverted to the east in the 1920's by means of a shortcut canal (Fig. 5.1). An abandoned delta resulted, characterized by a reduction of the sediment discharge after the inactivation of the river branch. Consequently, the northward progradation of the delta was halted and the canalization heralded a phase of retrogression of the inactivated delta, and the formation of a delta at the newborn river mouth. Fig. 5.1 illustrates the associated shoreline changes. Since the end of the 19th century the Ciujung delta has eroded some 3 km. A considerable portion of the erosion occurred in the period between 1970 and 1995, which suggests that the present coastal system not yet has reached an equilibrium and is thus still eroding. The bay's present bathymetry is displayed in Fig. 5.1.

The tidal regime in the bay is mixed, mainly diurnal, with a maximum surface elevation range of 85 cm. The tide-induced currents are primarily bidirectional and parallel to the bay's isobaths (Fig. 5.2). Despite the micro-tidal conditions, currents reach peak velocities of 65 cm/s. In between the island of Pamujan Besar and the

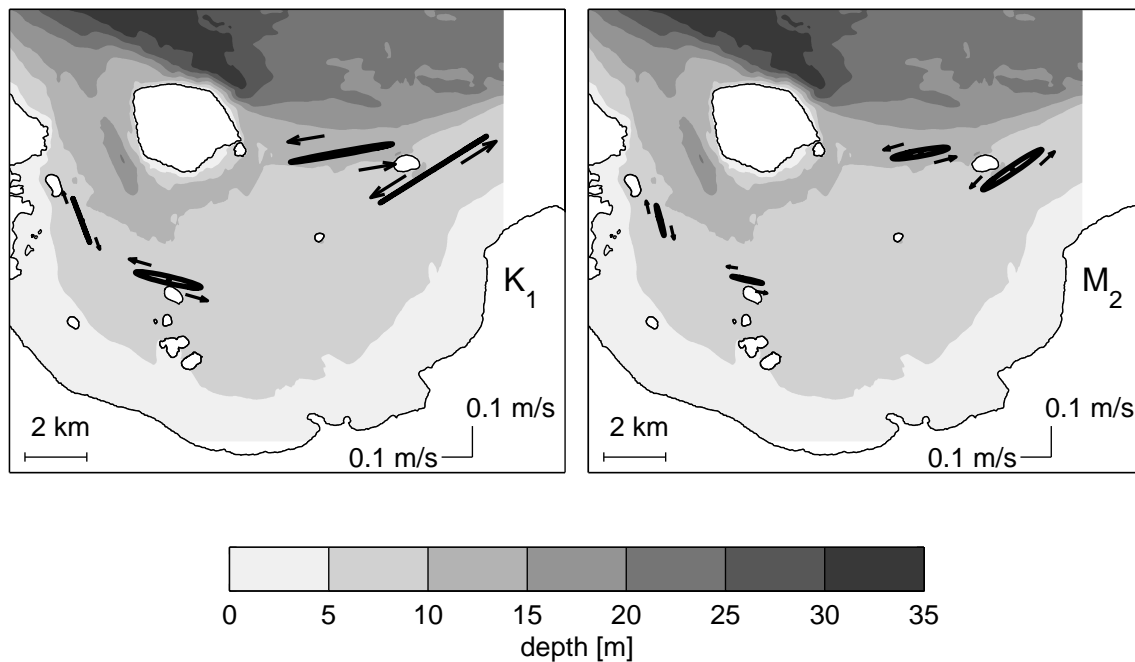


**Figure 5.2.** Surface current ellipses of the major diurnal and semidiurnal tidal constituents, viz.  $K_1$  and  $M_2$ . Tidal currents are largely bidirectional, and strongest at the submarine platform in front of the old delta. Arrows indicate the direction of rotation and the shading represents depth in meters.

former delta, the tidal flow is funnelled through an 8-m deep submarine platform that borders the eroding delta front. The delta hydrodynamically acts as a headland, which explains the relatively strong currents over the submarine delta front platform. At the northern margin of the bay, the late Pleistocene-Holocene coastline can be distinguished where depths increase typically from 12 to 20 m over a cross-shore distance of 1 to 2 km. North of Panjang Island, a northwest directed former river valley is present. The gullies at the southeastern and -western flanks of Panjang are respectively 12 and 20 m deep and represent scour trenches maintained by the tidal flow. At a smaller scale, the bed morphology surrounding Pamujan Besar Islet shows two similar scour trenches along its southern and northern margins, with depths of 15 and 19 m, respectively.

The continuous erosion of the former delta is at the expense of a thin stroke of mangrove area that separates fish and shrimp ponds from the Java Sea. Over the time span between 1970 to 1995, the southeastern shoreline of the Bay of Banten has accreted substantially, increasing the local land surface area by 2.5 km<sup>2</sup>. Consequently, two coral reef islets jointly named Pulau Dua have been grown together with the coast by tombolas (Fig. 5.1). The surviving patch reefs in the bay emerge partly during low tide and in most cases exhibit a small coral cay on top of the reef flat. Living coral occurs in a very narrow depth range in between 0.5 and 4 m (E.H. Meesters, unpubl. data). Following the ranking supported by Kleypas (1999), the coral reefs in the bay may be considered marginal, due to the prevailing high levels of turbidity

in between 3 and 10 mg/l. Based on RNA/DNA ratios of coral samples, Meesters et al. (2002) demonstrated that the scleractinian corals in the bay may have partially adapted to the high turbidity regime. The data they present show that the metabolic functioning, or health, of the corals increases with increasing distance from the shore.

## 5.4 Data acquisition and processing

Field measurements were concentrated in the wet season of November 1998 through March 1999. An Electromagnetic Flowmeter (EMF) combined with a pressure sensor was attached to a wooden fishing platform at 11 m depth, at a site labelled Utara (Fig. 5.1). Two-hourly wave measurements were taken for an intermittent period of three months in 1998 and 1999 at 4 Hz, with a burst length of 1028 s. For each burst a directional wave spectrum was calculated using the maximum entropy method as described by Hashimoto (1997). Two additional self-contained wave gauges were deployed, but yielded unreliable data as a result of instrumental errors. However, due to the central position of the Utara site, which is exposed irrespective of the dominant wave direction, the single-point data provided satisfying synopses of the wave field.

A mobile anemometer recorded wind speeds and directions, at 8 m above ground, sampling every 10 minutes during the observations (Fig. 5.1). The wind speed time-series were low-pass filtered to exclude oscillations with frequencies higher than 0.8 cpd. Periods when the wind speed was below 0.5 m/s were not used for analysis, as the vane of the anemometer behaves rather erratically under these conditions. The meteorological and wave field data were supplemented by a wind and wave climatology of the southwestern part of the Java Sea, obtained from satellite observations over the past 15 years, covering a 400 by 400 km area (ARGOSS, 2001).

Flow measurements were also taken with a broad-banded 1.2 MHz Acoustic Doppler Current Profiler (ADCP) at sites nearby Kubur and Besar (Fig. 5.1). The ADCP was deployed at a research vessel for 25-hour anchor station observations and at fishing platforms at approximately the same location for long-term moorings. At both the field sites, situated at the 8-m isobath in the central and eastern part of the bay (respectively), a mooring was performed that lasted three weeks. During these ADCP surveys, profiles of salinity, temperature and suspended sediment concentration (SSC) were obtained hourly during daytime using a CTD probe (*Conductivity Temperature Depth*) with attached OBS (*Optical Backscatter*) sensor, which was calibrated *in situ*. Two additional OBS sensors were deployed at a site at the 3-m isobath labelled Delta Front (Fig. 5.1), sampling synchronously at a frequency of 0.2 min<sup>-1</sup> over a time-span of nearly a fortnight.

## 5.5 Transport of terrigenous sediment by monsoon-driven flow

This section considers the coupling between wave-induced resuspension, gravitational circulation and throughflow in the bay, which protects the coral reefs in the bay from direct exposure to high-turbidity sediment suspensions generated in the old delta. A



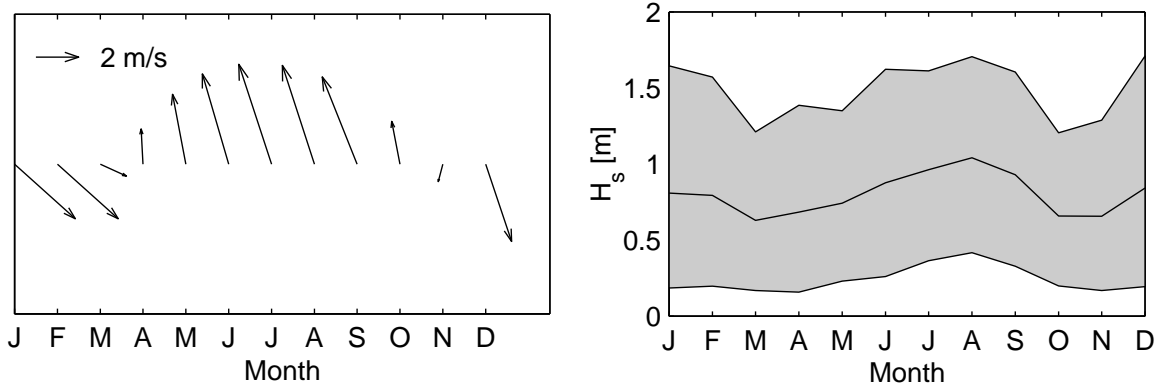


**Figure 5.3.** Left panel: time-averaged wind vectors for the western part of the Java Sea, representing a 400 by 400 km grid centered at  $4^{\circ}45' \text{ S } 107^{\circ}45' \text{ E}$ . Right panel: wave climatology for the same area where the solid line reflects the mean significant wave height ( $H_s$ ); 5% of time  $H_s$  surpasses the upper bound of the shaded area and 5% of time  $H_s$  remains below the lower bound.

description of this coupling is preceded by a characterization of the wind and wave climate in the bay and by an analysis of wave-induced resuspension.

### 5.5.1 Monsoonal wind and wave climate

The Java Sea has a typical monsoonal climate. Fig. 5.3 displays a wind and wave climatology of the western part of the Java Sea, representing an area of 400 by 400 km. The northwest monsoon runs from December through February, whereas the Southeast Monsoon occurs from May until October. In both seasons winds are predominantly gentle and steady. During the transitional periods winds are light and more variable as a result of local land-sea breezes, which are then relatively influential. The significant wave height ( $H_s$ ) in the southeastern Java Sea is within the range of 0.2 to 1.7 m for 90% of time, and is smallest during the transitional periods. Due to the location of Teluk Banten in the outer southwestern part of the Java Sea, only waves from the northeasterly quadrant may have developed over a considerable distance. Since northeasterly winds are rare, waves in the bay are expected to be fetch-limited and largely depending on the local wind field.

Fig. 5.4 displays a frequency diagram of wind speed and direction, and a time-averaged directional wave energy spectrum, based on the wet season measurements of 1998/1999. The observations confirm that waves in the bay are predominantly locally generated. The wave periods are short, generally remaining within range of 2 and 3 s. Waves from the north only account for a small portion of the total wave energy and have a typical wave period of 5 s. The largest recorded waves occurred during a storm event, culminating with  $H_s=1.08$  m. During that storm, a large number of fishing platforms collapsed under wave action, which indicates that waves in Teluk Banten exceed 1 m only incidentally. Local fishermen argued that similar wave events occur once every year or two.

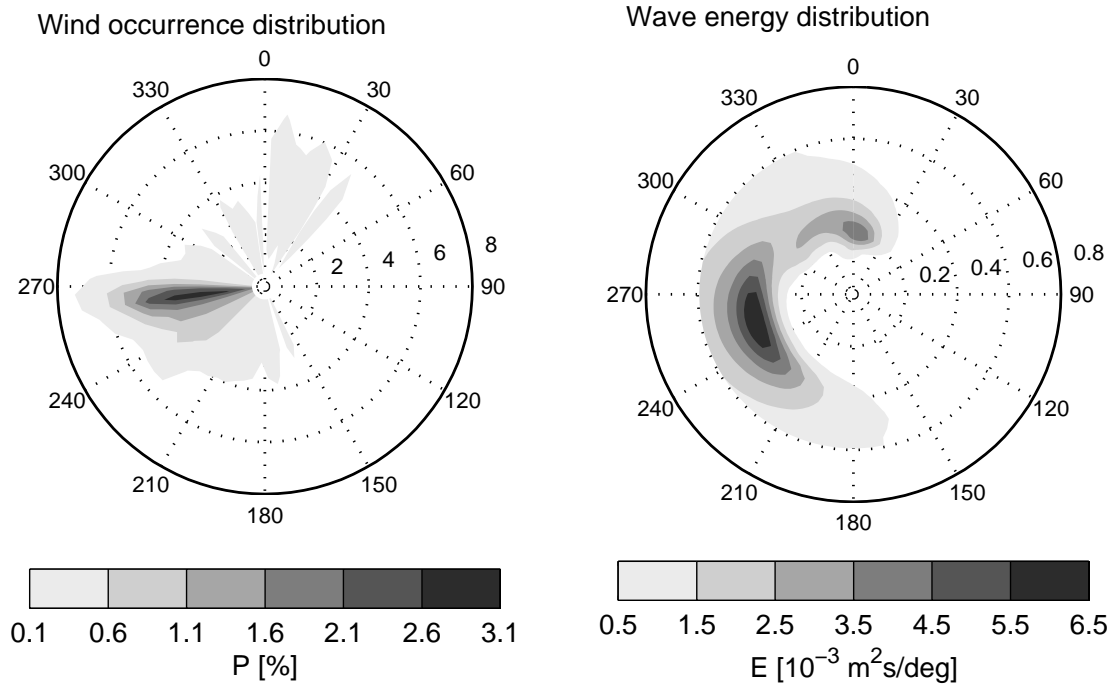


**Figure 5.4.** Wind frequency distribution and a time-averaged directional wave spectrum representing the wet season of 1998/1999. Spokes in the wind frequency plot are assigned to wind speed in m/s; in the wave energy plot the spokes indicate frequency with unit  $s^{-1}$ .

### 5.5.2 Resuspension by waves

Using linear wave theory and assuming an initiation of motion threshold of 0.1 m/s for the near-bed orbital velocity, the short-period waves are only able to resuspend sediment in the shallow and exposed parts of the bay, at depths less than 3.5 m. Fig. 5.5 illustrates the dependence of SSC in the former delta on the wave field and the phase of the tidal and subtidal flow. Near-surface and near-bed SSC patterns are largely congruent, yet the near-surface SSC is slightly lower and lags on the near-bed SSC. Peaks in SSC generally occur at the end of a period of reduced flow velocity, which can be explained as follows. During slack water, waves that travel eastward in the bay transfer their kinetic energy into the mobilization of sediment at the shallow-water delta front, where stagnant nearshore waters become increasingly muddy. Subsequently, the tidal flow conveys the turbid water masses in either of the two opposing directions along the local isobaths, whereas the waters supplied to the delta front are comparatively clear. Due to the prevalence of an eastward throughflow at the time of the observations in the bay, sediment suspensions generated in the old delta were intermittently advected in easterly direction, leaving the bay at its northeastern margin.

Fig. 5.5 also demonstrates that the short-period waves propagating eastward are more efficient in resuspending sediment at the delta front than waves from the Java Sea, which can be illustrated by focussing on the second and fourth of February 1999. On the second of February, local waves from the west peaked at 0.55 m and instantly raised near-bed SSC levels over 100 mg/l. On the fourth of February, the bay was

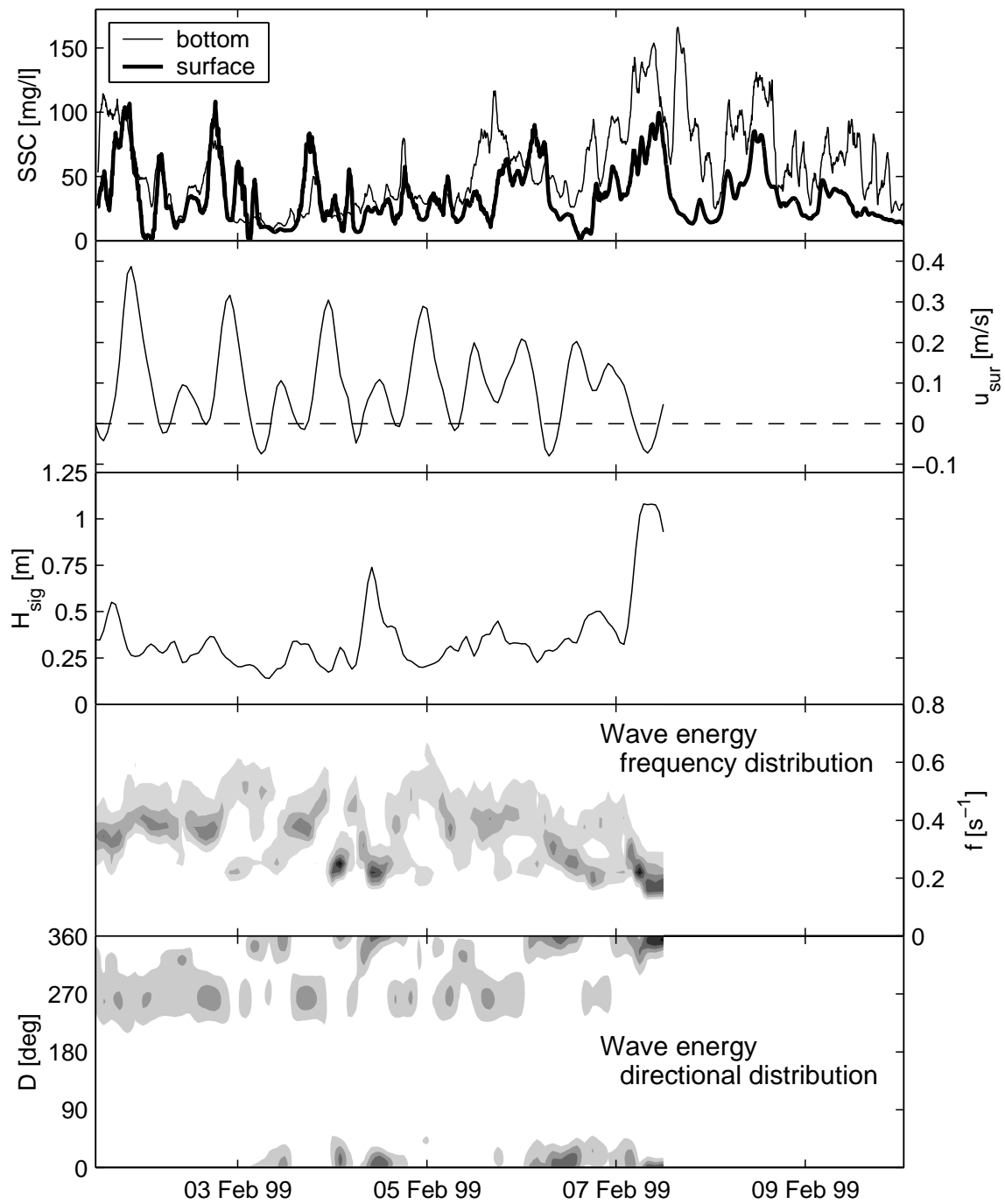


**Figure 5.5.** Turbidity variation at the abandoned delta front (top panel) compared to hydrodynamic conditions at Utara (lower four panels). From top to bottom: near-surface and near-bed SSC, along-isobath flow velocity at 1 m below local datum, significant wave height, wave energy frequency distribution and wave energy directional distribution. Positive and negative values of  $U$  coincide with an eastward and westward circulation along the bay's isobaths, respectively.

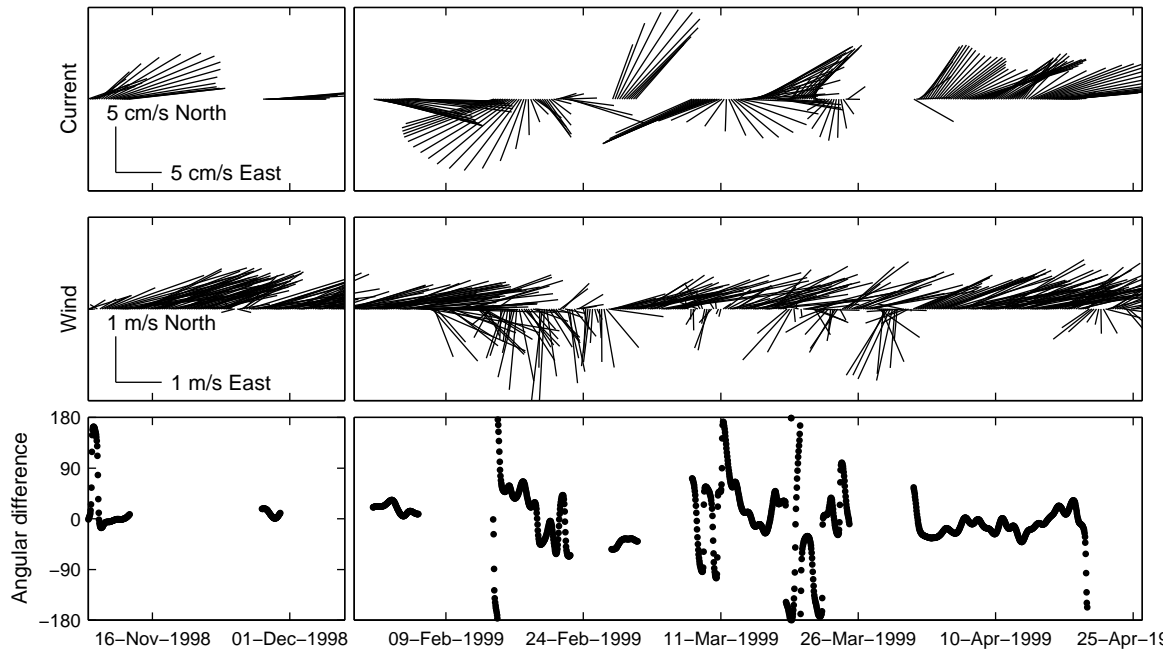


**Figure 5.6.** Vector plot of low-passed surface current velocity at Utara (top panel), low-passed wind velocity at Bojonegara (middle panel), and the angular difference between current and wind vectors (bottom panel); wind vectors follow currents criteria, i.e. sticks indicate where the wind is blowing to.

subjected to incident waves from the north up to 0.75 m, which did not induce a significant raise of SSC levels. However, during the storm event around the seventh of February, waves from the north did generate a pronounced peak of especially the near-bed SSC, whereas the near-surface SSC variation differed little from fair-weather conditions. Nevertheless, it seems credible that waves from the north have a smaller impact on SSC fluctuation at the delta front than these from the west, as a result of the relatively low frequency of occurrence of storm events.

### 5.5.3 Seasonal coupling between wave attack, wind-driven throughflow and river discharge

The throughflow in the bay, though subject to considerable directional spreading (Fig. 5.6), is primarily driven by the monsoonal winds, which is confirmed by a correlation between low-passed surface currents at Utara and wind speeds along the principal flow direction ( $r^2=0.79$ ). The spatial coherence of the low-frequency currents in the bay is large, which appeared from the simultaneous ADCP and EMF measurements of surface currents (Fig. 5.7). The Northwest Monsoon thus concurrently generates waves that cause resuspension in the old delta and an easterly throughflow, which advects the created sediment suspensions in easterly direction. Both the easterly throughflow and wave-induced resuspension intensify as the local winds turn to become more westerly, i.e. directed to the east. Hence, the easterly throughflow protects

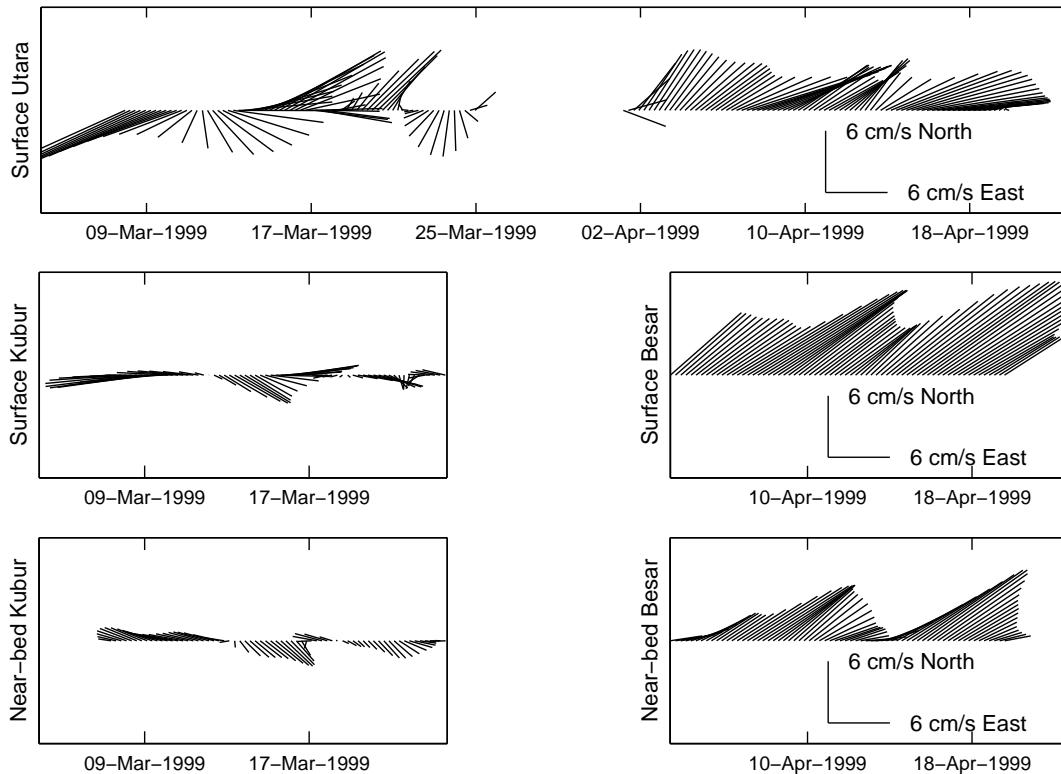


**Figure 5.7.** Vector plot of simultaneous low-passed currents, demonstrating the strong coherence of the low-frequency flow in the bay; Utara observations are from EMF samples; Kubur and Besar observations are from ADCP measurements.

the corals in the bay from sediment that is resuspended in the old delta. Although no measurements were taken during the Southeast Monsoon, it is anticipated that the associated offshore winds generate far smaller waves in the embayment than these that occur during the Northwest Monsoon. Consequently, the westerly throughflow in the bay that then may develop is expected to carry little resuspended terrestrial sediment.

The Northwest and Southeast Monsoons coincide with the wet season and dry season, respectively. The wind-driven throughflow is therefore not only coupled to the incident wave heights in the former delta, but also to the discharge of freshwater and river sediment into the bay. The creeks that debouch into the bay issue an estimated total discharge ranging in between 1 and 30 m<sup>3</sup>/s. Disregarding episodic peak events, the associated sediment discharge is virtually negligible and the Coriolis-induced flow along the bay's isobaths is subordinate to the monsoon-driven throughflow. The gravitational circulation in the cross-isobath direction features an offshore moving surface layer over an onshore return current. In Chapter 3 it was demonstrated that during the Northwest Monsoon the Ekman-forcing on the wind-driven along-isobath flow reinforces this circulation. At Besar, the offshore surface drift flow averaged 0.8 cm/s over the three weeks of measurement, or 0.7 km/day. The finer fraction of the resuspended sediment may be conveyed by this drift flow, containing sediment with

a relatively small settling velocity. However, once the sediment enters the onshore moving lower layer, part of the offshore displacement may be cancelled.

## 5.6 Tidally-driven residual transport

The present section focusses on the residual sediment transport in the bay due to tidal asymmetry and spatial differences in tidal current amplitude. Prior to a description of these mechanisms, the response of suspended sediment concentration to flow variation in the bay is analyzed.

### 5.6.1 Flow-induced resuspension

In offshore coastal waters, at depths larger than 4 m and at distance from the reef islets, SSC's rapidly decrease to a level that rarely exceeds 20 mg/l. During the mooring at Besar, which is at 8-m water depth, diurnal flow events evidently induced resuspension and subsequent deposition of sediment (Fig. 5.8). At slack water, SSC levels drop but never reduce to zero, which suggests the presence of a washload fraction in the sediment suspension consisting of particles with a small fall-velocity at the timescale under consideration. By contrast, the depth-mean SSC level at Kubur is virtually constant (Fig. 5.9), due to a negligible influence of local resuspension.

Using the simultaneous measurements of flow velocity and SSC, the resuspension and deposition events in April 1999 at the submarine platform bordering the delta front can be simulated using the relaxation model proposed by Groen (1967):

$$\frac{\partial h\bar{c}}{\partial t} = w_s(\bar{c} - \bar{c}_e) \quad (5.1)$$

Herein,  $h$  denotes water depth,  $w_s$  is the bulk particle fall velocity,  $c$  is the instantaneous suspended sediment concentration,  $c_e$  is an equilibrium suspended sediment concentration and the over bars indicate  $c$  and  $c_e$  to be depth-averaged. Adopting the theory of Bagnold (1966),  $c_e$  can be related to the depth-mean flow velocity,  $\bar{u}$ , as in:

$$c_e = k\bar{u}^p \quad (5.2)$$

where  $k$  is a constant of proportionality and  $p$  is a constant power.

Fig. 5.8 exhibits an interpretation of the SSC variation in April 1999, where the relaxation model was applied to the resuspension fraction of the total suspended load. The washload and resuspension fractions are assumed to be separated by a second order polynomial. The values of  $k$  and  $p$  are determined by best-fitting a function of the form  $y = kx^p$ , through a scatter plot of samples of  $(\bar{u}, \bar{c})$  for which  $\partial\bar{c}/\partial t=0$ . During these events, upward forcing of sediment particles due to turbulence is balanced by downward forcing from gravity. After substitution of  $\partial\bar{c}/\partial t=0$ , combination of Eqs. 5.1 and 5.2 results in  $\bar{c} = \bar{c}_e = k\bar{u}^p$ . For the Besar mooring this method yields  $k = 0.08$  and  $p = 2.51$ . Subsequently,  $w_s$  is obtained by minimizing the mean absolute error in the modelled SSC's, which results in  $w_s=0.77$  mm/s. For a water depth of 8 m, this implies an adaptation time of SSC to flow velocity of  $h/w_s=2.9$  hours.

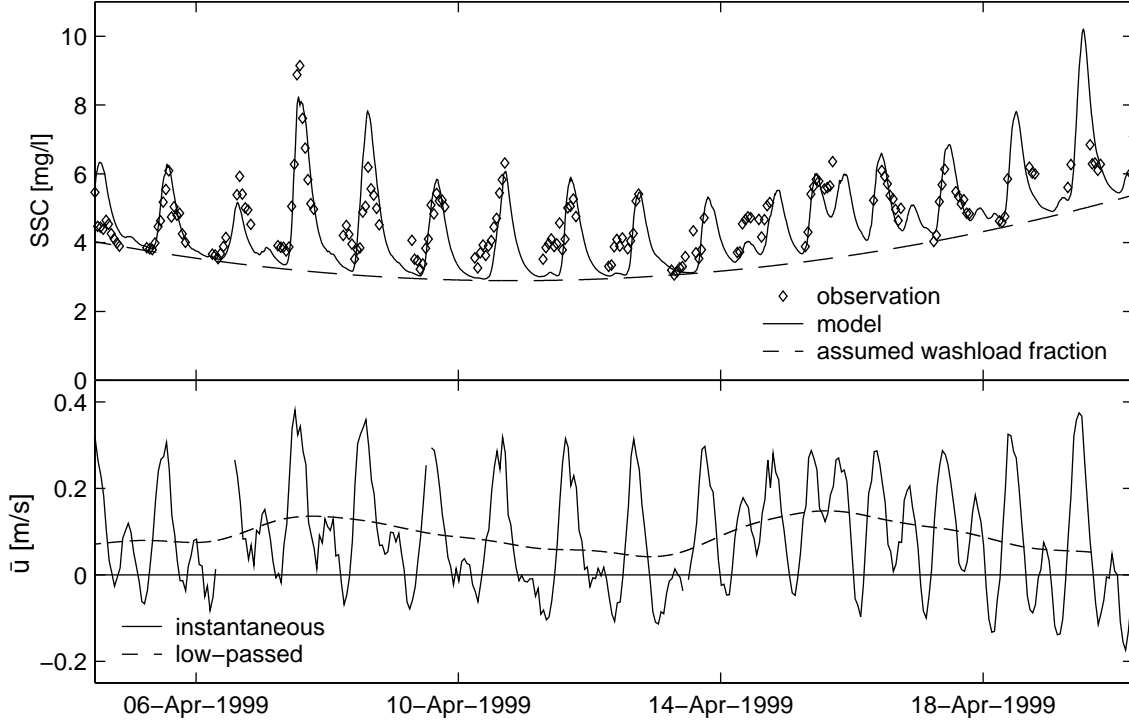


**Figure 5.8.** Interpretation of the depth-mean SSC variation in the former delta region at 8-m water depth, which is in response to current variation. Observed suspended load is composed of a slowly varying washload component and a flow-induced fluctuating resuspension component, modelled based on Eqs. 5.1 and 5.2

### 5.6.2 Residual transport associated with tidal asymmetry

The tidal regime in Teluk Banten is mixed, mainly diurnal. In Chapter 4 the role of tidal asymmetry in the residual suspended sediment transport in diurnal regimes was addressed. It was found that a current velocity signal composed of the tidal constituents  $K_1$ ,  $O_1$  and  $M_2$  exhibits an asymmetrical cycle with a period of 13.66 days. Due to the nonlinear relation between SSC and flow velocity (Eq. 5.2), persistent tidal asymmetries may induce residual suspended sediment transport. This can be illustrated on the basis of the relaxation model defined by Eqs. 5.1 and 5.2, in which the depth-mean tidal velocity component takes the form:

$$\begin{aligned}
 \bar{u} = & A_{K_1} \cos((\omega_1 + \omega_2)t - \phi_{K_1}) \\
 & + A_{O_1} \cos((\omega_1 - \omega_2)t - \phi_{O_1}) \\
 & + A_{M_2} \cos(2\omega_1 t - \phi_{M_2})
 \end{aligned} \tag{5.3}$$

where  $A_N$  and  $\phi_N$  denote the amplitude and phase of constituent  $N$ , respectively, and the basic astronomical frequencies  $\omega_1$  and  $\omega_2$  coincide with 14.4921 deg/h and 0.5490 deg/h, respectively. Neglecting depth variation of  $u$  and  $c$ , the sediment transport rate  $S$  can be approximated as the product of  $\bar{c}$  and  $\bar{u}$ . Under the assumption of  $b = 2$  in Eq. 5.2, this approximation allows for an analytical expression for the residual

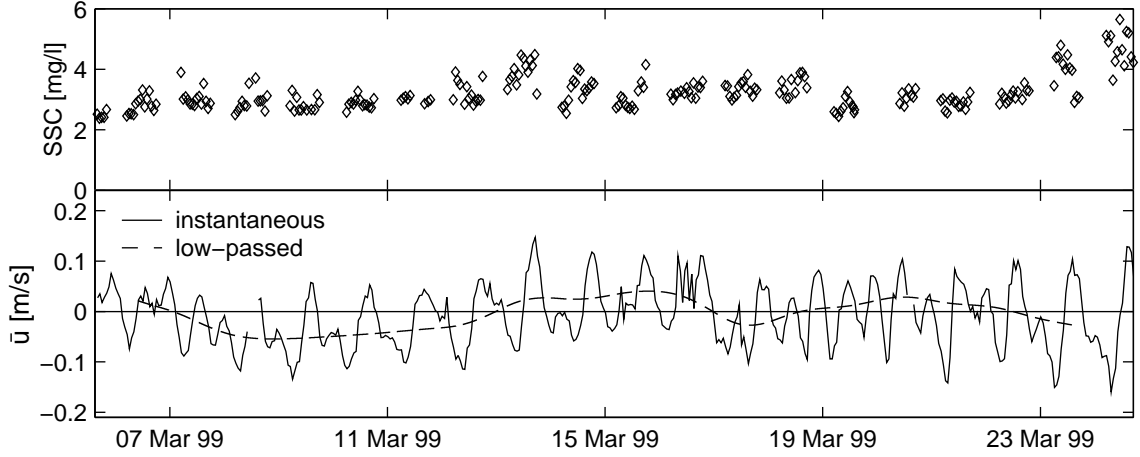


**Figure 5.9.** Variation of depth-mean SSC and along-isobath flow at Kubur. The SSC level is not responding to flow variation.

suspended sediment transport which reads (Chapter 4):

$$\begin{aligned}
 \langle S \rangle_{\infty} &= \langle \bar{c} \bar{u} \rangle_{\infty} \\
 &= \lim_{\tau \rightarrow \infty} \frac{1}{\tau} \int_0^{\tau} \bar{u} e^{-\frac{t}{T_a}} \left\{ c_0 + \int_0^t \frac{k \bar{u}^2}{T_a} e^{\frac{t'}{T_a}} dt' \right\} dt \\
 &= \frac{3}{2} k A_{K_1} A_{O_1} A_{M_2} F
 \end{aligned} \tag{5.4}$$

where

$$\begin{aligned}
 F &= \frac{\cos \Theta + 2T_a \omega_1 \sin \Theta}{3 + 12T_a^2 \omega_1^2} \\
 &\quad + \frac{\cos \Theta - T_a(\omega_1 + \omega_2) \sin \Theta}{3 + 3T_a^2(\omega_1^2 + 2\omega_1\omega_2 + \omega_2^2)} \\
 &\quad + \frac{\cos \Theta - T_a(\omega_1 - \omega_2) \sin \Theta}{3 + 3T_a^2(\omega_1^2 - 2\omega_1\omega_2 + \omega_2^2)}
 \end{aligned} \tag{5.5}$$

$$\Theta = \phi_{K_1} + \phi_{O_1} - \phi_{M_2} \tag{5.6}$$

Herein,  $T_a$  equals  $h/w_s$  and  $F$  is an attenuation factor within the range of -1 and 1. Note that if  $T_a$  is negligibly small as in the case of bedload transport, Eq. 5.5 reduces to  $F = \cos \Theta$ . The residual suspended sediment transport rate is primarily dependent on the relative phased difference  $\Theta$  and the flow amplitudes of  $K_1$ ,  $O_1$  and  $M_2$ .

The tidal signal in the Bay of Banten is persistently asymmetrical due to the interaction of  $K_1$ ,  $O_1$  and  $M_2$ , yet the asymmetry is generally masked by the remaining subordinate tides and by the concurrent monsoon-induced flows. After performing a harmonic analysis on the current velocity component directed along the bay's isobaths, a velocity signal can be reconstructed that is exclusively composed of  $K_1$ ,  $O_1$  and  $M_2$  oscillation. Fig. 5.10 displays the asymmetrical cycles of the tidal flow along the local isobaths at Kubur and Besar, induced by the  $K_1$ ,  $O_1$  and  $M_2$  tides. At spring tide, peak flow velocities in the bay are largest towards the east, whereas at neap tide, westward currents are strongest.



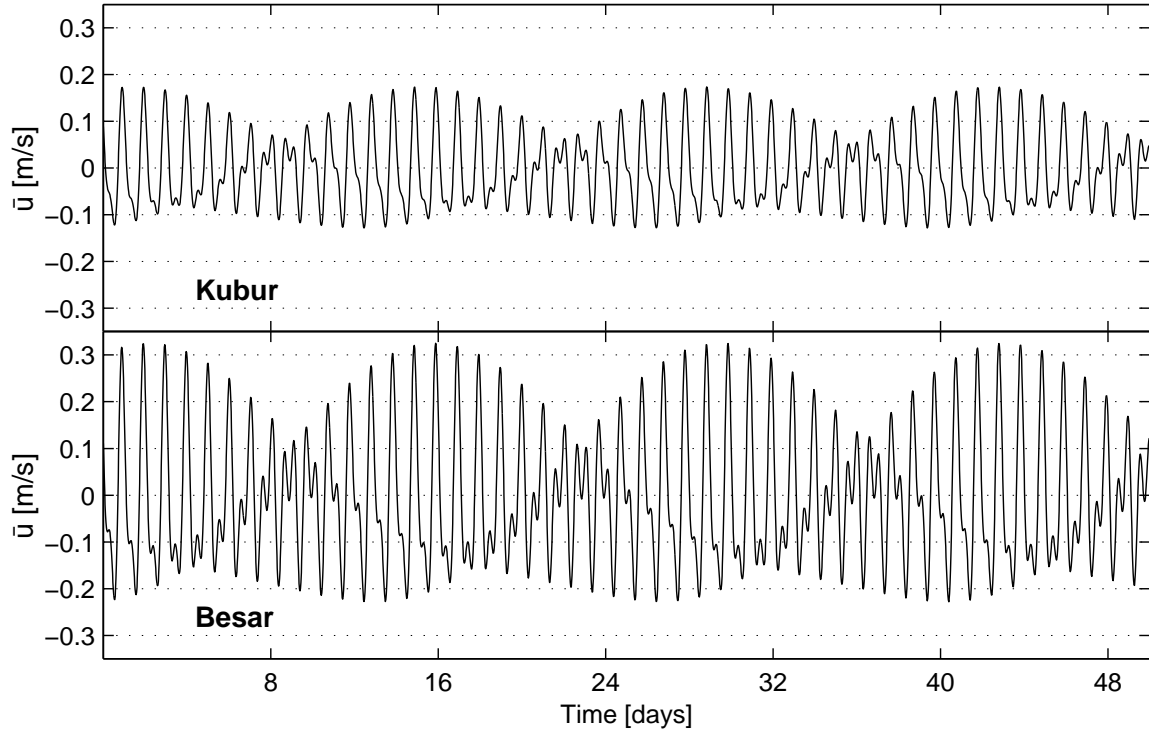


**Figure 5.10.** Asymmetrical tidal cycles induced by  $K_1$ ,  $O_1$  and  $M_2$  oscillation at Kubur and Besar. The tidal amplitudes and phases were obtained from a harmonic analysis performed on the depth-mean flow velocity along the local isobaths. Positive axes have  $103^\circ$  (Kubur) and  $58^\circ$  (Besar) inclination angles, clockwise from north. At spring tide, eastward tidal flow is generally strongest, whereas at neap tide, strongest currents occur towards the west.

Using the tidal phases obtained from the harmonic analysis and presuming  $T_a=2.9$  hours, as observed during the mooring at Besar, the attenuation factor  $F$  was calculated to be virtually equal for the cases of Kubur and Besar, amounting to 0.54 and 0.55, respectively. Therefore, the asymmetry-induced difference between the residual transport at Kubur and Besar depend primarily on spatial variation of  $k$  and difference in the product  $A_{K_1} \cdot A_{O_1} \cdot A_{M_2}$ , which is seven times larger at Besar than at Kubur. Kubur and Besar are situated approximately at the same pathway of the tidal flow, along the 8-m isobath. Along the interval in between the two sites, the tidal asymmetry generates an easterly residual transport that increases towards Besar, which favors the coral reefs in the bay.

### 5.6.3 Residual effect of spatial current variation

The residual sediment transport associated to a decrease of the tidal current amplitude in a coastal inlet, generally known as the settling-lag/scour-lag effect, was described by Van Straaten & Kuenen (1958) and later elaborated by Postma (1961). This mechanism bears a general applicability for any tidal flow, either or not symmetrical, with a spatially varying current amplitude. The net result of the time-lags is to carry sediment from a region of strong tidal currents along a flow pathway in the direction where tidal current amplitudes are smaller. Although lag effects were ignored in Eq.

5.2, the zero response of SSC to flow variation at Kubur (Fig. 5.9) proves that least an erosion threshold is applicable in the bay and thus that lag effect are relevant. This may be clarified by a Lagrangian type of reasoning. When following the westward tidal flow, sediment that is brought into suspension in the former delta region is likely to settle down in the central parts of the bay, due to the decrease of sediment transport capacity of the decelerating water mass. During the subsequent eastward flow, little sediment is being entrained in other parts of the bay than the submarine platform in front of the former delta, leaving a large portion of the earlier deposited sediment to consolidate. This implies a divergence of sediment at the submarine platform, representing a current amplitude maximum, and convergence of sediment in the central and western part of the bay, as a result of the relatively weak currents in this area.

The settling-lag/scour-lag mechanism thus potentially may result in a residual transport of reworked sediment from the 8-m deep submarine platform between Besar and the delta front to the scattered reefs in the center of the embayment, including Kubur. A characteristic length scale for erosion and deposition reads:

$$D = \frac{Uh}{w_s} \quad (5.7)$$

where  $U$  is a typical depth-mean velocity. Assuming  $w_s=0.77$  mm/s,  $U=0.4$  m/s and an average depth of 8 m along a current pathway, a typical length scale is given by  $D=4$  km. This scaling analysis demonstrates that the bulk of sediment entrained at the former delta may have settled before reaching the reefs in the center of the bay. Merely a small portion of the sediment entrained at the submarine delta front platform, consisting of especially fine grains with small fall velocity, may actually arrive at these reefs. The coarser grains settle most rapidly, and therefore remain on the eastern side of the bay. Based on gravity cores, Van den Bergh (unpubl. data) indeed found an east to west gradient in the mean particle grain size of seafloor sediment, with the coarser particles occurring at the submarine delta front platform. Focussing on the area enclosed by the 6 and 10-m isobaths, this can be regarded the long-term result of the settling-lag/scour-lag mechanism. Van den Bergh's geological analysis further confirmed that the submarine platform bordering the delta front is subject to erosion, whereas in the central and southern bay areas accumulation takes place.

## 5.7 Summary and discussion

The present study has provided insight into the oceanographic mechanisms that enhance or resist the supply of terrigenous sediment, derived from an eroding delta system, to shallow-water coral reefs in an adjacent embayment. The coupling between the monsoon-induced coastal processes, including wind-driven throughflow and wave attack on the eroding delta, protects the coral reefs in the Bay of Banten from prolonged inundation by high-turbidity water masses, originating in the eroding delta. The highest incident waves occur during the Northwest Monsoon, which drives an eastward throughflow in the bay that conveys the resuspended sediments to a loca-

tion outside the bay. River discharges also culminate during the Northwest Monsoon, yet the creeks debouching into the bay are too small to have an eminent influence.

The mixed, mainly diurnal tidal flow in the bay is principally bidirectional and asymmetric as maximum velocities to the east systematically exceed these to the west. The tidal flow asymmetry is due to the interaction of the  $K_1$ ,  $O_1$  and  $M_2$  tides, and was found to be a second mechanism resisting westward sediment transport, in favor of the patch reefs in Teluk Banten. Along the 8-m deep submarine platform adjacent to the eroding Ciujung delta, tidal currents accelerate as a topographic effect of the protruding delta, which acts as a headland. These currents are strong enough to induce events of resuspension and subsequent deposition, and the dominance of eastward currents suggests an eastward residual transport component. However, part of the sediment that is released from the submarine delta front platform may apparently accumulate in the central region of the bay as a result of the settling-lag/scour-lag mechanism (Van Straaten & Kuenen, 1958; Postma, 1961). Analogous to shoreward fining associated to the tidal amplitude decrease in tidal inlets, this mechanism may explain why seafloor sediment in the central region of the bay is significantly finer than in front of the delta.

The importance of throughflow to the survival of the patch reefs in the Bay of Banten confirms the results of Kitheka (1997), who found that wind-driven flushing of Gazy Bay, Kenya, during the wet season supports the persistence of coral reefs in the very near vicinity of high-turbidity water masses. Other examples of reef systems favored by seasonal coupling of coastal processes include the Berau Barrier Reef system, north of the Berau delta, and the fringing reef complex north of the Mahakam delta (Tomascik et al., 1997). Both these reef complexes are located along the East Kalimantan Coast, which is separated from Sulawesi by the Makassar Strait. The peak discharges of the rivers Mahakam and Berau coincide with a southerly throughflow in the Makassar Strait during the wet season (Wyrтки, 1961). By contrast, the Bay of Jakarta exemplifies a patch reef complex that is overexposed to terrestrial sediment due to the coupling of monsoon-induced flow, river discharge and wave erosion of the Cisadane delta. During the wet season, the Cisadane delta is most exposed (Verstappen, 1988) and the eastward residual current along the north coast of Java conveys riverine and resuspended sediment to the Bay of Jakarta.

Recognition of the settling-lag/scour-lag mechanism in tropical coastal systems provides an explanation for what may have been intuitively clear: inlets and bays where longshore tidal currents retard are prone to become accumulation areas of especially fine-grained sediment. Woolfe & Larcombe (1998, 1999) argue that the sediment accumulation rate is even a more fundamental control on the reef development than turbidity, as it determines substrate availability. Despite that the turbidity response to tidal current variation on tropical continental shelves is often weak (Larcombe et al., 2001), or merely noticeable in a thin bottom layer (Geyer & Kineke, 1995), the continuous transport capacity of the tidal flow may be sufficient to affect the accumulation rates.

The Indonesian Archipelago constitutes the single largest regional source of sediment to the global ocean (Milliman et al., 1999), and simultaneously may be regarded the preeminent center of coral reef diversity (Tomascik et al., 1997). The seasonal coupling between river outflow, monsoon-driven longshore flow and wave erosion, can be

expected to apply in many near-equatorial parts of Indonesia where monsoon winds provide the dominant driving force for residual longshore flows. In view of the increased sediment yields of the Indonesian rivers (Douglas, 1996), river mouths may exhibit a lee and a luff side and the survival of coral reefs may consequently be topography dependent. However, predictions regarding the future sedimentary regimes of coral reef systems require not merely knowledge of river plume dynamics, but also a thorough understanding of the tidal and subtidal hydrodynamics and associated sediment transport on a regional scale. In this respect, the interaction of diurnal and semidiurnal tidal constituents may be relevant to sediment transport in a large portion of the Indonesian coastal zones, as the diurnal tidal constituents dominate the tidal motion all through the Java Sea and the Indonesian part of the South China Sea (Wyrтки, 1961).

# 6

## Observation of fine-grained suspended sediment from ADCP and OBS measurements

*To be submitted to Journal of Sea Research*

### 6.1 Abstract

Acoustic backscatter devices are commonly used for the measurement of suspended sediment concentration (SSC) and to determine particle size distributions. Although it was designed to measure current velocity, an Acoustic Doppler Current Profiler (ADCP) can accordingly be used to obtain information about the abundance and particle sizes of suspended matter. Alternatively, SSCs can be deduced more accurately from Optical Backscatter (OBS) measurements. The ability of a 1.2 MHz ADCP to measure SSC and to infer temporal particle size variability has been investigated by comparison of ADCP echo intensity to levels of optical backscatter. Experiments were conducted in the Bay of Banten, Indonesia, where clays and silts in the range of 3 to 55  $\mu\text{m}$  are prevalent. The ADCP backscatter co-varies both with SSC and the size of the scatterers. The suspended sediment concentration was found to be generally proportional to the acoustically normative grain size squared. Using this relation, the ADCP backscatter indeed could be converted to SSC, but the calibration was both spatially and seasonally dependent. Differences in the calibrations could not be completely ascribed to grain size variation, due to the largely unknown influences of aggregates and organic scatterers. Qualitatively, however, the ADCP backscatter provided insight into diurnal events of erosion and subsequent deposition and spatial turbidity patterns. An increase or decrease of SSC generally coincided with a raise or decline of the average grain size in the sediment suspension (respectively).

### 6.2 Introduction

Regarding the measurement of suspended sediment concentration (SSC) in coastal waters, optical and acoustical devices have different pros and cons and may therefore

be complementary. Optical devices include transmissometers and optical backscatter sensors, which have been successfully used in many applications often focussing on fine-grained sediments (cf. Bryce et al. (1998), Green et al. (2000), Van Weering et al. (2002)). Estimates of SSC from these instruments may be regarded point measurements, which restricts either the spatial or temporal resolution of the SSC observations, unless a suite of instruments is available. Moreover, the optical devices are intrusive, as they disturb the local flow field.

Acoustic profilers are capable of yielding SSC estimates over the depth range which is ensonified, at a high temporal and spatial resolution. They are non-intrusive as the sediment suspension is being monitored at distance. The disadvantage of the acoustic approach is the comparatively strong dependence on sediment properties such as particle size, shape and density, and the sensitivity for air bubbles. In particular, irregularities of the particle size distribution restrict the accuracy of the acoustic SSC estimates, which can be partly overcome by using multiple frequencies (Hay & Sheng, 1992). The assumption of a homogeneous distribution of particle sizes in marine environments is commonly valid for sand suspensions (Sheng & Hay, 1988; Hanes, 1988; Thorne et al., 1993), enabling acoustic devices to be used for sand concentration measurements. Few studies, however, have addressed the performance of acoustic concentration meters in marine environments where silt or clay is prevalent.

The backscattered intensity from a homogeneous sediment suspension ensonified by an acoustic device is proportional to the product  $M f_p^2/d$ , where  $M$  denotes mass concentration,  $f_p$  is a representative particle form factor and  $d$  a representative particle radius (Lynch et al., 1994). For particles that are small compared to the acoustic wave length, i.e.  $kd \ll 1$ , where  $k$  is the acoustic wave number, the Rayleigh scattering law applies and  $f_p^2/d$  reduces to  $d^3$  (Rayleigh, 1945). For increasing particle size in the regime where  $kd$  is close to unity or larger, the sensitivity of the backscattered intensity to particle size decreases. Hence, the acoustic response generally grows more rapidly with size for smaller particles.

Optical backscatter intensity is comparatively insensitive to changes in particle size distribution, and generally features a linear response to changes in mass concentration within the range of 0 to 10 kg/m<sup>3</sup> (Kineke & Sternberg, 1992). Simultaneous OBS and acoustic measurements therefore may yield particle size information of fine-grained sediments. Lynch et al. (1994) stress the restrictions of the determination of absolute particle size information following such an approach, which mainly concern the calibration of the optical and acoustic devices. Fine particles like clays and silts can be irregular and form aggregates which are difficult to retrieve unaltered and undamaged for assessment of the particle size distribution in the laboratory. Moreover, samples may suffer from aging, due to organic mass production and aggregation of the particles while they are stored.

The primary objective of the present chapter is to establish the potential of a 1.2 MHz ADCP for measurement of SSC in a tropical coastal environment composed of mixture of silt and clay. An additional aim is to explore the possibility to derive qualitative information on particle size distributions from simultaneous ADCP and OBS measurements. Particular attention is focussed on the error mechanisms that are to be expected, including aggregation of sediment particles and backscattering from anomalous particles such as plankton. This chapter is organized as follows. In

Section 2, a brief theory of acoustic backscattering and sound attenuation in turbid seawater is presented. Section 3 discusses the experimental site, the instruments used and the protocols for data logging and filtering. The calibration of the OBS and the conversion of ADCP backscatter information to estimates of suspended mass concentration is presented in Section 4. In Section 5 a comparison is made between the ADCP and OBS estimates of suspended mass concentration, which is further discussed in Section 6. Section 7 concludes this chapter by summarizing the main results.

## 6.3 Acoustic formulation

### 6.3.1 Application of the sonar equation

The ADCP backscatter of sound from an aqueous suspension containing sediment can be modelled by the well-known sonar equation (Medwin & Clay, 1998). It constitutes a balance between the difference between emitted and received energy and the energy lost during the round trip of the acoustic pulse. After elaboration, a relation can be obtained between received backscatter to transmission, radiation, backscattering, returning and reception of an acoustic signal. A working version of the sonar equation in units of decibel is adopted here, formulated by Deines (1999), which reads:

$$S_v = 2\alpha R + K_c(E - E_r) + 10 \log_{10} \left[ \frac{T_T R^2}{L P_T} \right] + C \quad (6.1)$$

Herein,  $S_v$  denotes the volume backscattering strength (Section 6.3.2) [dB],  $R$  is the slant range or range along the central beam axis [m],  $\alpha$  is the attenuation coefficient (Section 6.3.3) [dB/m],  $E$  is the echo strength [counts],  $E_r$  is received noise [counts],  $K_c$  is a scale factor [dB/count],  $T_T$  is the transducer temperature [°C],  $L$  denotes transmit pulse length [m],  $P_T$  is the transmit power [W] and  $C$  is a constant.

The values of  $E_r$  and  $K_c$  are beam specific and may be determined from calibration. The ADCP records  $T_T$ ,  $P_T$  and  $E$  and computes  $R$  from the time span between emission and reception of the acoustic pings, using a simplified formula for the speed of sound (Medwin, 1975):

$$c = 1449.2 + 4.6T - 0.055T^2 + 0.00029T^3 + (1.34 - 0.01T)(Sal - 35) + 0.016z \quad (6.2)$$

where  $Sal$  is salinity,  $T$  is water temperature and  $z$  denotes depth, calculated by transforming the slant range to the system vertical. Depth variation of  $T$  and  $Sal$  and temporal variation of  $Sal$  therefore influence the accuracy of the estimation of bin depths. This accuracy may be increased by post processing, using simultaneous auxiliary data on  $T$  and  $Sal$ .

### 6.3.2 Volume backscattering strength related to SSC

The volume backscattering strength,  $S_v$ , can be expressed in terms of the density of scatterers within a scattering volume,  $n_b$ , and the mean square backscattering cross

section,  $\langle \sigma_{bs} \rangle$  (Medwin & Clay, 1998):

$$S_v = 10 \log_{10}(n_b \langle \sigma_{bs} \rangle) \quad (6.3)$$

For spherical particles, the density of scatterers relates to the volume mass concentration ( $M$ ) as in:

$$M = n_b \rho_s \frac{4}{3} \pi \langle d^3 \rangle \quad (6.4)$$

The acoustical scattering cross section depends on the size of a scatterer relative to the length of the effective plane wave incident on the sediment particle, which is captured in the product  $kd$ . In Rayleigh scatter, where  $kd \ll 1$ , the acoustical scattering cross section is very much smaller than the geometrical cross section, because the sound waves bend around, and are hardly affected by, acoustically small nonresonant bodies (Medwin & Clay, 1998). For a spherical particle acting as a Rayleigh scatterer, the acoustical scattering cross section can be represented by (Rayleigh, 1945):

$$\sigma_{bs} = 4\pi a^2 \vartheta (kd)^4 \quad (6.5)$$

Herein,  $\vartheta$  is a material parameter which reads (Anderson, 1950):

$$\vartheta = \left( \frac{e-1}{3e} \right)^2 + \frac{1}{3} \left( \frac{g-1}{2g+1} \right) \quad (6.6)$$

where  $e$  is the ratio of the elasticity of the sphere to that of the medium and  $g$  is the ratio of the density of the sphere to that of the medium. Combining (6.3), (6.4) and (6.5) gives:

$$S_v = 10 \log_{10} \left[ \frac{3\vartheta k^4}{\rho_s} \langle d^3 \rangle M \right] \quad (6.7)$$

The value  $kd=1$  can be considered an upper limit of the validity of the Rayleigh regime (Urlick, 1983). Johnson (1977) formulated a high-pass model to account for reduction of  $\sigma_{bs}$  if  $kd$  is in the order of unity or larger, which reads

$$\sigma_{bs} = \frac{2\pi\alpha(kd)^4 d^2}{2 + 3(kd)^4} \quad (6.8)$$

Using Johnson's model, the Rayleigh scattering law overestimates  $\sigma_{bs}$  for  $kd=1$  by 9%.

### 6.3.3 Sound absorption

Sound absorption in seawater,  $\alpha$  may be due to relaxation in seawater with dissolved substances,  $\alpha_w$  [dB/m], and attenuation due to the suspended load,  $\alpha_s$  [dB/m], which depends on sound scattering and viscous absorption by suspension material:

$$\alpha = \alpha_w + \alpha_s \quad (6.9)$$



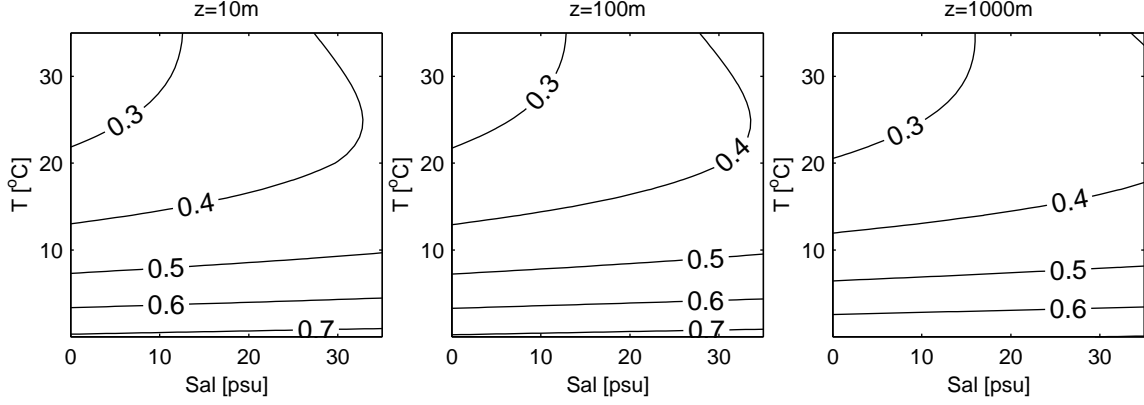


**Figure 6.1.** Isolines of  $\alpha_w$  based on Eq. 6.10, for  $pH=8$ ,  $f=1.2$  MHz,  $c=1500$  m/s and  $z=10, 100$  and  $1000$  m.

The empirical research on the attenuation of sound in seawater with only dissolved substances has been summarized by François & Garrison (1982a,b). The total absorption is the sum of relaxation due to a boric acid component, a magnesium sulfate component and a viscosity component:

$$\alpha_w = \frac{A_1 P_1 f_1 f^2}{f^2 + f_1^2} + \frac{A_2 P_2 f_2 f^2}{f^2 + f_2^2} + A_3 P_3 f^2 \quad (6.10)$$

where for the boric acid component:

$$\begin{aligned} A_1 &= \frac{0.00868}{c} 10^{0.78pH-5} \\ P_1 &= 1 \\ f_1 &= 2.8 \sqrt{Sal/35} 10^{4-1245/(273+T)} \end{aligned}$$

where  $pH$  denotes the acid degree, for the magnesium sulfate component:

$$\begin{aligned} A_2 &= 0.02144 \frac{Sal}{c} (1 + 0.025T) \\ P_2 &= 1 - 1.37 \cdot 10^{-4} z + 6.2 \cdot 10^{-9} z^2 \\ f_2 &= \frac{8.17 \cdot 10^{[8-1990/(273+T)]}}{1 + 0.0018(Sal - 35)} \end{aligned}$$

and for the viscosity component:

$$\begin{aligned} A_3 &= 4.937 \cdot 10^{-7} - 2.59 \cdot 10^{-8} T + 9.11 \cdot 10^{-10} T^2 - 1.5 \cdot 10^{-11} T^3 \quad \text{if } T \leq 20^\circ C \\ A_3 &= 3.964 \cdot 10^{-7} - 1.146 \cdot 10^{-8} T + 1.45 \cdot 10^{-10} T^2 - 6.5 \cdot 10^{-13} T^3 \quad \text{if } T > 20^\circ C \\ P_3 &= 1 - 3.83 \cdot 10^{-5} z + 4.9 \cdot 10^{-10} z^2 \end{aligned}$$

The influence of variation in acid and speed of sound is generally marginal. Fig. 6.1 illustrates how  $\alpha_w$  varies as function of  $T$  and  $Sal$ , for  $pH=8$ ,  $c=1500$  m/s,  $f=1.2$

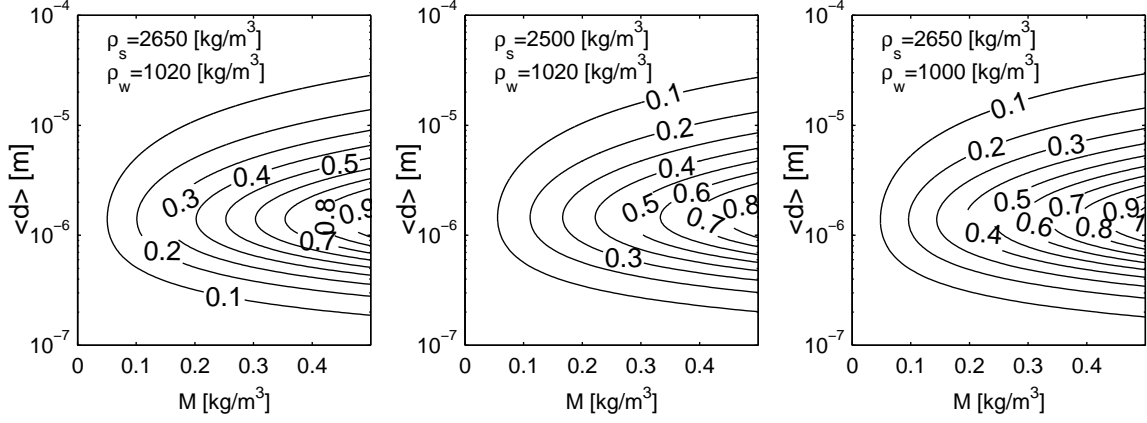


**Figure 6.2.** Isolines of  $\alpha_s$  based on Eq. 6.11, for  $f=1.2$  MHz,  $c=1500$  m/s and  $\rho_w$  and  $\rho_s$  as indicated. Note the logarithmic scaling for  $\rho_s$

MHz and  $z=10, 100$  and  $1000$  m. In the nearshore zone, at depths below 30 m, the depth dependence is negligible. For temperatures over  $25$  °C,  $\alpha_w$  is dominated by salinity fluctuation and values of  $T$  below  $15$  °C, temperature variations are dominant.

Sound attenuation due to suspended sediment was analyzed by Urlick (1948), who demonstrated that the absorption by the suspension material is given by

$$\alpha_s = \left[ \frac{k^4 d^3}{96 \rho_s} + \frac{k(\sigma - 1)^2}{2 \rho_s} \frac{s}{s^2 + (\sigma + \delta)^2} \right] \frac{20}{\ln(10)} M$$

$$s = \frac{9}{2\beta \langle d \rangle} \left[ 1 + \frac{2}{\beta \langle d \rangle} \right]$$

$$\sigma = \frac{\rho_s}{\rho_w}, \quad \delta = \frac{1}{2} \left[ 1 + \frac{9}{\beta \langle d \rangle} \right], \quad \beta = \sqrt{\frac{\pi f}{\nu}} \quad (6.11)$$

provided  $kd$  is small compared with unity and  $\beta d$ . Herein,  $k$  is the wave number [ $\text{m}^{-1}$ ], equal to  $2\pi/\lambda$ ,  $M$  is the sediment mass concentration [ $\text{kg}/\text{m}^3$ ],  $\rho_w$  is the seawater density [ $\text{kg}/\text{m}^3$ ],  $\rho_s$  is the sediment density [ $\text{kg}/\text{m}^3$ ],  $\langle d \rangle$  is the mean particle diameter [m] and  $\nu$  is the kinematic viscosity of water [ $\text{m}^2\text{s}^{-1}$ ]. As  $\nu$  may be attributed a value of  $1 \cdot 10^{-6} \text{ m}^2\text{s}^{-1}$ , the condition  $kd < \beta d$  is generally satisfied for realistic values of  $k$ . Fig. 6.2 exhibits the variation of  $\alpha_s$  as a function of  $M$  and  $\langle d \rangle$ , for  $f=1.2$  MHz,  $c=1500$  m/s,  $\rho_s=2500$  and  $2650 \text{ kg}/\text{m}^3$ , which is typical of coral sediment and quartz sand, and  $\rho_w=1020$  and  $1000 \text{ kg}/\text{m}^3$ , which is typical of seawater and fresh water, respectively. Values of  $\alpha_s$  depend only marginally on  $\rho_w$  and  $\rho_s$ . The viscous absorption increases linear with  $M$ , and is larger for particles with grain sizes closer to  $0.7 \mu\text{m}$ , for this acoustic frequency.

## 6.4 Site and instrumentation

The Bay of Banten is situated along the north coast of Java, close to the Strait Sunda that separates Java from Sumatra (Fig. 6.3). The bay has a mean depth of about 8

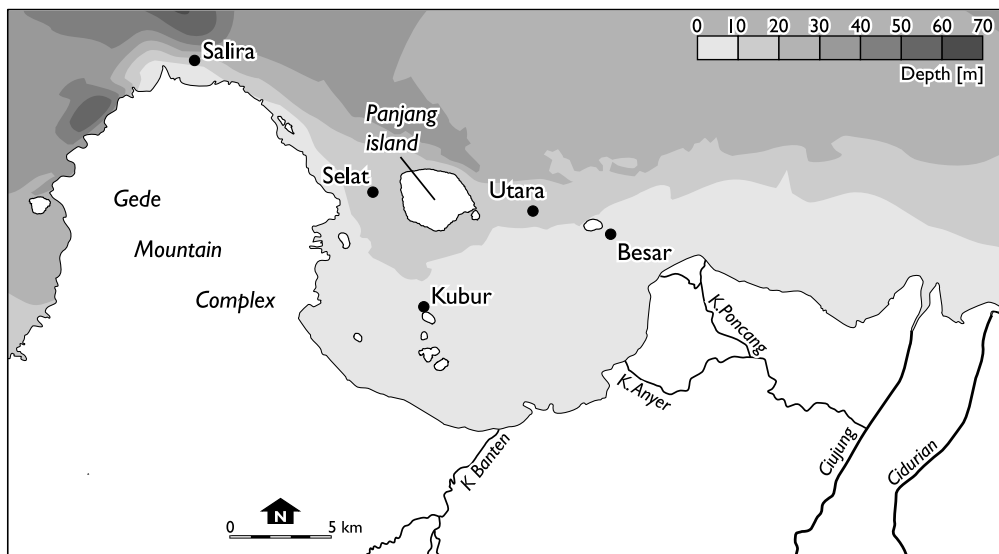
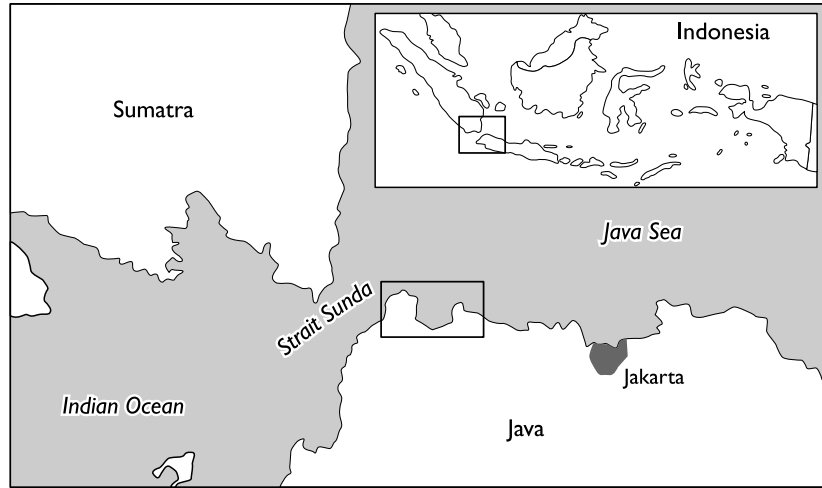


**Figure 6.3.** Map showing the location of the five experimental sites.

m and harbors over ten reef-built islets, of which Pulau Panjang is the largest. Along the seaward edge of the bay the 10-m isobath marks a steepening of the bottom that connects the bay to the southwestern Java Sea, where depths are typically 20 m. Four of the five measuring sites are located inside the bay (Fig. 6.3). Besar and Kubur were chosen in the bay's eastern and central areas, respectively, and are both at an approximate depth of 8 m. Utara and Selat are located at the foreslope east and west of Pulau Panjang, at depths of about 11 and 13 m, respectively. Salira, finally, is located in the Java Sea at the 18 m isobath north of the Gede mountain complex, that shapes the western margin of the bay.

The bottom sediments in the bay were analyzed by *Van den Bergh et al.* (submitted a,b). They distinguish between the eastern part of the bay, where currently erosion takes place, the aforementioned foreslope that is subject to relatively high accumulation rates and the remainder of the bay, where accumulation rates are notably

smaller. The erosive eastern part of the bay coincides with a subtidal inactive delta front, where wind and tide-driven currents are comparatively strong (Chapter 3). The tidal flow at the foreslope is characterized by strong shears, which are associated to the time lag between tidal currents in the bay and at the Java Sea. In the remainder of the bay, currents gradually reduce in magnitude when moving southward.

Throughout the bay, sediments in the top few centimeters of the bed constitute a fairly homogeneous layer of fine-grained silty clays and clayey silts. From six sediment samples taken at 2.5 cm below the bed in the southern, central and eastern part, the average values of  $d_{50}$ ,  $d_m$  and  $d_{90}$  amounted to 6, 15 and 35  $\mu\text{m}$ , respectively, where  $d_{50}$  and  $d_m$  respectively denote the median and mean particle grain size and  $d_{90}$  is the grain diameter exceeded by 10%, by weight of sample. The sample with the finest grains was extracted in the south, with  $d_{50}=3$   $\mu\text{m}$ ,  $d_m=9$   $\mu\text{m}$  and  $d_{90}=22$   $\mu\text{m}$ , and the one with the coarsest grains was taken from the subtidal delta, with  $d_{50}=11$   $\mu\text{m}$ ,  $d_m=23$   $\mu\text{m}$  and  $d_{90}=55$   $\mu\text{m}$ . The particle size distributions of the sediments in suspension are presumed to be largely comparable to these of the bottom sediments, yet differences due to bed armoring and flocculation are acknowledged. The results of samples taken in the western part of the bay are ignored because they contain substantial amounts of faecal pellets, which are unlikely to become resuspended (Van den Bergh et al., in prep a). The faecal pellets caused a peak in the particle size distribution at approximately 100  $\mu\text{m}$ .

At each of the five measuring sites, shipboard measurements were taken twice over the time span of 25-hours, in different seasons. A downward looking ADCP operated for ten minutes every hour storing velocity and backscatter data, when an OBS attached to a CTD probe was winched down to a level of about 50 cm from the bed and back, within a few meters of the ADCP. In addition, long-term surveys were carried out at Besar and Kubur, lasting 20 days at both sites. During these observations, the ADCP was mounted on a wooden fishing platform and operated nearly continuously. From the fishing platforms, a depth profile of optical backscatter, salinity and temperature was obtained once every hour during daytime. The observations took place during surveys in March 1998, October 1998 and February through April 1999. A total of 92 in-situ bottle samples of sediment suspensions were taken for calibration of the OBS sensor, spread out over the three survey periods and a number of locations in the bay.

The ADCP stored data with a vertical resolution of 25 cm, except for the Salira observations, where the bin size was chosen 50 cm. The ADCP transmitted 8 pings per ensemble at 1.2 MHz, in four beams at an angle of  $20^\circ$  to the vertical. Accordingly, four independent backscatter profiles were obtained once every 3 s. The depth registration of the ADCP was corrected for variations in the sound propagation speed by applying Eq. 6.2, using the temperature and conductivity obtained from the CTD casts. The acoustic samples for which the maximum difference between the synchronous backscatter intensities exceeded 2 dB were discarded. This corresponds to a maximum disagreement between the four concentration estimates of 58%. This filtering method provides for the removal of spikes which may be due to fish, and excludes the observations made during periods of strong spatial variability of SSC.

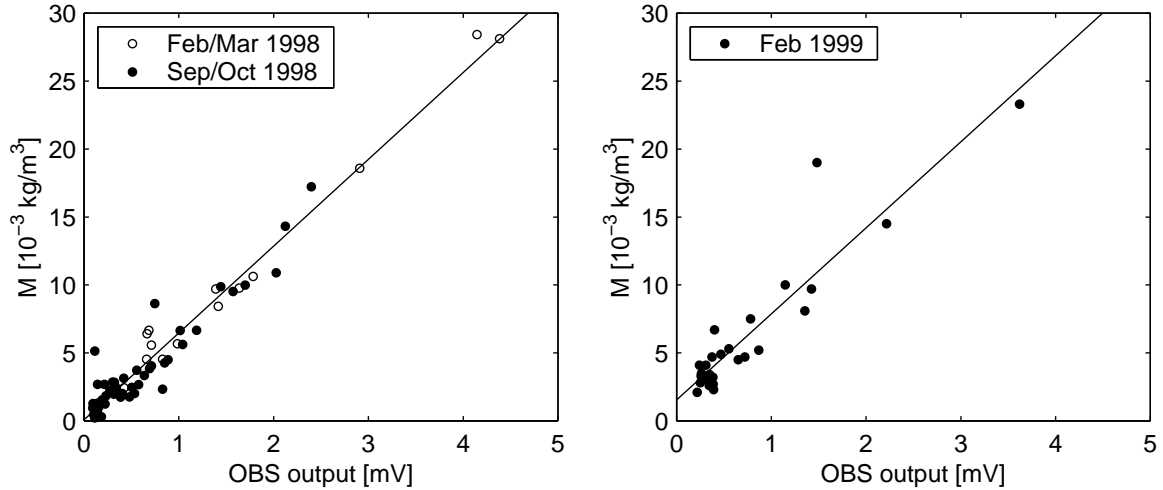


**Figure 6.4.** OBS calibration using the *in situ* mass in water samples. Due to scratching of the OBS window, the regression line of February 1999 has slightly shifted compared to the foregoing periods.

## 6.5 Calibrations

### 6.5.1 OBS calibration using water samples

The suspended mass content of the water samples was measured by vacuum filtration of a fixed amount of water on pre-weighed polycarbonate filters with a pore size of  $0.4 \mu\text{m}$ . After filtration, the filters were cleaned with nano-pure water to remove salts, washed with alcohol, and dried and weighted. The regression results of the SSC measurements taken from water samples with OBS voltage is shown in Fig. 6.4. A slight reduction of the OBS response occurred in the course of the field work, which may be attributed to micro scratching of the OBS window. Separate linear regression lines were used for the measurements in 1998 and 1999. The OBS measurements are here treated as 'ground truth', yet it is noted that OBS measurements may also have a weak size dependent response. A recent laboratory study performed by Hatcher et al. (2001) elucidated that size-related OBS responses are primarily due to flocculation, which frustrates the expected linear relation between suspended mass concentration and particle projected area. The optical backscatter from a flocculating suspended mass declines due to the fact that the particle projected area of a floc is smaller than the sum of the particle projected areas of the primary particles in the disaggregated situation.

### 6.5.2 ADCP backscatter conversion to SSC

The mass concentrations in the bay varied between 0 and  $30 \cdot 10^{-3} \text{ kg/m}^3$  (Fig. 6.4). Using typical, maximum and minimum values for the variables in (6.11), the sound attenuation due to the prevailing sediments in suspension appeared to be negligible. The acoustic scattering from particles in the range of 3 to  $55 \mu\text{m}$ , subjected to 1.2

MHz sound pulses, is generally within the Rayleigh regime. For these particles the values of  $kd$  vary between 0.02 and 0.28, assuming a sound propagation speed of 1500 m/s. The un-flocculated, resuspended sediments may therefore be considered Rayleigh scatterers. For aggregates up to a 100  $\mu\text{m}$ ,  $kd$  remains below 1, yet it is uncertain whether flocs may acoustically be considered spherical. From (6.7) it was established that within the Rayleigh regime,  $\exp(S_v/10)$  is proportional to the product  $\langle d^3 \rangle M$ . The particle size and mass concentration are often correlated, however, which needs to be accounted for to obtain an unambiguous relation between acoustic backscatter and suspended mass concentration.

There is empirical evidence for a relation between the particle fall velocity ( $w_s$ ) and  $M$  of the form (Dyer, 1994; Van Leussen, 1994; Whitehouse et al., 2000):

$$w_s = a M^b \quad (6.12)$$

where  $a$  is an empirical constant and  $b$  an empirical exponent. The well-known Stokes' law, in turn, provides for a relation between  $w_s$  and  $d$  for  $1 < d \leq 100\mu\text{m}$ , which reads:

$$w_s = \frac{(\rho_s - \rho_w)gd^2}{18\nu} \quad (6.13)$$

Equating (6.12) to (6.13) provides for a relation between  $M$  and  $d$ , if  $b$  is known. In absence of particle size measurements of the sediments in suspension, a default value of  $b=1.0$  is adopted here, as suggested by Whitehouse et al. (2000). Combining (6.7), (6.12) and (6.13) then results in:

$$10^{(S_v/10)} = \frac{3\vartheta k^4}{\rho_s} \left[ \frac{18a\nu}{(\rho_s - \rho_w)g} \right]^{1.5} M^{2.5} \quad (6.14)$$

or

$$M \propto 10^{(S_v/25)} \quad (6.15)$$

The validity of (6.15) depends most crucially on the assumptions of a constant value of  $a$ , and  $b=1$ , which implicitly prescribe the effect of flocculation on the mean particle size. Although it is widely accepted that (6.12) is valid for concentrations within the range of 0.002-5  $\text{kg}/\text{m}^3$  (Dyer, 1994), there are studies where no correlation is found between mean particle size and concentration, which challenge the general capability of (6.12) to properly reflect the flocculation process. The applicability of (6.12) may therefore be context dependent. Studies on aggregation behavior in tropical environments comparable to the setting in Teluk Banten, with concentrations in the range 0 to 0.03  $\text{kg}/\text{m}^3$ , are sparse. Dyer & Manning (1999) recently found from a laboratory study that low concentrations promote flocculation. Berhane et al. (1996) presented an analysis on flocculation behavior on the Amazon Continental Shelf, where concentrations varied from 0.001 to 0.076  $\text{kg}/\text{m}^3$ . They found a strong correlation ( $r^2=0.94$ ) between volume concentration and the maximum aggregate diameter. In their photographic analysis, the smallest particles measurable from the images were in the order of 125  $\mu\text{m}$  and no information was presented on the size distribution of the primary particles.

Correlations between the mean concentration and the bulk particle fall velocity may not merely be due to flocculation. Winterwerp (1999) argues that such correlations are spurious, as higher concentrations generally occur at stronger currents,

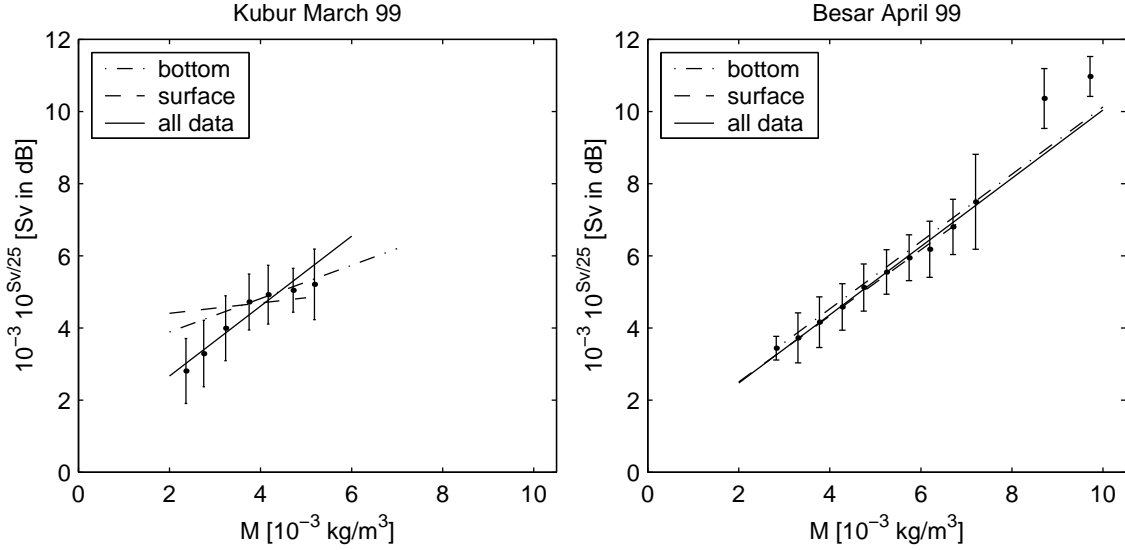


**Figure 6.5.** Calibration of the ADCP signal volume strength for the 20-day moorings at Besar and Kubur. The original measurements were clustered in discrete intervals of  $0.5 \cdot 10^{-3} \text{ kg/m}^3$ , where the dots and bars indicate the mean values and standard deviations for each cluster, respectively. The solid lines are a least-squares fits, regressed through the original measurements. The dashed and dash-dotted lines are least-squares fits, regressed through the measurements from the top and bottom meter only, respectively.

when larger particles may be mobilized with larger fall velocities. If only two sediment classes are involved, with different threshold values for erosion and deposition, the existence of an unambiguous relation between mass concentration and fall velocity becomes implausible. Moreover, suchlike concept disregards the time lag between change of hydrodynamic conditions and the genesis or breakup of flocs and (6.12) may only be valid in the case of an instantaneous adaptation of the number of flocs that pertains to the occurring concentration. Finally, the fact that an increase of the concentration may be partially due to the formation of aggregates contradicts the underlying assumptions of the Stokes' law, which is valid for spherical, massive particles. In particular for larger flocs, the fall velocity may be considerably smaller than predicted by (6.13). Taking these annotations into account, (6.15) will be considered a hypothesis that needs evaluation *a posteriori*.

## 6.6 Comparison of ADCP and OBS estimates of mass concentration

### 6.6.1 20-day moorings

The correlations between  $\exp(S_v/25)$  and  $M$  obtained from OBS measurements were significant both for the 20-day mooring at Kubur ( $r^2=0.64$ ) and the one at Besar ( $r^2=0.83$ ). For presentation purposes, the samples were clustered in intervals of  $0.5 \cdot 10^{-3} \text{ kg/m}^3$  and of each cluster, the average and standard deviation were calculated

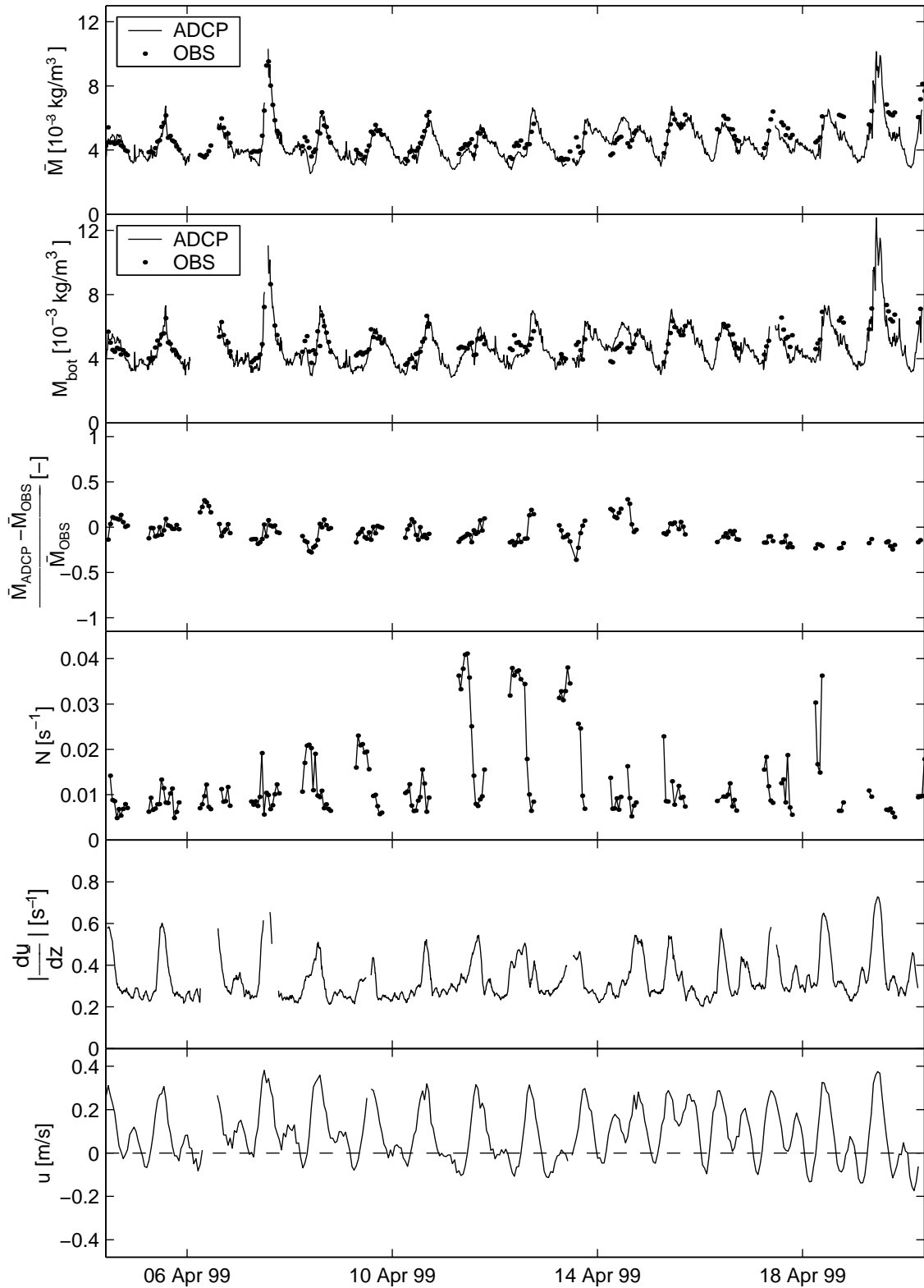


**Figure 6.6.** Time-series of ADCP and OBS estimates of suspended mass concentration and environmental variables at Besar. From top to bottom: ADCP and OBS estimates of the depth-mean mass concentration ( $\bar{M}$ ), ADCP and OBS estimates of the average mass concentration in the bottom meter ( $M_{bot}$ ), the relative difference between ADCP and OBS estimates of  $\bar{M}$ , the buoyancy frequency ( $N$ ), the depth-mean absolute velocity gradient ( $|du/dz|$ ) and the depth-mean flow velocity along the local isobath ( $u$ ).



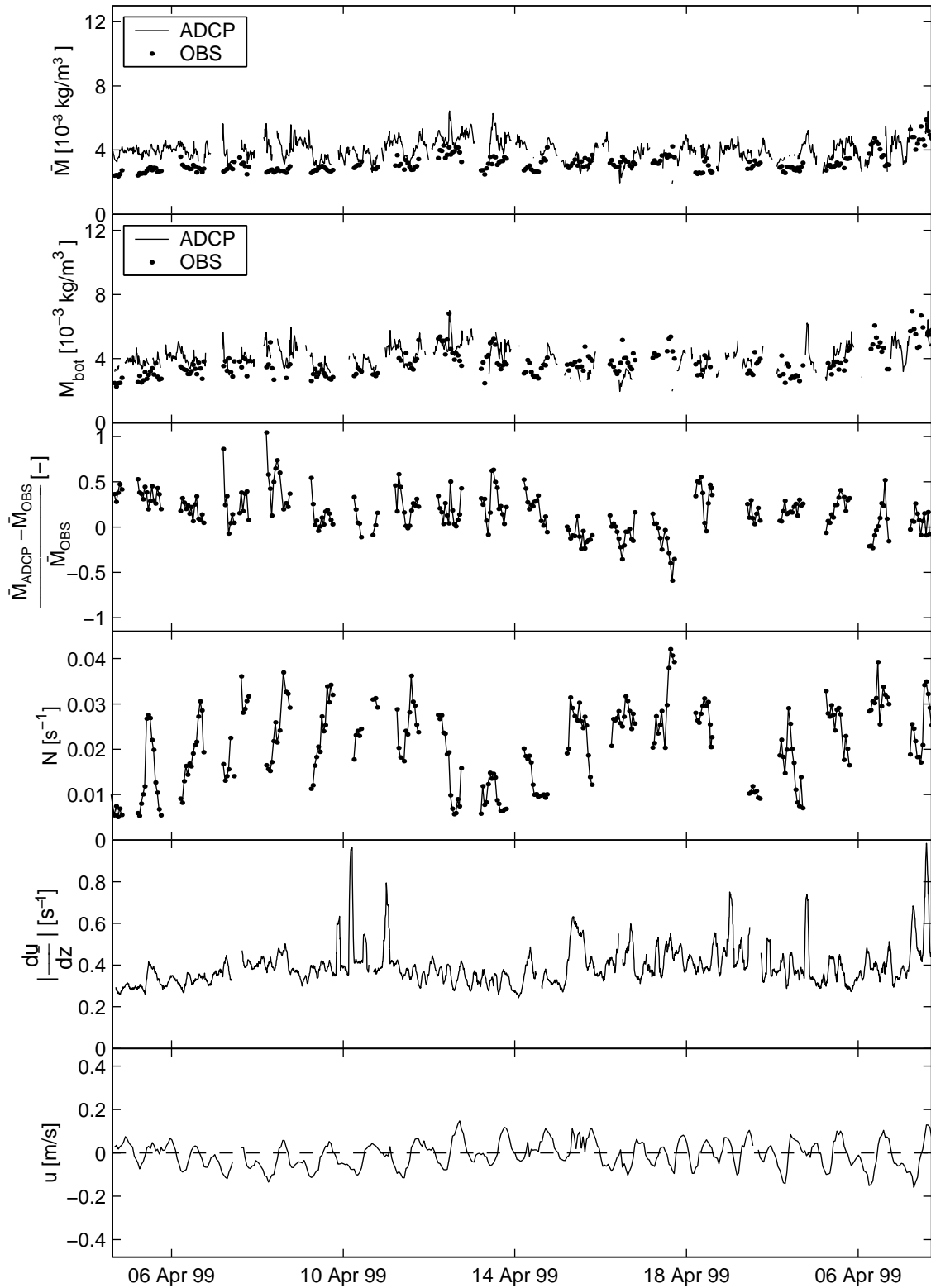


**Figure 6.7.** Time-series of ADCP and OBS estimates of suspended mass concentration and environmental variables at Kubur. From top to bottom: ADCP and OBS estimates of the depth-mean mass concentration ( $\bar{M}$ ), ADCP and OBS estimates of the average mass concentration in the bottom meter ( $M_{bot}$ ), the relative difference between ADCP and OBS estimates of  $\bar{M}$ , the buoyancy frequency ( $N$ ), the depth-mean absolute velocity gradient ( $|du/dz|$ ) and the depth-mean flow velocity along the local isobath ( $u$ ).

(Fig. 6.5). The regression lines through the total of samples at Besar and Kubur agreed well and confirmed the assumption of a linear relation between  $\exp(S_v/25)$  and  $M$ . Fig. 6.5 shows also regression lines for subsets of the data including samples from the bottom or top meter of the observation range only. At Kubur, both the bottom and near-surface samples had a relatively weak acoustic response, yet with a higher intercept. The regression lines of the bottom and near-surface samples at Besar were virtually identical to the one for the total of measurements. These results suggest there is no persisting depth variation in the properties of sediments in suspension at Besar, at least over the time span of observations. At Kubur, dominant sediment properties may vary over depth to some extent. A smaller slope indicates finer primary particles to be prevalent in the sample, which seems plausible for near-surface sediment in suspension, but unlikely for near-bottom sediments. It should be noted in this respect, that part of the differences in the slopes of the regression lines at Kubur, as well as the smaller correlation coefficient compared to Besar, is a direct result of the narrow concentration range. Compared to the horizontally-averaged variation of  $M$ , the inevitable errors due to the fact that the ADCP and OBS measurements were not taken exactly at the same place were therefore relatively large.

Using the best-fit linear lines through the total of samples at Besar and Kubur, Figs. 6.6 and 6.7 compare the OBS and ADCP estimates of the depth-mean mass concentration ( $\bar{M}$ ), the mass concentration averaged over the bottom meter ( $M_{bot}$ ) and the difference between  $\bar{M}_{ADCP}$  and  $\bar{M}_{OBS}$  to environmental variables. As the wind and tide-driven flow in the bay is largely bidirectional and along the bay's isobaths (Chapter 3), the flow velocity was represented by the along-isobath flow velocity,  $u$ . Floc-forming and -destroying mechanisms are primarily governed by the dissipation parameter  $G$  (Van Leussen, 1988), which reads:

$$G = \sqrt{\frac{\varepsilon}{\nu}} \quad (6.16)$$

Herein,  $\varepsilon$  denotes the energy dissipation per unit mass and time [ $\text{J kg}^{-1} \text{s}^{-1}$ ] and  $\nu$  is the kinematic viscosity [ $\text{m}^2 \text{s}^{-1}$ ]. In turbulent flow,  $\varepsilon$  relates to the eddy viscosity ( $N_z$  with unit  $\text{m}^2 \text{s}^{-1}$ ) and the velocity shear as in (Lewis, 1997):

$$\varepsilon = N_z \left( \frac{du}{dz} \right)^2 \quad (6.17)$$

Substitution of (6.17) in (6.16) results in:

$$G = \sqrt{\frac{N_z}{\nu}} \left| \frac{du}{dz} \right| \quad (6.18)$$

For seawater,  $\nu$  has only a weak temperature dependence and is generally attributed a value of  $1 \cdot 10^{-6} \text{ m}^2 \text{ s}^{-1}$ . The eddy viscosity, however, depends on the turbulence field in a complex manner. It increases with an increase of velocity shear and declines with a raising degree of density stratification. Consequently,  $G$  not only depends on the absolute velocity shear, but also on the degree of density stratification. In Figs. 6.6 and 6.7, depth-mean values of  $du/dz$  are presented. As a density stratification index,

the buoyancy frequency was calculated, which reads (Emery & Thomson, 2001):

$$N = \sqrt{\frac{g}{\rho} \frac{d\rho}{dz}} \quad (6.19)$$

The water masses in the bay are generally in between well-mixed and continuously stratified (Chapter 3). A representative value of  $d\rho/dz$  could therefore be obtained from the slope of the best-fit linear line through scatter plots of  $\rho$  versus  $z$ .

The time-series from the Besar mooring (Fig. 6.6) exhibit a general agreement between the ADCP estimates of  $\bar{M}$  and  $M_{bot}$  with the corresponding OBS estimates. The tidal flow at Besar induces diurnal variation of the depth-averaged velocity shear and daily events of resuspension and subsequent settling of sediment. Values of  $du/dz$  generally remain below a level for which turbulence is likely to destroy flocs. This suggests that the proportionality between the acoustically normative grain size  $d$  and  $\bar{M}^2$  may be due to flocculation during increasing flow velocities and differential settling of flocs at the time of flow deceleration. However, if the formation and destruction of flocs were the dominant process that causes increase and decrease of the acoustically normative grain size over the time span of a day, respectively, a time lag between  $\bar{M}_{OBS}$  and  $\bar{M}_{ADCP}$  would have emerged from the data due to the inertia of the flocculation process. The level of  $\bar{M}_{ADCP}$  would then culminate after the peak in the actual suspended mass concentration, whereas  $\bar{M}_{OBS}$  would peak simultaneously with the actual level of  $\bar{M}$ , irrespective of a possible reduction of the optical backscatter response associated to flocculation.

Winterwerp (1999) postulates that the timescale for aggregation is inversely proportional to the product of  $M$  and  $G$ . Although the constant of proportionality needs to be assessed empirically, his parameterizations suggest that due to the low concentrations and low rates of energy dissipation, the timescales for aggregation and breakup of flocs in the Bay of Banten are in the order of days rather than hours. Assuming sediment to enter the water column near the bed as unpacked primary particles, the time-scale of the erosion and subsequent deposition events is thus too small to involve aggregation and subsequent disaggregation. Therefore, co-varying of suspended mass concentration and the acoustically normative grain size will be primarily due to a relative enrichment or depletion of large or small primary particles in suspension (respectively).

At the Kubur site, the relative error of  $\bar{M}_{ADCP}$  is substantially larger than at Besar. Currents are weaker, and the degree of density stratification is comparatively high, exhibiting a diurnal oscillation superimposed on a weekly undulation (Fig. 6.7). Despite the weak currents, the depth-mean absolute velocity gradient is maintained at a steady level of  $0.39 \text{ s}^{-1}$  on average, which is larger than for the case of Besar, where the average amounted to  $0.34 \text{ s}^{-1}$ . The steady suspended mass concentration sustained by the vertical shear at Kubur may involve a relatively long residence time of suspended particles in the water column, allowing for aggregation and disaggregation mechanisms to occur. These could explain the larger error in  $\bar{M}_{ADCP}$ , since floc-forming and -destroying influences optical and acoustic backscatter differently. Since the absolute velocity gradient is relatively constant, imbalance between floc forming and floc destroying may be controlled by the alterations in the buoyancy frequency.

Synthesizing the results from the moorings at Besar and Kubur, it seems plausible that the proportionality between  $d$  and  $\bar{M}^2$  is primarily due to a relative enrichment or depletion of large or small primary particles in suspension, whereas aggregation and disaggregation mechanisms are likely to introduce error in the ADCP estimates of the suspended mass concentration.

### 6.6.2 25-hour anchor stations

The regression results from the 25-hour anchor stations demonstrate that both seasonal and spatial differences in the relation between  $S_v$  and  $M$  in the embayment can be substantial (Fig. 6.8). The calibrations show that a linear relation between  $\exp(S_v)$  and  $M$  is generally valid, but the slopes of the best-fit linear lines may differ. Contrary to the regression lines for the total of samples in Fig. 6.5, the intercepts in Fig. 6.8 are significant. Since a zero intercept is expected from theory (Eq. 6.14), this reveals the limitations of the adopted approach.

Despite the possible influence of organic scatterers, large differences between the slopes in Fig. 6.8 may be at least partially attributed to grain size variations. The influence of other properties of the marine sediments than size such as density, relative compressibility and roundness is expected to be subordinate. Taking the regression results from Besar in April 1999 as a reference, the slope of the regression line from Salira in October 1998 is substantially larger, indicating larger grain sizes. This is in accordance with what may be expected from the fact that Salira is located in an area of strong tidal currents in the order of 0.7 m/s, which are forced to bypass the Gede Mountain Complex (Fig. 6.3).

The regression line for the case of Besar in October 1998 agrees well with the regression line at the same location in February 1999, but its slope is significantly smaller than the slope corresponding to regression from Besar in April 1999 (see Fig. 6.8). In February 1999, the  $\bar{M}$  varied between 6 and 17  $10^{-3}$  kg/m<sup>3</sup> at Besar, largely in response to variation of the flow velocity  $u$ . As  $u$  remained in between -10 and 20 cm/s, currents were not exceptionally strong and the values of  $\bar{M}$  from the OBS are notably high. The proportionality between  $u$  and  $\exp(S_v/25)$ , however, was approximately the same as for the mooring in April 1999. Similarly, the range of  $M$  at Kubur in October 1998 is notably large (1-10  $10^{-3}$  kg/m<sup>3</sup>) when compared to the range of observed mass concentrations during the three weeks of measurement in March 1999 (1-6  $10^{-3}$  kg/m<sup>3</sup>), in absence of an anomalous flow event. Again, this discrepancy was not observed in the ADCP backscatter, resulting in a relatively gentle slope of the regression line between  $M$  and  $\exp(S_v/25)$  for the case of Kubur in October 1998. The ADCP backscatter indicate the high mass concentrations of suspended sediment to contain an ample amount of relatively fine grained material, which is comparatively easily resuspended by the tidal flow. Therefore, the total amount of suspended mass that the flow is able to carry is larger if the sediments available for resuspension are smaller.

The positive intercepts can be explained by the prevalence of anomalous scatterers in the water column, having a relatively strong acoustic response. These could include air bubbles and plankton, the latter of which relate to the biological productivity in the bay. The vertical extent of bubbles entrained by waves ( $l$ ) was analyzed by Thorpe

(1986), who estimates  $l$  to be within the range of 2.5 to 4 times the significant wave height. Wave-induced air bubbles therefore did not affect the acoustic response, as the significant wave heights remained below 0.5 m and the distance between the range of acoustic measurements and the water surface exceeded 2 m at all time.

The sensitivity of acoustic and optical backscatter to plankton depends highly on the species (Flagg & Smith, 1989). There is a long cascade of plankton concentration structures ranging from 1 to 100 km. Phytoplankton are known to have distributions similar to those of physical quantities, such as sea surface temperature, whereas zooplankton populations have marked a more fine scale structure (Massel, 1999). In tropical shelf environments, plankton populations are generally dominated by phytoplankton. Phytoplankton not only hinder acoustic measurements of SSC, but also affect the response of optical instruments (Bunt, 1999). Walker (1981) postulated that the concurrent resuspension of organic and inorganic bottom particles and the associated temporal relationship between chlorophyll concentration and SSC is a widespread feature of turbid coastal regions in the tropics, which was confirmed by results of Wolanski et al. (1981). Therefore, not only the intercepts but also the slopes of the regression lines in Fig. 6.8 may be affected by phytoplankton variation.

## 6.7 Spatial turbidity patterns

The ADCP backscatter can be used to render spatial patterns of SSC in turbid coastal waters. Applications may include the visualization of e.g. sediment plumes that develop during dredging and the turbidity maximum in estuaries. Fig. 6.9 displays the turbidity structure around a coral reef island in the Bay of Banten as an example, based on ADCP backscatter converted to SSC using the calibration results of the Kubur mooring (Fig. 6.5). At distance from the reefs, a nepheloid layer can be distinguished, presumably generated by the prevailing currents. In the wake of the island, currents are virtually stagnant although turbidity is relatively high. High turbidity in island wakes is generally associated to eddies, which are known to generate upwelling in the center of the eddy (Wolanski et al., 1984a).

## 6.8 Discussion

The present study has provided insight into the potential of ADCP backscatter for the measurement of SSC and for the detection of qualitative grain size variation, in combination with OBS measurements. The general validity of a linear relation between  $M_{OBS}$  and  $\exp(S_v/25)$  demonstrates that the ADCP backscatter can be converted to a valuable measure of SSC. Accordingly, ADCP transects and time-series may yield high-resolution information on the coherence between flow and SSC patterns. In a qualitative manner, the ADCP backscatter in combination with OBS measurements has been shown useful to distinguish temporal and spatial grain size variations. For the case of Teluk Banten, it was established that an increase or decrease of the mass concentration respectively involves an enrichment or depletion of larger particles in suspension, associated to flow-induced diurnal events of erosion and subsequent deposition. In a region of strong currents at some distance outside

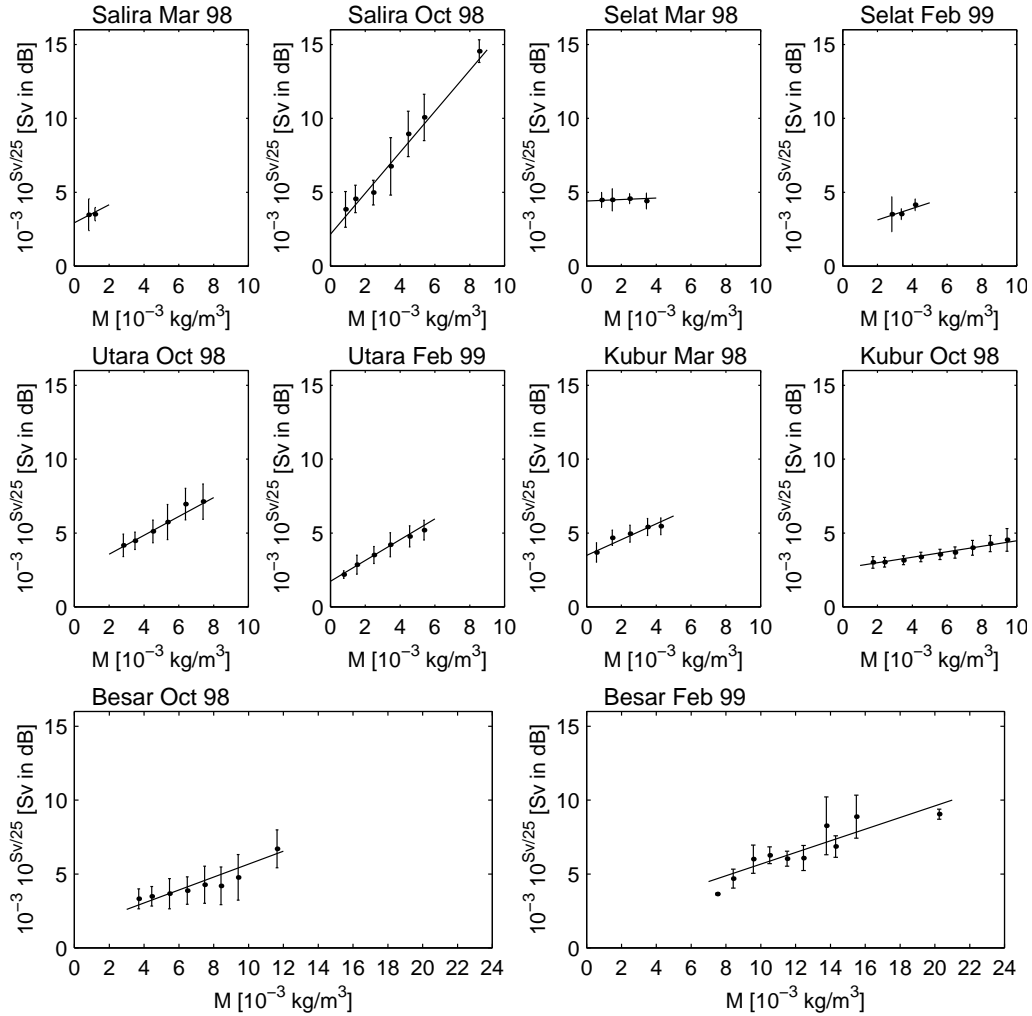


**Figure 6.8.** Calibration of the ADCP signal volume strength for the shipboard 25-hour measurements. The original measurements were clustered in discrete intervals of  $1 \cdot 10^{-3} \text{ kg/m}^3$ , where the dots and bars indicate the mean values and standard deviations for each cluster, respectively. The solid lines are least-squares fits, regressed through the original measurements.

the bay the ADCP backscatter levels were found to be comparatively large, which suggests marine sediments at the shelf to be coarser than these inside the bay. The synchronous OBS and ADCP measurements revealed that the response of the depth-mean mass concentration to variation in flow velocity is sometimes disproportionately strong, when the acoustically normative grain sizes are small. This suggests that the flow in the bay is able to carry a larger mass of sediment, if the grain size of the particles available for resuspension is smaller.

Holdaway et al. (1999) argue that variation in suspended sediment sizes is the primary reasons for differences between SSC estimates derived from ADCP and transmissometer measurements. In the present work, two additional drawbacks were put forward that complicate the adequate interpretation of ADCP backscatter. In the first place, the formation and destruction of flocs in a sediment suspension of constant mass may result in an increase and decrease of the acoustic backscatter (respectively), due

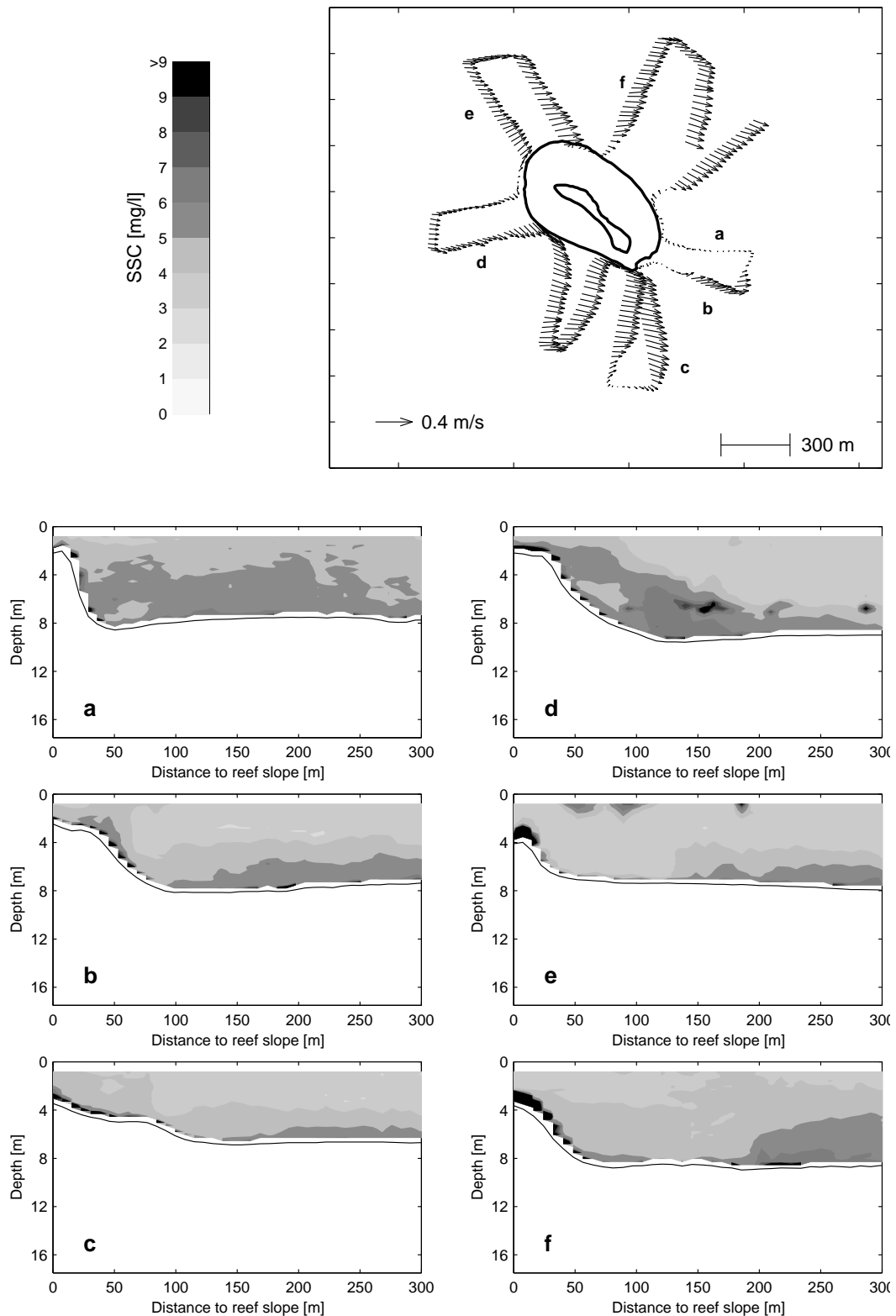


**Figure 6.9.** Quasi-synoptic spatial turbidity patterns at the reef slope of Kubur during eastward flow conditions, based on SSC estimates inferred from ADCP backscatter intensity. Vectors in the top panel indicate the depth-mean current velocity around the island

to the expected change of the acoustically normative grain size. In this respect, the time-scales involved in the aggregation and disaggregation mechanisms are of interest, which increase for decreasing SSC or particle size. In areas with low levels of SSC and fine particles, the time-scales of aggregation may exceed the duration of events of erosion and subsequent deposition by an order of magnitude. In that case, the error introduced by the aggregation and disaggregation mechanisms may be detectable.

The use of ADCP backscatter for the measurement of SSC is further complicated by the prevalence of anomalous scatterers in the water column, of which phytoplankton species are likely dominant. The positive intercepts as observed in the linear relations between  $\exp(S_v/25)$  and  $M$  suggest that organic scatterers, being generally insignificant by mass, may cause a relatively strong acoustic gain. The abundance of organic particles such as phytoplankton in a marine environment depends on the biological productivity, which is particularly high in tropical nearshore areas.

With respect to the calibration procedure, the OBS measurements or water samples never represent exactly the same unit volume at exactly the same point in time as the corresponding ADCP signal volume strengths. This problem can be overcome by excluding measurements made during unfavorable conditions characterized by a large spatial variability of SSC, which can be detected by comparing the independent backscatter levels from the four beams. In the present analysis, measurements for which the maximum difference in backscatter gain exceeded 2 dB were discarded for this reason, which resulted in a removal of only short intervals of data. The consistency of the acoustical SSC estimates may also be determined from an analysis of the backscatter frequency distributions. However, in the light of the foregoing, the adequate interpretation of backscatter frequency distributions requires information on the acoustic response of the total of scatterers in the water column, including flocs and plankton. Empirical research on the acoustic response of organic particles and sediment aggregates would offer further insights into the limitations of the use of ADCP backscatter as turbidity measure.

## 6.9 Conclusion

An investigation has been conducted into the use of a 1.2 MHz ADCP for the measurement of fine-grained suspended sediment concentrations. An overview of the theory of acoustic backscattering and sound attenuation was presented, which highlights that fine-grained particles for which  $kd < 0.5$ , in which  $k$  is the acoustic wave number and  $d$  the acoustically normative particle size, the backscatter relates to  $d^3M$ , where  $M$  is suspended mass concentration. Measurements performed in the Bay of Banten, a small embayment located in West Java, Indonesia, containing a mixture of clay and silt showed that at certain location, within a time span in the order of weeks,  $M$  is generally proportional to  $d^2$ . Using this relation, the ADCP backscatter can be converted to  $M$ , but the calibration is both spatially and seasonally dependent. Increase and decrease of the suspended mass concentration is primarily governed by events of erosion and subsequent deposition, which thus involve an enrichment and subsequent depletion of relatively large grains in suspension.

Particles that are long enough in suspension may form flocs, which presumably



have an acoustic response that relates to their sizes. ADCP estimates of SSC at a dynamical site characterized by diurnal events of resuspension and subsequent deposition contained less error than at a site where SSC levels were relatively steady. Supposed that the steady conditions promote floc formation, this indicates that flocs hinder the accurate measurement of the suspended mass concentration using acoustics. A second source of inaccuracy are organic scatterers, which are generally insignificant by mass, but may have a relatively strong acoustic response. Despite the influences of flocs and organic scatterers, pronounced differences in the relation between acoustic backscatter and suspended mass concentration may be attributed to grain size variation. The combined results of ADCP and OBS observations suggest that the tide and monsoon-driven flow in the Bay of Banten is able to carry a larger amount of suspended mass if the particles in suspension are smaller in size.

# 7

## Tidally-induced clouds of suspended sediment connected to shallow-water coral reefs

*To be submitted to Marine Geology*

### 7.1 Abstract

The Bay of Banten, West Java, Indonesia, represents a shallow coastal embayment harboring coral reefs subject to extremely turbid conditions. The sedimentary regime and flow structure of two contrasting coral reef islands in the embayment were investigated to identify the mechanisms responsible for peak levels of suspended sediment concentration around the reefs. Arrays of *in situ* calibrated optical backscatter sensors were deployed across the reef slopes, revealing the multi-periodicity of suspended sediment variation in the ambient reef waters. Hydrographic surveys were conducted using an Acoustic Doppler Current Profiler (ADCP) attached to a small fishing boat, navigating transects perpendicular to the reef islands. Resuspension of sediment at the lower half of the reef slope was found to be the dominant mechanism generating clouds of suspended sediment covering the reef fringes. The entrained sediment disperses upward across the reef slopes, which is likely due to a secondary current associated with bending of the flow along the curved, hydraulically rough reef slopes, in weakly stratified ambient waters. Changes in sediment availability, variable critical shear stresses for erosion and deposition, and the formation and evanescence of island wakes may explain the high variability of the SSC levels at the reef slopes.

### 7.2 Introduction

Coral reefs are generally associated with blue-water marine environments where visibility is high. However, a considerable portion of the reef-covered area in the tropics is surrounded by turbid coastal waters resulting from terrestrial runoff (Spalding et al., 2001). It has been well established that high levels of turbidity restrict reef development by limiting light penetration and compressing the depth range over which flour-

ishing of corals is feasible (Hayward, 1982; Rogers, 1990; Hopley, 1994). Few studies have focussed on SSC variation in turbid, or marginal reef environments, which leaves the nature of these regimes largely unexplored. This chapter examines hydrodynamic processes controlling turbidity variation in the ambient reef waters of two contrasting patch reefs, Kubur and Pamujan Besar, located in the Bay of Banten, Indonesia (Fig. 7.1). The Bay of Banten represents a 10 by 15 km wide, 8-m deep tidal embayment where coral reefs are exposed to very high levels of suspended sediment concentration (SSC), over 40 mg/l.

Existing time series on SSC at coral reefs suggest that wind and especially swell waves are the dominant cause of high levels of turbidity in the direct vicinity of coral reefs, whereas tidal and wind-driven currents seem less important there (Larcombe et al., 1995, 2001). However, studies using remotely sensed images have shown that flow processes do influence the suspended sediment dynamics of shallow-water islands, by upwelling suspended particles of various kinds (Wolanski et al., 1984a; Pattiaratchi et al., 1986; Ingram & Chu, 1987). Much effort has been devoted to the understanding of eddy formation in the wake of shallow-water islands, which are often sharply separated from the surrounding flow (Black & Gay, 1987; Tomczak, 1988; Wolanski, 1988; Deleersnijder et al., 1992; Wolanski et al., 1996; Tseng, 2002). Within these eddies, bottom friction generates a closed circulation characterized by strong upwelling in the bulk of the eddy and an even larger downwelling in a narrow zone along the edges of the eddy (Wolanski et al., 1984a). Merely a small part of the edge of the eddy is connected to the reef island, which restricts the direct impact on near-reef turbidity.

The present study focusses on turbidity in the direct environment of reef fringes, which constitutes a boundary condition for corals. The Bay of Banten provides a nice example of a marginal reef environment where turbidity is controlled by tidal currents, generating clouds of suspended sediment. Observations using nephelometers demonstrate that the most intense SSC variation initiates at the lower parts of the reefs, at locations too deep for wave stirring. The turbidity events cannot be explained by advection, since far-field SSC's are almost an order of magnitude smaller than these nearby the reef fringes. A quasi-synoptic view of spatial SSC patterns around the reef islands is presented, using ADCP backscatter as a measure of turbidity.

The remainder of this chapter is arranged as follows. After discussing the observational program and methods in Section 7.4, Section 7.3 gives a brief field description. Subsequently, the observed flow-induced clouds of suspended sediment are analyzed in Section 7.5. Section 7.6 characterizes the flow around the islands, stressing the influence of morphological adaptations. Section 8.3 addresses the implications of the turbidity events for reef development. It is argued that sedimentation is likely a more fundamental control on aggregate reef development than turbidity. Sections 7.8 and 7.9 conclude this chapter with a discussion and conclusions.

### 7.3 Field site

The Bay of Banten is subject to a mixed, mainly diurnal tidal regime, characterized by a maximum vertical tidal range of 85 cm. Tidal currents in the embayment are largely bidirectional, parallel to the local isobaths and attain local peak values exceeding 60

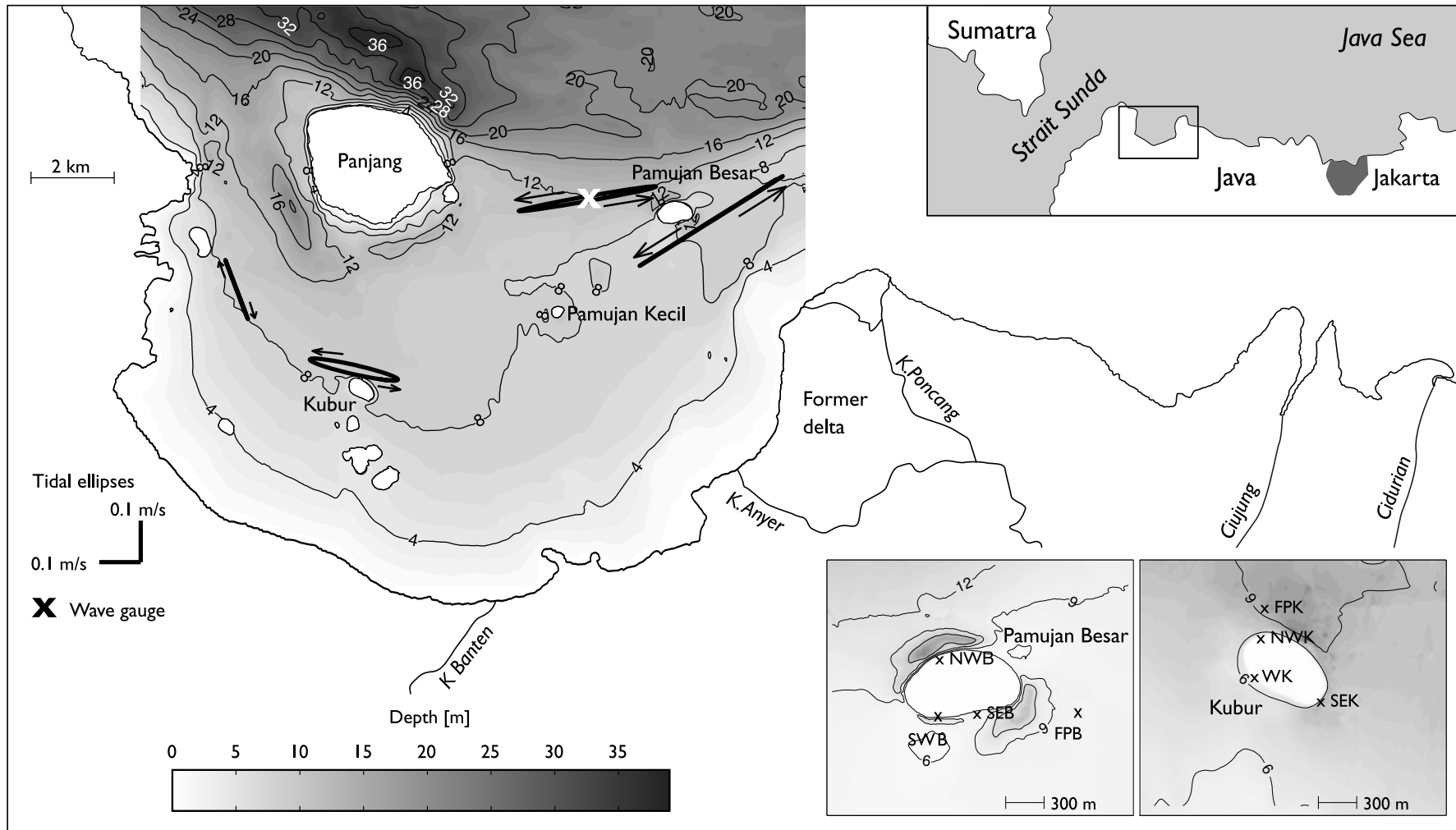


**Figure 7.1.** Bathymetry and tidal flow properties of the Bay of Banten, Indonesia, and location of the sample stations. The tidal regime in the bay is mixed, mainly diurnal and the tidally-induced currents are largely bidirectional, parallel to the bay's isobaths. The exhibited surface current tidal ellipses represent the principal diurnal constituent (viz.  $K_1$ ).

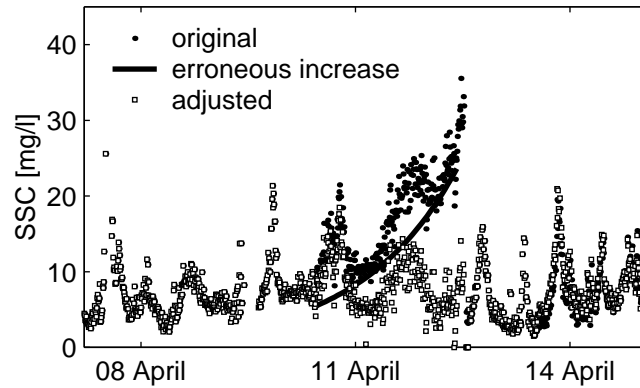


**Figure 7.2.** Example of an OBS-derived SSC time series corrupted by algae growth, which is adjusted to allow for a spectral analysis of the entire time series.

cm/s. The rivers that directly debouch into the bay deliver too little freshwater to induce a substantial gravitational circulation (Chapter 3). A seasonally-dependent monsoon-driven current in the order of 5 cm/s is superimposed on the tidal flow. In Chapter 5 it was argued that the prevailing reefs in the bay benefit from the seasonal coupling between river outflow, wave erosion at the eastern shorelines and monsoon-driven throughflow. During the wet season, an easterly circulation induced by the Northwest Monsoon protects the reefs from both the culminating discharges of the rivers Ciujung and Cidurian (Fig. 7.1) and from turbid water masses generated by west to east heading waves, attacking the erosive former delta front that shapes the east coast of the bay. Short-period wind waves are generally in the order of 0.4 m, and remain below 1.5 m for 95% of time. Swell occurs merely sporadic when winds are from the north or northeast.

## 7.4 Observational program and methods

### 7.4.1 Field surveys

The majority of the observations were made during the period from March through April 1999 in the wet season. A wave gauge including an electromagnetic flow meter (EMF) and a pressure sensor was moored at a fishing platform in the mid-north of the bay, to measure wave height and direction during the observational period (Fig. 7.1). Ten OBS sensors were placed in three arrays across the reef slopes of the islands Kubur and Pamujan Besar, successively. At different depths, a sensor was attached to a rod at about 0.5 m above the slope. From 1 to 23 March 1999, the OBS sensors were placed at Kubur at four different depths at the site labelled NWK, at four depths at WK and at two depths at SEK. The measurements at Pamujan Besar lasted from 2 to 16 April 1999, when four OBS sensors were located at NWB, four at SEB and two at SWB. During each of the two surveys, a broad-banded 1.2 MHz ADCP monitored the far-field flow conditions at a fishing platform nearby the island under investigation (FPK and FPB in Fig. 7.1). From the same platforms, Conductivity, Temperature

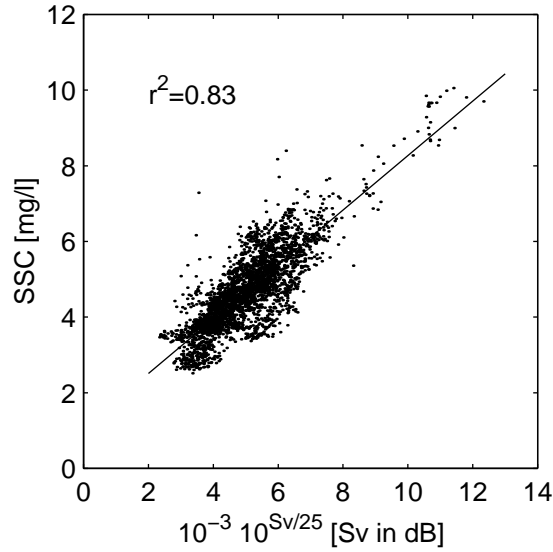


**Figure 7.3.** Calibration of the ADCP backscatter intensity, converted to  $\exp(Sv/25)$ , using concurrent OBS derived estimates of SSC.

and Depth (CTD) casts were taken to yield a depth profile of temperature and salinity once every hour, during daytime. To obtain a quasi-synoptic view of the current structure of the ambient reef waters, the ADCP was attached to a fishing boat with limited draft, which navigated transects perpendicular to the reef slopes. Finally, the seabed morphology and geometry of the reefs was established by echo-sounding and levelling.

#### 7.4.2 Directional wave spectra

The EMF with combined pressure sensor sampled at 4 Hz, in bursts of 1028 s, once every two hours. For each burst a directional wave spectrum was calculated using the maximum entropy method as described by Hashimoto (1997).

#### 7.4.3 OBS calibration

The OBS sensors were calibrated in the lab using *in situ* water samples. The suspended mass content of the water samples was measured by vacuum filtration of a fixed amount of water on pre-weighed polycarbonate filters with a pore size of  $0.4 \mu\text{m}$ . After filtration, the filters were cleaned with nano-pure water to remove salts, washed with alcohol, and dried and weighted. The correlations between OBS voltage and mass content were high ( $r^2 > 0.92$ ). The calibration was repeated without permitting light penetration, to assess the effect of light penetration into the water column on the OBS measurements. In some cases the regression coefficient altered noticeable, but differences did not exceed three percent. Therefore, the former calibration was used for all sensors. The OBS sensors acquired 6 recordings per hour, each recording being the average over a minute of sampling at 0.2 Hz. Spikes due to the abundance of fish in the vicinity of the sensors were replaced by a 3-hour averaging of the neighboring data points. If either two consecutive measurements differed over 5 mg/l, or

the difference between a measurement and that of 20 or 30 minutes earlier exceeded 10 or 15 mg/l, respectively, the sample was regarded invalid. It was verified that the presence of spikes did not relate to either location or depths.

#### 7.4.4 SSC spectra

Incidentally, algae may cover the OBS sensors, particularly at the top few meters of reef slopes. As a result, 6 of the 20 OBS signals were partly corrupted by an exponential increase from the start of algae growth until cleaning of the sensor, which was after 3 days at maximum. The corrupted parts of the OBS signals were adjusted by subtracting a best-fit exponential curve through low-value points and adding up the average over the non-affected part of the signal, to allow for a spectral analysis of the full time series (Fig. 7.2). The partly adjusted OBS time series, disposed of spikes and denoted  $y_t$ , were detrended by subtracting a 36-hour moving average  $s_t$  of the form:

$$s_t = \sum_{i=-108}^{108} w_i y_{t+i} \quad (7.1)$$

where the weights  $w_{-108}$  and  $w_{108}$  equal  $1/432$  and  $w_i = 1/216$  otherwise, resulting in the residual time series  $r_t$  which satisfies:

$$r_t = y_t - s_t \quad (7.2)$$

Subsequently, the variance density spectra of  $r_t$  were calculated, denoted  $f_r(\omega)$ . The spectral estimates were computed using a fast Fourier transform length of 1024 data points, with 75% overlapping segments, resulting in 8 and 18 degrees of freedom for the cases of Pamujan Besar and Kubur, respectively. The spectra were corrected to account for the influence of trend removal on the autocorrelation structure of  $r_t$  (Diggle, 1990):

$$f_r(\omega) = |a(\omega)|^2 |f_y(\omega)| \quad (7.3)$$

where  $f_y$  is the corrected spectrum and  $a(\omega)$  is a transfer function defined as:

$$a(\omega) = w_0 + 2 \sum_{j=1}^{108} w_j \cos(j\omega) \quad (7.4)$$

#### 7.4.5 Calibration of ADCP backscatter intensity

ADCP backscatter intensity can be used as a measure of SSC (Holdaway et al., 1999), at least in a qualitative manner (Chapter 6). The functional relation between a volume backscatter strength ( $S_v$  [dB]) and ADCP echo strength ( $E$  [counts]) reads (Deines, 1999):

$$S_v = 2\alpha R + K_c(E - E_r) + 10 \log_{10} \left[ \frac{T_T R^2}{L P_T} \right] + C \quad (7.5)$$

Herein,  $R$  is the slant range or range along the central beam axis [m],  $\alpha$  is the attenuation coefficient [dB/m],  $E_r$  is the received noise [counts],  $K_c$  is a scale factor [dB/count],  $T_T$  is the transducer temperature [°C],  $L$  denotes transmit pulse length [m],  $P_T$  is the transmit power [W] and  $C$  is a constant. The attenuation can be decomposed into parts due to water and sediment, respectively:

$$\alpha = \alpha_w + \alpha_s \quad (7.6)$$

In regions where the SSCs remain below 50 mg/l as in the Bay of Banten, attenuation due to sediment is negligible (cf. Urick, 1948), whereas  $\alpha_w$  is a function of salinity and temperature (François & Garrison, 1982a,b). Assuming spherical particles and Rayleigh scattering (Urick, 1983),  $S_v$  relates to the normative grain diameter  $d$  and SSC as:

$$10^{S_v/10} \propto \langle d^3 \rangle SSC \quad (7.7)$$

where the angled brackets denote the average over a target volume. The problem of particle size dependence was solved by assuming that the bulk particle fall velocity  $w_s$  to be proportional to  $d^2$ , based on Stoke's law, and by supposing  $w_s$  is proportional to SSC, which yields  $SSC \propto d^2$ . The latter assumption is based on the suggestion made by Whitehouse et al. (2000), who stated that in the relation  $w_s = aSSC^b$  the exponent  $b$  equals approximately 1 in most environments where cohesive sediments prevail. The calibration was based on the moored OBS and ADCP data at FPK and FPB (Fig. 7.1). Using the OBS-derived estimates of SSC, the relation between  $\exp(S_v/25)$  and  $SSC$  was found to be linear, which confirms the above assumptions (Fig. 7.3). As for the calibration,  $\alpha_w$  could be inferred from the CTD-derived estimates of temperature and salinity. Considering the small variance of  $\alpha_w$ , which ranged between 0.40 and 0.41 dB/m, a constant value of 0.40 dB/m was taken in the conversion procedure of the ADCP transect data to SSC.

## 7.5 Turbidity variation

The SSC variation at various depths across the reef slopes of the two coral islands under investigation was generally capricious. For most of the reef transects, both mean and maximum SSC levels at the reef slopes increased with depth and surpassed those in the far field (Table 7.1). Maximum SSCs at the reef slopes frequently exceeded 40 mg/l, whereas the free stream SSCs generally remained below 10 mg/l. Buoyant river plumes occurred merely sporadically on the reef slopes, raising SSC's in the near-surface waters to 20 mg/l for only short intervals (<1 hour). As the measurements were taken in the heart of the wet season, the direct influence of river plumes can be considered insignificant throughout the year. The direct response of SSC to periodic wave forcing was incidentally observed, but it is not persisting as was established from low correlations between wave height and SSC (see also Hoitink, 2000). Moreover, no relation was found between average SSC levels and wave exposure of the sites. The absence of persisting wave influence is largely due to the short periods and limited heights of the locally generated waves. Consequently, wave action at the reef slopes is merely significant in those regions where coral cover is largest, and little



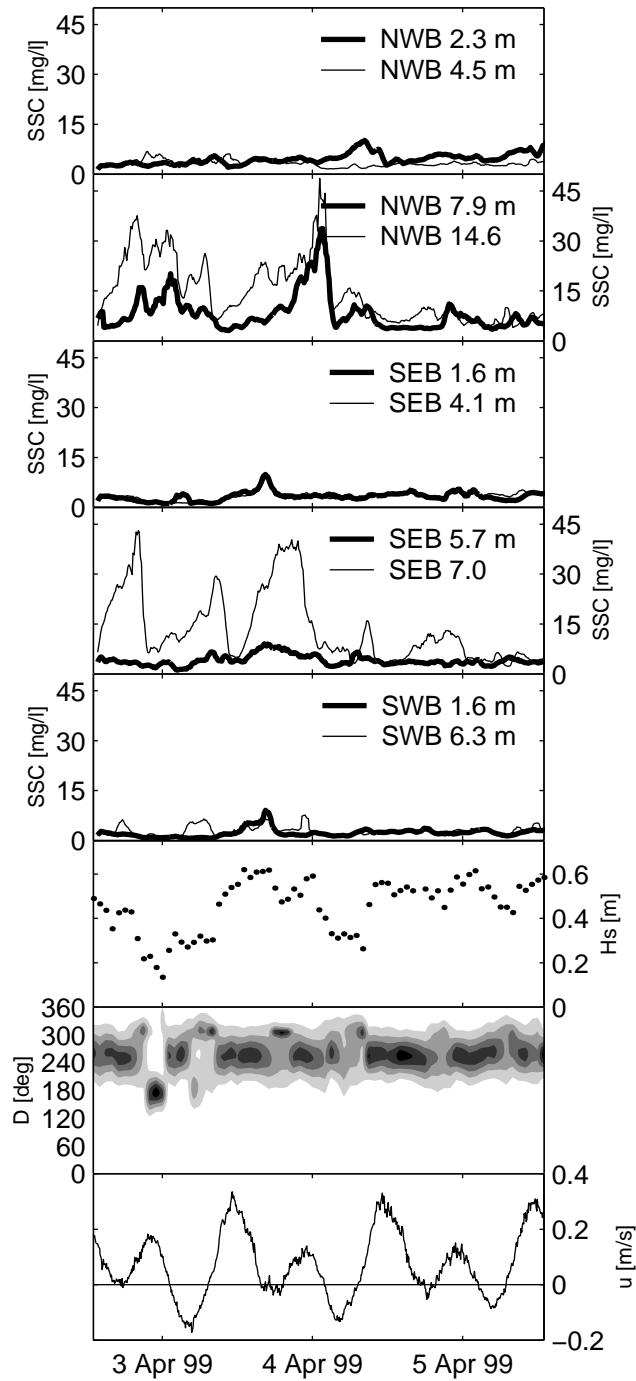


**Figure 7.4.** From top to bottom: SSC variation at the reef slope of Besar, where the location (Fig. 7.1) and depth of the OBS sensor is indicated in the legend, wave height ( $H_s$ ) and wave energy directional distribution at Utara ( $f(D)$ , directions positively clockwise from true north), and along-isobath flow velocity at the far-field station near Besar (u).

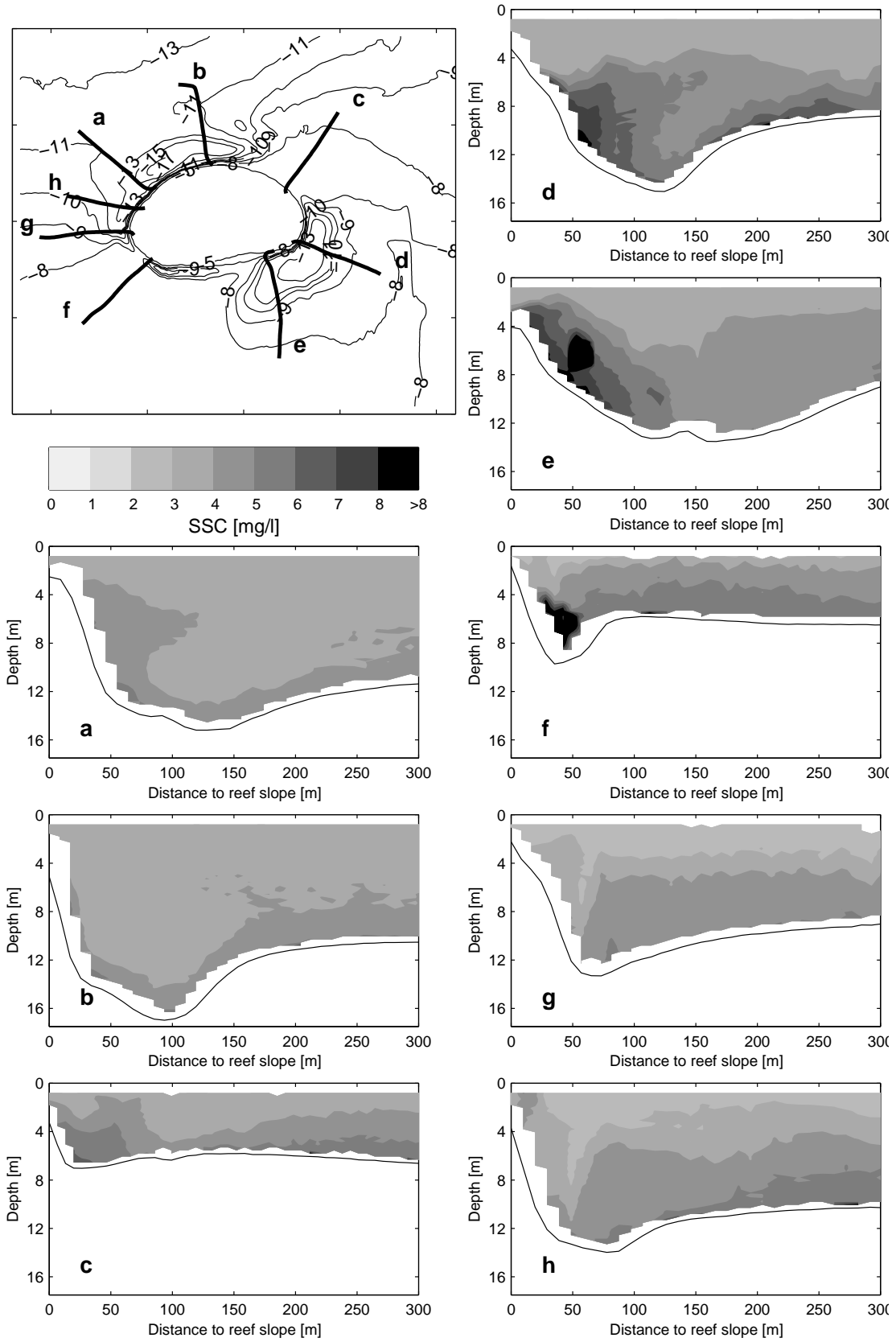


**Figure 7.5.** Quasi-synoptic spatial turbidity patterns at the reef slope of Pamujan Besar during eastward flow conditions, based on SSC estimates inferred from ADCP backscatter intensity.

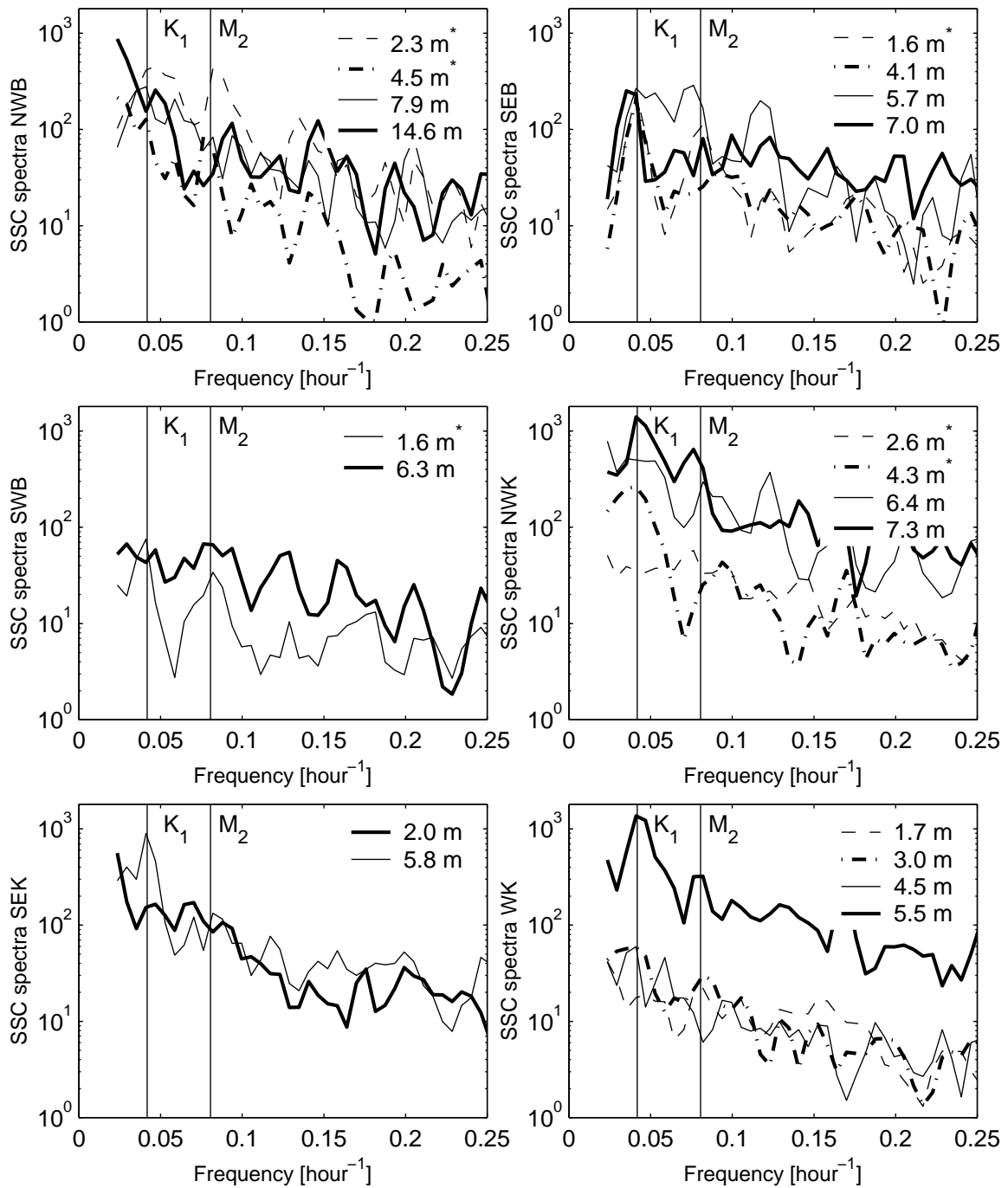


**Figure 7.6.** SSC spectra from OBS measurements at the reef slopes of Kubur and Pamujan Besar. See Fig. 7.1 for location codes. Vertical lines marked by  $K_1$  and  $M_2$  indicate the angular speeds of the corresponding tidal constituents. Note the logarithmic scaling of the vertical axes. Spectra marked by an asterisk were partly adjusted to correct for the erroneous SSC increase due to algae growth.

**Table 7.1.** Mean and maximum of hourly averaged SSC [mg/l] at Kubur and Pamujan Besar. See Fig. 7.1 for site locations. The far field stations correspond to FPK (Kubur) and FPB (Pamujan Besar).

Kubur reef slope										
	NW 2.6	NW 4.3	NW 6.4	NW 7.3	W 1.7	W 3.0	W 4.5	W 5.5	SE 2.0	SE 5.8
mean	3.16	2.48	10.14	8.73	3.35	3.03	3.92	9.74	4.91	6.31
max.	22.33	16.08	72.84	91.00	32.10	23.31	23.66	73.23	34.92	38.99
Kubur far field										
	bottom	depth	surface							
	meter	average	meter							
mean	2.90	3.10	3.80							
max.	11.81	7.30	11.29							
P. Besar reef slope										
	NW 2.3	NW 4.5	NW 7.9	NW 14.6	SW 1.6	SW 6.3	SE 1.6	SE 4.1	SE 5.7	SE 7.0
mean	7.35	4.85	8.29	7.98	4.35	6.20	5.88	5.62	6.85	9.92
max.	28.00	21.30	51.07	82.25	20.30	51.47	25.57	25.65	53.27	72.78
P. Besar far field										
	bottom	depth	surface							
	meter	average	meter							
mean	4.32	4.59	4.93							
max.	10.70	9.17	10.45							

sediment is available for resuspension. Long-term wave data derived from satellite observations (ARGOSS, 2001) confirmed that the wave heights encountered during the field campaign were representative of the wet-season, when typically the highest waves occur.

Fig. 7.4 exhibits a turbidity event which provides a clue that the highest turbidity peaks are due to sediment clouds generated at the deeper parts of the reef slopes. The largest SSC peak occurred at the deepest OBS sensor at the northwestern transect (NW 14.6 m), which was located fairly sheltered as waves were heading east to northeast. Along the same transect, the SSC variation observed at mid-depth (NW 7.9 m) agreed well with the SSC variation at NW 14.6 m, whereas the former persistently lagged on the latter. These sites were clearly located too deep for wave stirring at the bed, since waves were below 0.7 m and the northwestern edge of Besar island was unexposed during the time-span considered. The time-lag indicates that the suspended sediment, either locally entrained or supplied from nearby the seabed, disperses upward across the reef slope.

The spatial structure of the reef-connected sediment clouds at Besar is visualized in Fig. 7.5, which displays SSC estimates inferred from ADCP backscatter intensity. The peaks in SSC occurred either at mid-depth or at the toe of the reef slope (transects d, e and f in Fig. 7.5), and the ambient SSC elevation extended over approximately 150 m. When comparing the SSC levels in Figs. 7.4 and 7.5 it appears that the SSCs at 0.5 m from the reef slopes, as observed by the OBS sensors, are significantly higher than the SSCs in ambient waters at more than 1 m from the reef slope, as observed by the ADCP. The level of turbidity within the clouds thus decreases rapidly with increasing distance from the reef slope.

The SSC spectra generally featured a strong decrease of variance density with increasing frequency, and illustrate the multi-periodicity of the SSC oscillation at the reef slopes (Fig. 7.6). The dominance of flow-induced resuspension of sediment at the reef slopes is marked by peaks at the diurnal and semidiurnal frequencies. These were particularly pronounced for the near-surface time series at Pamujan Besar, and

**Table 7.2.** Coherence between SSC and  $u^2$  oscillation, at frequencies  $f_{K_1}$  and  $f_{M_2}$ . For the cases of Kubur and Besar,  $u$  corresponds to the depth-mean alongshore current velocity at FPK and FPB (Fig. 7.1), respectively. Values of  $u^2$  are supposed to relate linearly to the local shear stress at the reef slope.

Kubur										
	NW 2.6	NW 4.3	NW 6.4	NW 7.3	W 1.7	W 3.0	W 4.5	W 5.5	SE 2.0	SE 5.8
$C(f_{K_1})$	0.06	0.65	0.15	0.26	0.47	0.07	0.51	0.05	0.39	0.26
$C(f_{M_2})$	0.13	0.43	0.11	0.40	0.60	0.25	0.13	0.12	0.24	0.29
P. Besar										
	NW 2.3	NW 4.5	NW 7.9	NW 14.6	SW 1.6	SW 6.3	SE 1.6	SE 4.1	SE 5.7	SE 7.0
$C(f_{K_1})$	0.72	0.88	0.82	0.53	0.93	0.38	0.89	0.95	0.72	0.20
$C(f_{M_2})$	0.68	0.68	0.74	0.14	0.92	0.85	0.83	0.42	0.61	0.60

for the deeper time-series at Kubur. The stronger peaks in the deeper areas of Kubur are in accordance with the expectation that the clouds are generated near the seabed, where most sediment is available. At Pamujan Besar, current amplitudes are larger, which enlarges the chance that the sediment clouds, which may intensify and reduce as a function of the mixed, mainly diurnal tides, reach shallow waters. In the deeper parts of Besar, interference of successive turbidity events may be the cause of absence of a clear diurnal or semidiurnal oscillation.

To determine how well the diurnal oscillations of SSC were linearly related to current shear stresses, the coherence between oscillation of SSC and  $u^2$  was determined, for each of the SSC time series and at frequencies corresponding to the  $K_1$  tide and  $M_2$  tide ( $f_{K_1}$  and  $f_{M_2}$ , respectively). Table 7.2 demonstrates that the diurnal SSC variation at Pamujan Besar predominantly coheres well with diurnal variation of  $u^2$ , which is in contrast with the case of Kubur. For both locations, the coherence of SSC with semidiurnal variation of  $u^2$  is generally weaker than with diurnal variation of  $u^2$ , which is in accordance with the dominance of diurnal currents. The distinction between the two islands may be due to the differences in current amplitudes and structure of the flow, which are the subject of the next section.

## 7.6 Flow structure and coastal morphology

High levels of turbidity are thus primary generated by tidal currents, which are known to be complex in the surroundings of islands (Wolanski & Hamner, 1988; Wolanski et al., 1996). This can be illustrated by the instantaneous horizontal flow structure corresponding to transect  $e$  in Fig. 7.5, which is depicted in Fig. 7.7. It shows significant veering in the vertical velocity structure of the current velocity field. The accuracy of the ADCP-derived vertical velocity component is insufficient to adequately quantify the associated vertical current component. However, based on continuity, the horizontal flow pattern suggests that the reef slope is subject to upwelling, which would explain the upward transport of sediment across the reef slope. It appears likely that the secondary flow conveys sediment that is being entrained at the toe of the reef slope in up-slope direction, until the flow turns and transports the sediment away from the reef, where it may commence to settle from suspension.

The SSC level at Besar, averaged over all time series, was 21% higher than at Kubur. This may certainly be associated with current strength. The  $K_1$  tidal amplitudes of the surface flow along the principal axis amount to 20.3 cm/s and 10.9

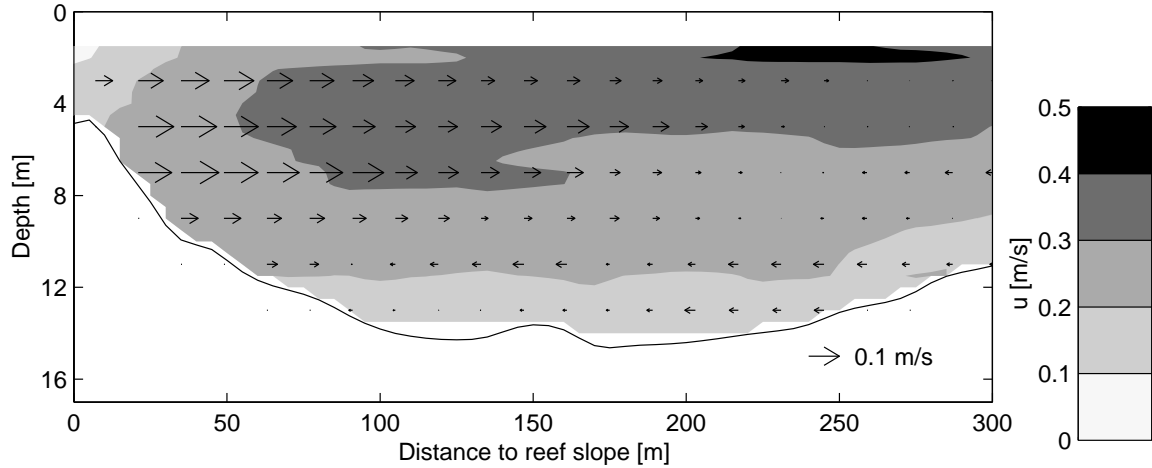


**Figure 7.7.** Horizontal flow affected by flow curvature and the high hydraulic roughness of the island fringe, observed at transect *e* in Fig. 7.5 (pertaining to Pamujan Besar). Gray shading and arrows represent the streamwise and transverse current components, respectively.

cm/s for the cases of Besar and Kubur, respectively. The distinction between average turbidity levels may also relate to a difference in the flow structure between the two islands. Fig. 7.8 displays the quasi-synoptic depth-mean flow structure at the islands under investigation, featuring flow separation in the lee of Kubur, whereas the flow at Besar may be considered quasi-potential. The flow at Kubur separates from the island fringe, creating a region of stagnant water. No fronts were observed during the field campaign, which excludes the possibility of a pronounced eddy with associated upwelling (cf. Wolanski et al., 1996). The turbidity levels in the wake that forms during eastward tidal flow (site NWK in Fig. 7.1), were comparable to these of the other stations.

Wolanski et al. (1984a) and Pattiaratchi et al. (1986) suggested that island wake dynamics are controlled by the island wake parameter:

$$P = \frac{UH^2}{K_z W} \quad (7.8)$$

where  $U$ ,  $H$  and  $W$  are the free-stream current velocity, depth and width of the island (respectively) and  $K_z$  is the vertical diffusion coefficient. For  $P \ll 1$ , friction dominates and quasi-potential flow is expected; a stable wake is characterized by  $P \simeq 1$  and when  $P \gg 1$  a Karman vortex street (e.g. Ingram & Chu, 1987) may develop. Attributing the observed values at Besar (Fig. 7.8, right panel), i.e.  $U=0.3$  m/s,  $H=10$  m,  $W=550$  m and taking  $K_z = 0.003HU$  m<sup>2</sup>/s (e.g. Fischer et al., 1979) gives  $P=6.1$ . Theoretically, either a stable wake or a Karman vortex street should occur, whereas the observed flow pattern is rather quasi-potential. By contrast, the depth-mean flow structure at Kubur does exhibit flow separation, whereas attributing  $U=0.2$  m/s,  $H=8$  m,  $W=450$  m yields  $P=5.9$ , which is virtually equal to the case of Besar. The reason for the established discrepancy between theory and field observations at Besar is the neglect of scour trenches when evaluating the island wake parameter, which presumes a flat bed. The scour trench on the northwestern flank of Besar reaches

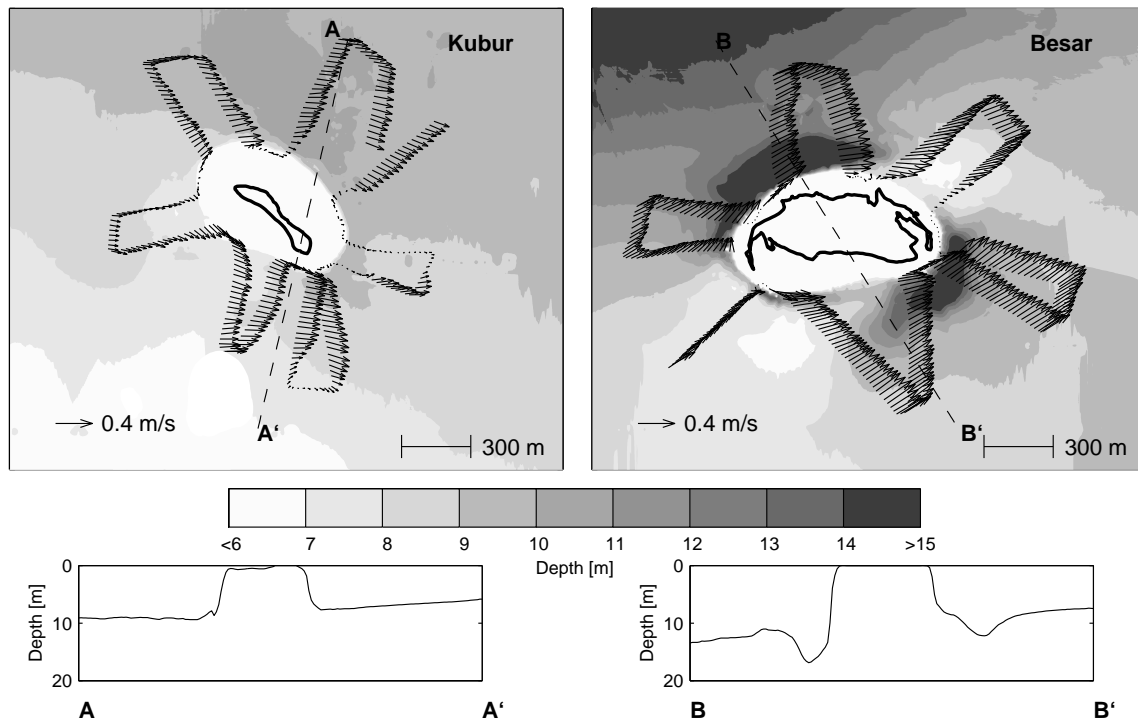


**Figure 7.8.** Depth-mean flow structure around Kubur (left panel) and Besar (right panel), where the bold lines reflect the borderline between reef flat and coral cay. Relatively strong currents at Besar have modified the bed morphology, which is marked by the scour trenches and results in quasi-potential flow. At Kubur, currents are too weak to adjust the bed morphology and flow separation occurs.

a maximum depth of 15 m (Fig. 7.1). The discharges through scour trenches along the flanks of the islands diminish flow accelerations, and therefore reduce horizontal gradients of current velocity.

## 7.7 Implications for reef development

Living corals in the Bay of Banten occur only over very narrow depth range (Meesters et al., 2002), which is due to high levels of turbidity induced by tidal currents. The limited wave influence on turbidity levels, as established, seems to contradict with the observed morphology of the subaqueous parts of the islands, as well as with the shape of the emerging cays (Fig. 7.8). The emerging cays feature well-developed overwashes and spit systems, which are clearly a product of wave driven transport of coral rubble. The distribution of coral rubble, in turn, may determine the availability of substrate for coral growth. The subaqueous parts of the islands are convex towards the north to northeast, orientated towards the direction where the highest waves enter the bay due to the associated long fetch (Fig. 7.1). The reefs in the Bay of Banten thus demonstrate that waves may control reef development in a highly turbid environment, despite that tides control the sedimentary dynamics.

Although flow-induced turbidity variations may not have an eminent influence on the development of the aggregate reef systems, it may determine the metabolic

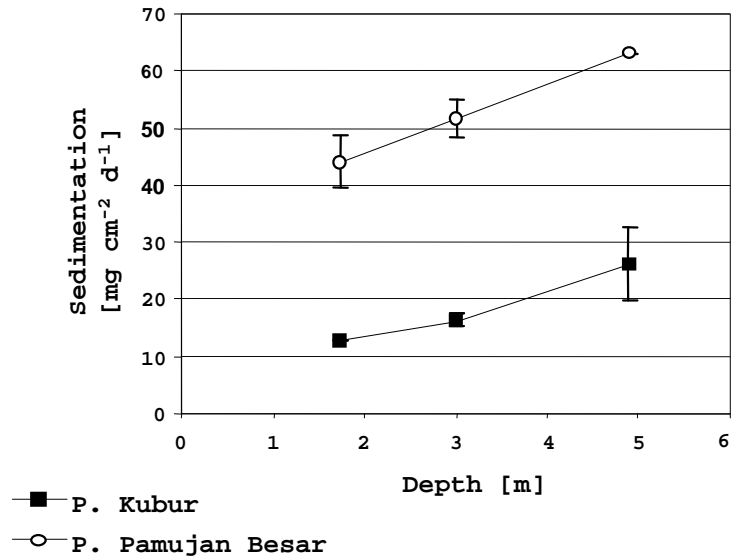


**Figure 7.9.** Sedimentation in tube traps deployed at Kubur and Pamujan Besar, as a function of depth (averages over the period 30 July till 15 August 1998  $\pm$  standard error). Adapted from E.H. Meesters (unpubl. data)

functioning, or health of the individual coral colonies (Meesters et al., 2002). Meesters (unpubl. data) established that the species richness and topographic complexity of the coral colonies were significantly higher at Pamujan Besar than at Kubur, whereas sedimentation and light extinction were most favorable for reef development at Kubur (Fig. 7.9). Meesters et al. (in prep) reports average light-extinction coefficients ( $k'$ ) of 0.42 and 0.50 for the cases of Kubur and Pamujan Besar, respectively, which confirms that SSC levels are highest at Pamujan Besar. The sedimentation measurements seem to disagree with the comparatively healthy status of the reefs, yet they were taken using tube traps, which indicate the potential sedimentation rather than the actual rates of sedimentation. Within the near-surface layer, waves and currents may exert a significant influence on the local sedimentary regime without being responsible for gross turbidity variation, by preventing settling of sediment. Sediment that has settled in the tube traps is substantially sheltered from wave stirring and current drag. Prevention of the settlement of sediment due to both currents and waves likely is the reason for the relatively good condition of the reefs at Pamujan Besar, despite the strong flow-induced turbidity peaks and associated high light extinction. The comparatively tranquil ambient hydrodynamic conditions after turbidity events at Kubur allow for 'unhindered' settlement of the entrained sediment.

## 7.8 Discussion

In particular the coherence and time lag between turbidity variation at different depths of the reef slopes indicate that suspended sediment disperses vertically upwards across the reef slope. Although this is only circumstantial evidence, it is consistent with flow mechanisms that may occur at the reef slopes. To some extent, the transverse ve-



locity structure resembles the secondary flow induced by the curved flow around a headland (Kalkwijk & Booij, 1986; Geyer & Signell, 1990; Geyer, 1993). However, unlike the theoretically transverse velocity profile derived by Kalkwijk & Booij (1986), the observed transverse current nearby the bottom, is substantially smaller than the reversed transverse current near the surface (Fig. 7.7). This discrepancy may relate to the high hydraulic roughness of the corals, and the steepness of the island slopes. Due to the steepness of the island slopes, the flow region nearby the islands can be regarded as a corner boundary layer. Perkins (1970) describes a laboratory experiment of a corner boundary layer in a straight non-circular duct, where transverse secondary circulations were generated including an upward velocity component at the vertical boundary. The discrepancy between the observed and an idealized secondary circulation in a curving flow may be further explained by stratification of the ambient waters, which mix in the turbulent boundary layer above the reef slope inducing a downward flux of buoyancy (Phillips et al., 1986; Wolanski & Hamner, 1988). The associated secondary current is directed toward the solid boundary both near the surface and near the bottom, and has a component away from the boundary in between, as visualized by Phillips et al. (1986) from experiments. The degree in which Phillips's mechanism may apply to low levels of stratification, in absence of a pronounced pycnocline as in the case of the Bay of Banten, is indefinite.

The results in this chapter partly confirm the findings by Larcombe & Woolfe (1999) and Larcombe et al. (2001), who argue that the turbidity and sedimentation regimes of nearshore reefs are controlled predominantly by the hydrodynamics of their environment and the nature and availability of bed sediment, rather than by sediment supply to the region or to the nearshore zone in particular. Both in the central Great Barrier Reef and at the northwestern coast of Java, turbidity peaks in ambient reef waters are thus not the direct result of inundation by river plumes. However, river discharges may indirectly affect the sedimentary regime of nearshore reefs by influencing the availability of bed sediment. Larcombe et al. (2001) further conclude that waves are the primary hydrodynamic mechanism generating high turbidity, which disagrees with the established flow dominance in this chapter. With reference to the Great Barrier Reef region, the southwestern Java Sea experiences relatively strong tidal currents, whereas winds and associated wind and swell waves are of low intensity. The comparatively strong tidal currents in the Bay of Banten and adjacent waters are due to three sources of tidal energy, viz. the resonant response of the Java Sea basin to diurnal forcing (Ali, 1992), penetration of semidiurnal tidal energy through the Strait Sunda (Fig. 7.1), and input of diurnal and semidiurnal tidal energy along the eastern margin of the Java Sea (Wyrтки, 1961). Within the Bay of Banten, coastal currents near Besar are enhanced by the protruding subaqueous delta that shapes the east coast of the bay.

The causes of the capricious SSC response to tidal current forcing in ambient reef waters remain largely inconclusive, but general experience in silty coastal regions does provide some clues. Bass et al. (2002) describe the factors associated with fine particles that may create phase shifts in concentrations derived from idealized scenarios of events of erosion and subsequent deposition, which complicate the interpretation of suspended sediment signals. These include variable floc size and hence settling velocity, bed consolidation, advection from nonlocal sources and variable critical erosion

and deposition shear stresses. Whereas SSCs between 1 to 40 mg/l are high for reef environments, these are low values within the context of flocculation studies, which generally deal with higher concentrations. However, using measurements from the Tamar estuary described by Fennessy et al. (1994), Dyer & Manning (1999) recently inferred that low concentrations promote flocculation. Actual observations of flocculation in a tropical region where SSC levels are comparable to these in the Bay of Banten were reported by Berhane et al. (1996). Probably each of the factors listed by Bass and coworkers is relevant to the sedimentary dynamics of shallow-water coral reefs. The observed capricious SSC response to current forcing may be enhanced by the transient character of the complex flow structures surrounding the reefs and by the spatially and temporally variable sediment availability at the reef slopes. The flow structures may be highly dependent on the exact direction of the ambient coastal flow.

The island wake parameter proposed by Wolanski et al. (1984a) has a limited predictive potential in a coral reef embayment where especially scour trenches influence the flow structure of the coral islands. This subscribes to the study by Furukawa & Wolanski (1998), who conclude that details of the bathymetry of Rattray Island are important to the hydrodynamics in its wake. Substitution of  $K_z = 0.003HU$  (e.g. Fischer et al., 1979) in Eq. 7.8 yields  $P=H/(0.003W)$ , which suggests that the flow structure in shallow-water island wakes is largely independent of the strength of the current. However, stronger currents are more likely to reshape the bed morphology, as they exceed the threshold for initiation of motion of the bottom sediments more often. Moreover, the alternating lee sides of islands subject to strong tidal currents may act as a sediment intercept where the sediment eroded along the flanks is deposited, which indeed was perceptible from the morphology surrounding Besar (Fig. 7.8). These accumulation areas effectively streamline the bed morphology and therefore resist flow separation to some extent. The occurrence of local morphological adjustments restrict the applicability of the island wake parameter to regions where the surrounding seafloor is either non-erodible and or subject to currents that remain below the threshold for initiation of motion of the bottom sediment.

## 7.9 Conclusions

The observations presented in this chapter show the presence of clouds of suspended sediment surrounding the fringes of coral reefs. ADCP backscatter data has provided a valuable measure of SSC, revealing the spatial structure of the reef-connected sediment clouds. Correspondence between OBS-derived time series of SSC at different depths at the reef slopes indicate that suspended sediment is dispersed upwards across the reef slopes. Since the SSC levels close to the reef slope are considerably higher than the SSCs in the ambient reef waters at larger distance, raised levels of turbidity are due to local hydrodynamic processes rather than the result of advection. From the peaks in the diurnal and semidiurnal frequency bands of SSC spectra, and the large depths where the turbidity variation initiates, it can be inferred that tidal currents are the main cause of turbidity generation. The influence of wave action on suspended sediment dynamics is confined to the top few meters of the reef slopes, where little sediment is readily available for resuspension. The ADCP-derived three-dimensional

current structure suggests that secondary circulation, which likely develops due to flow curvature and the hydraulic roughness of the reef fringes, plays an important role in the upward fluxes of suspended sediment. The flow structure, in turn, interacts with the seafloor morphology surrounding the shallow-water islands, which emerged from scour trenches and areas of accretion. These morphological adjustments counteract flow separation, resulting in quasi-potential flow in regions where currents are strongest. Comparison of two studied marginal reefs subject to stronger and weaker currents (respectively) indicates that the health of the living corals, nor the aggregate reef morphology are directly linked to turbidity conditions. High-energy wave incidence and sedimentation causing temporary silt cover are seemingly more fundamental controls on shallow-water reef development.

# 8

## Synthesis

### 8.1 Introduction

The Bay of Banten represents a coral reef environment characterized by:

- a mixed, mainly diurnal tidal regime
- low-energy wave conditions
- small-scale river input
- a monsoon-dominated throughflow
- high turbidity
- an eroding delta that shapes the eastern shorelines
- a high degree of siltation

Section 8.2 synthesizes the physical processes that determine the principal environmental conditions of coral reefs in the bay. In succession, the direct influence of river discharges, regional sediment transport and local sedimentary processes are described. Section 8.3 highlights the general implications of the results and concludes this thesis with recommendations.

### 8.2 Physical processes in the Bay of Banten

#### 8.2.1 Direct river impacts

The direct influence of low-salinity/high-turbidity river plumes on coral reefs in the bay is restricted to incidental events, and not a primary stress factor. Despite the micro-tidal regime, tidal currents are strong enough to breakdown stratification in the freshwater input region during peak current velocities. This is a topographic effect induced by a protruding, semi-inactivated delta, which obstructs the tidal flow that drains and refills the bay. The delta hydrodynamically acts as a headland, where currents accelerate and where upwelling may occur due to flow curvature. Both

upwelling and shear-induced mixing associated with the relatively strong currents provide for well-mixed conditions near the delta, where small rivers debouch into the bay. Thus, local river discharges in the bay mix rapidly with marine waters.

Restriction of river influences also results from the coupling between the monsoon-induced throughflow and river discharge, which is highest during the wet season when the residual circulation is towards the east. The monsoon-induced residual current is strong enough to overcome the Coriolis force, and advects the river discharges mixed with marine waters. Consequently, coral reefs in the bay are protected from direct exposure to suspensions containing recent river discharges, which inundate the reefs merely incidentally in the wet season. During the dry season, the throughflow associated with the Southeast Monsoon may convey buoyancy and suspended sediment derived from the remote rivers Cijung and Cidurian, yet salinity remains well above the stressing limits.

### **8.2.2 Regional sediment supply**

The Bay of Banten constitutes a Holocene sediment wedge composed of a mixture of silt and clay. Processes of bottom erosion and deposition operate continuously throughout the embayment and are governed by both waves and currents. Waves resuspend sediment especially in the nearshore zone along the eastern margin of the bay, at depths smaller than about 3 m, where delta deposits are being reworked. Like the river discharges, wave attack and the resulting shoreline erosion in the delta culminate during the Northwest Monsoon, when the monsoon-driven circulation is towards the east. The seasonal coupling of wave-induced erosion and monsoon circulation favors the ambient turbidity conditions of coral reefs in the bay.

Currents resuspend sediment in a broader depth range, most persistently in front of the semi-inactivated delta where currents accelerate. The mixed, mainly diurnal tidal flow is essentially bidirectional, along the bay's isobaths, and displays an asymmetric pattern as maximum velocities to the east systematically exceed those to the west. Due to the nonlinear response of sediment transport to current velocity, the tidal asymmetry promotes an eastward drift of sediment, away from the patch reefs in the bay.

The combination of spatial variation in current amplitudes, settling lags and scour lags does provide a mechanism causing residual sediment transport towards the reefs in the bay. When following the westward tidal flow, sediment that is brought into suspension at the submarine delta is likely to settle down in the central parts of the bay, due to the decrease of sediment transport capacity of the decelerating water mass. During the subsequent eastward flow, little sediment may be entrained in other parts of the bay than the submarine platform in front of the former delta, leaving a large portion of the earlier deposited sediments to consolidate. This mechanism may be enhanced during the Southeast Monsoon, when a westward residual circulation is superimposed on the tidal flow.

### 8.2.3 Local sedimentary processes at coral reefs

Regional sediment supply determines the availability of readily erodible sediment in the ambient reef waters. Local physical processes, in turn, dominate turbidity variation and sedimentation rates in the reef environments, whereas regional advection generally plays a subordinate role. Peak tidal currents induce clouds of suspended sediment connected to the reef slopes. However, these clouds behave rather capriciously, which may relate to the complex reef morphology that generates versatile three-dimensional current structures. An observed time-lag between turbidity variation near the bottom and at mid-depth above the reef slope has indicated that the suspended sediment, either locally entrained or supplied from nearby the seabed, disperses upwards across the reef slope. The upwelling of resuspended sediment may be associated with the curvature of flow pathways along the reef slopes, with the high hydraulic roughness of the reefs and with weak stratification. Scour trenches flanking the reef islands counteract flow separation, as the flow obstruction due to the island is compensated by the discharge through the trench. These morphological adaptations strengthen the connection between the flow and the curved, hydraulically rough reef slopes, and consequently may enhance upward sediment fluxes across the reef slopes.

The high levels of turbidity associated with the tidally-induced clouds of suspended sediment limits the depth range in which coral can subsist in the bay. However, it is unlikely that turbidity plays a primary role in modern reef development, since the shape of the islands obviously relates to wave exposure, and reefs situated in a more turbid regime can be in a better health state. Waves act particularly in a shallow layer near the surface, where coral cover is highest and little bed sediment is available for resuspension. Whereas tidal currents are the primary cause of high turbidity, locally generated waves may be important in preventing sediment to settle from suspension, and smother coral polyps. During tranquil conditions the water clarity may be high, yet corals are being covered by a thin film of deposited sediment. During high-energy conditions, turbidity may increase but shear stresses clear the reefs from settled sediment. Hence, sedimentation in the embayment is likely a more fundamental control on the shallow-water coral reefs than turbidity.

## 8.3 General implications and recommendations

### 8.3.1 Coral reefs in marginal regimes

The major determinants of coral reef distribution include temperature, salinity, light, aragonite saturation and nutrients. The physical analysis of the Bay of Banten has exemplified a shallow-water reef environment that may be classified as marginal, due to siltation stresses and the proximity of freshwater and nutrient sources. The example revealed that the key issues determining the delicate subsistence of shallow-water reefs include (1) mixing in the freshwater source region, (2) the seasonal coupling between wave-induced erosion, river discharge and residual flow and (3) local sedimentary processes. The topography-controlled mixing of small-scale river discharges with the ambient marine waters inhibits the direct exposure of coral reefs to river-derived sediment suspensions, high nutrient loads and low salinity. Human coastal interventions,

such as land reclamation for fish ponds and jetty construction to facilitate transshipment, generally alter flow patterns and consequently change the tide-induced mixing capacity. Marginal reefs benefit from the increase of current amplitudes in the freshwater source regions, and suffer from changes that enhance stratification. In the Indonesian context, extensive fish ponds of brackish water in the coastal zone cause salinity gradients to shift inland, which may reduce the potential problem of low salinity.

Monsoonal cycles of river discharge, wave height and direction and throughflow are often very regular. Indeed, the seasonal coupling of river discharge, wave attack and residual flow may create a lee and a luff side on the flanks of a river mouth. However, the dominance of local hydrodynamic processes controlling the sedimentary regimes of the near-coastal reefs puts the importance of regional sediment supply in perspective. It is questionable whether the ambient reef waters would gradually become more transparent if less recent river sediment would be injected to the coastal system. It appears unlikely that a decline or increase of terrestrial sediment input would have an immediate impact on the sedimentary regime of near-coastal reefs. The sediment that is already available may be resuspended and deposited repeatedly. Moreover, a portion of the suspended sediment may consist of carbonate sands produced by the coral reefs themselves. Consolidation and biological sediment fixation constitute important processes that may interrupt cycles of erosion and deposition. Both these processes were not addressed in this thesis, and await future research.

### 8.3.2 Physical oceanography of continental shelves

The present analysis has demonstrated that tidal asymmetry in mixed, mainly diurnal regimes may lead to residual sediment transport. The asymmetry associated with the  $K_1$ ,  $O_1$  and  $M_2$  tides may occur not merely in the shallow coastal region, but also in deeper waters of continental shelves where diurnal tides are significant, since each of the tidal constituents is astronomical. It would be of interest to analyze the implications of sediment transport due to the interaction of the  $K_1$ ,  $O_1$  and  $M_2$  to morphological behavior on the scale of a tidal basin such as the Java Sea. This would require a detailed modelling study similar to the one performed by Ali (1992), with the attention focussed on the phase angle relationship  $\Theta_d = \phi_{K_1} + \phi_{O_1} - \phi_{M_2}$ , and the amplitude product  $A_{K_1} \cdot A_{O_1} \cdot A_{M_2}$ . Ideally, such an analysis would include the monsoon-driven circulation, in particular since the results of Wyrтки (1961) demonstrate that the opposing monsoons create dissimilar spatial patterns of residual currents. Consequently, the distortion of the tidal motion due to the monsoon-driven residual currents may not average out over the time span of a year.

The morphological adaptations in the surrounding island waters, which effectively streamline the reefs, suggest that scattered reefs produce less mixing than what may be expected from literature (Wolanski et al., 1984a; Pattiaratchi et al., 1986; Furukawa & Wolanski, 1998). Many authors have stressed that islands can have a significant influence on horizontal dispersion (Okubo, 1974; Sanderson et al., 1995; Inoue & Wiseman Jr., 2000; Tseng, 2002). Okubo (1974) has analytically derived an equation for the effective horizontal mixing coefficient ( $K_x$ ) due to trapping of water in island

wakes:

$$K_x = \frac{K'}{1+r} + \frac{rU_0^2}{2k(1+r+\sigma/k)(r+r)^2} \quad (8.1)$$

where  $r$  is the ratio of trapped to nontrapped fluid,  $k$  is the inverse of the exchange times between the trapped fluid and the main flow,  $\sigma$  is the tidal frequency,  $U_0$  is the tidal flow amplitude, and  $K'$  is the normal mixing coefficient without islands. Whereas it is tempting to scale  $k$  with  $\sigma$ , to predict the radius of the island wake using the theory of Wolanski et al. (1984a), and subsequently to estimate the regional mixing effect using equation 8.1, the present study discourages such an approach. If morphological adaptations occur, including scour trenches and deposition areas in the island wakes, currents around reef islands may mimic quasi-potential flow in spite of high current velocities and large depth to width ratios, which renders the island wake parameter inappropriate. Bathymetric data are lacking to assess whether the morphological adaptations as observed are common, or representative of coral reef systems in silty coastal environments in the tropics. Further research is recommended on the morphological characteristics influencing wake behavior, since these may be essential to both local and regional mixing processes.



# Samenvatting

## Introductie

Koraalriffen zijn van vitaal belang voor het leven in tropische kustzeeën. De mondiale distributie van koraal is gerelateerd aan watertemperatuur, zoutgehalte, lichtdoordringing en de concentratie van voedingsstoffen. Koraal is sterk afhankelijk van de lokale marine condities en is daardoor kwetsbaar voor natuurlijke en antropogene verstoringen in het kuststelsel. Deze kwetsbaarheid manifesteert zich met name bij riffen in de kustnabije zone, waar de ontwikkeling van rivierdelta's de marine condities beïnvloedt. De hedendaagse ontwikkelingen in tropische rivierdelta's zijn vaak terug te voeren op de ontbossing van stroomgebieden, waardoor bodemerosie plaatsvindt. Dit gaat gepaard met een toename van de sedimentlast in rivieren en een verhoging van piekafvoeren van water dat rijk is aan voedingsstoffen. Ontwikkelingen in rivierdelta's kunnen van invloed zijn op koraal in de kustnabije zone door de initiatie of verandering van processen zoals het opwerpen van riviersediment, hetgeen het zicht onder water verkleint, sedimentatie op het rif, aanvoer van voedingsstoffen en menging van zout en zoet water. Dit proefschrift draagt bij aan de kennis omtrent

- de fysische mechanismen die bepalend zijn voor de regionale variatie in troebelheid, zoutgehalte, verticale menging van zout en zoet water en de aanvoer van riviersediment in de omgeving van riffen bij de kust, en
- lokale sedimentaire processen ter plaatse van koraalrifhellingen, welke van invloed zijn op zeezicht en het neerslaan van sediment op koraal assemblages.

Als studiegebied is gekozen voor de Baai van Banten (West Java, Indonesië). Deze fysisch geografische studie is onderdeel het 'Teluk Banten Research Programme', dat deel uitmaakt van het 'Global Change Programme' van de Koninklijke Nederlandse Academie van Wetenschappen. Het project is gecoördineerd door Stichting voor Wetenschappelijk Onderzoek van de Tropen en Ontwikkelingslanden.

## Studiegebied

De Baai van Banten ligt aan de zuidwestelijke rand van de Java Zee, nabij de Straat Sunda. Het gebied heeft een typisch moessonklimaat, hetgeen resulteert in regelmatige cycli van wind en neerslag. De kust wordt gevormd door laaggelegen moddervlaktes,

veelal begroeid met mangroves. Louter kleine krekens monden uit in de baai. De belangrijkste bronnen van zoetwater en riviersediment zijn gelegen langs de oostelijke kustlijn, welke is gevormd door de Ciujung delta. De Ciujung is tussen 1920 en 1930 omgelegd middels de aanleg van een kanaal, waarna de verlaten delta in de Baai van Banten begon te eroderen. Een deel van het geërodeerde sediment heeft voor aangroei van de zuidoostelijke kustlijn van de baai gezorgd. Recente topografische kaarten wijzen erop dat dit proces momenteel nog aan de gang is.

De baai accommodeert meer dan tien koraalrif eilanden, die in de meeste gevallen deels verheven zijn boven de maximale hoogwaterstand. De supra-getijdegebieden zijn grotendeels begroeid en zijn ontstaan door een verlaging van de zeespiegel, welke tijdens het Mid-Holeceen minimaal 2 m boven de huidige zeespiegel stond. De rifen staan zonder twijfel onder invloed van de dynamica van gesuspendeerd sediment en gerelateerde kustmorfologische processen. Zo zijn door de kustaanwas langs de zuidoost rand van de baai twee tombolo's ontstaan, tezamen genaamd Pulau Dua. Dit proces is nog gaande, waardoor de twee schiereilanden zich geleidelijk verenigen met de kust, waarbij koraal bedekt raakt. De maximale diepte tot waar levend koraal voorkomt in de baai is over het algemeen in de orde van 3 m en dus zeer beperkt. De hoge troebelheid comprimeert het bereik waarover koraalgroei mogelijk is.

## **Topografische invloed op menging en gelaagdheid in een ondiepe getijde baai**

Het getij in de baai is gemengd enkel- en dubbeldaags, waarbij het dagelijkse verticale getijverschil zelden 85 cm overschrijdt. Ondanks dit microgetij kunnen de getijgedreven stroomsnelheden lokaal oplopen tot 65 cm/s. De getijstromen lopen hoofdzakelijk parallel aan de dieptecontouren, en zijn daarmee grotendeels oost-west georiënteerd. Op de getijstroom is een quasi-stationaire moessonstroming gesuperponeerd van ongeveer 10 cm/s. Ondanks de beperkte aanvoer van zoet water kan er aanzienlijke gelaagdheid in de waterkolom optreden, als gevolg van verticale gradiënten in zoutgehalte. De fluctuaties in verticale gelaagdheid en menging vinden plaats over een breed frequentiespectrum. De enkel- en dubbeldaagse fluctuaties worden veroorzaakt door de sterktevariatie van de getijstroom die de turbulente uitwisseling over de waterkolom bevordert. De laagfrequente fluctuaties zijn een gevolg van differentiële zoutaanvoer over de waterkolom. In geval van een moessonstroming vanuit de richting van de zoetwaterbron ter plaatse van een meetlocatie neemt het zoutgehalte aan de oppervlakte sneller af dan bij de bodem, door de hogere stroomsnelheid aldaar. Hierdoor treedt een gelaagdheid op die kan worden opgeheven door het omgekeerde proces.

De mate van verticale menging en gelaagdheid van water massa's in de baai is dus afhankelijk van de sterkte van de getijstroom, de locatie ten opzichte van de belangrijkste zoetwaterbron en de oriëntatie van de moesson-gedreven doorstroom. De sterkte van de getijstroom varieert door de baai, onder invloed van de topografie. Hydrodynamisch gezien fungeert de verlaten delta als een kaap die voor obstructie van de getijstroom zorgt, waardoor de snelheden lokaal hoger zijn. Zodoende komt de zoetwater bron overeen met het gebied waar gelaagdheid van de waterkolom het

meest wordt tegengewerkt, door een sterke turbulente uitwisseling. Het netto effect is dat in de nabijheid van de verlaten delta de waterkolom dagelijks een periode volledig gemengd is, terwijl in de meer centrale en westelijke delen van de baai de kritieke grens van volledige menging tijdens maximale stroomsnelheid soms dagenlang niet wordt overschreden. Dit is enigszins contraintuïtief, aangezien de zoetwater effecten dus beter merkbaar zijn op enige afstand van de zoetwaterbron.

## **Asymmetrie van zeestromingen door astronomische getijden: implicaties voor het residuaal transport van sediment**

Het gemengde enkel- en dubbeldaagse karakter van het getij in de Baai van Banten gaf aanleiding tot een verkennende studie naar de verschillen tussen eb- en vloedstromen in dit type regime. Asymmetrie van het getij wordt doorgaans veroorzaakt door niet-lineaire processen op ondiep water, waar bodemwrijving en topografische effecten een rol spelen. Ervaring op dit terrein is met name opgedaan in dubbeldaagse getij milieus, waar veelal een viermaal daagse getij component ( $M_4$ ) wordt gegenereerd. In het geval van een gemengd enkel- en dubbeldaags getij kan asymmetrie echter ook worden veroorzaakt door interactie van de twee enkeldaagse hoofdcomponenten, te weten  $K_1$  en  $O_1$  met de dubbeldaagse hoofdcomponent,  $M_2$ . Als gevolg daarvan is de maximale stroomsnelheid over de tijdsperiode van een cyclus van springtij tot doodtij persistent in dezelfde richting voor opeenvolgende cycli. De asymmetrie van de getij curve is identiek voor opeenvolgende springtij/doodtij cycli. Naast de genoemde drie hoofdcomponenten speelt een aantal getijcomponenten een rol die doorgaans een relatief kleine amplitude hebben.

Asymmetrie van getijstroming kan residuaal bodemtransport van sediment tot gevolg hebben, door de niet-lineaire respons van sediment transport nabij de bodem op stroomsnelheidsvariatie. De asymmetrie inherent aan een stromingscomponent  $V$  opgebouwd uit de bijdragen van de  $K_1$ ,  $O_1$ ,  $M_2$  en  $M_4$  veroorzaakt een residuaal bodemtransport dat in dit proefschrift is geanalyseerd door afleiding van de lange termijn gemiddelden van  $V^3$  en  $V^5$ . Suspensief sediment transport reageert met een vertraging op variatie van de stroomsnelheid, als gevolg van de tijd die nodig is voor het opwerpen en uitzakken van sediment. Daardoor wordt het transport van suspensief sediment niet alleen beïnvloed door verschillen in de maximale stroomsnelheid tijdens eb en tijdens vloed, maar ook door genuanceerde verschillen in versnelling en vertraging van de stroming tijdens eb en vloed. De vertragingseffecten zijn geanalyseerd met behulp van een relaxatiemodel. Verschillen in pieksnelheden blijken in potentie ongeveer een vijf maal belangrijkere bijdrage te leveren aan het residuaal transport van suspensief sediment dan vertragingseffecten.

## Hydrodynamische controle op het transport van kust- en riviersediment naar koraal riffen

De koraalriffen in de Baai van Banten liggen op enige afstand van een eroderende, verlaten delta, waar kreken uitmonden die met name in het natte seizoen sediment aan het kuststelsel leveren. Bij de aanvoer van sediment naar de koraal riffen in de baai is de seizoenskoppeling tussen kustprocessen van belang. Zo vindt erosie van de kustlijn met name plaats tijdens de noordwest moesson, wanneer de golven hoofdzakelijk vanuit het westen invallen. De noordwest moesson genereert een oostwaarts gerichte doorstroom in de baai, waardoor veel van het in suspensie gebrachte sediment de baai wordt uitgevoerd, zich verwijderend van de riffen. Tijdens de zuidwest moesson is de wind vaak landafwaarts, waardoor de golfaanval minder sterk is. Een soortgelijke seizoenskoppeling vindt plaats tussen de rivierafvoeren en de moessongedreven stroming. De noordoost moesson komt overeen met het natte seizoen, waarin de rivierafvoeren het hoogst zijn. De moessongedreven stroming weegt doorgaans op tegen het effect van de draaiing van de aarde, waardoor de rivierafvoeren met deze laagfrequente stroming worden mee getransporteerd, wederom zich verwijderend van de riffen in de baai.

Naast kusterosie door golfwerking en rivierinvloed is resuspensie de getijstroom een oorzaak van troebelheid en sedimenttransport, met name in de regio van de verlaten delta op dieptes in de orde van 6 à 10 meter. Twee getij-gerelateerde mechanismen leiden tot een residuaal transport. Allereerst is de getijstroom asymmetrisch door interactie van de getij componenten  $K_1$  en  $O_1$  met  $M_2$ . Als gevolg daarvan is de pieksnelheid van de getijstroom over duur van een springtij/doodtij cyclus persistent naar het oosten gericht. Dit resulteert in residuaal sediment transport naar het oosten, hetgeen gunstig is voor de riffen in de baai die ten westen van de voornaamste sedimentbron zijn gelegen. Een tweede transportmechanisme komt voort uit de ruimtelijk verschillen in de amplitude van de getijstroomsnelheid. Deze amplitudevariatie, in combinatie met vertragingen bij het opwervelen en uitzakken van sediment, resulteren in een residuaal transport van een grote amplitude van de getijstroom naar een kleine. Meebewegend met de getijstroom naar het westen wordt in het voorgebied van de verlaten delta sediment in suspensie gebracht, hetgeen uitzakt in de centrale delen van de baai waar de getijstroom snelheid mindert. De snelheid van de daaropvolgende westelijke getijstroom is overwegend onvoldoende om het bezonken sediment weer in suspensie te brengen. Om die reden is het grootste gedeelte van de baai een regio van netto depositie.

## Observatie van fijnkorrelig gesuspendeerd sediment met behulp van ADCP en OBS metingen

Akoestische stroomsnelheidsmetingen met behulp van een ADCP (*Acoustic Doppler Current Profiler*) levert kwalitatieve informatie over korrelgroottes en concentraties van sediment in suspensie. Met behulp van simultane metingen met een optisch instrument is het potentieel van dergelijke ADCP informatie geanalyseerd, met het oog

op toepassing in de Baai van Banten. Op basis van theorie en vergelijking met optische metingen is afgeleid dat de concentratie suspensief sediment lineair gerelateerd is aan de korrelgrootte in het kwadraat. Een toename van de concentratie suspensief sediment, veelal als gevolg van een toename van de stroomsnelheid, gaat dus gepaard met een kwadratische toename van de korrelgrootte. Dit laatste is niet verwonderlijk, aangezien de getijstroom bij een grotere stroomsnelheid in staat is om grover materiaal in suspensie te brengen.

Gebruik makend van de gevonden relatie tussen korrelgrootte en concentratie suspensief sediment kan de ADCP echointensiteit worden geconverteerd naar de concentratie suspensief sediment, op basis van een calibratie. De calibratie blijkt echter seizoen- en regioafhankelijk, hetgeen de algemene toepasbaarheid beperkt. Het is aanmerkelijk dat de seizoen- en regioafhankelijkheid van de calibratieresultaten kunnen worden toegeschreven aan de grotendeels onbekende invloed van flocculatie en aan de aanwezigheid van organische stof op ADCP echointensiteit. Ondanks deze beperkende factoren kan de ADCP echointensiteit op zijn minst een kwalitatief beeld geven van temporele of ruimtelijke patronen van de concentratie suspensief sediment.

## **Getij-geïnduceerde wolken van suspensief sediment rondom koraal riffen op ondiep water**

De koraal riffen in de Baai van Banten zijn gelegen in een regio waar sediment accumuleert. De locale hydro- en sediment dynamica rondom de riffen wijkt echter af van het regionale beeld. Aan de bovenstroomse zijde ontstaat een gebied waar het water stagneert. Aan de benedenstroomse zijde ontstaan wervels die relatief klein van afmeting zijn. De vorming van wervels wordt tegengewerkt door geulen parallel aan de stroomrichting, die stroomvoerend zijn de weerstand van het eiland deels compenseren. Boven de rifeellingen is het water troebeler dan in het omringende water. Variatie in troebelheid in de diepere delen ijlt na op troebelheidsvariatie meer bij de oppervlakte. Dit suggereert dat de getijstroom langs het rif sediment in suspensie brengt, waardoor sub-mariene sediment wolken ontstaan. Het ruimtelijke beeld van deze sediment wolken is in beeld gebracht door de ADCP echointensiteit te gebruiken als maat voor de concentratie suspensief sediment, na calibratie. Een spectraal analyse demonstreert dat de dominante perioden van troebelheidsvariaties rond het rif overeenkomen met die van het enkeldaagse en dubbeldaagse getij.

De golven in de baai zijn slechts sporadisch hoger dan 1.5 m. Daardoor is golfwerking over het algemeen alleen significant in de bovenste drie meter van de waterkolom. Aangezien de koraalbedekking het hoogst is op de bovenste drie meter van de rifeelling, vervullen de golven ondanks hun beperkte hoogte een belangrijke functie. In het bijzonder zorgen zij ervoor dat het sediment in suspensie niet neerslaat, waardoor het levende koraal zou kunnen worden bedekt. Golven bepalen tevens de herverdeling van koraal brokstukken op het rifplateau. Dergelijke brokstukken die over de rand van het rif vallen en zich hechten aan de rifeelling vormen substraat voor nieuw koraal. De golfwerking is zodoende met name van invloed op de laterale ontwikkeling van het levende deel van het rif, terwijl de getijwerking de dieptelimiet van koraalgroei bepaalt.

## Synthese

Koraalriffen dicht bij de kust staan vaak bloot aan vertroebeling van de omringende kustwateren door rivierafvoeren en erosieprocessen. Het onderzoek in de Baai van Banten heeft aangetoond dat koraalriffen kunnen voortbestaan in de nabijheid van een eroderende riviermonding, dankzij menging en door het optreden van een seizoenskoppeling tussen verschillende fysische kustprocessen. De troebelheid rond de koraalriffen in de baai limiteert de diepte tot waar koraalgroei mogelijk is. De belangrijkste oorzaak van deze troebelheid is de lokale opwerveling van sediment door de getijstroom. De riffen komen maar zelden direkt met rivierpluimen in contact; het riviersediment wordt eerst afgezet alvorens stromingen door wind en getij voor verspreiding zorgen. De troebelheid hoeft niet *perse* af te nemen indien de regionale aanvoer van sediment stagneert. Hetzelfde sediment kan immers herhaaldelijk opwervelen en weer uitzakken.

# Bibliography

- ACHITUV, Y. & Z. DUBINSKY (1990), Evolution and zoogeography of coral reefs. In: Z. Dubinski, ed., *Ecosystems of the world* 25, chap. 1, Elsevier, Amsterdam, pp. 1–9.
- ALI, E. M. (1992), The Tidal Dynamics of the Java Sea. Master's thesis, School of Earth Science, Flinders University of South Australia.
- ALLEN, G. P., D. LAURIER & J. THOUVENIN (1979), Etude sédimentologique du delta de la Mahakam. *Notes et Mémoires, Total Paris, Compagnie Française des Pétroles* 15, 156 pp.
- ANDERSON, V. C. (1950), Sound scattering from a fluid sphere. *Journal of the Acoustic Society of America* 22, pp. 426–431.
- ANDREWS, J. C. & G. L. PICKARD (1990), The physical oceanography of coral-reef systems. In: Z. Dubinsky, ed., *Coral Reefs, Ecosystems of the world* 25, chap. 2, Elsevier, pp. 11–48.
- ARGOSS (2001), CLAMS: An Online Offshore Climate Assessment Tool, Vollenhove, the Netherlands.
- AUBREY, D. G. & C. T. FRIEDRICH (1988), Seasonal climatology of tidal non-linearities in a shallow estuary. In: D. G. Aubrey & L. Weishar, eds., *Hydrodynamics and Sediment Dynamics of Tidal Inlets, Lecture Notes on Coastal and Estuarine Studies*, 29, Springer-Verlag, pp. 103–124.
- AUBREY, D. G. & P. E. SPEER (1985), A study of non-linear tidal propagation in shallow inlet/estuarine systems part 1: Observations. *Estuarine, Coastal and Shelf Sciences* 21, pp. 185–205.
- BABCOCK, R. & P. DAVIES (1991), Effects of sedimentation on settlement of *Acropora millepora*. *Coral Reefs* 9, pp. 205–208.
- BAGNOLD, R. (1966), An approach to the sediment transport problem from general physics. *Physiographic and hydraulic studies of rivers*, Washington: USGPO. Professional paper US Geological Survey no. 422-1.
- BASS, S. J., J. N. ALDRIDGE, I. N. MCCAVE & C. E. VINCENT (2002), Phase relationships between fine sediment suspensions and tidal currents in coastal seas. *Journal of Geophysical Research, part Oceans* 107. 3146, doi:10.1029/2001JC001269.
- BERHANE, I., R. W. STERNBERG, G. C. KINEKE, T. G. MILLIGAN & K. KRANCK (1996), The variability of suspended aggregates on the Amazon Continental shelf. *Continental Shelf Research* 17, pp. 267–285.
- BLACK, K. P. (1993), The relative importance of local retention and inter-reef dispersal of neutrally buoyant material on coral reefs. *Coral Reefs* 4, pp. 201–211.
- BLACK, K. P. & S. L. GAY (1987), Eddy formation in unsteady flows. *Journal of Geophysical Research, part Oceans* 92, pp. 9514–9522.
- BOON, J. D. (1988), Temporal variation of shallow-water tides in basin-inlet systems. In: D. G. Aubrey & L. Weishar, eds., *Hydrodynamics and Sediment Dynamics of Tidal Inlets*, Springer-Verlag, pp. 125–136.

- BOWDEN, K. (1953), Note on wind drift in a channel in the presence of tidal currents. *Proceedings of the Royal Society (A)* 219, pp. 426–446.
- BOWDEN, K. (1983), *Physical oceanography of coastal waters*. Ellis Horwood series in marine science, Ellis Horwood Limited.
- BROWN, B. E. (1997), Adaptations of reef corals to physical environmental stress. *Advances in Marine Biology*, pp. 221–299.
- BRYCE, S., P. LARCOMBE & P. V. RIDD (1998), The relative importance of landward-directed tidal sediment transport versus freshwater flood events in the Normanby River estuary, Cape York Peninsula, Australia. *Marine Geology* 149, pp. 55–78.
- BUNT, J. A. C. (1999), Quantifying the response of optical backscatter devices and transmissometers to variations in suspended particulate matter. *Continental Shelf Research* 19, pp. 1199–1220.
- CHALKER, B. E. (1981), Simulating light-saturation curves for photosynthesis and calcification by reef-building corals. *Marine Biology* 63, pp. 135–141.
- COLES, S. L. & Y. H. FADLALLAH (1991), Reef coral survival and mortality at low temperatures in the Arabian Gulf: New species-specific lower temperature limits. *Coral Reefs* 9, pp. 231–226.
- COLES, S. L. & P. JOKIEL (1992), Effects of salinity on coral reefs. In: D. W. Connell & D. W. Hawker, eds., *Pollution in tropical aquatic systems*, chap. 6, CRC Press, pp. 147–166.
- DE RUIJTER, W. P. M. (1983), Effects of Velocity Shear in Advective Mixed-Layer Models. *Journal of Physical Oceanography* 13, pp. 1589–99.
- DE RUIJTER, W. P. M., A. W. VISSER & W. G. BOS (1997), The Rhine outflow: A prototypical pulsed discharge plume in a high energy shallow sea. *Journal of Marine Systems* 12, pp. 263–276.
- DE VRIEND, H. J. (1981), Steady flow in shallow channel bends. Ph.D. thesis, Delft University of Technology, Delft, The Netherlands.
- DEFANT, A. (1961), *Physical oceanography*. Oxford: Pergamon Press.
- DEINES, K. L. (1999), Backscatter estimation using broadband acoustic doppler current profilers. In: *Oceans 99 MTS/IEEE Conference Proceedings*, San Diego.
- DELEERSNIJDER, E., A. NORRO & E. WOLANSKI (1992), A three-dimensional model of the water circulation around an island in shallow water. *Continental Shelf Research* 12, pp. 891–906.
- DIGGLE, P. J. (1990), *Time Series - A Biostatistical Introduction*. Oxford Statistical Science Series, Oxford: Clarendon Press, 5 edn.
- DOODSON, A. T. (1921), The harmonic development of the tide generating potential. *Proc. Roy. Society of London A100*, pp. 305–329. Reprinted in the *International Hydrographic Review*, 1954.
- DOUGLAS, I. (1996), The impact of land-use changes, especially logging, shifting cultivation, mining and urbanization on sediment yield in tropical Southeast Asia: a review with special reference to Borneo. *Int. Assoc. Hydrol. Sci.* 236, pp. 463–472.
- DRONKERS, J. (1986), Tide-induced residual transport of fine sediment. In: J. van de Kreeke, ed., *Physics of Shallow Estuaries and Bays*, Springer Verlag, Berlin, pp. 228–258.
- DYER, K. R. (1986), *Coastal and Estuarine Sediment Dynamics*. New York: John Wiley&Sons.
- DYER, K. R. (1994), Sediment transport and depositional processes. In: K. Pye, ed., *Estuarine sediment transport and deposition*, chap. 6, Blackwell Scientific Publications, Oxford, pp. 193–218.
- DYER, K. R. & A. J. MANNING (1999), Observation of the size, settling velocity and



- effective density of flocs, and their fractal dimensions. *Journal of Sea Research* 41, pp. 87–95.
- EMERY, W. J. & R. E. THOMSON (2001), *Data Analysis Methods in Physical Oceanography*. Elsevier Science BV.
- FABRICIUS, K. E. & E. WOLANSKI (2000), Rapid Smothering of Coral Reef Organisms by Muddy Marine Snow. *Estuarine, Coastal and Shelf Science* 50, pp. 115–120.
- FENNESSY, M. J., K. R. DYER & D. A. HUNTLEY (1994), Size and settling velocity distributions of flocs in the Tamar Estuary. *Neth. J. Aqu. Ecol.* 28, pp. 275–282.
- FISCHER, H. B., E. J. LIST, R. C. Y. KOH, J. IMBERGER & N. H. BROOKS (1979), *Mixing in Inland and Coastal Waters*. Academic Press, Inc.
- FLAGG, C. N. & S. L. SMITH (1989), On the use of the acoustic doppler current profiler to measure zooplankton abundance. *Deep Sea Res.* 36, pp. 455–474.
- FONG, D. A., W. R. GYER & R. P. SIGNELL (1997), The wind-forced response on a buoyant coastal current: Observations of the western Gulf of Maine plume. *Journal of Marine Systems* 12, pp. 69–81.
- FRANÇOIS, R. E. & G. R. GARRISON (1982a), Sound absorption based on ocean measurements. part I: pure water and magnesium sulfate contributions. *Journal of the Acoustic Society of America* 72, pp. 896–907.
- FRANÇOIS, R. E. & G. R. GARRISON (1982b), Sound absorption based on ocean measurements. part II: boric acid contribution and equation for total absorption. *Journal of the Acoustic Society of America* 72, pp. 1879–90.
- FRIEDRICHS, C. (1988), Non-linear tidal distortion in shallow well-mixed estuaries: a synthesis. *Estuarine, Coastal and Shelf Science* 27, pp. 521–545.
- FURUKAWA, K. & E. WOLANSKI (1998), Shallow-water Frictional Effects in Islands Wakes. *Estuarine, Coastal and Shelf Science* 46, pp. 599–608.
- GEYER, W. R. (1993), Three-dimensional tidal flow around a headland. *Journal of Geophysical Research*, part Oceans 98, pp. 955–966.
- GEYER, W. R. (1995), Tide-induced mixing in the Amazon frontal zone. *Journal of Geophysical Research*, part Oceans 100, pp. 2341–2353.
- GEYER, W. R. & G. C. KINEKE (1995), Observations of currents and water properties in the Amazon frontal zone. *Journal of Geophysical Research*, part Oceans 100, pp. 2321–2339.
- GEYER, W. R. & R. SIGNELL (1990), Measurements of tidal flow around a headland with a shipboard acoustic doppler current profiler. *Journal of Geophysical Research*, part Oceans 95, pp. 3189–3197.
- GEYER, W. R. & J. D. SMITH (1987), Shear instability in a highly stratified estuary. *Journal of Physical Oceanography* 17, pp. 1668–1679.
- GODIN, G. (1972), *The analysis of tides*. Liverpool University Press.
- GOURLAY, M. R. (1988), Coral cays: products of wave action and geological processes in a biogenic environment. In: *Proceedings of the 6th International Coral Reef Symposium, Australia*, vol. 2.
- GOURLAY, M. R. (1994), Wave transformation on a coral reef. *Coastal Engineering* 23, pp. 17–42.
- GREEN, M. O., R. G. BELL, T. J. DOLPHIN & A. SWALES (2000), Silt and sand transport in a deep tidal channel of a large estuary (Manukau Harbour, New Zealand). *Marine Geology* 163, pp. 217–240.
- GREENSPAN, H. P. (1968), *The theory of rotating fluids*. Cambridge University Press. 327 pp.
- GROEN, P. (1967), On the residual transport of suspended matter by an alternating tidal

- current. Netherlands Journal of Sea Research 3-4, pp. 564–574.
- HALLOCK, P. & W. SCHLAGER (1986), Nutrients excess and the demise of coral reefs and carbonate platforms. *Palaios* 1, pp. 389–398.
- HANES, D. M. (1988), Intermittent Sediment Suspension and its Implications to Sand Traces Dispersal in Wave-dominated Environments. *Marine Geology* 81, pp. 175–183.
- HASHIMOTO (1997), Analysis of the directional wave spectrum from field data. In: P.-F. Liu, ed., *Advances in Coastal Engineering Vol. 3*, World Scientific, Singapore, pp. 103–143.
- HATCHER, A., P. HILL & J. GRANT (2001), Optical backscatter of marine flocs. *Journal of Sea Research* 46, pp. 1–12.
- HAY, A. E. & J. SHENG (1992), Vertical profiles of suspended sand concentration and size from multifrequency acoustic backscatter. *Journal of Geophysical Research, part Oceans* 97, pp. 15661–15667.
- HAYWARD, A. B. (1982), Coral reefs in a clastic sedimentary environment: fossils (Miocene, SW Turkey) and moderns (Recent, Red Sea) analogues. *Coral Reefs* 1, pp. 109–114.
- HOEKSTRA, P., R. F. NOLTING & H. A. VAN DER SLOOT (1989), Supply and dispersion of water and suspended matter of the rivers Solo and Brantas into the coastal waters of East Java, Indonesia. *Netherlands Journal of Sea Research* 23, pp. 501–515.
- HOITINK, A. J. F. (2000), Three dimensional velocity structure and suspended sediments at coral reefs in Teluk Banten. In: B. L. Edge, ed., *Coastal Engineering 2000*, Sydney, Australia: ASCE (American Society of Civil Engineers), pp. 3345–3358.
- HOLDAWAY, G. P., P. D. THORNE, D. FLATT, S. E. JONES & D. PRANDLE (1999), Comparison between ADCP and transmissometer measurements of suspended sediment concentration. *Continental Shelf Research* 19, pp. 421–441.
- HOPLEY, D. (1994), Continental shelf reef systems. In: R. W. G. Carter & C. D. Woodroffe, eds., *Coastal evolution: late quaternary shoreline morphodynamics*, Cambridge University Press, Cambridge, pp. 303–340.
- HOWARTH, M. J. & D. T. PUGH (1983), Observations of tides over the continental shelf. In: J. Noye, ed., *Physical oceanography of coastal and shelf seas*, vol. 35 of *Elsevier oceanography series*, Amsterdam: Elsevier.
- HUBBARD, D. K. (1986), Sedimentation as a control of reef development: St. Croix, US.V.I. *Coral Reefs* 5, pp. 117–125.
- INGRAM, R. G. & V. H. CHU (1987), Flow Around Islands in Rupert Bay: An Investigation of the Bottom Friction Effect. *Journal of Geophysical Research, part Oceans* 92, pp. 14521–14533.
- INOUE, M. & W. J. WISEMAN JR. (2000), Transport, Mixing and Stirring Processes in a Louisiana Estuary: A Model Study. *Estuarine, Coastal and Shelf Science* 50, pp. 449–466.
- JAMES, M., C. CRABBE & D. J. SMITH (2002), Comparison of two reef sites in the Wakatobi Marine National Park (SE Sulawesi, Indonesia) using digital image analysis. *Coral Reefs* 21, pp. 242–244.
- JOHNSON, R. K. (1977), Sound scattering from a fluid sphere revised. *Journal of the Acoustic Society of America* 61, pp. 375–377.
- JORDAN, C. F., R. J. WHARTON & R. E. COOK (1993), The sedimentology of Kepulauan Seribu: A modern patch reef complex in the west Java Sea, Indonesia. In: *Modern Carbonates and their Ancient Counterparts in Indonesia: A Guide to Interpreting and Understanding Carbonate Reservoirs*, Indonesian Petroleum Association, pp. 2.1–2.6.
- KALKWIJK, J. P. T. & R. BOOIJ (1986), Adaptation of secondary flow in nearly-horizontal flow. *Journal of Hydraulic Engineering* 24, pp. 19–37.
- KINEKE, G. C. & R. W. STERNBERG (1992), Measurements of high concentration suspended sediments using the optical backscatterance sensor. *Marine Geology* 108, pp.

253–258.

- KITHEKA (1997), Coastal tidally-driven circulation and the role of water exchange in the linkage between tropical coastal ecosystems. *Estuarine, Coastal and Shelf Science* 45, pp. 177–187.
- KLEYPAS, J. A. (1999), Environmental Limits to Coral Reef Development: Where Do We Draw the Line? *American Zoologist* 39.
- LARCOMBE, P. & K. J. WOOLFE (1999), Increased sediment supply to the Great Barrier Reef will not increase sediment accumulation at most coral reefs. *Coral Reefs* 18, p. 163:169.
- LARCOMBE, P., P. V. RIDD, A. PRYTZ & B. WILSON (1995), Factors controlling suspended sediment on inner-shelf coral reefs, Townsville, Australia. *Coral Reefs* 14, pp. 163–171.
- LARCOMBE, P., A. COSTEN & K. J. WOOLFE (2001), The hydrodynamic and sedimentary setting of nearshore coral reefs, central Great Barrier Reef shelf, Australia. *Sedimentology* 48, pp. 811–835.
- LEWIS, R. (1997), Dispersion in estuaries and coastal waters. John Wiley&Sons Ltd.
- LYNCH, J. F., J. D. IRISH, C. R. SHERWOOD & Y. C. AGRAWAL (1994), Determining suspended sediment particle size information from acoustical and optical backscatter measurements. *Continental Shelf Research* 14, pp. 1139–1165.
- MARMORINO, G. O., T. F. DONATO, M. A. SLETTEN & C. L. TRUMP (2000), Observations of an inshore front associated with the Chesapeake Bay outflow plume. *Continental Shelf Research* 20, pp. 665–684.
- MASSEL, S. R. (1993), Extended refraction-diffraction equation for surface waves. *Coastal Engineering* 19, pp. 97–126.
- MASSEL, S. R. (1996), *Ocean Surface Waves: Their Physics and Prediction*, vol. 11 of *Advanced Series on Ocean Engineering*. World Scientific Publishing Co. Pte. Ltd.
- MASSEL, S. R. (1999), *Fluid Mechanics for Marine Ecologists*. Springer-Verlag.
- MEDWIN, H. (1975), Speed of sound in water: a simple equation for realistic parameters. *Journal of the Acoustic Society of America* 56, pp. 1318–19.
- MEDWIN, H. & C. S. CLAY (1998), *Fundamentals of Acoustical Oceanography*. Academic Press.
- MEESTERS, E. H., R. P. M. BAK, S. WESTMACOTT, M. RIDGLEY & S. DOLLAR (1998), A fuzzy logic model to predict coral reef development under nutrient and sediment stress. *Conserv. Biol.* 12, pp. 957–965.
- MEESTERS, E. H., G. NIEUWLAND, G. C. A. DUINEVELD, A. KOK & R. P. M. BAK (2002), RNA/DNA ratios of scleractinian corals suggest acclimatisation/adaptation in relation to light gradients and turbidity regimes. *Mar. Ecol. Prog. Ser.* 227, pp. 233–239.
- MEESTERS, E. H., G. NIEUWLAND, M. P. A. VAN ROUVEROY VAN NIEUWAAL, P. Q. TERPSTRA & R. BAK (in prep), Ecological adaptations of scleractinian corals in marginal reefs: nearshore high turbidity reefs in the Indonesian Archipelago.
- MILLER, R. L. & J. F. CRUISE (1995), Effects of Suspended Sediments on Coral Growth: Evidence from Remote Sensing and Hydrologic Modeling. *Remote Sens. Environ.* 53, pp. 177–187.
- MILLIMAN, J. D. & R. H. MEADE (1983), Worldwide delivery of river sediment to the oceans. *Journal of Geology* 91, pp. 1–21.
- MILLIMAN, J. D., K. L. FARNSWORTH & C. S. ALBERTIN (1999), Flux and fate of fluvial sediments leaving large islands in the East Indies. *Journal of Sea Research* 41, pp. 97–107.
- MITCHELL, W. M., D. A. BEARD, P. J. BILLS & B. J. NOYE (1984), An application of a three-dimensional tidal model to the gulf of carpentaria. In: J. Noye, ed., *Computational techniques for differential equations*, vol. 83 of *North-Holland mathematics studies*, North-

- Holland.
- MUNCHOW, A. & R. W. GARVINE (1993), Dynamical properties of a buoyancy-driven coastal current. *Journal of Geophysical Research*, part Oceans 98, pp. 20063–77.
- MUNK, W. & E. ANDERSON (1948), Note on the theory of the thermocline. *Journal of Marine Research* 7, pp. 276–295.
- NEPF, H. M. & W. R. GEYER (1996), Intratidal variations in stratification and mixing in the Hudson estuary. *Journal of Geophysical Research*, part Oceans 101, pp. 12,079–86.
- NICHOLS, M. M. & J. D. BOON (1994), Sediment transport processes in coastal lagoons. In: B. Kjerfve, ed., *Coastal Lagoon Processes*, Elsevier Oceanography Series, 60, chap. 7, Elsevier Science Publishers B.V., pp. 157–219.
- NUNES VAZ, R. A. & G. W. LENNON (1991), Modulation of estuarine stratification and mass flux at tidal frequencies. In: B. B. Parker, ed., *Tidal Hydrodynamics*, chap. 26, John Wiley&Sons, pp. 505–520.
- OKUBO, A. (1974), Some speculations on oceanic diffusion diagrams. In: Rapp. P.-V. Reun. Cons. Int. Explor. Mer, 167, pp. 77–85.
- PARKER, B. B. (1991), The relative importance of the various nonlinear mechanisms in a wide range of tidal interactions (review). In: B. B. Parker, ed., *Tidal Hydrodynamics*, chap. 13, John Wiley&Sons, Inc., pp. 237–268.
- PATTIARATCHI, C., A. JAMES & M. COLLINS (1986), Island wakes and headland eddies: a comparison between remotely sensed data and laboratory experiments. *Journal of Geophysical Research*, part Oceans 92, pp. 783–794.
- PERKINS, H. J. (1970), The formation of streamwise vorticity in turbulent flow. *Journal of Fluid Mechanics* 44, pp. 721–740.
- PHILLIPS, O. M., J. HWA SHYU & H. SALMUN (1986), An experiment on boundary mixing: mean circulation and transport rates. *Journal of Fluid Mechanics* 173, pp. 473–499.
- PICKARD, G., D. J.R., C. HENIN & F. ROUGERIE (1977), A review of the physical oceanography of the Great Barrier Reef and western Coral Sea, vol. 2 of *Monograph Series*. Australian Institute of Marine Science. 134 pp.
- PINGREE, R. D. & D. K. GRIFFITHS (1979), Sand transport paths around the British Isles resulting from  $M_2$  and  $M_4$  tidal interactions. *Journal of the Marine Biological Association of the United Kingdom* 59, pp. 497–513.
- PINGREE, R. D. & L. MADDOCK (1978), The  $m_4$  tide in the english channel derived from a nonlinear numerical model of the  $m_2$  tide 25, pp. 53–63.
- POSTMA, H. (1961), Transport and accumulation of suspended matter in the Dutch Wadden Sea. *Netherlands Journal of Sea Research* 1, pp. 148–190.
- PUGH, D. (1987), *Tides, surges and mean sea-level*. John Wiley&Sons.
- RANASINGHE, R. & C. PATTIARATCHI (2000), Tidal inlet velocity asymmetry in diurnal regimes. *Continental Shelf Research* 20, pp. 2347–2366.
- RAYLEIGH, L. J. W. S. (1945), *The Theory of Sound*, vol. 1 and 2. New York Dover Publications.
- RIDDERINKHOF, H. (1988a), Tidal and residual flows in the Western Dutch Wadden Sea, I: Numerical model results. *Netherlands Journal of Sea Research* 22, pp. 1–21.
- RIDDERINKHOF, H. (1988b), Tidal and residual flows in the Western Dutch Wadden Sea, II: An analytical model to study the constant flow between connected tidal basins. *Netherlands Journal of Sea Research* 22, pp. 185–198.
- ROBERTS, H. H., P. A. WILSON & A. LUGO-FERNÁNDEZ (1992), Biologic and geologic responses to physical processes: examples from modern reef systems of the Caribbean-Atlantic region. *Continental Shelf Research* 12, pp. 809–834.
- ROGERS, C. S. (1990), Responses of coral reefs and reef organisms to sedimentation. *Marine*

- Ecological Progress Series 62.
- SANDERS, T. M. & R. W. GARVINE (2001), Fresh water delivery to the continental shelf and subsequent mixing: An observational study. *Journal of Geophysical Research*, part Oceans 106, pp. 27,087–27,101.
- SANDERSON, B. G., A. OKUBO, I. R. WEBSTER, S. KIOROGLU & R. APPELDOORN (1995), Observations and Idealized Models of Dispersion on the Southwestern Puerto Rican Insular Shelf. *Mathl. Comput. Modelling* 21, pp. 39–63.
- SCHRAMA, E. J. O. & R. D. RAY (1994), A preliminary tidal analysis of topex/poseidon altimetry. *Journal of Geophysical Research*, part Oceans 99, pp. 24799–24808.
- SHARPLES, J. (1992), Time Dependent Stratification in Regions of Large Horizontal Gradient. Ph.D. thesis, Univ. Wales, Bangor.
- SHARPLES, J. S. & J. H. SIMPSON (1995), Semi-diurnal and longer period stability cycles in the Liverpool Bay region of freshwater influence. *Continental Shelf Research* 15, pp. 295–313.
- SHENG, J. & A. E. HAY (1988), An examination of the spherical scatter approximation in aqueous suspension of sand. *Journal of the Acoustic Society of America* 83, pp. 598–610.
- SIMPSON, J. H. (1997), Physical processes in the ROFI regime. *Journal of Marine Systems* 12, pp. 3–15.
- SIMPSON, J. H., J. BROWN, J. MATTHEWS & G. ALLEN (1990), Tidal Straining, Density Currents, and Stirring in the Control of Estuarine Circulation. *Estuaries* 13, pp. 125–132.
- SOULSBY, R. L. (1983), The bottom boundary layer of shelf seas. In: B. Johns, ed., *Physical Oceanography of Coastal and Shelf Seas*, chap. 5, Elsevier, pp. 189–266.
- SPALDING, M. D., C. R. RAVILOUS & E. P. GREEN (2001), *World Atlas of Coral Reefs*. University of California Press, in association with UNEP World Conservation Monitoring Centre.
- SZMANT, A. M. (1997), Nutrient effects on coral reefs: A hypothesis on the importance of topographic and trophic complexity to reef nutrient dynamics. In: *Proc. 8th Int. Coral Reef Sym.*, 2, pp. 1527–1532.
- THOMPSON, E. R. & E. J. WOLANSKI (1984), Tidal period upwelling within Raine Island Entrance, Great Barrier Reef. *Journal of Marine Research* 42, pp. 787–808.
- THOMPSON, R. O. R. Y. & T. J. GOLDING (1981), Tidally-induced upwelling by the Great Barrier Reef. *Journal of Geophysical Research*, part Oceans 86, pp. 6517–6521.
- THORNE, P. D., P. J. HARDCASTLE & R. L. SOULSBY (1993), Analysis of Acoustic Measurements of Suspended Sediment. *Journal of Geophysical Research*, part Oceans 98, pp. 899–910.
- THORPE, S. A. (1971), Experiments on instability and turbulence in a stratified shear flow. *Journal of Fluid Mechanics* 61, pp. 731–751.
- THORPE, S. A. (1986), Measurements with an automatically recording inverted echo sounder; ARIES and the bubble clouds. *J. Phys. Oceanogr.* 16, pp. 1462–78.
- TOMASCIK, T., A. J. MAH, A. NONTJI & M. K. MOOSA (1997), The Ecology of the Indonesian Seas, Part One, vol. 7 of *The Ecology of Indonesia Series*. Singapore: Periplus Editions (HK) Ltd.
- TOMCZAK, M. (1988), Island Wakes in Deep and Shallow Water. *Journal of Geophysical Research*, part Oceans 93, pp. 5153–5154.
- TROWBRIDGE, J. H. & G. C. KINEKE (1994), Structure and dynamics of fluid muds over the Amazon Continental Shelf. *Journal of Geophysical Research*, part Oceans 99, pp. 865–874.
- TSENG, R. S. (2002), On the dispersion and diffusion near estuaries and around islands. *Estuarine, Coastal and Shelf Science* 54, pp. 89–100.

- URICK, R. J. (1948), The absorption of sound in irregular particles. *Journal of the Acoustic Society of America* 20, pp. 283–289.
- URICK, R. J. (1983), *Principles of Underwater Sound*. McGraw-Hill Book Company.
- VAN AKEN, H. M. (1986), The onset of seasonal stratification in shelf seas due to differential advection in the presence of a salinity gradient. *Continental Shelf Research* 5, p. 475:485.
- VAN DE KREEKE, J. (1997), Tidal variations in suspended sediment concentration in the Ems estuary: origin and resulting sediment flux. *Netherlands Journal of Sea Research* 38, pp. 1–16.
- VAN DE KREEKE, J. & K. ROBACZEWSKA (1993), Tide-induced residual transport of coarse sediment; application to the Ems estuary. *Netherlands Journal of Sea Research* 31, pp. 209–220.
- VAN DEN BERGH, G. D., T. C. E. VAN WEERING & W. BOER (2001), Recent sediments and sediment accumulation rates in Teluk Banten, Indonesia. In: *Royal NIOZ jaarverslag 2001*, pp. 44–47.
- VAN DEN BERGH, G. D., T. C. E. VAN WEERING & H. DE HAAS (in prep a), Holocene sedimentation and shallow seismic stratigraphy of Teluk Banten (NW Java, Indonesia). *Netherlands Institute for Sea Research*.
- VAN DEN BERGH, G. D., T. C. E. VAN WEERING & R. VAN WIJHE (in prep b), Tsunami deposits and recent sedimentation in Teluk Banten (NW Java, Indonesia). *Netherlands Institute for Sea Research*.
- VAN DER MOLEN, J. (2000), A 2DH numerical model of tidally induced sand transport in the Southern North Sea. In: T. Yanagi, ed., *Interactions between Estuaries, Coastal Seas and Shelf Seas*, Terra Scientific Publishing Company, Tokyo.
- VAN LEUSSEN, W. (1988), Aggregation of particles, settling velocity of mud flocs; a review. In: J. Dronkers & W. Van Leussen, eds., *Physical Processes in Estuaries*, Springer-Verlag, pp. 347–403.
- VAN LEUSSEN, W. (1994), Estuarine macroflocs and their role in fine-grained sediment transport. Ph.D. thesis, Faculty of Earth Sciences, Utrecht University.
- VAN STRAATEN, L. & P. KUENEN (1958), Tidal action as a cause of clay accumulation. *Journal of Sedimentary Petrology* 28, pp. 406–413.
- VAN WEERING, T. C. E., H. C. DE STIGTER, W. BOER & H. DE HAAS (2002), Recent sediment transport and accumulation on the NW Iberian margin. *Progress in Oceanography* 52, pp. 349–371.
- VERSTAPPEN, H. T. (1988), Old and New Observations on Coastal Changes of Jakarta Bay: An Example of Trends in Urban Stress on Coastal Environments. *Journal of Coastal Research* 4, pp. 573–587.
- VISSER, A. W., A. J. SOUZA, K. HESSNER & J. H. SIMPSON (1994), The influence of water column stratification on tidal current profile in a ROFI system. *Oceanology Acta* 17, pp. 369–381.
- WALKER, T. A. (1981), Dependence of phytoplankton chlorophyll on bottom resuspension in Cleveland Bay, northern Queensland. *Australian Journal of Marine and Freshwater Research* 32, pp. 831–886.
- WANG, Z. B., T. LOUTERS & H. J. DE VRIEND (1995), Morphodynamic modelling for a tidal inlet in the Wadden Sea. *Marine Geology* 126, pp. 289–300.
- WANG, Z. B., M. C. J. L. JEUKEN & H. J. DE VRIEND (1999), Tidal asymmetry and residual sediment transport in estuaries. Tech. Rep. Z2749, WL|Delft Hydraulics.
- WHITEHOUSE, R., R. SOULSBY, W. ROBERTS & H. MITCHENER (2000), *Dynamics of estuarine muds*. HR Wallingford Limited and Thomas Telford Limited.
- WIENS, H. J. (1962), *Atoll Environment and Ecology*. New Haven: Yale University Press.

532 pp.

- WINTERWERP, H. (1999), On the dynamics of high-concentrated mud suspensions. Ph.D. thesis, Department of Civil Engineering and Geosciences, Delft University of Technology.
- WL|Delft Hydraulics (1997), Getijsys Manual Version 3.00.
- WOLANSKI, E. (1988), Island wakes in shallow waters. *Journal of Geophysical Research*, part Oceans 93, pp. 1335–1336.
- WOLANSKI, E. (2001), *Oceanographic Processes of Coral Reefs - Physical and biological links in the Great Barrier Reef*. CRC Press. 356 pp.
- WOLANSKI, E. & W. M. HAMNER (1988), Topographically controlled fronts in the Ocean and Their Biological Influence. *Science* 241, pp. 177–181.
- WOLANSKI, E. & G. L. PICKARD (1985), Long-term observations of currents on the central great barrier reef. *Coral Reefs* 4, pp. 47–57.
- WOLANSKI, E. & J. SARSENSKI (1997), Dispersion in coral reefs and mangroves. *American Scientist* 85, pp. 236–243.
- WOLANSKI, E. & S. SPAGNOL (2000), Sticky Waters in the Great Barrier Reef. *Estuarine, Coastal and Shelf Science* 50, pp. 27–32.
- WOLANSKI, E., M. JONES & W. T. WILLIAMS (1981), Physical Properties of Great Barrier Reef Lagoon Waters near Townsville. II Seasonal Variations. *Australian Journal of Marine and Freshwater Research* 32, pp. 321–334.
- WOLANSKI, E., J. IMBERGER & M. L. HERON (1984a), Island Wakes in Shallow Coastal Water. *Journal of Geophysical Research*, part Oceans 93, pp. 10.553–10.569.
- WOLANSKI, E., G. L. PICKARD & D. L. B. JUPP (1984b), River Plumes, Coral Reefs and Mixing in the Gulf of Papua and the Northern Great Barrier Reef. *Estuarine, Coastal and Shelf Science* 18, pp. 291–314.
- WOLANSKI, E., T. ASAEDA, A. TANAKA & E. DELEERSNIJDER (1996), Three-dimensional island wakes in the field, laboratory experiments and numerical models. *Continental Shelf Research* 16, pp. 1437–1452.
- WOLANSKI, E., S. SPAGNOL, B. KING & T. AYUKAI (1999), Patchiness in the Fly River plume in Torres Strait. *Journal of Marine Systems* 18, pp. 369–381.
- WOODS, A. W. & R. C. BEARDSLEY (1988), On the barotropic discharge of a homogeneous fluid onto a continental shelf. *Continental Shelf Research* 8, pp. 307–327.
- WOOLFE, K. J. & P. LARCOMBE (1998), Terrigenous sediment accumulation as a regional control on the distribution of reef carbonates. *Spec. Publs Int. Ass. Sediment* 25, pp. 295–310.
- WOOLFE, K. J. & P. LARCOMBE (1999), Terrigenous sedimentation and coral reef growth: a conceptual framework. *Marine Geology* 155, pp. 331–345.
- WYRTKI, K. (1961), *Physical oceanography of the southeast Asian waters*. Tech. Rep., University of California, San Diego. NAGA report, 195 pp.
- WYRTKI, K. (1987), Indonesian throughflow and the associated pressure gradient. *Journal of Geophysical Research*, part Oceans 92, pp. 12.941–12.946.

# Curriculum Vitae

Ton Hoitink was born on 20 December 1973 in Hoogkarspel (The Netherlands). He started to study Civil Engineering Technology and Management in 1992, at the University of Twente in Enschede. In 1996, he joined an irrigation project in Mendoza, Argentina, where he specialized in cost-benefit analysis within the framework of a traineeship. Once returned to the Netherlands he started to do research for his MSc thesis in 1997, which was concerned with the morphological impact of large-scale marine sand extraction from the North Sea. For that purpose he was stationed in Delft at WL|Delft Hydraulics. He obtained his Master's degree in November 1998.

Subsequent to his master's studies he participated in the Teluk Banten Research Programme, focussing on the marine physics of tropical coastal systems as a PhD student at the Physical Geography Department, Utrecht University. Throughout his PhD study he was employed by the Foundation for the Advancement of Tropical Research (WOTRO), which is a multi-disciplinary funding organization residing under the Netherlands Organisation for Scientific Research (NWO). He had the privilege to spend nine month in Indonesia doing field measurements, in 1998 and 1999.

At present Ton is working on a project under the umbrella of the East Kalimantan Research Programme. In July a reconnaissance survey is planned in which the deltas formed by the rivers Mahakam and the Berau will be explored. From May 2003 onward he will have a temporary position at the Department of Physical Geography, Utrecht University.

